UNIVERSITY OF CALIFORNIA,
IRVINE

Applying New Tools to Study Aβ-derived Oligomers

DISSERTATION

submitted in partial satisfaction of the requirements
for the degree of

DOCTOR OF PHILOSOPHY

in Chemistry

by

Gretchen Guaglianone

Dissertation Committee:
Professor James S. Nowick, Chair
Professor Rachel W. Martin
Assistant Professor Elizabeth N. Bess

2022

DEDICATION

To

the family, friends, and wonderful lab mates

that kept me going

For the graduate students,

the best way out is always through

Robert Frost

For the scientists,

We must accept infinite disappointment, but we must never lose infinite hope

Martin Luther King Jr.

For the women,

Give 'em hell

TABLE OF CONTENTS

	Page
LIST OF FIGURES	vi
LIST OF SCHEMES	viii
ACKNOWLEDGEMENTS	ix
VITA	x
ABSTRACT OF THE DISSERTATION	xv
CHAPTER 1: Exploring Amyloid Oligomers with Peptide Model Systems	1
Preface to Chapter 1	1
Introduction	2
Synthesis of Macrocyclic β-Hairpin Peptides	4
Methods for Studying the Self-Assembly of Macrocyclic β-Hairpin Peptides	9
Conclusion	13
Acknowledgements	15
References	16
CHAPTER 2: Elucidating the Oligomerization and Cellular Interactions of a Trimer Derived from Aβ Through Fluorescence and Mass Spectrometric Studies	22
Preface to Chapter 2	22
Introduction	23
Results and Discussion	24
Design and synthesis of 2AT-L	24
Preparation of fluorescently labeled 2AT-L	25
Oligomerization of 2AT-L and fluorescently labeled 2AT-L analogues by SDS-PAGE	26
Oligomerization of 2AT-L and fluorescently labeled 2AT-L analogues by native IM-MS	28
Oligomerization of 2AT-L-sCy3 and 2AT-L-sCy5 by FRET	30
Fluorescence microscopy of 2AT-L-sCy3 and 2AT-L-sCy5	32
FLIM-FRET studies of 2AT-L-sCy3 and 2AT-L-sCy5	34
Summary and Conclusions	38
Acknowledgements	40
References and Notes	41
Supporting Information	50
Table of Contents	50
Supporting Figures	51

Materials and Methods 58
References and Notes 68
Characterization Data 71

CHAPTER 3: Isomorphic Trimers Derived from Aβ Exhibit Different Oligomerization and Biological Properties 94
Preface to Chapter 3 94
Introduction 96
Results and Discussion 98
Synthesis of 2AT and KLT 98
Assembly of 2AT and KLT by SDS-PAGE 99
Investigating the cytotoxicity of 2AT and KLT 100
Preparation of fluorescently labeled 2AT and KLT 102
Fluorescence microscopy of 2AT-sCy3 and KLT-sCy3 102
Summary and Conclusions 108
References and Notes 110
Supporting Information 117
Table of Contents 117
Materials and Methods 118
References and Notes 125
Characterization Data 127

CHAPTER 4: Investigating the Gas- and Solution-Phase Assembly of Three Trimers Derived from Aβ 153
Preface to Chapter 4 153
Introduction 154
Results and Discussion 156
Design and Synthesis of 2AT, KLT, and QKT 156
Oligomers of 2AT, KLT, and QKT observed by native MS 159
Oligomers of 2AT, KLT, and QKT observed by native IM-MS 161
Oligomers of 2AT, KLT, and QKT observed by mass photometry 164
Oligomers of 2AT, KLT, and QKT observed by SDS-PAGE 166
Cell viability of SH-SY5Y cells treated with 2AT, KLT, and QKT 167
Summary and Conclusions 168
References and Notes 172
Supporting Information 180
Table of Contents 180
Materials and Methods 184
References and Notes 193
Characterization Data 195

CHAPTER 5: Knowledge Acquired From My Experience As The Mass Spectrometry

Fellow at UCI 210
Introduction 210
General Principles and Instruments of Mass Spectrometry 210
Biomolecule Sample Preparations 215
Analysis Tools 219
Conclusions 220
References 221
EPILOGUE 224

LIST OF FIGURES

		Page
Figure 1.1	Aβ-derived macrocyclic β-hairpin peptides	4
Figure 1.2	Techniques to study supramolecular assembly	10
Figure 1.3	Silver-stained SDS-PAGE	11
Figure 2.1	Chemical structures of β-hairpin peptide 2AT-L	25
Figure 2.2	SDS-PAGE of 2AT-L and fluorescently labeled analogues	28
Figure 2.3	Native IM-MS of 2AT-L and fluorescently labeled analogues	30
Figure 2.4	Fluorescence emission of 2AT-L-sCy3 and 2AT-L-sCy5	32
Figure 2.5	Micrographs of fluorescently labeled 2AT-L analogues	33
Figure 2.6	Micrographs of a fluorescently labeled 2AT-L analogue and a lysosomal marker	34
Figure 2.7	Phasor analysis of FLIM micrographs	37
Figure S2.1	Micrograph of 2AT-L-sCy3 with SH-SY5Y cells	52
Figure S2.2	Micrograph of 2AT-L-sCy5 with SH-SY5Y cells	53
Figure S2.3	Micrograph of concentration gradient of 2AT-L-sCy5 with SH-SY5Y cells	54
Figure S2.4	Micrograph of 2AT-L-sCy3 with Lysotracker Green	55
Figure S2.5	Fractional intensity of quenched donor (D_q)	56
Figure S2.6	Representative clouds on phasor plot	57
Figure 3.1	Chemical structures of β-hairpin peptides 2AT and KLT	99
Figure 3.2	SDS-PAGE of 2AT and KLT	100
Figure 3.3	Caspase 3/7 Assay of 2AT and KLT	101
Figure 3.4	Fluorescence micrographs of 2AT-sCy3	103
Figure 3.5	Fluorescence micrographs of 2AT-sCy3 and a lysosomal marker	104
Figure 3.6	Fluorescence micrographs of KLT-sCy3	105
Figure 3.7	Fluorescence micrographs of KLT-sCy3 and a lysosomal marker	106
Figure 3.8	Fluorescence micrographs of KLT-sCy3 and 2AT-sCy5	107
Figure 4.1	Chemical structures of 2AT, KLT, and QKT	158

Figure 4.2	Native MS of 2AT, KLT, and QKT	160
Figure 4.3	Native IM-MS of 2AT, KLT, and QKT	163
Figure 4.4	Mass photometry of 2AT, KLT, and QKT	165
Figure 4.5	SDS-PAGE of 2AT, KLT, and QKT	167
Figure 4.6	Cell viability assay of 2AT, KLT, and QKT	168
Figure S4.1	LC-MS of QKM_{CC} oxidation reaction	181
Figure S4.2	Native IM-MS of trimers with 0 h incubation	182
Figure S4.3	Caspase 3/7 activation assay of 2AT, KLT, and QKT	183
Figure 5.1	Schematic of ionization techniques	213
Figure 5.2	Schematic of mass analyzers	215
Figure 6.1	Fluorescence micrographs of fluorescently labeled Aβ	226
Figure 6.2	Study of peptides derived from familial mutations of Aβ	227
Figure 6.3	Representation of the urgency to move a course online	228
Figure 6.4	Cytotoxicity of teixobactin-derived prodrugs	229
Figure 6.5	Structures of β-hairpin peptides derived from Aβ12–40	230

LIST OF SCHEMES

Page

Scheme 1.1	Dde protecting group deprotection	6
Scheme 1.2	Cyclization of a β-hairpin peptide	7
Scheme 1.3	Oxidation of macrocyclic β-hairpin	8

ACKNOWLEDGEMENTS

I would like to thank my advisor Professor James S. Nowick for his support over the last five years. I am grateful for his support for my project endeavors and encouragement to explore my interests in new instruments and techniques. He allowed me the freedom to delve into different analytical techniques and find my passion in mass spectrometry. Without his guidance, the completion of this degree would not have been possible.

I would also like to thank Dr. Felix Grün and Benjamin Katz, who served as mentors in my time as the fellow in the Mass Spectrometry Core Facility. Their lively stories conveying years of wisdom about both mass spectrometry and life have taught me many lessons I will carry forward. I am thankful to them for creating a supportive environment where I could explore the limits of mass spectrometry and not be afraid to break a few things along the way. They have given me a foundation of knowledge and experience that is invaluable.

I would like to thank my collaborators for their contributions, teachings, and patience. Specifically, Prof. Enrico Gratton and Dr. Belén Torrado in the Laboratory for Fluorescence Dynamics, and Prof. Vicki Wysocki and Leon Lin of The Ohio State University.

For the friends that started this journey with me and the ones I made along the way, I am forever grateful. Thank you Katie, Sara, Kira and Taylor for answering all of the late night phone calls, hearing all of my complaining on the golf course, and listening to my anxieties while floating on a surfboard. To the senior graduate students who offered their mentorship, I appreciate your time and your kindness. And to the greatest group of lab mates I could ask for, I thank you deeply for your support. The ability for this group to pick each other up is incredible. It takes a village to get a PhD and you were my village. The memories of the early mornings, late nights, and lunch breaks will stay close to my heart. I implore you, never discount the power of comedic relief and a good “that’s what she said” joke. We laugh so we don’t cry.

To my brothers, I thank them for the holidays spent together recharging. They always knew how to ground me when lab work felt overwhelming. And, while they didn’t know much chemistry when I started this degree, I hope they learned something about chemistry along the way. To my mom for talking me out of quitting more times than I can count and my dad for reminding me that life is meant to be enjoyed, I cannot express the power of your love and encouragement. And to Dave, you made me happy when the proverbial skies were gray. Your patience is limitless and I am immensely appreciative.

I thank Elsevier for the permission to publish Chapter 1, which was originally published in *Methods in Enzymology*. The text of this chapter is a reprint of the material as it appears in *Methods in Enzymology*. I thank Prof. James Nowick, the corresponding author listed on this publication, who directed and supervised research which forms the basis for this dissertation and Dr. Adam Kreutzer, a co-author listed on this publication, for his contributions to X-ray crystallography.

VITA

Gretchen Guaglianone

Education

University of California, Irvine 2017-2022
PhD, Chemistry

University of California, Los Angeles 2012-2016
Bachelor of Science, Chemistry

Skills

Mass Spectrometry and LC Instrumentation	• Waters Synapt G2 • Sciex MALDI TOF/TOF 5800 • Bruker utrafleXtreme MALDI-TOF/TOF • Waters GCT Premier • Waters LCT Premier • Waters Xevo G2-XS QTof • Waters Acquity UPLC-QDa • Shimadzu preparative HPLC • Rainin Dynamax preparative HPLC • Agilent analytical HPLC 1200 and 1260 • Chemstation and Masslynx software • Scroll pump maintenance
Chemical Biology	• High resolution mass confirmation for peptides, nucleotides, proteins, and small molecules • LC purification method development for peptides and small proteins • MALDI imaging tissue sample preparation • Confocal and fluorescence microscopy • Mammalian cell culture • Cytotoxicity and cell viability • FPLC • Circular dichroism • Solid phase peptide synthesis

Awards

UCI Mass Spectrometry Innovation Fellowship (Irvine, CA) 2020-2022
UC Irvine

- Experience in instrument maintenance and operation, and method development for the mass spectrometric analysis of small molecules, nucleotides, peptides, and proteins.
- Pioneering the use of IM-MS and MALDI imaging for research of the Aβ peptide and Alzheimer's disease at UCI.
- Trained new graduate, industry, and undergraduate users on UCI open access MS instruments.

Professional Experience

Graduate Student Researcher (Irvine, CA) 2017-2022
University of California, Irvine
Professor James S. Nowick

- Synthesis and characterization of macrocyclic peptide models to study the self-assembly of biologically relevant amyloid beta, responsible for Alzheimer's disease.
- Led and mentored 2 undergraduate research assistants and collaborated with a team of graduate students to design, synthesize, and assess macrocyclic peptides capable of mimicking toxic proteins in Alzheimer's and other neurodegenerative diseases using solid-phase peptide synthesis, mass spectrometry, SDS-PAGE, fluorescence microscopy, western blot, HPLC, CD, and cytotoxicity assays. Familiar with FPLC, SEC, and X-ray crystallography.
- Communicated my scientific results and research progress in 7 scientific publications, and at 4 regional and national scientific conferences to multidisciplinary audiences.

GlaxoSmithKline (Raleigh, North Carolina) 2016-2017
Future Leaders Program, GMS Quality Associate

- Assisted in the evaluation of new Raman Spectroscopy technology for incorporation into GMP workflow and revitalized Analytical Workshop presentations to promote discussion of current topics and concerns within the analytical community.

Sanofi Pasteur (Swiftwater, PA) Summer 2015
Quality Control, Analytical Scientist

- Participated in maintenance of High pH Anion-Exchange Chromatography with Pulsed Amperometric Detection instrument and developed Reagents Database containing vital data for all reagents necessary for procedural testing.

Clinlogix (Ambler, PA) Summer 2014

Clinical Project Assistant

- Prepared for new studies by obtaining required regulatory approvals for protocols and amendments and assembled necessary medical documentation for physicians, patients, and research.

Publications

Guaglianone, G.; Torrado, B.; Lin, Y-F.; Watkins, M. C.; Wysocki, V. H.; Gratton, E.; Nowick, J. S. Elucidating the oligomerization and cellular interactions of a trimer derived from Aβ through fluorescence and mass spectrometric studies. *Submitted to ACS Chem. Neurosci.*

Samdin, T. D.; **Guaglianone, G**.; Kreutzer, A. G.; Wierzbicki, M.; Nowick, J. S. A Tetrameric β-Barrel-Like Oligomer Formed by a Macrocyclic β-Hairpin Peptide Derived from Aβ12–40. *Submitted to Nat. Commun.*

Jones, C. R.; **Guaglianone, G**.; Lai, G.; Nowick, J. S. Teixobactin-Derived *O*-Acyl Isopeptide Prodrugs. *Submitted to ChemSci*

Howitz, W. J.; **Guaglianone, G**.; McKnelly, K. J.; Nowick, J. S. Macrocyclic Peptides Derived from Familial Alzheimer's Disease Mutants Show Charge-Dependent Oligomeric Assembly and Toxicity. *ACS Chem. Neurosci*. **2022**, *13*, 714-720.

Guaglianone, G.; Kreutzer, A. G.; Nowick, J. S. Synthesis and Study of Macrocyclic β-Hairpin Peptides for Investigating Amyloid Oligomers. *Method. Enzymol.* **2021**, *656*, 123-168.

Zhang, S.; **Guaglianone, G**.; Morris, M. A.; Yoo, S.; Howitz, W. J.; Jusuf, H.; Huizar, G.; Lim, J.; Kreutzer, A. G.; Nowick, J. S. Expression of N-Terminal Cysteine $A\beta_{42}$ and Conjugation to Generate Fluorescent and Biotinylated $A\beta_{42}$. *Biochemistry* **2021**, *60*, 1191-1200.

Kreutzer, A. G.; Krumberger, M.; Diessner, E. M., Parrocha, C. M. T.; Morris, M. A.; **Guaglianone, G**.; Butts, C. T., Nowick, J. S. A Cyclic Peptide Inhibitor of the SARS-CoV-2 Main Protease. *Eur. J. Med. Chem.* **2021**, *218*, 11390.

Howitz, W. J.; **Guaglianone, G**.; King, S. M. Converting a third quarter organic chemistry course to an online format in two weeks: Design and implementation. *J. Chem. Educ.* **2020**, *97*, 2581-2589.

Haerianardakani, S.; Kreutzer, A. G.; Salveson, P. J.; Samdin, T. D.; **Guaglianone, G**.; Nowick, J. S. Phenylalanine Mutation to Cyclohexylalanine Facilitates Triangular Trimer Formation by β-Hairpins Derived from Aβ. *J. Am. Chem. Soc*. **2020**, *142*, 20708-20716.

Kreutzer, A. G.; Samdin, T. D.; **Guaglianone, G**.; Spencer, R. K.; Nowick, J. S. X-ray Crystallography Reveals Parallel and Antiparallel β-Sheet Dimers of a β-Hairpin Derived from Aβ16–36 that Assemble to Form Different Tetramers. *ACS Chem. Neurosci*. **2020**, *11*, 2340-2347.

Conferences and Workshops

"Understanding the assembly of oligomers derived from Aβ by IMS-MS" Presented at the ASMS Asilomar Conference, Asilomar, CA	Dec 2021
" Understanding the assembly of oligomers derived from Aβ by IMS-MS" Presented at the American Society for Mass Spectrometry Annual Conference, Philadelphia, PA	Oct 2021
Waters Young Investigator Summit	August 2021
Native Mass Spectrometry Workshop	March 2021
"Illuminating the assembly and cellular interactions of a trimer derived from Aβ" Presented at Peptide Therapeutics Symposium Poster Session at The Salk Institute, La Jolla, CA	October 2019
"Illuminating the assembly and cellular interactions of a trimer derived from Aβ" Presented at the Gordon Research Conference Poster Session, Ventura, CA.	February 2020
"Illuminating the assembly and cellular interactions of a trimer derived from Aβ" Presented at the Gordon Research Seminar Poster Session, Ventura, CA.	February 2020

Mentorship and Leadership

Incoming Graduate Student Mentor (Irvine, CA) 2019-2022
Chemistry TA Mentorship Program

- Hosted orientation and met with mentees twice a quarter to prepare for teaching assignments, set goals, develop good teaching practices, discuss mid-quarter feedback, and reflect on progress in teaching.

Founding Member (Irvine, CA) 2019-2022

Business and Consulting Club for STEM Scientists

- Helped Ph.D. students and postdocs explore careers in business by coordinating events and creating an environment focused on consulting career opportunities, case interviews, and networking.

Lead Instructor (Norco, CA) 2018-2022
Prison Education Project

- Designed course content and lead eight week math courses for 25-30 incarcerated people, navigating challenges with restricted resources.

Teaching

Teaching Assistant (Irvine, CA) 2017-2022
UC Irvine

- Chem 177, Medicinal Chemistry, Winter 2018
- Chem 51B, Organic Chemistry Lecture, Winter 2019
- Chem 1LC, General Chemistry Lab, Spring 2019
- Chem 1B, General Chemistry Lecture, Winter 2020
- Chem 51C, Organic Chemistry Lecture, Spring 2020
- Chem 51C, Organic Chemistry Lecture, Summer 2020

Memberships

American Society of Mass Spectrometry 2021-present
Business and Consulting for STEM Scientists 2019-present
American Chemical Society 2016-present

Certificates

Business Concepts for STEM Scientists Certificate
Activate to Captivate, Public Speaking Certificate

ABSTRACT OF THE DISSERTATION

Applying New Tools to Study Aβ-derived Oligomers

by

Gretchen Guaglianone

Doctor of Philosophy in Chemistry

University of California, Irvine, 2022

Professor James S. Nowick, Chair

The formation of aggregates of the amyloidogenic peptide β-amyloid (Aβ), termed oligomers, is central to Alzheimer's disease, where oligomers play a central role in neurodegeneration. The use of chemical model systems can help provide insights into the structures and interactions of oligomers, which are otherwise difficult to study because they are heterogeneous and metastable. In my dissertation, I describe the application of new tools to study Aβ-derived oligomers to better understand the molecular basis of Alzheimer's disease.

Chapter 1 describes the use of macrocyclic β-hairpin peptides as model systems to study amyloid oligomers. The first part of the chapter describes the chemical synthesis of the macrocyclic β-hairpin peptides and covalent assemblies thereof. The second part of the chapter describes the characterization of the oligomers formed by the macrocyclic β-hairpin peptides, focusing on SDS-PAGE, size-exclusion chromatography (SEC), and X-ray crystallography. This chapter focuses on the β-amyloid peptide (Aβ), but these strategies are applicable to a broad range of amyloid-derived peptides and proteins. The subsequent chapters study the covalently stabilized trimers derived from residues 16–36 of Aβ as model systems to understand Aβ oligomers.

Chapter 2 expands the toolset to study Aβ-derived oligomers using the emerging techniques of fluorescence lifetime imaging microscopy (FLIM) and native mass spectrometry (native MS) to better understand the assembly and interactions of the oligomer model system 2AT-L in aqueous solutions and with cells. Oligomer model 2AT-L and fluorescently labeled 2AT-L analogues assemble in the membrane-like environment of SDS-PAGE, showing diffuse bands of oligomers in equilibrium. Native ion mobility-mass spectrometry (native IM-MS) of 2AT-L allows for the identification of discrete oligomers in solution and shows similar patterns of oligomer formation between 2AT-L and fluorescently labeled analogues. Fluorescence microscopy with SH-SY5Y cells reveals that fluorescently labeled 2AT-L analogues co-localize within lysosomes. FLIM studies with phasor analysis further elucidate the assembly of 2AT-L within cells and establish the occurrence of FRET, suggesting intracellular oligomerization.

Chapter 3 explores how differences in β-hairpin registration can affect biophysical and biological activity. The prevalence of β-sheet rich structures of Aβ, where the central and *C*-terminal regions fold to form a β-hairpin has been established as important secondary structure of Aβ oligomers. Using our laboratory's template for oligomer models, two isomorphic trimers were synthesized and fluorescently labeled. The differences in the two trimers' interactions with cells are explored through fluorescence microscopy. Results suggest that the alignment of the β-hairpin can affect cellular interactions and support the principle that function follows form.

Chapter 4 introduces additional mass spectrometry techniques as tools in the investigation of the complex behavior of oligomer model systems. In particular, native MS is a powerful technique for the study of non-covalent assemblies that complements other biophysical techniques. In this study, the oligomeric assemblies of three isomorphic trimers are investigated

by two native MS techniques, mass photometry, SDS-PAGE, and cellular cytotoxicity. These studies affirm the need for multiple techniques to accurately characterize oligomer behavior.

Chapter 5 details techniques learned from my experience working in the UCI Mass Spectrometry Core Facility as the Mass Spectrometry Fellow. I have distilled the knowledge gathered through literature and experience into a simple guide that outlines the types of mass spectrometry instruments available in the UCI Mass Spectrometry Core Facility, sample preparation requirements and instrument compatibility, and data analysis resources.

Finally, in my epilogue, I describe a selection of collaborative projects I have contributed to in my time in the Nowick laboratory. These collaborations include research related to amyloidogenic peptides, antibiotic peptides, and online organic chemistry teaching methods.

Chapter 1[a]

Exploring Amyloid Oligomers with Peptide Model Systems

Preface to Chapter 1

Chapter 1 describes guidance on how to synthesize and study self-assembling macrocyclic β-hairpin peptides. The procedures described in Chapter 1 formed the foundation of all of my subsequent projects, where assays could not be performed if successful peptide synthesis and trimer stabilization could not be completed. I had the opportunity to publish this guide which encompasses many years of troubleshooting from generations of graduate students in the Nowick laboratory. We thank Dr. Ryan Spencer, Dr. Adam Kreutzer, Dr. Patrick Salveson, Dr. Nicholas Truex, Dr. Hyun-Jun Yang, and Dr. Tuan Samdin for developments in these procedures over the past decade and Dr. Adam Kreutzer for his contributions to the X-ray crystallography section.

[a] This chapter is adapted from Guaglianone, G.; Kreutzer, A. G.; Nowick, J. S. Synthesis and Study of Macrocyclic β-Hairpin Peptides for Investigating Amyloid Oligomers. *Meth. Enzymol.* ***2021****, 656, 123–168.*

INTRODUCTION

Amyloidogenic peptides and proteins are characterized by their ability to self-assemble to form oligomers and fibrils and are involved in many neurodegenerative diseases including Parkinson's disease, Huntington's disease, and Alzheimer's disease. Aggregates of these peptides are a hallmark of amyloid diseases; however, the underlying mechanisms leading to aggregation are not well understood.[1–3] The process of aggregation, whereby monomeric units assemble into oligomers and fibrils, is difficult to study because of the transitory and dynamic nature of assembly.[4–6] Amyloid oligomers are highly heterogeneous in size and structure, hindering investigation of structure-activity relationships.[7–9] Often in the oligomeric and fibrillar state, amyloidogenic peptides and proteins adopt a β-sheet conformation, frequently known as the amyloid fold.[5,10–12] It has become apparent that the oligomeric assemblies contribute to the toxicity observed in amyloid diseases. Understanding the oligomerization of amyloidogenic peptides and proteins is vital for understanding the molecular basis of amyloid diseases and for discovering potential treatments of these diseases.[4,13,14]

There are limitations to studying full-length amyloidogenic peptides and proteins. Isolating soluble oligomers, the suspected toxic species, and developing therapies targeting these dynamic species has thus far been unsuccessful.[15] Model systems consisting of fragments of amyloidogenic peptides or proteins have emerged as accessible methods to increase understanding of the biophysical properties of amyloid oligomers.[3,4,16,17] Our laboratory has pioneered the synthesis and study of macrocyclic β-hairpin peptides derived from the β-amyloid peptide (Aβ), an amyloidogenic peptide that aggregates to form the hallmark plaques in Alzheimer's disease.[18–26]

Here we detail methods to synthesize and study macrocyclic β-hairpin peptides (**Figure 1.1**). We describe procedures to constrain peptide fragments into a β-hairpin using the turn mimic δ-linked ornithine, with the option to incorporate additional residues onto the *N*-terminus of the macrocyclic β-hairpin peptide and modify the peptide backbone to prevent uncontrolled aggregation.[27,28] We also provide methods to incorporate cysteine mutations into the native sequence to create covalently linked, stable oligomers through disulfide bonds. Finally, we provide detailed methods to study the self-assembly of macrocyclic β-hairpin peptides, including SDS-PAGE, SEC, and X-ray crystallography. These methods are not limited to peptides derived from Aβ and can be applied to other amyloidogenic peptides and proteins to further elucidate the role of amyloid assemblies in neurodegenerative and somatic diseases.

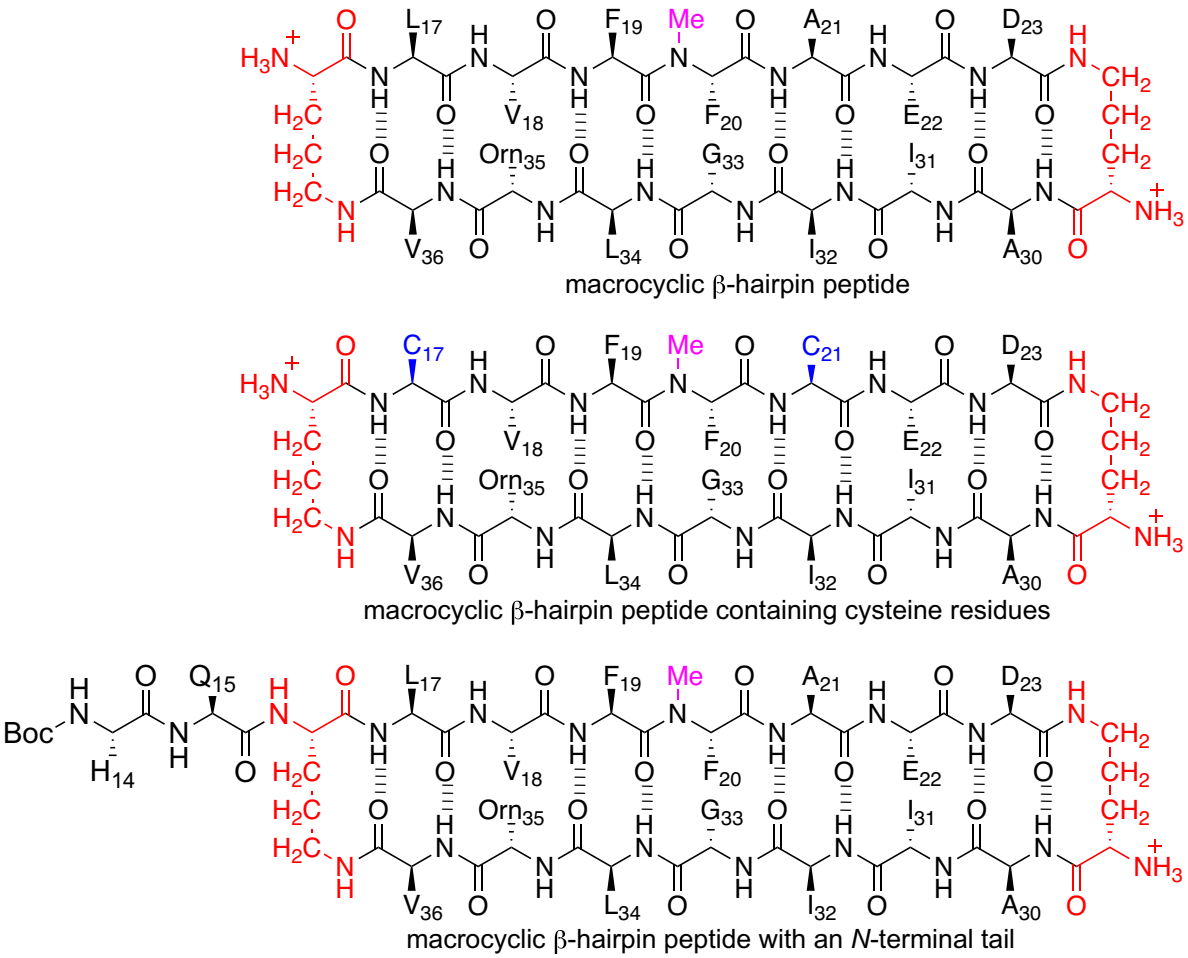

Figure 1.1 Aβ-derived macrocyclic β-hairpin peptides highlighting the use of *N*-methyl-phenylalanine at position 20 (magenta) to prevent uncontrolled aggregation, δ-ornithine turn mimics (red) to induce β-hairpin formation, and cysteine residues at positions 17 and 21 (blue) to permit disulfide crosslinking.

SYNTHESIS OF MACROCYCLIC β-HAIRPIN PEPTIDES

Studying the self-assembly of amyloidogenic peptides and proteins into oligomers is difficult because oligomers are heterogeneous and metastable. Our laboratory has developed techniques to synthesize and study oligomers of the β-amyloid peptide (Aβ), using macrocyclic β-hairpin peptides derived from Aβ that allow for the formation of more stable and homogeneous oligomers. In these macrocyclic peptides, δ-linked ornithine ($^{\delta}$Orn) turn mimics are used to

constrain fragments from the central and *C*-terminal regions of Aβ into a β-hairpin. An *N*-methyl group on the backbone of the peptide prevents uncontrolled aggregation. The corresponding $^{\delta}$Orn and *N*-methyl amino acids are easily incorporated into the macrocyclic β-hairpin peptides using standard solid-phase peptide synthesis with Fmoc-protected amino acids. Additionally, a $^{\delta}$Orn orthogonally protected with Dde and Fmoc allows additional *N*-terminal amino acids to be appended to the macrocycle (**Scheme 1.1**). Solution-phase cyclization generates the macrocyclic ring (**Scheme 1.2**). Cysteine residues can be incorporated into macrocyclic peptides that exhibit well-defined self-assembly and then oxidized to create covalently stabilized oligomers with disulfide crosslinks (**Scheme 1.3**). Detailed below is a description for the synthesis of a macrocyclic β-hairpin peptide using 2-chlorotrityl chloride resin on a 0.1 mmol scale following standard solid-phase peptide synthesis procedures using Fmoc-protected amino acids.

Synthesis of the macrocyclic β-hairpin peptide begins with by loading 2-chlorotrityl chloride resin with the first Fmoc-protected amino acid. After loading for 12 h, drain the solution and cap unreacted resin sites with a solution of dichloromethane, methanol, and N,N-diisopropylethylamine (8.5:1:0.5 mL). Following capping, subject the loaded resin to cycles of peptide coupling. In each cycle, 20% piperidine is used to remove the Fmoc protecting group from the amine. An amino acid is then activated with coupling agents and added to extend the amino acid chain. When synthesizing a peptide containing an *N*-methyl amino acid, begin the synthesis from the $^{\delta}$Orn proximal to the *C*-terminal side of the desired *N*-methyl residue.

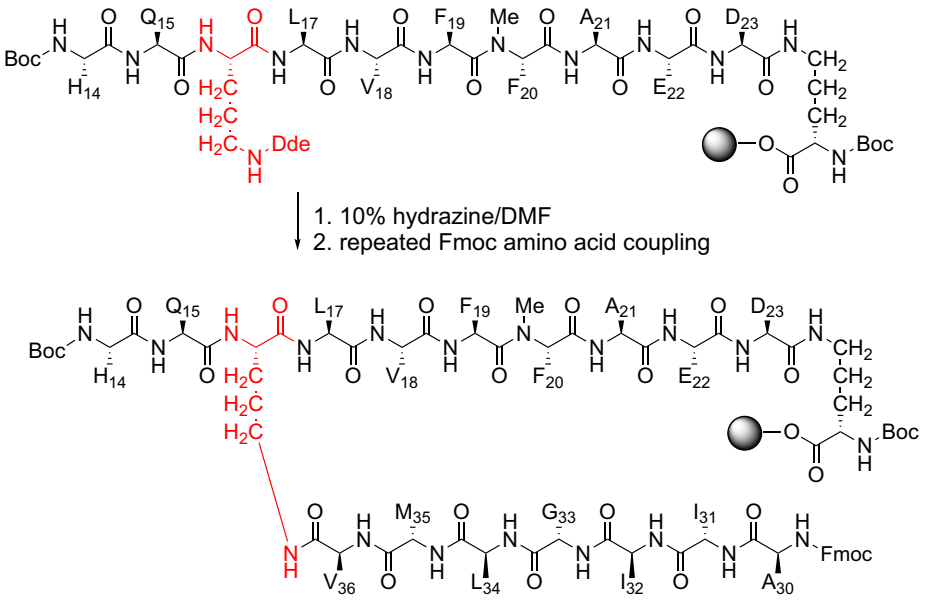

Scheme 1.1 Removal of the Dde protecting group in the synthesis of a macrocyclic β-hairpin peptide that incorporates additional *N*-terminal residues.

It is optional to extend the *N*-terminus off of the α-amino group of δOrn using Fmoc-Orn(Dde)-OH. Continue to couple the desired *N*-terminal extended of amino acids, using a Boc-protected α-amino acid for the final amino acid. Then, remove the orthogonal protecting group Dde with 10% hydrazine in dimethylformamide (10 mL) and continue to couple the bottom strand of amino acids following standard Fmoc-based solid-phase peptide synthesis. If you do not wish to extend the *N*-terminus, use Boc-Orn(Fmoc)-OH and extend the bottom strand by standard Fmoc-based solid-phase peptide synthesis.

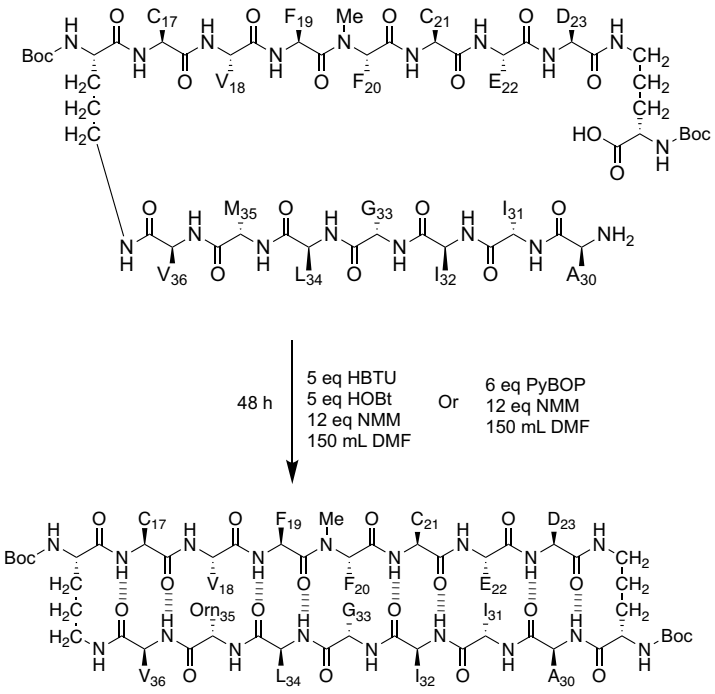

Scheme 1.2 Cyclization to generate a macrocyclic β-hairpin peptide.

The completed peptide is cleaved from resin and proceeds through the final amide bond formation in solution to yield a macrocycle. The macrocycle is globally deprotected with a solution of trifluoroacetic acid (TFA), triisopropylsilane (TIPS), and water (18:1:1 mL) to remove trityl (Trt),O-tert-butyl (OtBu), tert-butyloxycarbonyl (Boc), and pentamethyldihydrobenzofuran-5-sulfonyl (Pbf) amino acid side chain protecting groups. This step does not remove other protecting groups, such as acetamidomethyl (Acm), benzyloxycarbonyl (Cbz), Alloc, or Dde. After one hour, the deprotected peptide is precipitated with ether. The precipitated, pelleted peptide is then purified by RP-HPLC. The peptide pellet is dissolved in a solution of water and acetonitrile equivalent to the ratio of water and acetonitrile of which the HPLC instrument is equilibrated. Typically, this is 20% acetonitrile or less. If the peptide is not soluble at this ratio, you may need to add more acetonitrile and adjust the injection water:acetonitrile ratio on the HPLC instrument to match the acetonitrile percentage in which the

peptide is dissolved. After a gradient elutes the peptide, fractions containing pure peptide are combined and concentrated by rotary evaporation. The solution is frozen and lyophilized to yield dry peptide.

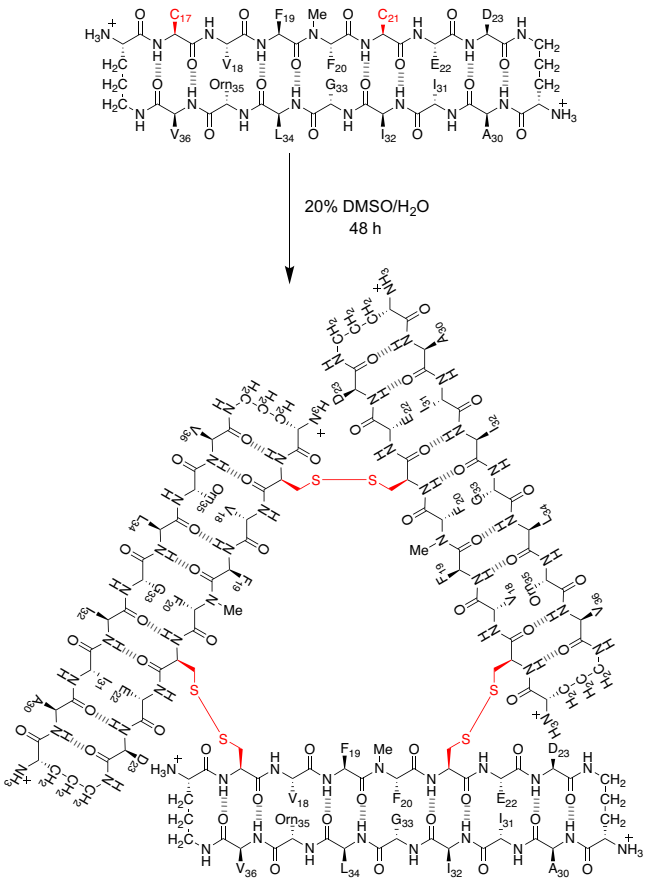

Scheme 1.3 Oxidation of a macrocyclic β-hairpin peptide containing cysteine residues to generate a covalently stabilized trimer with disulfide crosslinks.

The purified macrocyclic β-hairpin peptide is subject to oxidation into crosslinked oligomers in 20% aqueous dimethyl sulfoxide for 48 h. The reaction is purified by RP-HPLC. Fractions containing pure trimer are combined and concentrated by rotary evaporation. The remaining solution is frozen and lyophilized to yield dry trimer.

METHODS FOR STUDYING THE SELF-ASSEMBLY OF MACROCYCLIC β - HAIRPIN PEPTIDES

A wide variety of methods are available to study the supramolecular assembly of amyloidogenic peptides and proteins. Below are three methods we have found to be the most reliable techniques that provide insights into the assembly and structure of macrocyclic β-hairpin peptides: SDS-PAGE, SEC, and X-ray crystallography (**Figure 1.2**). SEC provides information about the size and molecular weight of the peptide assembly that forms in solution. SDS-PAGE offers additional information about the peptide assembly in the lipid-like environment of SDS micelles. X-ray crystallography provides high-resolution structures of the peptide assemblies that form. A combination of these techniques can elucidate the structures and self-assembling behavior of macrocyclic β-hairpin peptides. These robust techniques are frequently supported with additional techniques such as ion mobility mass spectrometry, NMR, analytical ultracentrifugation, and dynamic light scattering, to better understand the biophysical properties of self-assembling peptides.

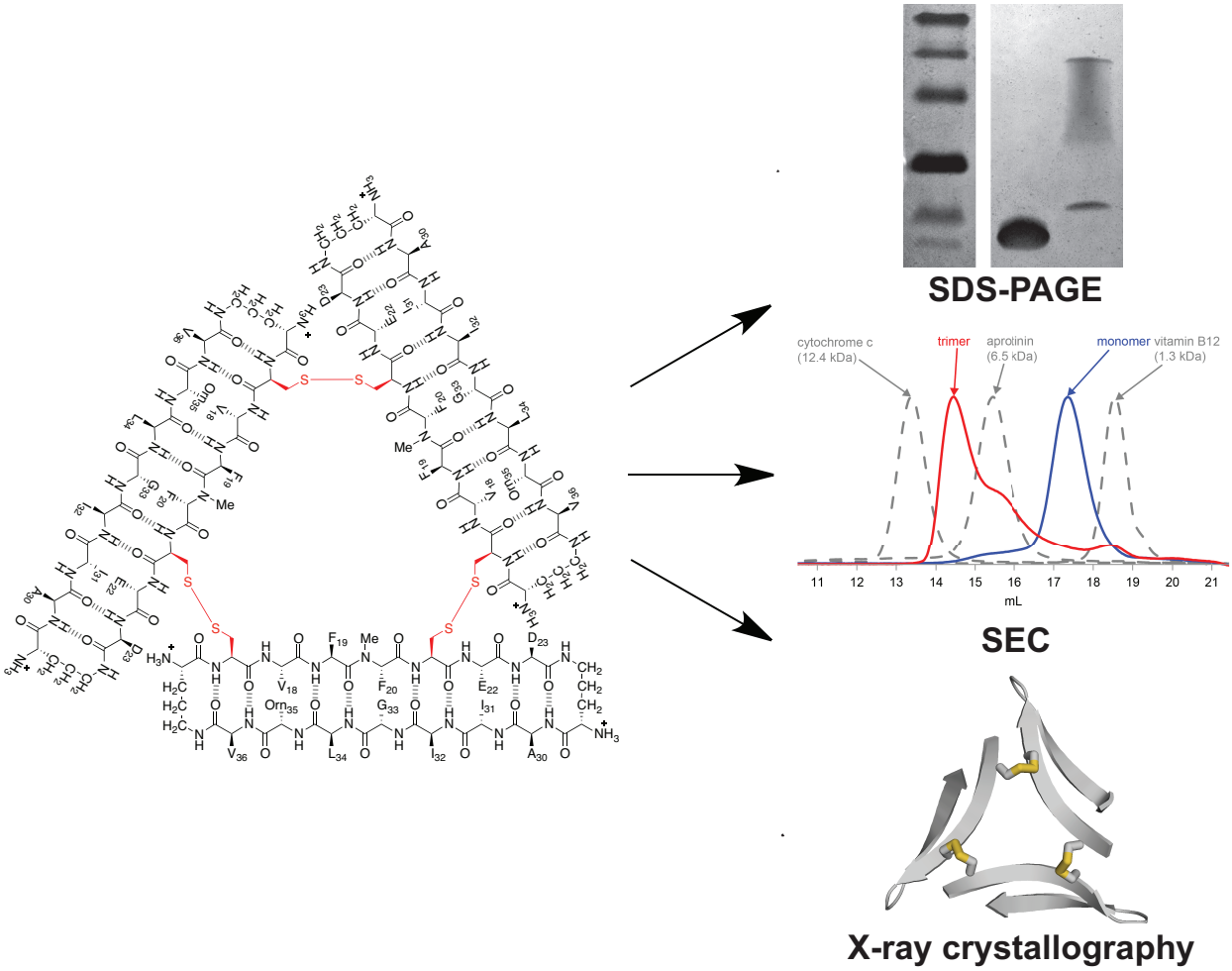

Figure 1.2 Three techniques used to study the supramolecular assembly of macrocyclic β-hairpin peptides and crosslinked oligomers: X-ray crystallography, SEC, and SDS-PAGE.

Polyacrylamide gel electrophoresis (PAGE) is a technique used to separate peptides and proteins. SDS (sodium dodecyl sulfate) is an anionic surfactant added to coat the peptides with a negatively charged layer, allowing the peptides to separate on the basis of molecular weight as they migrate in the applied electric field. Many of the Aβ-derived macrocyclic peptides and subsequent crosslinked oligomers that we have created form SDS-stable assemblies.[19,20,24,29] In fact, SDS appears to promote higher-order assembly of many of our Aβ-derived peptides and

oligomers (**Figure 1.3**). These observations are consistent with those for full-length Aβ, which also appears to form SDS-promoted assemblies.[30]

Various techniques can be used to visualize the peptide bands within the gel. The most common method we use is silver staining, which relies on the reduction of silver ions to elemental silver, in a fashion similar to the development of a black-and-white photograph.[31,32] We occasionally perform Coomassie staining to visualize the bands in the gel. Coomassie staining relies on adsorption of the dye to the hydrophobic side chains of the amino acids contained in the peptide to visualize the peptide assemblies.[31,33] Visualization via InstantBlue Coomassie protein stain is reversible and compatible with subsequent mass spectrometric analysis of the gel bands. While silver staining is more sensitive than Coomassie staining, it is not reversible and thus not compatible with potential subsequent mass spectrometric analysis of the gel bands. Although other visualization methods are available, our lab has found these two to be the most effective for the visualization of our macrocyclic β-hairpin peptides.

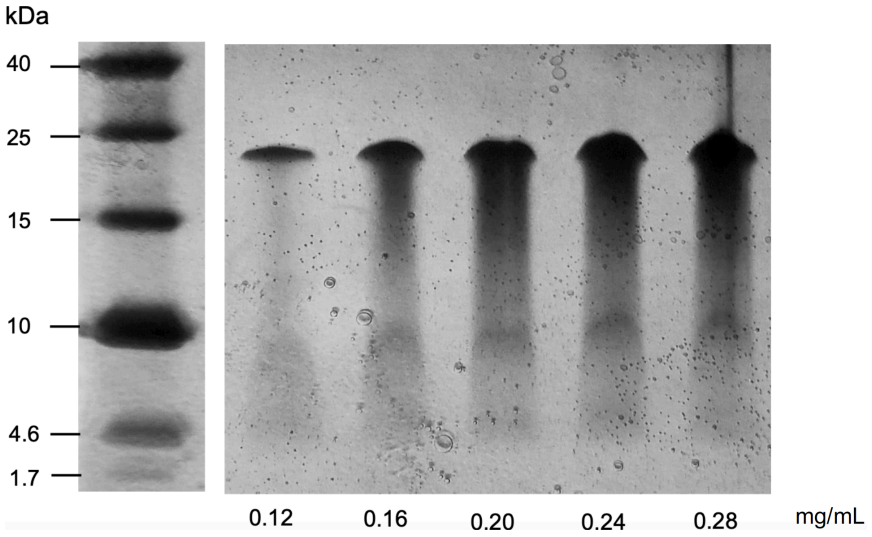

Figure 1.3 Silver-stained SDS-PAGE gel showing a macrocyclic β-hairpin peptide at varying concentrations. Streaking of the bands illustrates the equilibrium of the oligomer with monomer and lower-order oligomers.

Size-exclusion chromatography offers insight into the sizes and molecular weights of the assemblies that the macrocyclic β-hairpin peptides and crosslinked oligomers form in aqueous solution. Peptide assemblies of various sizes are separated through a gel matrix with larger molecular weight peptide assemblies eluting first, followed by smaller molecular weight assemblies and peptide monomers, which better enter the pores within the gel matrix. The peptides and reference standards that elute from the column pass through a UV absorbance detector and the absorbance signal is monitored. We typically monitor absorbance at 214 nm, however, for peptides that contain tyrosine or tryptophan, absorbance at 280 nm may be used. The mass of the peptide assembly and number of peptide monomer units can be determined by comparing the elution time of the peptide to multiple reference standards.[7,34]

It is important to identify a buffer and pH in which the peptide of interest is completely soluble and does not precipitate. Comparison of the UV absorbance of a solution of the peptide in buffer before and after centrifugation can help detect loss of peptide by precipitation or aggregation. Buffers systems that have been successful for our macrocyclic β-hairpin peptides and crosslinked oligomers include 50 mM Tris buffer at pH 7.4 with 150 mM NaCl, 10 mM glycine and 50 mM NaCl at pH 3.0, and 50 mM sodium acetate and 50 mM acetic acid at pH 4.7.[19–21] Phosphate buffers have often led to precipitation. Once an appropriate buffer system is determined, peptide samples and references standards can be run and analyzed quickly.

X-ray crystallography is a powerful technique for elucidating the three-dimensional structures of the higher-order assemblies that macrocyclic β-hairpin peptides form. These peptides are well suited for X-ray crystallography, because they adopt conformationally homogeneous β-hairpin structures that are prone to self-assemble and form a crystal lattice. We

have adapted the tools of protein crystallography to crystallize and elucidate the crystal structures of macrocyclic β-hairpin peptides.[35]

CONCLUSIONS

Macrocyclic β-hairpin peptides provide useful model systems for studying the elusive peptide and protein oligomers associated with amyloid diseases. Understanding amyloid oligomer structures and their biophysical and biological properties is critical for understanding and developing treatments of amyloid diseases. Throughout this chapter, we outline simple synthetic methods for incorporating $^{\delta}$Orn turn linkers to constrain fragments of Aβ and *N*-methyl amino acids to limit uncontrolled aggregation of the peptide. These modifications create macrocyclic β-hairpin peptides derived from amyloidogenic peptides and proteins that self-assemble to form oligomers. The structures of these oligomers can be elucidated at high-resolution using X-ray crystallography, and the oligomers can be further studied by techniques such as SDS-PAGE and SEC.

Our laboratory has demonstrated the utility of these synthetic modifications to make macrocyclic β-hairpin peptides derived from a variety of amyloidogenic peptides and proteins.[22,36–39] These powerful tools have led to the discovery of oligomers—elucidated through SEC, SDS-PAGE, and X-ray crystallography—ranging from dimers (2 monomers) to dodecamers (12 monomers) to large annular pore-like structures. The oligomers formed by our macrocyclic β-hairpin peptides are far more homogeneous than native oligomers formed by full-length amyloidogenic peptides and proteins, which are inherently heterogeneous. The homogeneity of the oligomers formed by macrocyclic β-hairpin peptides allows for a more direct correlation of oligomer structure with oligomer biology. In our own laboratory, we have

correlated the oligomers formed by our macrocyclic β-hairpin peptides with oligomers formed by full-length Aβ using the oligomer-specific antibody A11.[19,40] We envision that experiments of this sort can also be done for other amyloidogenic peptides and proteins.

Current studies in our laboratory also focus on better understanding the biological significance of the oligomeric assemblies that we create and correlating these assemblies with biogenic Aβ oligomers and other oligomers of full-length Aβ. Antibodies feature heavily among the tools that we are using in these studies, and we are looking at the cross-reactivity of antibodies generated against our macrocyclic β-hairpin peptides with biogenic Aβ oligomers. Through these studies, we aim to learn what our macrocyclic β-hairpin peptides can reveal about the structures and biology of oligomers that occur in the brain in Alzheimer's disease. We hope this chapter advances the study and understanding of amyloidogenic peptides and proteins and their relationship to amyloid diseases.

ACKNOWLEDGEMENTS: We thank Tuan Samdin for providing the gel image in Figure 1.3. We thank Dr. Ryan Spencer, Dr. Patrick Salveson, Dr. Nicholas Truex, and Dr. Hyun-Jun Yang for contributions to predecessors of the protocols in this guide that have been developed over the past decade. We thank the National Institutes of Health (NIH) National Institute of General Medical Sciences (NIGMS, GM097562) and National Institute on Aging (NIA, AG062296), and the National Science Foundation (Grant CHE-1808096) for support that allowed the development of these protocols.

REFERENCES

(1) Li, D.; Liu, C. Structural Diversity of Amyloid Fibrils and Advances in Their Structure Determination. *Biochemistry* **2020**, *59* (5), 639–646. https://doi.org/10.1021/acs.biochem.9b01069.

(2) Lashuel, H. A.; Overk, C. R.; Oueslati, A.; Masliah, E. The Many Faces of α-Synuclein: From Structure and Toxicity to Therapeutic Target. *Nat. Rev. Neurosci.* **2013**, *14* (1), 38–48. https://doi.org/10.1038/nrn3406.

(3) Benilova, I.; Karran, E.; De Strooper, B. The Toxic Aβ Oligomer and Alzheimer's Disease: An Emperor in Need of Clothes. *Nat. Neurosci.* **2012**, *15* (3), 349–357. https://doi.org/10.1038/nn.3028.

(4) Straub, J. E.; Thirumalai, D. Principles Governing Oligomer Formation in Amyloidogenic Peptides. *Curr. Opin. Struct. Biol.* **2010**, *20* (2), 187–195. https://doi.org/10.1016/j.sbi.2009.12.017.

(5) Gallardo, R.; Ranson, N. A.; Radford, S. E. Amyloid Structures: Much More than Just a Cross-β Fold. *Curr. Opin. Struct. Biol.* **2020**, *60* (Lc), 7–16. https://doi.org/10.1016/j.sbi.2019.09.001.

(6) Larson, M. E.; Lesné, S. E. Soluble Aβ Oligomer Production and Toxicity. *J. Neurochem.* **2012**, *120* (SUPPL. 1), 125–139. https://doi.org/10.1111/j.1471-4159.2011.07478.x.

(7) Hall, D.; Huang, L. On the Use of Size Exclusion Chromatography for the Resolution of Mixed Amyloid Aggregate Distributions: I. Equilibrium Partition Models. *Anal. Biochem.* **2012**, *426* (1), 69–85. https://doi.org/10.1016/j.ab.2012.04.001.

(8) Ono, K.; Condron, M. M.; Teplow, D. B. Structure-Neurotoxicity Relationships of Amyloid β-Protein Oligomers. *Proc. Natl. Acad. Sci. U. S. A.* **2009**, *106* (35), 14745–

14750. https://doi.org/10.1073/pnas.0905127106.

(9) Marina, G. B.; Kirkitadze, D.; Lomakin, A.; Vollers, S. S.; Benedek, G. B.; Teplow, D. B. Amyloid β-Protein (Aβ) Assembly: Aβ40 and Aβ42 Oligomerize through Distinct Pathways. *Proc. Natl. Acad. Sci. U. S. A.* **2003**, *100* (1), 330–335. https://doi.org/10.1073/pnas.222681699.

(10) Celej, M. S.; Sarroukh, R.; Goormaghtigh, E.; Fidelio, G. D.; Ruysschaert, J. M.; Raussens, V. Toxic Prefibrillar α-Synuclein Amyloid Oligomers Adopt a Distinctive Antiparallel β-Sheet Structure. *Biochem. J.* **2012**, *443* (3), 719–726. https://doi.org/10.1042/BJ20111924.

(11) Eichner, T.; Radford, S. E. A Diversity of Assembly Mechanisms of a Generic Amyloid Fold. *Mol. Cell* **2011**, *43* (1), 8–18. https://doi.org/10.1016/j.molcel.2011.05.012.

(12) Bitan, G. Structural Study of Metastable Amyloidogenic Protein Oligomers by Photo-Induced Cross-Linking of Unmodified Proteins. *Methods Enzymol.* **2006**, *413*, 217–236. https://doi.org/10.1016/S0076-6879(06)13012-8.

(13) Fantini, J.; Chahinian, H.; Yahi, N. Progress toward Alzheimer's Disease Treatment: Leveraging the Achilles' Heel of Aβ Oligomers? *Protein Sci.* **2020**, *29* (8), 1748–1759. https://doi.org/10.1002/pro.3906.

(14) Sakono, M.; Zako, T. Amyloid Oligomers: Formation and Toxicity of Aβ Oligomers. *FEBS J.* **2010**, *277* (6), 1348–1358. https://doi.org/10.1111/j.1742-4658.2010.07568.x.

(15) Rosenblum, W. I. Why Alzheimer Trials Fail: Removing Soluble Oligomeric Beta Amyloid Is Essential, Inconsistent, and Difficult. *Neurobiol. Aging* **2014**, *35* (5), 969–974. https://doi.org/10.1016/j.neurobiolaging.2013.10.085.

(16) Hawk, L. M. L.; Pittman, J. M.; Moore, P. C.; Srivastava, A. K.; Zerweck, J.; Williams, J.

T. B.; Hawk, A. J.; Sachleben, J. R.; Meredith, S. C. β-Amyloid Model Core Peptides: Effects of Hydrophobes and Disulfides. *Protein Sci.* **2020**, *29* (2), 527–541. https://doi.org/10.1002/pro.3778.

(17) Wang, Y.; Truex, N. L.; Vo, N. D. P.; Nowick, J. S. Effects of Charge and Hydrophobicity on the Oligomerization of Peptides Derived from IAPP. *Bioorganic Med. Chem.* **2018**, *26* (6), 1151–1156. https://doi.org/10.1016/j.bmc.2017.10.001.

(18) Liu, C.; Sawaya, M. R.; Cheng, P. N.; Zheng, J.; Nowick, J. S.; Eisenberg, D. Characteristics of Amyloid-Related Oligomers Revealed by Crystal Structures of Macrocyclic β-Sheet Mimics. *J. Am. Chem. Soc.* **2011**, *133* (17), 6736–6744. https://doi.org/10.1021/ja200222n.

(19) Kreutzer, A. G.; Yoo, S.; Spencer, R. K.; Nowick, J. S. Stabilization, Assembly, and Toxicity of Trimers Derived from Aβ. *J. Am. Chem. Soc.* **2017**, *139* (2), 966–975. https://doi.org/10.1021/jacs.6b11748.

(20) Haerianardakani, S.; Kreutzer, A. G.; Salveson, P. J.; Samdin, T. D.; Guaglianone, G. E.; Nowick, J. S. Phenylalanine Mutation to Cyclohexylalanine Facilitates Triangular Trimer Formation by β-Hairpins Derived from Aβ. *J. Am. Chem. Soc.* **2020**, *142* (49), 20708–20716. https://doi.org/10.1021/jacs.0c09281.

(21) Samdin, T. D.; Wierzbicki, M.; Kreutzer, A. G.; Howitz, W. J.; Valenzuela, M.; Smith, A.; Sahrai, V.; Truex, N. L.; Klun, M.; Nowick, J. S. Effects of N-Terminal Residues on the Assembly of Constrained β-Hairpin Peptides Derived from Aβ. *J. Am. Chem. Soc.* **2020**, *142* (26), 11593–11601. https://doi.org/10.1021/jacs.0c05186.

(22) Spencer, R. K.; Kreutzer, A. G.; Salveson, P. J.; Li, H.; Nowick, J. S. X-Ray Crystallographic Structures of Oligomers of Peptides Derived from B2-Microglobulin. *J.*

Am. Chem. Soc. **2015**, *137* (19), 6304–6311. https://doi.org/10.1021/jacs.5b01673.

(23) Salveson, P. J.; Spencer, R. K.; Kreutzer, A. G.; Nowick, J. S. X-Ray Crystallographic Structure of a Compact Dodecamer from a Peptide Derived from Aβ16-36. *Org. Lett.* **2017**, *19* (13), 3462–3465. https://doi.org/10.1021/acs.orglett.7b01445.

(24) Kreutzer, A. G.; Samdin, T. D.; Guaglianone, G.; Spencer, R. K.; Nowick, J. S. X-Ray Crystallography Reveals Parallel and Antiparallel β-Sheet Dimers of a β-Hairpin Derived from Aβ16-36that Assemble to Form Different Tetramers. *ACS Chem. Neurosci.* **2020**, *11* (15), 2340–2347. https://doi.org/10.1021/acschemneuro.0c00290.

(25) Kreutzer, A. G.; Nowick, J. S. Elucidating the Structures of Amyloid Oligomers with Macrocyclic β-Hairpin Peptides: Insights into Alzheimer's Disease and Other Amyloid Diseases. *Acc. Chem. Res.* **2018**, *51* (3), 706–718. https://doi.org/10.1021/acs.accounts.7b00554.

(26) Kreutzer, A. G.; Spencer, R. K.; McKnelly, K. J.; Yoo, S.; Hamza, I. L.; Salveson, P. J.; Nowick, J. S. A Hexamer of a Peptide Derived from Aβ16-36. *Biochemistry* **2017**, *56* (45), 6061–6071. https://doi.org/10.1021/acs.biochem.7b00831.

(27) Nowick, J. S.; Brower, J. O. A New Turn Structure for the Formation of β-Hairpins in Peptides. *J. Am. Chem. Soc.* **2003**, *125* (4), 876–877. https://doi.org/10.1021/ja028938a.

(28) Spencer, R.; Chen, K. H.; Manuel, G.; Nowick, J. S. Recipe for β-Sheets: Foldamers Containing Amyloidogenic Peptide Sequences. *European J. Org. Chem.* **2013**, *17*, 3523–3528. https://doi.org/10.1002/ejoc.201300221.

(29) Salveson, P. J.; Haerianardakani, S.; Thuy-Boun, A.; Kreutzer, A. G.; Nowick, J. S. Controlling the Oligomerization State of Aβ-Derived Peptides with Light. *J. Am. Chem. Soc.* **2018**, *140* (17), 5842–5852. https://doi.org/10.1021/jacs.8b02658.

(30) Walsh, D. M.; Selkoe, D. J. Aβ Oligomers - A Decade of Discovery. *J. Neurochem.* **2007**, *101* (5), 1172–1184. https://doi.org/10.1111/j.1471-4159.2006.04426.x.

(31) Winkler, C.; Denker, K.; Wortelkamp, S.; Sickmann, A. Silver-and Coomassie-Staining Protocols: Detection Limits and Compatibility with ESI MS. *Electrophoresis* **2007**, *28* (12), 2095–2099. https://doi.org/10.1002/elps.200600670.

(32) Merril, C. R. Development and Mechanisms of Silver Stains for Electrophoresis. *Acta Histochem. Cytochem.* **1986**, *19* (5), 655–667. https://doi.org/10.1267/ahc.19.655.

(33) Smejkal, G. B. The Coomassie Chronicles: Past, Present and Future Perspectives in Polyacrylamide Gel Staining. *Expert Rev. Proteomics* **2004**, *1* (4), 381–387. https://doi.org/10.1586/14789450.1.4.381.

(34) Winzor, D. J. Analytical Exclusion Chromatography. *J. Biochem. Biophys. Methods* **2003**, *56*, 15–52. https://doi.org/10.1016/S0165-022X(03)00071-X.

(35) Spencer, R. K.; Nowick, J. S. A Newcomer′s Guide to Peptide Crystallography. *Isr. J. Chem.* **2015**, *55* (6), 698–710. https://doi.org/10.1002/ijch.201400179.

(36) Spencer, R. K.; Li, H.; Nowick, J. S. X-Ray Crystallographic Structures of Trimers and Higher-Order Oligomeric Assemblies of a Peptide Derived from Aβ17-36. *J. Am. Chem. Soc.* **2014**, *136* (15), 5595–5598. https://doi.org/10.1021/ja5017409.

(37) Salveson, P. J.; Spencer, R. K.; Nowick, J. S. X-Ray Crystallographic Structure of Oligomers Formed by a Toxic β-Hairpin Derived from α-Synuclein: Trimers and Higher-Order Oligomers. *J. Am. Chem. Soc.* **2016**, *138* (13), 4458–4467. https://doi.org/10.1021/jacs.5b13261.

(38) Yoo, S.; Kreutzer, A. G.; Truex, N. L.; Nowick, J. S. Square Channels Formed by a Peptide Derived from Transthyretin. *Chem. Sci.* **2016**, *7* (12), 6946–6951.

https://doi.org/10.1039/C6SC01927G.

(39) Wang, Y.; Kreutzer, A. G.; Truex, N. L.; Nowick, J. S. A Tetramer Derived from Islet Amyloid Polypeptide. *J. Org. Chem.* **2017**, *82* (15), 7905–7912. https://doi.org/10.1021/acs.joc.7b01116.

(40) Kayed, R.; Head, E.; Thompson, J. L.; McIntire, T. M.; Milton, S. C.; Cotman, C. W.; Glabel, C. G. Common Structure of Soluble Amyloid Oligomers Implies Common Mechanism of Pathogenesis. *Science* **2003**, *300* (5618), 486–489. https://doi.org/10.1126/science.1079469.

Chapter 2[b]

Elucidating the Oligomerization and Cellular Interactions of a Trimer Derived from Aβ Through Fluorescence and Mass Spectrometric Studies

Preface to Chapter 2

Chapter 2 describes a project that aimed to use emerging tools to study a macrocyclic peptide derived from Aβ—a goal that could not have been achieved without the knowledge and support of my collaborators. Guidance through fluorescence lifetime imaging microscopy (FLIM) and processing data by the phasor method was supported by Dr. Belén Torrado and Prof. Enrico Gratton. Dr. Torrado dedicated many hours of her time with me collecting FLIM images, teaching me the process of applying the phasor method to visualize lifetime changes, and meeting with me to discuss figures and information for the manuscript. Her expertise was critical to the success of these experiments. Guidance through native ion mobility-mass spectrometry (native IM-MS) was supported by Leon Lin and Prof. Vicki Wysocki. Leon ran my samples on their cyclic IM-MS instrument and taught me how to process the data and prepare figures to represent the findings. Leon's knowledge and patience contributed greatly to this project.

[b] This chapter is adapted from Guaglianone, G.; Torrado, B.; Lin, Y-F.; Watkins, M. C.; Wysocki, V. H.; Gratton, E.; Nowick, J. S. Elucidating the Oligomerization and Cellular Interactions of a Trimer Derived from Aβ Through Fluorescence and Mass Spectrometric Studies. *Submitted to ACS Chem. Neurosci.*

INTRODUCTION

Elucidating the biological properties of Aβ oligomers and understanding their solution phase behavior are essential to better understanding Alzheimer's disease.[1] Accumulation of the β-amyloid peptide (Aβ) in the brain is a hallmark of Alzheimer's disease and is a key contributor to neurodegeneration.[2] Aβ aggregates to form toxic oligomers and the fibrils that make up the characteristic plaques observed in the brains from those with Alzheimer's disease. These oligomers are thought to be the main synaptotoxic species, but have proven difficult to study as they are inherently heterogeneous and metastable with a high propensity to form fibrils.[3–8] Trimers of $A\beta_{42}$ are among the most toxic oligomers and are implicated in neuronal cell death.[6,9–12]

Model systems of stabilized Aβ-derived oligomers have emerged as tools to better understand endogenous oligomers and provide further insight into the molecular basis of Alzheimer's disease.[12–14] Our laboratory has developed a series of covalently stabilized trimers derived from residues 17–36 of Aβ as chemical models of toxic amyloid oligomers associated with neurodegeneration in Alzheimer's disease.[15–20] One of the trimers, termed 4AT-L, is composed of three β-hairpins formed by an $A\beta_{17–36}$ peptide, with molecular templates designed to induce β-hairpin folding, block uncontrolled aggregation, and allow disulfide crosslinking of three β-hairpins to form a covalent trimer.[20] Trimer 4AT-L is toxic toward the neuronal cell line SH-SY5Y, assembles to form ball-shaped dodecamers composed of four trimers in the crystal state, and forms dodecamers in SDS-PAGE.

Fluorescence lifetime imaging microscopy (FLIM) and native mass spectrometry (native MS) have emerged as important new tools to probe the assembly and interactions of peptides and proteins.[21–25] Native MS provides information about the stoichiometry of oligomeric assemblies

present in solution and can thus complement the structural information elucidated from X-ray crystallography and SDS-PAGE to build a broader understanding of the solution-phase assembly of Aβ-derived oligomers.[26,27] Fluorescence microscopy to visualize Aβ-derived oligomers in the presence of cells and the application of FLIM to determine the occurrence of Förster resonance energy transfer (FRET) can complement the previously observed cellular cytotoxicity.[28–34] In the current study, we set out to apply these and other techniques to better understand the assembly and interactions of a covalently stabilized trimer derived from residues 17–36 of Aβ in aqueous solutions and with cells.

RESULTS AND DISCUSSION

Design and synthesis of 2AT-L. In trimer 4AT-L, the native phenylalanine at position 20 is replaced with cyclohexylalanine. For the current study, we prepared homologue 2AT-L, which behaves similarly but has the native phenylalanine at position 20. Trimer 2AT-L is composed of three crosslinked $A\beta_{17–36}$ β-hairpins. In each β-hairpin, a δ-linked ornithine ($^{\delta}$Orn) turn unit between residues 17 and 36 helps enforce a folded β-hairpin conformation, and an *N*-methyl group on phenylalanine 20 helps block uncontrolled aggregation (Figure 2.1A). In 2AT-L, residues 17 and 21 are replaced by cysteines, which provide covalent crosslinks that hold the trimer together by connecting the monomer subunits at the vertices (Figure 2.1B,C). The crosslinked trimers are homogeneous, stable, and mimic some of the biological properties of Aβ oligomers.[18,20]

We synthesized trimer 2AT-L by the same procedures that we previously used to prepare trimer 4AT-L. We first prepared macrocyclic peptide 2AM-L_{CC} by solid-phase peptide synthesis of the corresponding linear peptide on 2-chlorotrityl resin, followed by cleavage of the protected

peptide from the resin, solution-phase macrocyclization, deprotection, and purification by RP-HPLC. 2AM-L_{CC} was oxidized at 6 mM in 20% aqueous DMSO with 60 mM triethylamine for 48 h. 2AT-L was isolated from the oxidation reaction by RP-HPLC. Pure fractions were lyophilized, affording >95% pure 2AT-L as the trifluoroacetate (TFA) salt.

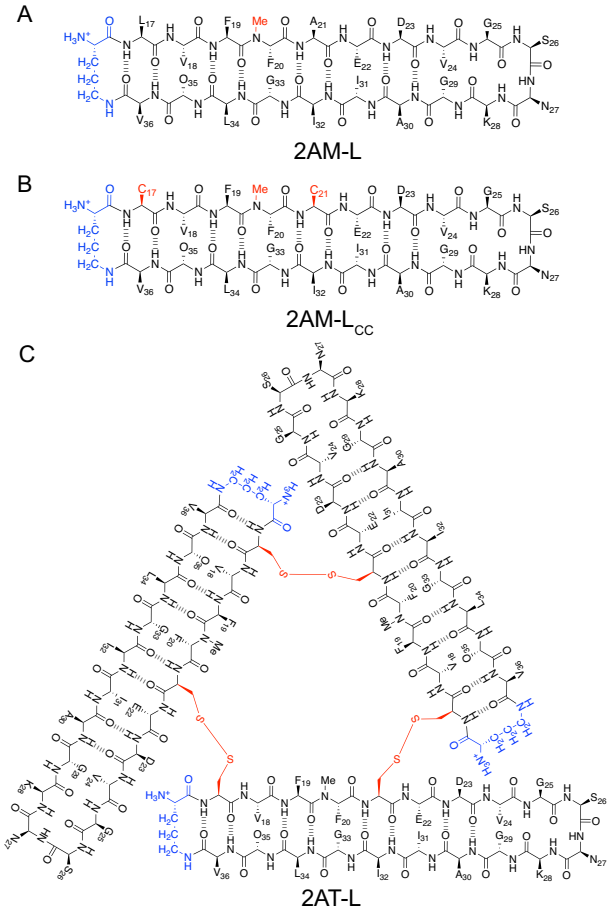

Figure 2.1 Chemical structures of β-hairpin peptides and a trimer derived from $A\beta_{17–36}$. **(A)** Macrocyclic β-hairpin 2AM-L incorporating an *N*-methyl residue to prevent uncontrolled aggregation and a $^{\delta}$Orn turn (blue) mimic to constrain the N- and C- termini. **(B)** β-Hairpin 2AM-L_{CC} incorporates cysteine mutations at residues 17 and 21. **(C)** Three 2AM-L_{CC} β-hairpins form covalently stabilized trimer 2AT-L through disulfide bonds.

Preparation of fluorescently labeled 2AT-L. Substoichiometric labeling of 2AT-L with fluorophore NHS esters permits the isolation of singly-labeled 2AT-L.[35] We developed a

labeling procedure in which 2AT-L is treated with 0.05 molar equivalents of the commercially available sulfo-cyanine3 (sCy3) or sulfo-cyanine5 (sCy5) NHS esters, the singly-labeled trimer is isolated by RP-HPLC, and the unlabeled trimer is recycled. We found that heating the HPLC column greatly facilitates the separation of the labeled trimer from the unlabeled trimer and also permits the removal of the small amounts of doubly-labeled trimer that form. We selected the bis-sulfonated analogues of the commonly used FRET partners Cy3 and Cy5 as fluorophores because they provide enhanced aqueous solubility and reduced aggregation. Labeling 3 mg of trimer by this procedure typically permits isolation of ca. 150 μg of singly-labeled trimer 2AT-L-sCy3 or 2AT-L-sCy5 as the TFA salt, which was sufficient for many of the experiments described below.

Oligomerization of 2AT-L and fluorescently labeled 2AT-L analogues by SDS-PAGE. We used SDS-PAGE to initially assess the effect of the sCy3 and sCy5 fluorophores on the assembly of 2AT-L into higher-order oligomers. In SDS-PAGE, trimer 2AT-L assembles to form higher-order oligomers. When 2AT-L (6.6 kDa) is run in SDS-PAGE and visualized by silver staining, it forms a downward-streaking band from ca. 32 kDa to ca. 13 kDa, suggesting assembly into oligomers ca. 2–5 trimers in size (Figure 2.2A). In contrast, the monomer 2AM-L (2.2 kDa) migrates at ca. 3 kDa, indicating the absence of assembly into oligomers. 2AT-L-sCy3 (7.2 kDa) migrates as a compact band at ca. 14 kDa, suggesting hexamer formation (2 trimers), while 2AT-L-sCy5 (7.2 kDa) migrates as a more diffuse band, from ca. 21 kDa to ca. 13 kDa, suggesting the formation of hexamers or perhaps hexamers and nonamers (2–3 trimers).

Fluorescence imaging provides additional insights into the bands formed by the trimers (Figure 2.2B,C). Notably, the diffuse band formed by 2AT-L-sCy5 shows an intense component

at ca. 14 kDa and a weaker component at ca. 21 kDa. The difference in shape between the bands formed by 2AT-L-sCy5 and 2AT-L-sCy3 may reflect the greater hydrophobicity and flat hydrophobic surface area provided by the larger sCy5 fluorophore. Both the sCy3 and sCy5 labels appear to impede the assembly, with hexamers as the main species observed, while the unlabeled 2AT-L forms predominantly larger oligomers.

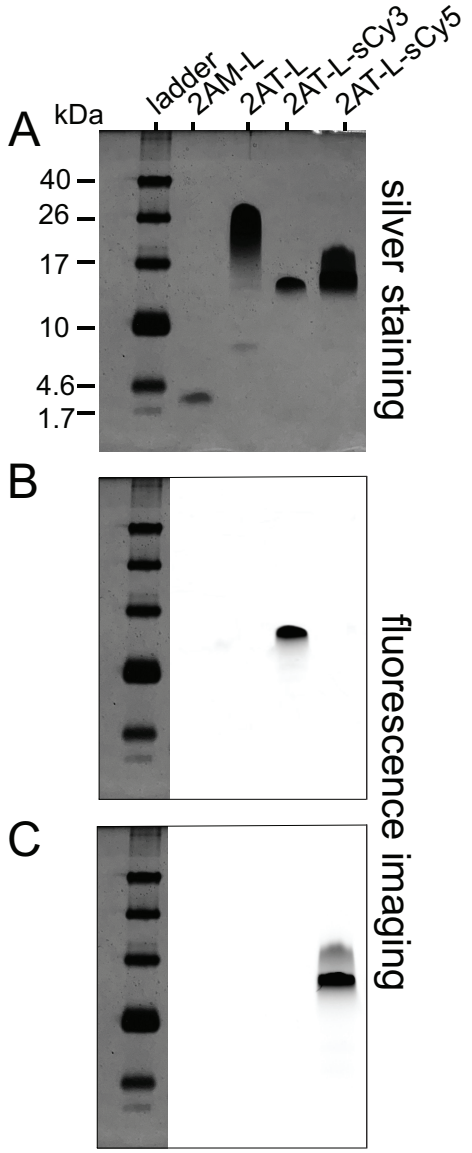

Figure 2.2 SDS-PAGE of peptides 2AM-L, 2AT-L, 2AT-L-sCy3, and 2AT-L-sCy5. **(A)** Silver-stained image. **(B)** Fluorescence image in the Cy3 channel. **(C)** Fluorescence image in the Cy5 channel. SDS-PAGE was performed in Tris buffer at pH 6.8 with 2% (w/v) SDS on a 16% polyacrylamide gel with 50 μM solutions of peptide in each lane. Fluorescence imaging was performed before silver staining.

Oligomerization of 2AT-L and fluorescently labeled 2AT-L analogues by native IM-MS.

We used native MS coupled with ion mobility spectrometry (IM) to investigate the oligomeric assembly of the trimers to complement the SDS-PAGE studies and avoid SDS-induced oligomer

formation.[36] In native IM-MS, oligomers and non-covalent assemblies are ionized and separated without dissociation. IM separates ionized oligomers of different size, shape, and charge in the gas-phase as they travel through the ion mobility device at different rates and their arrival times are measured.[37] The ions then are analyzed by a mass analyzer to determine their mass-to-charge ratio, *m/z* (Figure 2.3A). Trimer 2AT-L and fluorescently labeled 2AT-L analogues show a charge state distribution in the mass spectrum, leading to many overlapping *m/z* peaks that arise from multiple assemblies of trimers. The separation by arrival times that occurs in the ion mobility device permits separation of species with identical mass-to-charge ratio into their component oligomers.

Native IM-MS reveals that 2AT-L and fluorescently labeled 2AT-L analogues also assemble to form oligomers in aqueous solution. Each IM-MS experiment generates a *mobiligram*, in which the arrival time is plotted against mass-to-charge ratio, with the relative intensity displayed as a heat map. The IM-MS mobiligram for trimer 2AT-L shows that 2AT-L forms hexamers and nonamers, in addition to the trimer (Figure 2.3B). IM-MS shows that 2AT-L-sCy3 and 2AT-L-sCy5 also undergo assembly. The mobiligram for 2AT-L-sCy3 shows the formation of hexamers, as well as a low abundance of nonamers and dodecamers, in addition to the trimer (Figure 2.3C). The mobiligram for 2AT-L-sCy5 also shows the formation of hexamers, nonamers, and dodecamers, in addition to the trimer (Figure 2.3D).

The SDS-PAGE and native IM-MS experiments reveal that oligomers of 2AT-L and the fluorescently labeled 2AT-L analogues can form in either the presence or absence of SDS. Although the fluorophore labels appear to perturb the formation of higher-order oligomers in SDS-PAGE, similar perturbation is not seen in native IM-MS.

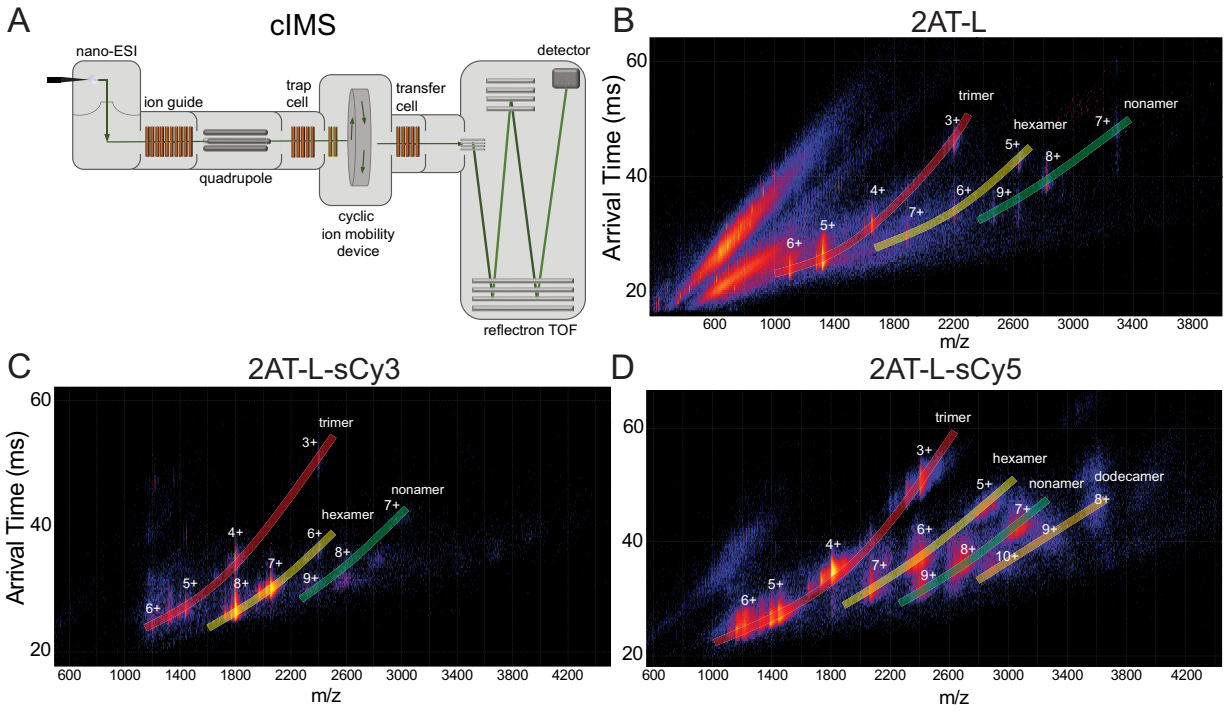

Figure 2.3 Native IM-MS of 2AT-L and labeled analogues. **(A)** Diagram of the cIMS instrument used to run native IM-MS experiments. Molecules are ionized through nano-electrospray ionization (nano-ESI), then travel through an ion guide and quadrupole. Ions reach a trap cell before entering the cyclic ion mobility device in which species are separated by size, shape, and charge. Ions exit the mobility device and proceed through a reflectron time-of-flight (TOF) mass analyzer to separate ions by mass-to-charge ratio. The time for an ion to travel through the mobility cell to detection is recorded as the arrival time. **(B**,**C**,**D)** Mobiligrams of 2AT-L, 2AT-L-sCy3, and 2AT-L-sCy5. Native IM-MS was performed on a SELECT SERIES Cyclic IMS Q-cIMS-TOF (cIMS) instrument (Waters Corporation). Numeric labels indicate the charge state of the corresponding oligomeric species. Samples of 2AT-L and fluorescently labeled 2AT-L analogues were prepared at a concentration of 40 μM in 400 mM ammonium acetate.

Oligomerization of 2AT-L-sCy3 and 2AT-L-sCy5 by FRET. We performed steady-state FRET experiments with mixtures of 2AT-L-sCy3 (donor) and 2AT-L-sCy5 (acceptor) to further assess the assembly of 2AT-L into higher-order oligomers in solution. The occurrence of FRET can be determined by selectively exciting at a wavelength absorbed by the donor and observing fluorescence at a wavelength emitted by the acceptor. In practice, it is often difficult to selectively excite only the donor. Thus, we used an excitation wavelength of 490 nm — which is well below the 548 nm λ_{max} of sCy3 — to minimize direct excitation of sCy5.[38] We monitored

fluorescence emission at 662 nm — the emission maximum of sCy5 — and varied the ratio of 2AT-L-sCy3 and 2AT-L-sCy5 from 100:0 to 0:100 while maintaining a total concentration of 5 μM.

When 2AT-L-sCy3 alone (100:0) is irradiated at 490 nm, emission (0.57 rfu) occurs at 662 nm (Figure 2.4). This emission is results from the sCy3 fluorophore, which has an emission maximum of 556 nm, but which extends weakly to 662 nm and beyond. When a 50:50 mixture of 2AT-L-sCy3 and 2AT-L-sCy5 is irradiated, the emission at 662 nm increases (1.00 rfu). The enhanced fluorescence reflects the occurrence of FRET and thus demonstrates the co-oligomerization of 2AT-L-sCy3 and 2AT-L-sCy5. Only modest emission (0.29 rfu) occurs from excitation of 2AT-L-sCy5 alone (0:100) at 490 nm, providing further evidence that the enhanced fluorescence in the 50:50 mixture results from FRET. Additional mixtures of 2AT-L-sCy3 and 2AT-L-sCy5 (80:20, 60:40, 40:60, 20:80) show intermediate levels of emission, providing further evidence for co-oligomerization and FRET.

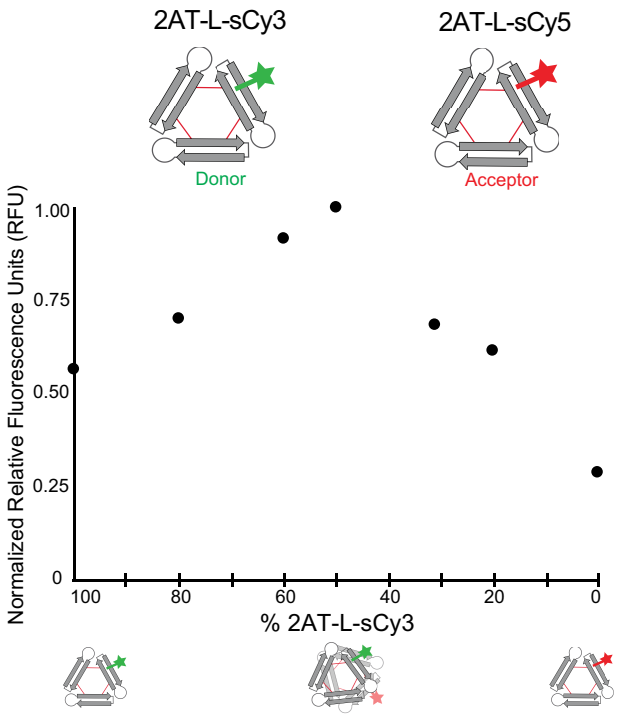

Figure 2.4 Fluorescence at the emission maximum of 2AT-L-sCy5 as a function of percentage of 2AT-L-sCy3. Fluorescence spectra of mixtures of varying ratios of 2AT-L-sCy3 and 2AT-L-sCy5 were acquired with excitation at 490 nm and observation at 662 nm. All spectra were collected on aqueous solutions of 2AT-L-sCy3 and 2AT-L-sCy5 with a total concentration of 5 μM.

Fluorescence microscopy of 2AT-L-sCy3 and 2AT-L-sCy5. To gain insights into the biological roles of the oligomers observed by SDS-PAGE, native IM-MS, and steady-state FRET experiments, we performed fluorescence microscopy with SH-SY5Y cells. Trimer 4AT-L is toxic toward SH-SY5Y cells, and trimer 2AT-L exhibits similar toxicity.[20] To further explore the interaction of Aβ-derived trimers with mammalian cells, we used fluorescence microscopy. SH-SY5Y cells were incubated with fluorescent analogues of 2AT-L at a total concentration of 5 μM. Cells were then counterstained with Hoechst 33342 nuclear stain (blue), washed with phenol red-free DMEM:F12 media, and imaged. Fluorescence micrographs were collected with emission observed in the respective Cyanine3 and Cyanine5 channels.

Fluorescence microscopy reveals that both 2AT-L-sCy3 and 2AT-L-sCy5 are internalized by cells. Incubation of SH-SY5Y cells with 2AT-L-sCy3 resulted in defined intracellular puncta and some small fluorescent features bound to the cell membrane (Figure S2.1). Incubation of SH-SY5Y cells with 2AT-L-sCy5 resulted in similar features (Figure S2.2). Incubation of SH-SY5Y cells with both 2AT-L-sCy3 and 2AT-L-sCy5 also resulted in similar features (Figure 2.5). Merged images, showing both the green (2AT-L-sCy3) and red (2AT-L-sCy5) channels, show a yellow hue, indicating co-localization of the fluorescently labeled trimers. Punctate features were observed as early as 5 h after treatment and at concentrations of fluorescently labeled 2AT-L as low as 8 nM (Figure S2.3).

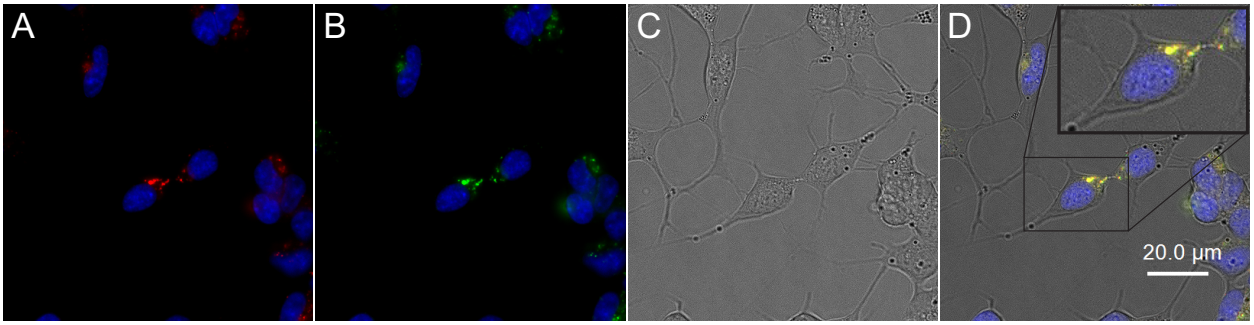

Figure 2.5 Micrographs illustrating intracellular co-localization of fluorescently labeled 2AT-L analogues in SH-SY5Y cells. **(A)** 2AT-L-sCy5 (red) and Hoechst 33342 nuclear stain (blue). **(B)** 2AT-L-sCy3 (green) and Hoechst 33342 nuclear stain (blue). **(C)** Brightfield image. **(D)** Merged fluorescent images with brightfield image. Cells were incubated with 5 µM 2AT-L-sCy3 and 5 µM 2AT-L-sCy5 for 6 h at 37°C, counterstained with Hoechst 33342 nuclear stain, and imaged.

The punctate intracellular features observed for the labeled 2AT-L are similar to those reported for fluorescently labeled $A\beta_{42}$, where uptake occurred primarily through endocytosis.[39–46] These studies have shown that Aβ localizes in lysosomes. To assess whether 2AT-L also localizes into lysosomes, we performed further experiments using the lysosomal marker Lysotracker Green. Treatment of SH-SY5Y cells with Lysotracker Green and either 2AT-L-sCy3

or 2AT-L-sCy5 showed co-localization, indicating sequestration in the lysosomes (Figure S2.4 and Figure 2.6). Thus, it appears that the uptake of 2AT-L occurs through endocytosis, in a fashion similar to that of Aβ.

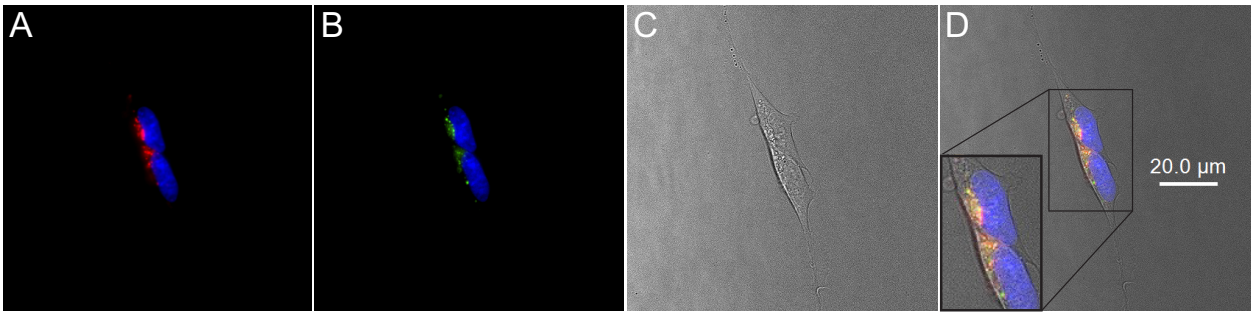

Figure 2.6 Micrographs illustrating intracellular co-localization of 2AT-L-sCy5 and Lysotracker Green in SH-SY5Y cells. **(A)** 2AT-L-sCy5 (red) and Hoechst 33342 nuclear stain (blue). **(B)** Lysotracker Green (green) and Hoechst 33342 nuclear stain (blue). **(C)** Brightfield image. **(D)** Merged fluorescent images with brightfield image. Cells were incubated with 5 µM 2AT-L-sCy5 and 100 nM Lysotracker Green for 6 h at 37°C, counterstained with Hoechst 33342 nuclear stain, and imaged.

Previous reports have suggested that oligomerization is a prerequisite for cellular uptake of Aβ.[47] The covalently stabilized oligomer model 2AT-L is readily taken up by cells and may thus serve as a model with which to further study the cellular uptake of Aβ oligomers. To continue to probe the assembly state of 2AT-L-sCy3 and 2AT-L-sCy5 and assess for higher-order oligomer formation, we turned to FRET microscopy.

FLIM-FRET studies of 2AT-L-sCy3 and 2AT-L-sCy5. We used fluorescence lifetime imaging microscopy (FLIM) to further investigate the intracellular puncta observed when fluorescently labeled 2AT-L analogues are incubated with cells. FLIM allows the detection of FRET and can thus reveal molecular co-localization at a resolution higher than can be achieved through confocal microscopy. If 2AT-L molecules bearing FRET partners co-assemble or are otherwise in close proximity (< 10 nm), FRET can occur and will manifest as a reduction in

fluorescence lifetime of the FRET donor through fluorescence quenching.[48] Measurement of fluorescence lifetimes through FLIM-FRET offers advantages over intensity-based FRET measurements, because the measurement of the lifetime is generally independent of the concentration of the fluorophores and does not require correction for spectral crosstalk.[49]

To assess FRET inside cells, we treated SH-SY5Y cells with either 2AT-L-sCy3 (donor) alone or with mixtures of 2AT-L-sCy5 (acceptor) and 2AT-L-sCy3 and looked for decreases in the fluorescence lifetime of sCy3 with increasing mole fraction of sCy5. Although 2AT-L-sCy3 oligomers or 2AT-L-sCy5 oligomers can form, only oligomers containing both 2AT-L-sCy3 and 2AT-L-sCy5 are expected to show decreased fluorescence lifetime (Figure 2.7A).[50] We used the phasor approach to analyze changes in fluorescence lifetime of sCy3. In this method, each pixel of a FLIM image is transformed to a point on a phasor plot, allowing for simple visualization of changes in the donor lifetime in a micrograph and thus facilitating the assessment of FRET.[51–54] Changes in fluorescence lifetime with increases in mole fraction of sCy5 manifest as changes in the positions of points on the phasor plot (Figure 2.7B), with greater changes corresponding to a greater fraction of molecules undergoing of FRET.[51,55,56]

We performed three sets of experiments, in which SH-SY5Y cells were treated with 2AT-L-sCy3 and 2AT-L-sCy5 in 100:0, 50:50, and 25:75 ratios while maintaining a total concentration of 5 μM. For each ratio, we collected 25–26 images of individual cells. We observed the photon intensity in the donor channel decrease as the fraction of 2AT-L-sCy5 increased (Figure 2.7C). The fluorescence decay from each pixel was determined, and the average from each image was plotted onto a phasor plot, with different colors (red, green, and violet) representing the three sets of ratios studied (Figure 2.7D,E). The resulting phasor plot shows significant decreases in

fluorescence lifetime with increasing fraction of sCy5 and thus provides compelling evidence for FRET, and hence intimate proximity of 2AT-L-sCy3 and 2AT-L-sCy5 in the cells.

The fluorescence lifetimes measured in FLIM-FRET can also be represented as a heat map, with each pixel of an image colored to reflect its relative fluorescence lifetime. We have thus represented the distribution of fluorescence lifetimes on three representative images at the 100:0, 50:50, and 25:75 ratios, with red representing the longest lifetimes and violet representing the shortest lifetimes, and colors ranging from orange to blue representing intermediate lifetimes (Figure 2.7F). The shift from red toward violet across the series of images reflects the decrease in fluorescence lifetime with increasing fraction of 2AT-L-sCy5 and further demonstrates that FRET increases with the addition of sCy5. Collectively, these FLIM-FRET experiments provide further evidence that 2AT-L-sCy3 and 2AT-L-sCy5 co-oligomerize in cells.

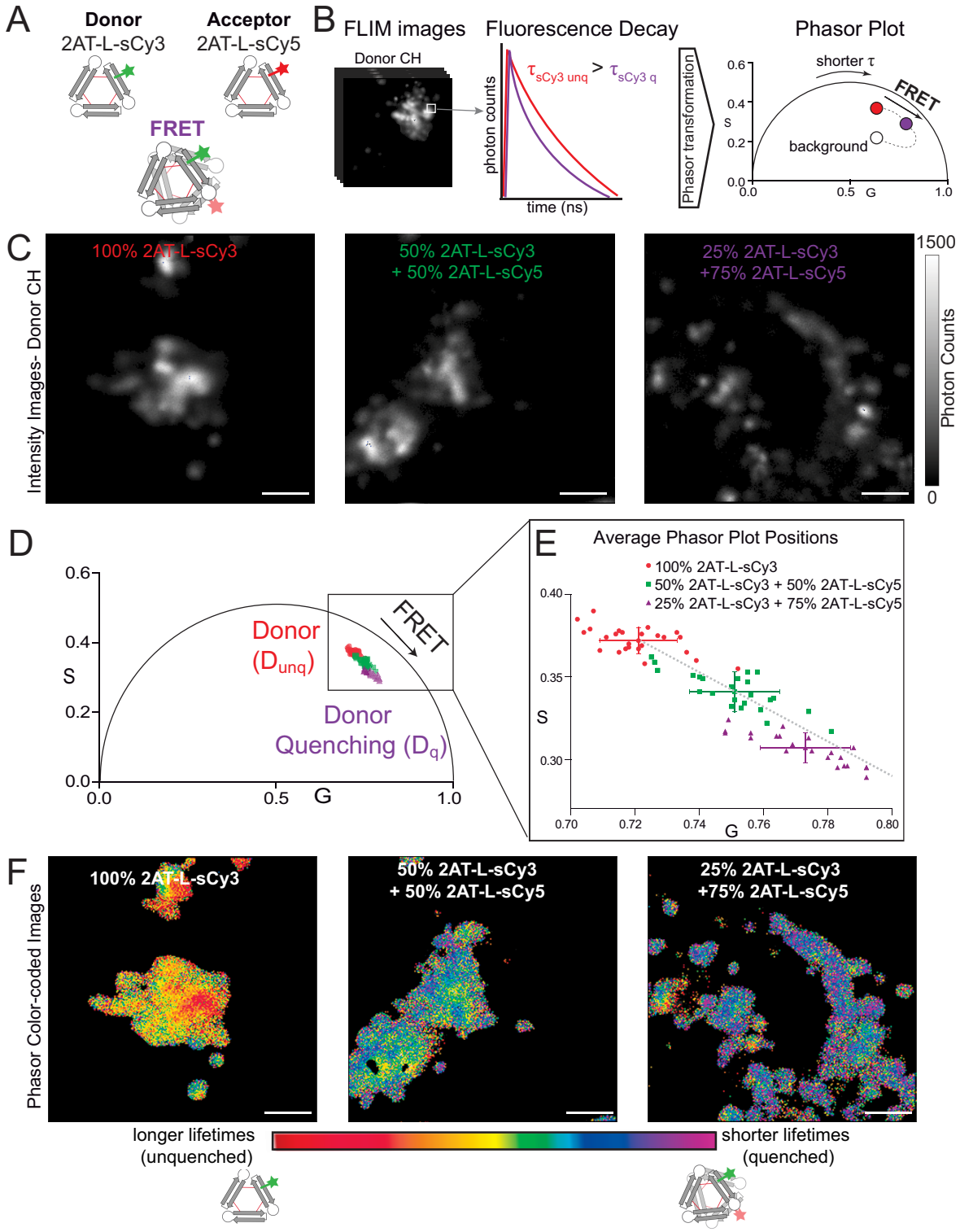

Figure 2.7 Phasor analysis of FLIM micrographs of SH-SY5Y cells treated with 2AT-L-sCy3 and 2AT-L-sCy5. Oligomeric assemblies of 2AT-L-sCy3 and 2AT-L-sCy5 within cells were analyzed by FLIM-FRET and the phasor approach. **(A)** Representation of the co-assembly of 2AT-L-sCy3

(donor) and 2AT-L-sCy5 (acceptor) and the occurrence of FRET. **(B)** Representation of the phasor transformation of FLIM images. Fluorescence lifetime of each pixel of each image is analyzed and plotted on a phasor plot. When FRET occurs, the excited state lifetime of the donor decreases and the phasor position shifts towards shorter lifetimes. The curved FRET trajectory (dotted line) follows the classical definition of FRET efficiency and is influenced by the background fluorescence lifetime. **(C)** Representative images showing photon intensity of SH-SY5Y cells treated with 2AT-L-sCy3 and 2AT-L-sCy5 in 100:0, 50:50, and 25:75 ratios. Images were acquired in the donor (sCy3) channel. Scale bar = 5 μm. **(D)** Phasor plot illustrating the average phasor position in each image. Images collected for the 100:0 ratio are represented by red points and correspond to unquenched donor (D_{unq}). Images collected for the 50:50 ratio are represented by green points. Images collected for the 25:75 ratio are represented by violet points and correspond to increased donor quenching (D_q). **(E)** Detail of phasor plot in D. Average phasor plot positions (±SD) from each image. **(F)** Representative images of SH-SY5Y cells with false color illustrating fluorescence lifetime. Longer fluorescence lifetimes are represented in red and orange, while shorter fluorescence lifetimes reflecting increased FRET are represented progressively in yellow, green, blue, and violet.

SUMMARY AND CONCLUSIONS

Our covalently stabilized Aβ-derived trimers mimic some of the assembly and biological properties of Aβ oligomers. In the crystal state, 2AT-L and homologue 4AT-L assemble to form ball-shaped dodecamers. In the membrane-like environment of SDS-PAGE, 2AT-L dodecamers are also observed but appear to be in equilibrium with oligomers ca. 2–5 trimers in size. Labeling 2AT-L with sCy3 and sCy5 appears to attenuate assembly in SDS-PAGE, with 2AT-L-sCy3 and 2AT-L-sCy5 migrating mainly as hexamers. Native IM-MS of 2AT-L identifies discrete hexamers and nonamers in solution. Native IM-MS of 2AT-L-sCy3 and 2AT-L-sCy5 shows similar oligomer formation to 2AT-L.[57]

Steady-state FRET experiments also show that 2AT-L-sCy3 and 2AT-L-sCy5 form oligomers in solution. Fluorescence microscopy shows that 2AT-L-sCy3 and 2AT-L-sCy5 form intracellular puncta in SH-SY5Y cells, which co-localize with a lysosomal marker, suggesting an uptake mechanism through endocytotic vesicles that is consistent with previous studies of Aβ.[45]

FLIM studies and phasor analysis establish the occurrence of FRET within cells treated with both 2AT-L-sCy3 and 2AT-L-sCy5, suggesting oligomerization within cellular vesicles.

The aggregation of Aβ to form oligomers is difficult to study in detail due to the complexity of the different species that form and the propensity of Aβ to ultimately form insoluble fibrils. Constraint of an Aβ-derived peptide into a stable trimer, 2AT-L, provides a model system that is easier to study and can be explored by a variety of biophysical and biological techniques. While X-ray crystallography provides a simple answer that assemblies of dodecamers form in the crystal state, the behavior in the solution state is more complex. SDS-PAGE shows multiple oligomeric states in equilibrium but does not allow the identification of discrete oligomers. Native IM-MS, on the other hand, allows the identification of individual oligomers. Addition of fluorescent labels is required to visualize the interactions of 2AT-L in cells, although SDS-PAGE shows that these labels can alter the oligomerization, at least somewhat. FLIM-FRET experiments with phasor analysis allow the observation of oligomerization of the labeled 2AT-L in cells. Collectively, the application of multiple complementary techniques helps better elucidate the complex behavior of the 2AT-L model system. We anticipate that these techniques may also be useful for understanding the yet more complex oligomerization of Aβ.

MATERIALS AND METHODS

Peptides 2AM-L, 2AM-L_{CC}, and 2AT-L were synthesized by procedures analogous to those described previously.[18] SDS-PAGE and silver staining were performed as described previously.[20] Procedures detailing the preparation of 2AT-L-sCy3 and 2AT-L-sCy5, native mass spectrometry studies, steady-state FRET experiments, fluorescence microscopy, and FLIM-FRET can be found in the Supporting Information.

ACKNOWLEDGMENTS

We thank Dr. Adam G. Kreutzer for helpful discussion and guidance, Dr. Suman Ranjit for useful discussions about FLIM-FRET, and the National Institutes of Health (NIH) for funding (AG072587). The Laboratory for Fluorescence Dynamics thanks the National Institutes of Health (NIH) for funding (P41-GM103540).

REFERENCES AND NOTES

(1) Mroczko, B.; Groblewska, M.; Litman-Zawadzka, A.; Kornhuber, J.; Lewczuk, P. Amyloid β Oligomers (AβOs) in Alzheimer's Disease. *J. Neural Transm.* **2018**, *125* (2), 177–191. https://doi.org/10.1007/s00702-017-1820-x.

(2) Pearson, H. A.; Peers, C. Physiological Roles for Amyloid β Peptides. *J. Physiol.* **2006**, *575* (1), 5–10. https://doi.org/10.1113/jphysiol.2006.111203.

(3) Ono, K.; Condron, M. M.; Teplow, D. B. Structure-Neurotoxicity Relationships of Amyloid β-Protein Oligomers. *Proc. Natl. Acad. Sci. U. S. A.* **2009**, *106* (35), 14745–14750. https://doi.org/10.1073/pnas.0905127106.

(4) Gray, A. L. H.; Sawaya, M. R.; Acharyya, D.; Lou, J.; Edington, E.; Best, M. D.; Prosser, R. A.; Eisenberg, D. S.; Do, T. D. Atomic View of an Amyloid Dodecamer Exhibiting Selective Cellular Toxic Vulnerability in Acute Brain Slices. *Protein Sci.* **2022**, 1–12. https://doi.org/10.1002/pro.4268.

(5) Sakono, M.; Zako, T. Amyloid Oligomers: Formation and Toxicity of Aβ Oligomers. *FEBS J.* **2010**, *277* (6), 1348–1358. https://doi.org/10.1111/j.1742-4658.2010.07568.x.

(6) Walsh, D. M.; Selkoe, D. J. Aβ Oligomers - A Decade of Discovery. *J. Neurochem.* **2007**, *101* (5), 1172–1184. https://doi.org/10.1111/j.1471-4159.2006.04426.x.

(7) LaFerla, F. M.; Green, K. N.; Oddo, S. Intracellular Amyloid-β in Alzheimer's Disease. *Nat. Rev. Neurosci.* **2007**, *8* (7), 499–509. https://doi.org/10.1038/nrn2168.

(8) Cline, E. N.; Bicca, M. A.; Viola, K. L.; Klein, W. L. The Amyloid-Oligomer Hypothesis: Beginning of the Third Decade. *J. Alzheimer's Dis.* **2018**, *64*, 567–610. https://doi.org/10.3233/JAD-179941.

(9) Jana, M. K.; Cappai, R.; Pham, C. L. L.; Ciccotosto, G. D. Membrane-Bound Tetramer

and Trimer Aβ Oligomeric Species Correlate with Toxicity towards Cultured Neurons. *J. Neurochem.* **2016**, *136* (3), 594–608. https://doi.org/10.1111/jnc.13443.

(10) Marina, G. B.; Kirkitadze, D.; Lomakin, A.; Vollers, S. S.; Benedek, G. B.; Teplow, D. B. Amyloid β-Protein (Aβ) Assembly: Aβ40 and Aβ42 Oligomerize through Distinct Pathways. *Proc. Natl. Acad. Sci. U. S. A.* **2003**, *100* (1), 330–335. https://doi.org/10.1073/pnas.222681699.

(11) Cleary, J. P.; Walsh, D. M.; Hofmeister, J. J.; Shankar, G. M.; Kuskowski, M. A.; Selkoe, D. J.; Ashe, K. H. Natural Oligomers of the Amyloid-β Protein Specifically Disrupt Cognitive Function. *Nat. Neurosci.* **2005**, *8* (1), 79–84. https://doi.org/10.1038/nn1372.

(12) Benilova, I.; Karran, E.; De Strooper, B. The Toxic Aβ Oligomer and Alzheimer's Disease: An Emperor in Need of Clothes. *Nat. Neurosci.* **2012**, *15* (3), 349–357. https://doi.org/10.1038/nn.3028.

(13) Hawk, L. M. L.; Pittman, J. M.; Moore, P. C.; Srivastava, A. K.; Zerweck, J.; Williams, J. T. B.; Hawk, A. J.; Sachleben, J. R.; Meredith, S. C. β-Amyloid Model Core Peptides: Effects of Hydrophobes and Disulfides. *Protein Sci.* **2020**, *29* (2), 527–541. https://doi.org/10.1002/pro.3778.

(14) Straub, J. E.; Thirumalai, D. Principles Governing Oligomer Formation in Amyloidogenic Peptides. *Curr. Opin. Struct. Biol.* **2010**, *20* (2), 187–195. https://doi.org/10.1016/j.sbi.2009.12.017.

(15) Kreutzer, A. G.; Nowick, J. S. Elucidating the Structures of Amyloid Oligomers with Macrocyclic β-Hairpin Peptides: Insights into Alzheimer's Disease and Other Amyloid Diseases. *Acc. Chem. Res.* **2018**, *51* (3), 706–718. https://doi.org/10.1021/acs.accounts.7b00554.

(16) Kreutzer, A. G.; Spencer, R. K.; McKnelly, K. J.; Yoo, S.; Hamza, I. L.; Salveson, P. J.; Nowick, J. S. A Hexamer of a Peptide Derived from Aβ16-36. *Biochemistry* **2017**, *56* (45), 6061–6071. https://doi.org/10.1021/acs.biochem.7b00831.

(17) Wang, Y.; Kreutzer, A. G.; Truex, N. L.; Nowick, J. S. A Tetramer Derived from Islet Amyloid Polypeptide. *J. Org. Chem.* **2017**, *82* (15), 7905–7912. https://doi.org/10.1021/acs.joc.7b01116.

(18) Kreutzer, A. G.; Yoo, S.; Spencer, R. K.; Nowick, J. S. Stabilization, Assembly, and Toxicity of Trimers Derived from Aβ. *J. Am. Chem. Soc.* **2017**, *139* (2), 966–975. https://doi.org/10.1021/jacs.6b11748.

(19) Kreutzer, A. G.; Samdin, T. D.; Guaglianone, G.; Spencer, R. K.; Nowick, J. S. X-Ray Crystallography Reveals Parallel and Antiparallel β-Sheet Dimers of a β-Hairpin Derived from Aβ16-36that Assemble to Form Different Tetramers. *ACS Chem. Neurosci.* **2020**, *11* (15), 2340–2347. https://doi.org/10.1021/acschemneuro.0c00290.

(20) Haerianardakani, S.; Kreutzer, A. G.; Salveson, P. J.; Samdin, T. D.; Guaglianone, G. E.; Nowick, J. S. Phenylalanine Mutation to Cyclohexylalanine Facilitates Triangular Trimer Formation by β-Hairpins Derived from Aβ. *J. Am. Chem. Soc.* **2020**, *142* (49), 20708–20716. https://doi.org/10.1021/jacs.0c09281.

(21) Hu, J.; Zheng, Q. Applications of Mass Spectrometry in the Onset of Amyloid Fibril Formation: Focus on the Analysis of Early-Stage Oligomers. *Front. Chem.* **2020**, *8*, 1–7. https://doi.org/10.3389/fchem.2020.00324.

(22) Ben-Nissan, G.; Sharon, M. The Application of Ion-Mobility Mass Spectrometry for Structure/Function Investigation of Protein Complexes. *Curr. Opin. Chem. Biol.* **2018**, *42*, 25–33. https://doi.org/10.1016/j.cbpa.2017.10.026.

(23) Matuszyk, M. M.; Garwood, C. J.; Ferraiuolo, L.; Simpson, J. E.; Staniforth, R. A.; Wharton, S. B. Biological and Methodological Complexities of Beta-Amyloid Peptide: Implications for Alzheimer's Disease Research. *J. Neurochem.* **2022**, *160* (4), 434–453. https://doi.org/10.1111/jnc.15538.

(24) Ueda, H. H.; Nagasawa, Y.; Murakoshi, H. Imaging Intracellular Protein Interactions/Activity in Neurons Using 2-Photon Fluorescence Lifetime Imaging Microscopy. *Neurosci. Res.* **2021**, In Press. https://doi.org/10.1016/j.neures.2021.10.004.

(25) Aliyan, A.; Cook, N. P.; Martí, A. A. Interrogating Amyloid Aggregates Using Fluorescent Probes. *Chem. Rev.* **2019**, *119*, 11819–11856. https://doi.org/10.1021/acs.chemrev.9b00404.

(26) Leney, A. C.; Heck, A. J. R. Native Mass Spectrometry: What Is in the Name? *J. Am. Soc. Mass Spectrom.* **2017**, *28* (1), 5–13. https://doi.org/10.1007/s13361-016-1545-3.

(27) Heck, A. J. R. Native Mass Spectrometry: A Bridge between Interactomics and Structural Biology. *Nat. Methods* **2008**, *5* (11), 927–933. https://doi.org/10.1038/nmeth.1265.

(28) Bacskai, B. J.; Skoch, J.; Hickey, G. A.; Allen, R.; Hyman, B. T. Fluorescence Resonance Energy Transfer Determinations Using Multiphoton Fluorescence Lifetime Imaging Microscopy to Characterize Amyloid-Beta Plaques. *J. Biomed. Opt.* **2003**, *8* (3), 368. https://doi.org/10.1117/1.1584442.

(29) Clegg, R. M. Chapter 1 Förster Resonance Energy Transfer—FRET What Is It, Why Do It, and How It's Done. *Lab. Tech. Biochem. Mol. Biol.* **2009**, *33*, 1–57. https://doi.org/10.1016/S0075-7535(08)00001-6.

(30) Jones, G. A.; Bradshaw, D. S. Resonance Energy Transfer: From Fundamental Theory to Recent Applications. *Frontiers in Physics*. **2019**, *7*, 1–19.

(31) Ma, L.; Yang, F.; Zheng, J. Application of Fluorescence Resonance Energy Transfer in Protein Studies. *J. Mol. Struc.* **2014**, *1077*, 87–100. https://doi.org/10.1016/j.molstruc.2013.12.071.

(32) Lou, J.; Scipioni, L.; Wright, B. K.; Bartolec, T. K.; Zhang, J.; Masamsetti, V. P.; Gaus, K.; Gratton, E.; Cesare, A. J.; Hinde, E. Phasor Histone FLIM-FRET Microscopy Quantifies Spatiotemporal Rearrangement of Chromatin Architecture during the DNA Damage Response. *Proc. Natl. Acad. Sci.* **2019**, *116* (15), 7323–7332. https://doi.org/10.1073/PNAS.1814965116.

(33) Ishikawa-ankerhold, H. C.; Ankerhold, R.; Drummen, G. P. C.; Biology, C.; Zeiss, C.; Gmbh, M.; Program, B.; Stress, C.; Program, A. Advanced Fluorescence Microscopy Techniques—FRAP , FLIP , FLAP , FRET and FLIM. *Molecules* **2012**, *17*, 4047–4132. https://doi.org/10.3390/molecules17044047.

(34) Chen, Y.; Mills, J. D. Protein Localization in Living Cells and Tissues Using FRET and FLIM. *Differentiation* **2003**, *71* (9–10), 528–541. https://doi.org/10.1111/j.1432-0436.2003.07109007.x.

(35) We chose to singly-label trimer 2AT-L to minimize perturbation of its assembly and interactions with cells.

(36) Pujol-Pina, R.; Vilaprinyó-Pascual, S.; Mazzucato, R.; Arcella, A.; Vilaseca, M.; Orozco, M.; Carulla, N. SDS-PAGE Analysis of Aβ Oligomers Is Disserving Research into Alzheimer's Disease: Appealing for ESI-IM-MS. *Sci. Rep.* **2015**, *5*, 1–13. https://doi.org/10.1038/srep14809.

(37) Snyder, D. T.; Jones, B. J.; Lin, Y. F.; Cooper-Shepherd, D. A.; Hewitt, D.; Wildgoose, J.; Brown, J. M.; Langridge, J. I.; Wysocki, V. H. Surface-Induced Dissociation of Protein

Complexes on a Cyclic Ion Mobility Spectrometer. *Analyst* **2021**, *146* (22), 6861–6873. https://doi.org/10.1039/d1an01407b.

(38) Miyawaki, R.; Tsien, R. Y. Monitoring Protein Conformations and Interactions by Fluorescence Resonance Energy Transfer between Mutants of Green Fluorescent Protein. *Meth. Enzymol.* **1999**, *327*, 472–500.

(39) Dutta, S.; Finn, T. S.; Kuhn, A. J.; Abrams, B.; Raskatov, J. A. Chirality Dependence of Amyloid β Cellular Uptake and a New Mechanistic Perspective. *ChemBioChem* **2019**, *20* (8), 1023–1026. https://doi.org/https://doi.org/10.1002/cbic.201800708.

(40) Hu, X.; Crick, S. L.; Bu, G.; Frieden, C.; Pappu, R. V.; Lee, J. M. Amyloid Seeds Formed by Cellular Uptake, Concentration, and Aggregation of the Amyloid-Beta Peptide. *Proc. Natl. Acad. Sci. U. S. A.* **2009**, *106* (48), 20324–20329. https://doi.org/10.1073/pnas.0911281106.

(41) Gorman, P. M.; Yip, C. M.; Fraser, P. E.; Chakrabartty, A. Alternate Aggregation Pathways of the Alzheimer β-Amyloid Peptide: Aβ Association Kinetics at Endosomal PH. *J. Mol. Biol.* **2003**, *325* (4), 743–757. https://doi.org/10.1016/S0022-2836(02)01279-2.

(42) Perez, R. G.; Soriano, S.; Hayes, J. D.; Ostaszewski, B.; Xia, W.; Selkoe, D. J.; Chen, X.; Stokin, G. B.; Koo, E. H. Mutagenesis Identifies New Signals for β-Amyloid Precursor Protein Endocytosis, Turnover, and the Generation of Secreted Fragments, Including Aβ42. *J. Biol. Chem.* **1999**, *274* (27), 18851–18856. https://doi.org/10.1074/jbc.274.27.18851.

(43) Yang, W. N.; Ma, K. G.; Chen, X. L.; Shi, L. L.; Bu, G.; Hu, X. D.; Han, H.; Liu, Y.; Qian, Y. H. Mitogen-Activated Protein Kinase Signaling Pathways Are Involved in

Regulating A7 Nicotinic Acetylcholine Receptor-Mediated Amyloid-β Uptake in SH-SY5Y Cells. *Neuroscience* **2014**, *278*, 276–290. https://doi.org/10.1016/j.neuroscience.2014.08.013.

(44) Esbjörner, E. K.; Chan, F.; Rees, E.; Erdelyi, M.; Luheshi, L. M.; Bertoncini, C. W.; Kaminski, C. F.; Dobson, C. M.; Kaminski Schierle, G. S. Direct Observations of Amyloid β Self-Assembly in Live Cells Provide Insights into Differences in the Kinetics of Aβ(1-40) and Aβ(1-42) Aggregation. *Chem. Biol.* **2014**, *21* (6), 732–742. https://doi.org/10.1016/j.chembiol.2014.03.014.

(45) Wesén, E.; Jeffries, G. D. M.; Dzebo, M. M.; Esbjörner, E. K. Endocytic Uptake of Monomeric Amyloid-β Peptides Is Clathrin- A Nd Dynamin-Independent and Results in Selective Accumulation of Aβ(1-42) Compared to Aβ(1-40). *Sci. Rep.* **2017**, *7* (1), 1–14. https://doi.org/10.1038/s41598-017-02227-9.

(46) Zhang, S.; Guaglianone, G.; Morris, M. A.; Yoo, S.; Howitz, W. J.; Xing, L.; Zheng, J. G.; Jusuf, H.; Huizar, G.; Lin, J.; Kreutzer, A. G.; Nowick, J. S. Expression of N-Terminal Cysteine Aβ42and Conjugation to Generate Fluorescent and Biotinylated Aβ42. *Biochemistry* **2021**, *60* (15), 1191–1200. https://doi.org/10.1021/acs.biochem.1c00105.

(47) Jin, S.; Kedia, N.; Illes-Toth, E.; Haralampiev, I.; Prisner, S.; Herrmann, A.; Wanker, E. E.; Bieschke, J. Amyloid-β(1- 42) Aggregation Initiates Its Cellular Uptake and Cytotoxicity. *J. Biol. Chem.* **2016**, *291* (37), 19590–19606. https://doi.org/10.1074/jbc.M115.691840.

(48) Jameson, D. M. *Introduction to Fluorescence*, 1st ed.; CRC Press., 2014. https://doi.org/https://doi.org/10.1201/b16502.

(49) Wallrabe, H.; Periasamy, A. Imaging Protein Molecules Using FRET and FLIM

Microscopy. *Curr. Opin. Biotechnol.* **2005**, 16, 19–27. https://doi.org/10.1016/j.copbio.2004.12.002.

(50) Levitt, J. A.; Matthews, D. R.; Ameer-Beg, S. M.; Suhling, K. Fluorescence Lifetime and Polarization-Resolved Imaging in Cell Biology. *Curr. Opin. Biotechnol.* **2009**, *20* (1), 28–36. https://doi.org/10.1016/j.copbio.2009.01.004.

(51) Digman, M. A.; Caiolfa, V. R.; Zamai, M.; Gratton, E. The Phasor Approach to Fluorescence Lifetime Imaging Analysis. *Biophys. J.* **2008**, *94* (2), 14–16. https://doi.org/10.1529/biophysj.107.120154.

(52) Jameson, D. M.; Gratton, E.; Hall, R. D. The Measurement and Analysis of Heterogeneous Emissions by Multifrequency Phase and Modulation Fluorometry. *Appl. Spectrosc. Rev.* **1984**, *20* (1), 55–106. https://doi.org/10.1080/05704928408081716.

(53) Clayton, A. H. A.; Hanley, Q. S.; Verveer, P. J. Graphical Representation and Multicomponent Analysis of Single-Frequency Fluorescence Lifetime Imaging Microscopy Data. *J. Microsc.* **2004**, *213* (1), 1–5. https://doi.org/10.1111/j.1365-2818.2004.01265.x.

(54) Malacrida, L.; Ranjit, S.; Jameson, D. M.; Gratton, E. The Phasor Plot: A Universal Circle to Advance Fluorescence Lifetime Analysis and Interpretation. *Annu. Rev. Biophys.* **2021**, *50*, 575–593. https://doi.org/10.1146/annurev-biophys-062920-063631.

(55) Giral, H.; Lanzano, L.; Caldas, Y.; Blaine, J.; Verlander, J. W.; Lei, T.; Gratton, E.; Levi, M. Role of PDZK1 Protein in Apical Membrane Expression of Renal Sodium-Coupled Phosphate Transporters. *J. Biol. Chem.* **2011**, *286* (17), 15032–15042. https://doi.org/10.1074/jbc.M110.199752.

(56) Hinde, E.; Cardarelli, F.; Digman, M. A.; Gratton, E. Changes in Chromatin Compaction

during the Cell Cycle Revealed by Micrometer-Scale Measurement of Molecular Flow in the Nucleus. *Biophys. J.* **2012**, *102* (3), 691–697. https://doi.org/10.1016/j.bpj.2011.11.4026.

(57) Bowers and coworkers observed assemblies of hexamers and dodecamers by nMS-IM and suggest these species to be central building blocks to the assembly of Aβ. Bleiholder, C.; Bowers, M. T. The Solution Assembly of Biological Molecules Using Ion Mobility Methods: From Amino Acids to Amyloid β-Protein. *Annu. Rev. Anal. Chem.* **2017**, *10*, 365–386. https://doi.org/10.1146/annurev-anchem-071114-040304.

Supporting information for:

Elucidating the Oligomerization and Cellular Interactions of a Trimer Derived from Aβ Through Fluorescence and Mass Spectrometric Studies

Table of Contents

Figure S2.1 Micrograph of 2AT-L-sCy3 with SH-SY5Y cells 52

Figure S2.2 Micrograph of 2AT-L-sCy5 with SH-SY5Y cells 53

Figure S2.3 Micrograph of concentration gradient of 2AT-L-sCy5 with SH-SY5Y cells 54

Figure S2.4 Micrograph of 2AT-L-sCy3 with Lysotracker Green 55

Figure S2.5 Fractional intensity of quenched donor (D_q) 56

Figure S2.6 Representative clouds on phasor plot 57

General Information 58

Synthesis of Macrocyclic Peptides 59

Synthesis of Fluorescently Labeled 2AT-L 59

SDS-PAGE 60

Steady-state FRET Experiments 61

Native IM-MS 61

Cell Culture 62

Fluorescence Microscopy 62

FLIM-FRET 64

References and Notes 68

Characterization Data

Characterization of 2AM-L 71

Characterization of 2AM-L_{CC} 75

Characterization of 2AT-L 79

Characterization of 2AT-L-sCy3 84

Characterization of 2AT-L-sCy5 89

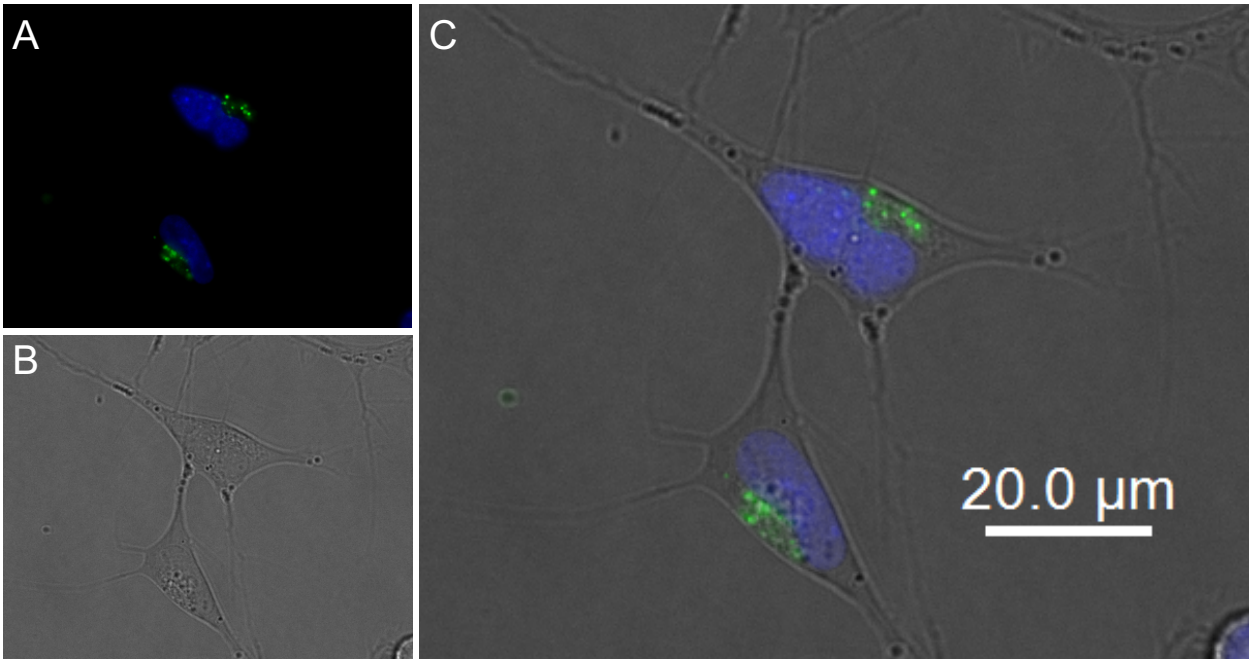

Figure S2.1 Micrographs illustrating intracellular localization of 2AT-L-sCy3 in SH-SY5Y cells. **(A)** 2AT-L-sCy3 (green) and Hoechst 33342 nuclear stain (blue). **(B)** Brightfield image. **(C)** Merged fluorescent image with brightfield image. Cells were incubated with 5 µM 2AT-L-sCy3 for 6 h at 37°C, counterstained with Hoechst 33342 nuclear stain (blue), and imaged.

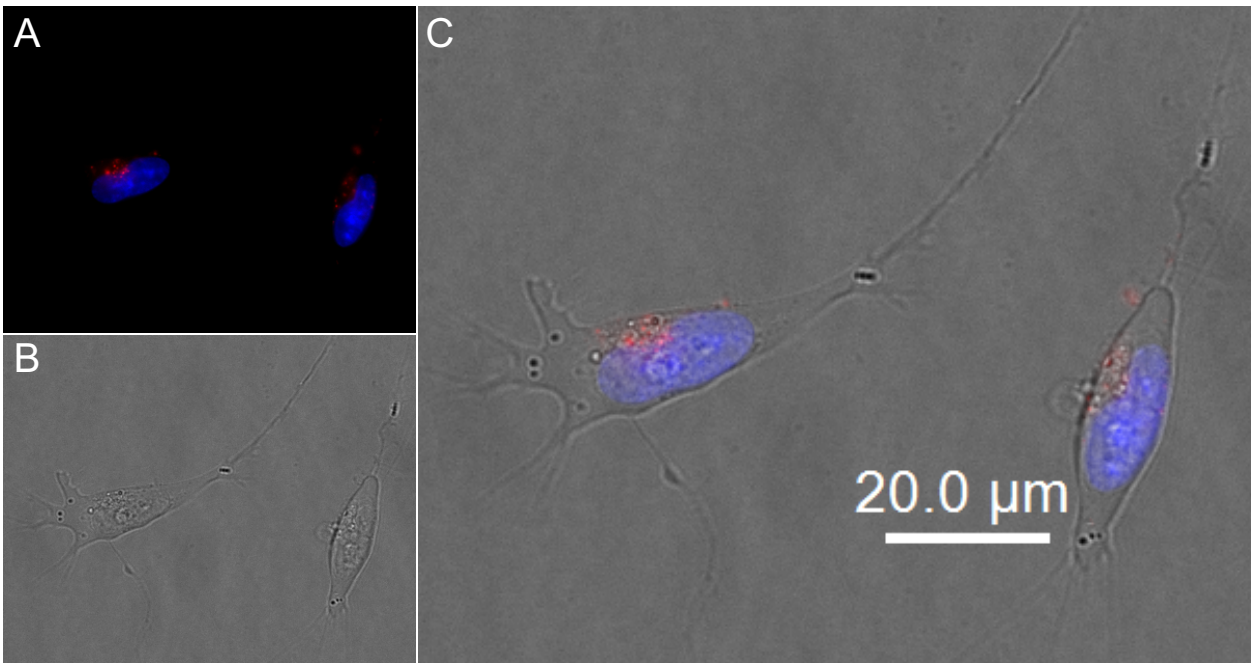

Figure S2.2 Micrographs illustrating intracellular localization of 2AT-L-sCy5 in SH-SY5Y cells. **(A)** 2AT-L-sCy5 (red) and Hoechst 33342 nuclear stain (blue). **(B)** Brightfield image. **(C)** Merged fluorescent image with brightfield image. Cells were incubated with 5 µM 2AT-L-sCy5 for 6 h at 37°C, counterstained with Hoechst 33342 nuclear stain (blue), and imaged.

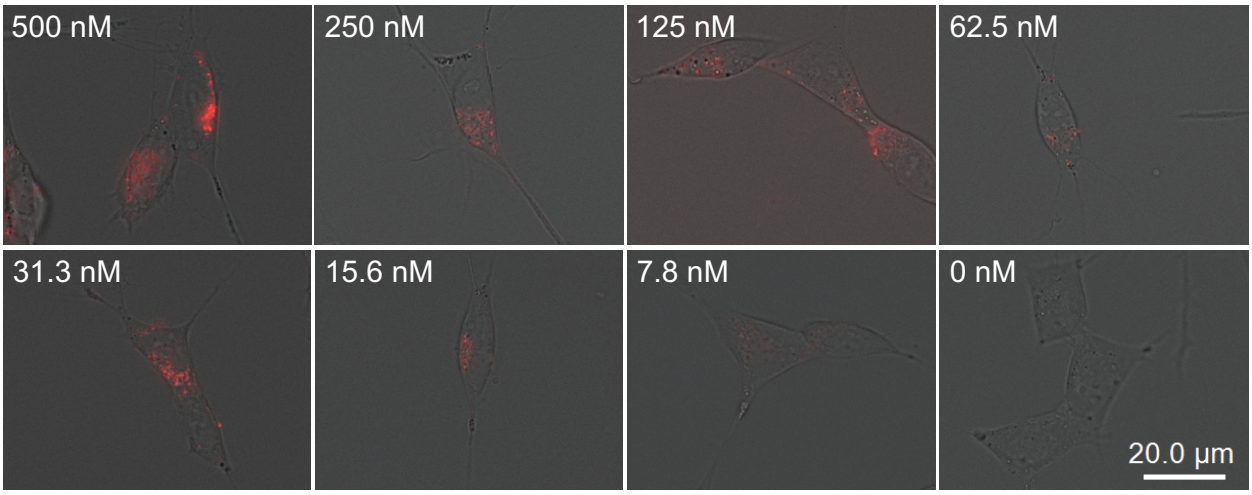

Figure S2.3 Merged fluorescent and brightfield micrographs of SH-SY5Y cells treated with 7.8–500 nM 2AT-L-sCy3. Cells were incubated with 2AT-L-sCy3 overnight at 37°C and imaged.

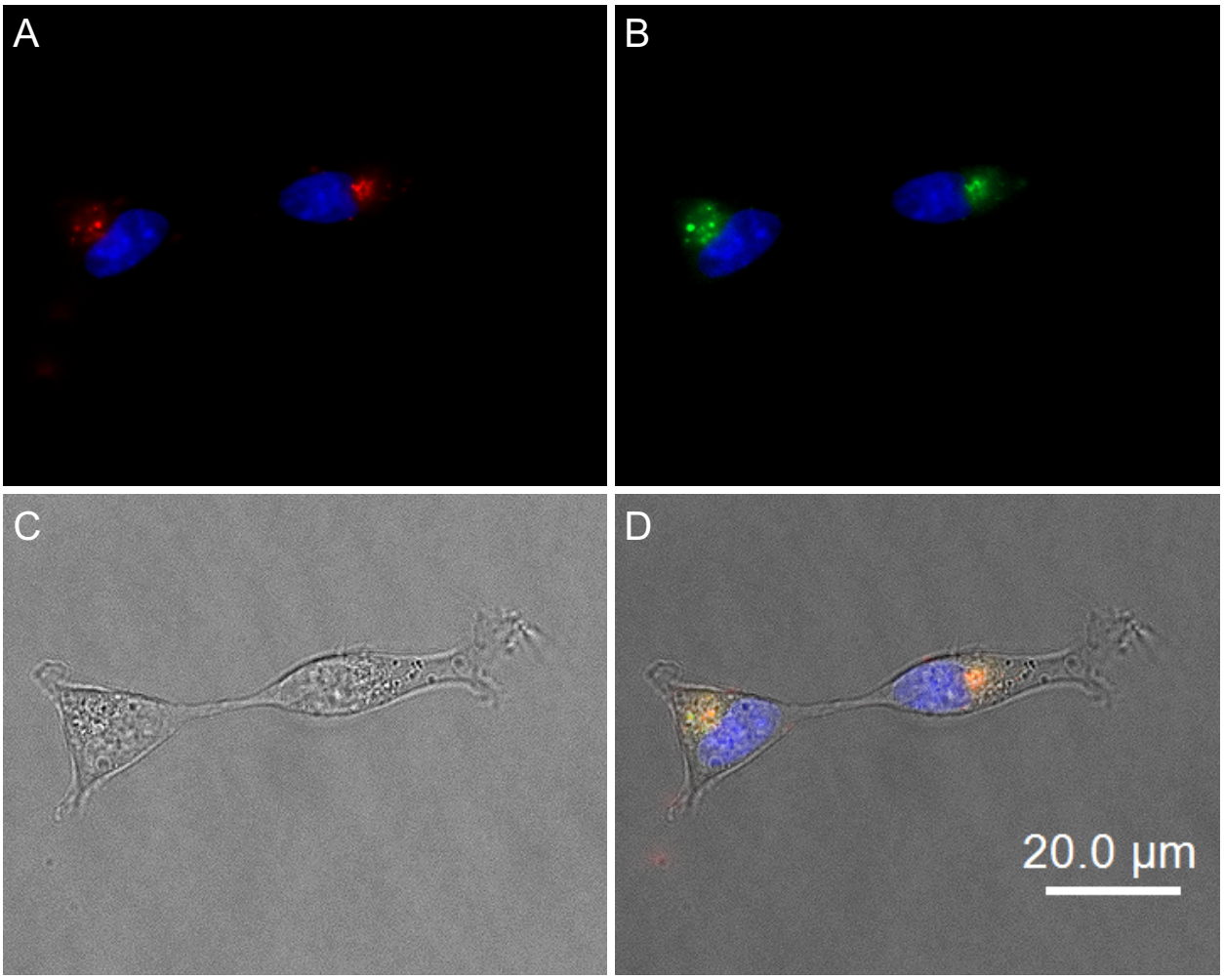

Figure S2.4 Micrographs illustrating intracellular co-localization of 2AT-L-sCy3 and Lysotracker Green in SH-SY5Y cells. **(A)** 2AT-L-sCy3 (red). **(B)** Lysotracker Green (green). **(C)** Brightfield cell image. **(D)** Merged fluorescent images with brightfield image. Cells were incubated with 5 µM 2AT-L-sCy3 and 100 nM Lysotracker Green for 6 h at 37°C, counterstained with Hoechst 33342 nuclear stain (blue), and imaged.

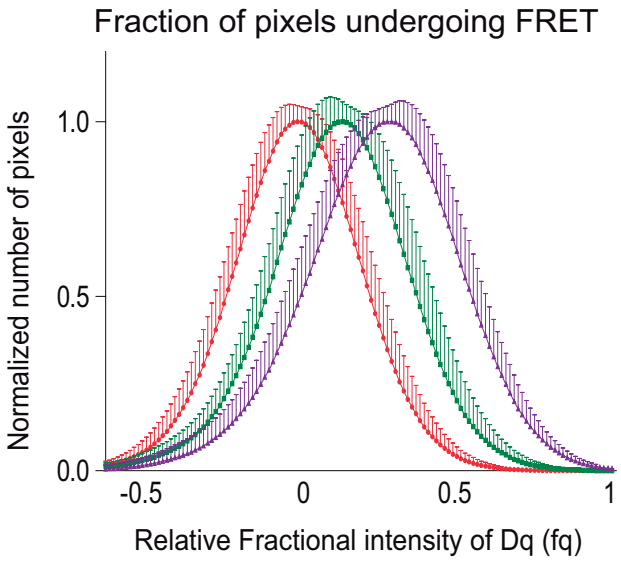

Figure S2.5 Fractional intensity of D_q (f_q) in all conditions. Fractional intensity is related to the molar fraction and the quantum yield. A shift to increasing values along the x axis is representative of an increase of the fraction of donor undergoing FRET.

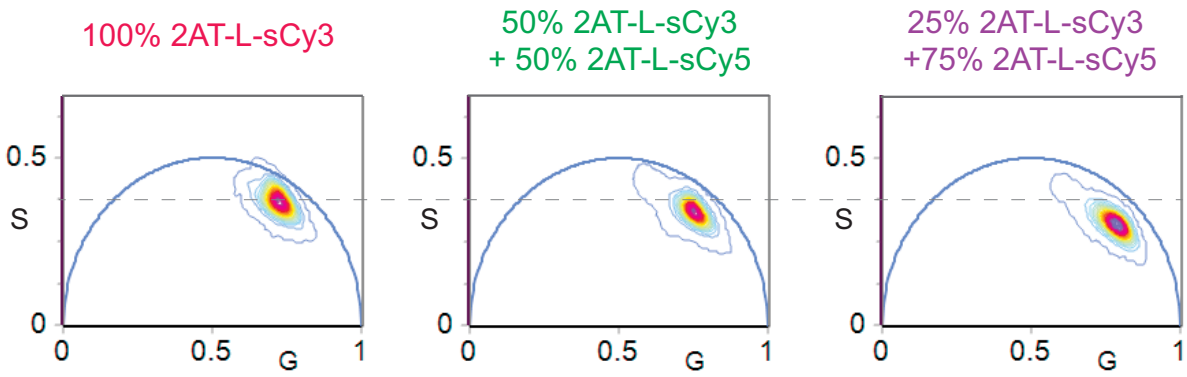

Figure S2.6 Phasor plot of every pixel from all images in each set of conditions creating a cloud. The red color indicates an increased density of pixels and blue-shifted colors indicate fewer pixels in that position on the phasor plot. Clouds between conditions shift, indicating FRET.

General Information[1]

All Fmoc-protected amino acids including the unnatural amino acid, Boc-ornithine(Fmoc)-OH, were purchased from Chem-Impex or Anaspec. 2-Chlorotrityl chloride resin was purchased from Chem-Impex. Trifluoroacetic acid (TFA), and HPLC grade acetonitrile (MeCN) were purchased from Fischer Scientific. Water was purified to 18 MΩ with a ThermoFisher Barnstead Nanopure water purification system. All other solvents and chemicals were purchased from Alfa Aesar and Sigma Aldrich. All amino acids, resins, solvents, and chemicals were used as received, with the exception that dichloromethane (DCM) and *N,N*-dimethylformamide (DMF) were dried by passage through dry alumina under argon. Analytical HPLC chromatograms were obtained using an Agilent 1260 Infinity II HPLC equipped with Phenomenex bioZen C18 column (150 mm × 4.6 mm, 2.6 μm particle size). HPLC grade acetonitrile (ACN) and 18 MΩ deionized water, each containing 0.1% trifluoroacetic acid, were used as the mobile phase running at 1 mL/min flow rate. Peaks for peptides without fluorophores were detected at 214 nm. Sulfo-cyanine3 labeled peptides were detected at 548 nm and sulfo-cyanine5 labeled peptides were detected at 646 nm in addition to 214 nm. All peptides were monitored using the provided HPLC OpenLAB software.

Semi-preparative scale purification of fluorescently labeled peptides was done using an Agilent Zorbax 300SB-C18 semi-preparative column (9.4 mm x 250 mm, 5 μm particle size) with a ZORBAX 300SB-C3 preparative guard column (9.4 x 15 mm) on a Rainin Dynamax HPLC with a flow rate of 5.0 mL/min. The C18 column and the guard column were heated to 60 °C in a water bath. Elution was monitored at 214 nm with the accompanying DA Rainin HPLC software. Liquid chromatography-mass spectrometry was performed using a Waters Xevo XS UPLC-QTOF. Spectra were analyzed using the accompanying Waters MassLynx software.

Synthesis of the Macrocyclic Peptide 2AM-L and 2AT-L

Synthesis of peptide 2AM-L and 2AT-L followed the previously outlined procedure of 4AM-L and 4AT-L.[2]

Synthesis of fluorescently labeled 2AT-L

2AT-L is labeled by treatment with 0.05 molar equivalents of sulfo-cyanine3 (sCy3) or sulfo-cyanine5 (sCy5) NHS esters as follows: 5 mg of NHS-ester sulfo-cyanine3 and NHS-ester sulfo-cyanine5 were purchased from Lumiprobe. The powder was dissolved in water and was transferred into Eppendorf in 17 μg aliquots of fluorophore. The tubes were immediately frozen and then lyophilized. A 75 mM sodium carbonate buffer solution was prepared gravimetrically and the pH was adjusted to 9.6. A 10 mg/mL solution of 2AT-L was prepared gravimetrically by dissolving the lyophilized trimer in the appropriate amount of 18 MΩ deionized water. 300 μL of 10 mg/mL stock solution was added to a fresh Eppendorf tube. 700 μL of carbonate buffer solution was added to the Eppendorf tube for a total volume of 1 mL. Lyophilized fluorophore was added to the reaction mixture by transferring 100 μL of solution into one aliquot of lyophilized fluorophore. The fluorophore was dissolved and the solution was transferred back to the larger reaction mixture. The reaction mixture was protected from light with black felt and rocked gently for 1 h. After 1 h, the reaction mixture was directly injected onto an RP-HPLC.

Semi-preparative scale purification of the fluorescently labeled peptides was done using an Agilent Zorbax 300SB-C18 semi-preparative column (9.4 mm x 250 mm, 5 μm particle size) with a ZORBAX 300SB-C3 preparative guard column (9.4 x 15 mm) on a Rainin Dynamax HPLC with a flow rate of 5.0 mL/min. The C18 column and the guard column were heated to 60 °C in a water bath and were eluted over a gradient of 20–45% MeCN over 80 min. Elution was

monitored at 214 nm with the accompanying DA Rainin HPLC software. Liquid chromatography-mass spectrometry was performed using a Waters Xevo XS UPLC-QTOF. Spectra were analyzed using the accompanying Waters MassLynx software. Pure fractions were concentrated by rotary evaporation and lyophilized. The purified labeled trimers were characterized by analytical HPLC and liquid chromatography-mass spectrometry. The fractions containing unlabeled 2AT-L were concentrated for subsequent use.

Stock solutions of fluorescently labeled analogues were prepared spectrophotometrically. Lyophilized peptide was dissolved in 18 MΩ deionized water and the absorbance was measured using the λ_{max} of the respective fluorophore (2AT-L-sCy3 λ_{max}= 548 nm, 2AT-L-sCy5 λ_{max}= 646 nm). The published molar extinction coefficients were used to calculate sample concentration. A typical synthesis yielded approximately 150 µL of 1 mg/mL solution. [Labeling 3 mg of trimer by this procedure typically permits isolation of ca. 150 µg of singly-labeled trimer 2AT-L-sCy3 or 2AT-L-sCy5 as the TFA salt.]

SDS-PAGE[3]

Solutions of the unlabeled peptides were prepared gravimetrically by dissolving the lyophilized peptide in the appropriate amount of 18 MΩ deionized water to achieve a 10 mg/mL stock. Stock solutions of the fluorescently labeled peptides were prepared and concentrations determined spectrophotometrically as described above. Stock solutions of all peptides were diluted with 18 MΩ deionized water to create 50 µM sample solutions.1 µL of 6X SDS-PAGE sample loading buffer (G Biosciences) was added per 5 µL sample solution to create working solutions. A 5 µL aliquot of each working solution was run on a 16% polyacrylamide gel with a 4% stacking polyacrylamide gel. The gel was run at a constant 60 volts for approximately 4 h.

Reagents and gels for Tricine SDS-PAGE were prepared according to recipes and procedures detailed in Schägger, H. *Nat. Protoc*. **2006**, *1*, 16–22.[4]

Prior to silver staining, a fluorescence image of the gel was obtained using a Gel Doc XR+ Gel Documentation System (BioRad) in the Cy3 and Cy5 channels. Staining with silver nitrate was then used to visualize the peptides in the gel. Reagents for silver staining were prepared according to procedures detailed in Simpson, R. J. *Cold Spring Harb. Protoc.* **2007**.[5] The gel was then silver stained following the procedures previously described.[3]

Steady-state FRET experiments

Freshly prepared stock solutions of fluorescently labeled trimer analogues were used to prepare samples. Each sample ratio was prepared immediately prior to analysis. Samples of 2AT-L-sCy3 and 2AT-L-sCy5 were prepared to a final volume of 150 μL at a total concentration of 5 μM in the following ratios: 100:0, 80:20, 60:40, 50:50, 40:60, 20:80, 0:100. Samples were prepared in Eppendorf tubes and transferred to a 10 mm quartz sub-micro fluorometer cell (Starna) for analysis. An Agilent Cary Eclipse Fluorescence Spectrophotometer was used to excite trimer mixtures at 490 nm record emission spectra. Emission was collected from 555 nm to 750 nm with a slit width of 5 nm. Sample emission at 662 nm (maximum emission of sCy5) was selected to graph emission output.

Native IM-MS

Solution of unlabeled trimer was prepared gravimetrically by dissolving the lyophilized peptide in the appropriate amount of 18 MΩ deionized water to achieve a 10 mg/mL stock. Stock solutions of the fluorescently labeled peptides were prepared and concentrations determined

spectrophotometrically as described previously. The stock solutions were diluted to 40 μM in 400 mM ammonium acetate immediately before each mass spectrometric experiment. A Waters SELECT SERIES Cyclic Ion Mobility Spectrometry System[6] (cIMS) was used to conduct mass spectrometry analysis. Samples were ionized using nanoelectrospray ionization (nano-ESI). Nano-ESI glass capillary tips were pulled in-house using a Sutter Instruments P-97 micropipette tip puller (Novato, CA). When performing experiments on the cIMS, the cIMS was tuned as follows: capillary voltage, 0.4 to 0.6 kV; cone voltage, 20 V; source temperature, 25 ℃; trap CE, 4 V; transfer CE, 4 V; trap and transfer gas, N_2 at 7.0 mL/min; IMS pressure, 1.8 mbar; TW static height, 22 V; TW velocity, 375 m/s; pushes per bin, 2.

Cell Culture

SH-SY5Y neuroblastoma cell cultures (ATCC® CRL-2266™) were maintained in 1:1 mixture of Dubelcco's modified Eagle medium and Ham's F12 (DMEM:F12) medium supplemented with 10% heat-inactivated fetal bovine serum (FBS), 100 U/mL penicillin and 100 μg/mL streptomycin at pH 7.4 in a humidified 5% CO_2 atmosphere at 37 °C using a Fischer Scientific Forma Series 3 Water Jacketed CO_2 Incubator. All experiments were performed using ca. 60–80% confluent cells on passages ranging from 2–10.

Fluorescence Microscopy[7]

Cell Preparation, Treatment, and Imaging. SH-SY5Y cells were plated in an Ibidi μ-Slide 8 Well Chamber Slide (Ibidi catalog number 80826) at 80,000 cells per well. Cells were incubated in 500 μL of a 1:1 mixture of DMEM:F12 media supplemented with 10% fetal bovine serum, 100 U/mL penicillin, and 100 μg/mL streptomycin at 37 °C in a 5% CO_2 atmosphere and

allowed to adhere to the bottom of the slide for 48 hours. A solution of 100 nM of lysotracker-containing media was prepared by adding Lysotracker Green DND-26 (ThermoFischer) into serum-free, phenol red-free 1:1 DMEM/F12 media. Solutions of 2AT-L-sCy3, 2AT-L-sCy5, or both were prepared to a final volume of 200 μL and a final concentration of 5 μM in either serum-free, phenol red-free 1:1 DMEM/F12 media or serum-free, phenol red-free 1:1 DMEM/F12 media with Lysotracker Green DND-26.

After cells were incubated for 48 hours, the media was removed and replaced with solutions with fluorescently labeled analogues with and without Lysotracker Green DND-26. Control wells were treated with media containing no peptide. The slide was incubated in the microscope chamber for 6 hours. media was removed from the well slide containing the cells and replaced with 200 μL of 1 μg/mL Hoechst 33342 in serum-free, phenol red-free 1:1 DMEM:F12 media. After 30 minutes, the Hoechst-containing media was removed and replaced with 200 μL of serum-free, phenol red-free 1:1 DMEM:F12 media. The cells were imaged using a Keyence BZ-X810 fluorescence microscope. Images were collected with a 60x oil immersion objective lens. Micrographs of treated cells were recorded using the DAPI filter cube [excitation wavelength = 350/50 nm (325–375 nm) and emission wavelength = 460/50 nm (435–485nm)] for Hoechst nuclear marker, the Cy3 filter cube [excitation wavelength = 545/25 nm (532.5–557.5 nm) and emission wavelength = 605/70 nm (570–640 nm)] for 2AT-L-sCy3, the Cy5 filter cube [excitation wavelength = 620/60 nm (590–650 nm) and emission wavelength = 700/75 nm (662.5–737.5 nm)] for 2AT-L-sCy5, and the GFP filter cube [excitation wavelength = 470/40 nm (450–490 nm) and emission wavelength = 525/50 nm (500–550 nm)] for Lysotracker Green DND-26 (ThermoFischer).The image brightness of the channels was adjusted using BZ-X810 Analyzer software.

FLIM-FRET

Sample Preparation and Imaging. SH-SY5Y cells were plated in an Ibidi µ-Slide 8 Well Chamber Slide (Ibidi catalog number 80826) at 80,000 cells per well. Cells were incubated in 500 µL of a 1:1 mixture of DMEM:F12 media supplemented with 10% fetal bovine serum, 100 U/mL penicillin, and 100 µg/mL streptomycin at 37 °C in a 5% CO_2 atmosphere and allowed to adhere to the bottom of the slide for 48 hours. After 48 h, media was removed from the Ibidi µ-Slide 8 Well Chamber Slide and replaced with 200 µL of 5 µM fluorescently labeled trimer solutions prepared in serum-free, phenol red-free DMEM:F12. Cells were incubated with peptide solutions for 6 h. Cells were incubated with the following ratios of 2AT-L-sCy3 and 2AT-L-sCy5: 100:0 (5 µM:0), 50:50 (2.5 µM: 2.5 µM), and 25:75 (1.25 µM: 3.75 µM). After 6 h, the media was removed and replaced with 200 µL serum-free, phenol red-free DMEM:F12 media and the cells were imaged.

All FLIM-FRET data was acquired using a two-channel ISS-ALBA5 confocal microscope equipped with a white laser source and acusto-optic tunable filter (NKT SuperK EXTREME, SuperK SELECT), and a digital frequency domain setup the ISS A320 FastFLIM acquisition unit for lifetime measurement. The repetition frequency of the laser is 78 MHz. A 60x oil immersion objective of 1.2 NA (Olympus) was used for all experiments. Intensity and lifetime data were simultaneously acquired by raster-scanning the one-photon laser. sCy3 was excited at 490 nm laser selected from the white laser, and a 488/25 dichroic mirror was used to separate the fluorescence signal from the laser light. The donor and acceptor signals were split between two avalanche photo-diodes detectors (Excelitas Technologies) using a long-pass 640 nm dichroic mirror. Additionally, bandwidth filters were placed in front of each detector: for

2AT-L-sCy3 a 575/50 (donor channel) and for 2AT-L-sCy5 a 679/41 (acceptor channel). Only the donor channel was used to analyze FLIM-FRET data. The acceptor channel was used only to obtain intensity images to check the presence of sCy5. The pixel frame size was set to 256, pixel size of 0.097 μm, and the pixel dwell time was set to 16 μs/pixel. For each FLIM experiment, 20 frames were integrated. All images accumulated contained from 0 to 2000 photons per pixel. Calibration of the system and phasor plot space was performed by measuring coumarin 6 (in ethanol), which has a known single-exponential lifetime of 2.4 ns.

Data Processing-Phasor Transformation. The FLIM data was collected and processed using the SimFCS software developed at the Laboratory for Fluorescence Dynamics (LFD) (available at https://www.lfd.uci.edu/). The FLIM data was analyzed using the phasor approach.[9–12] The intensity decays collected from each pixel of the image was transformed to the phasor plot using a fast Fourier transformation. The sine and cosine components are plotted against each other in the phasor plot, where the intensity decay from each pixel is transformed to a coordinate value, expressed by G (cosine) and S (sine). The uncertainty and hence the spread of the phasors position depends on the number of counts in each pixel. A background correction of 40 counts/pixel was employed using the intensity histogram. The extent of the autofluorescence signal was determined was determined by measuring cells without the presence of fluorophores using the same cell preparation as that of the treated samples and was ~ 3% of the total signal.

The G and S value for the phasor position corresponding to every single cell (each FLIM image) was determined from the center of the distribution of the phasor points from that cell using the method described before.[13] The phasor distribution of the of the donor only cells (unquenched, D_{unq}) were determined using cells incubated with 2AT-L-sCy3. The occurrence of FRET was analyzed in the phasor plot by quantifying the phasor shift occurring between the

donor only and the donor in the presence of acceptor (D_q). The FRET trajectory for the donor is curved as the donor lifetime is gradually quenched by the FRET process. The shape of the FRET trajectory and deviation from the linear combination between the donor only and donor-acceptor phasor positions is dependent on the contribution from background. The measurement of autofluorescence under the same excitation wavelength is required for the calculation of the trajectory.[14]

Each pixel of an image can contain donor only, donor-acceptor, or a combination of different fractions of donor (f_q) and donor-acceptor (f_{unq}). Hence, the resulting phasor appears along the line joining the phasor positions of the donor and donor-acceptor at a distance from D_{unq} that is proportional to the fraction of interacting donors f_q.[15,16] This can become curved if the donor only and donor-acceptor samples have different amount of fractional intensity contribution from the autofluorescence as donor-acceptor sample can be less fluorescent. In our experiments the donor only and donor-acceptor phasor positions were located along a line, not in the curved trajectory, due to the very small amount of autofluorescence and can be expressed as a simple liner combination of D_q and D_{unq} and not a curved trajectory. The fractional intensity of interacting donors f_q was calculated using linear additive properties of phasor plot.[13,16]

Phasor transformation was performed using SimFCS. The fluorescence lifetime decay curve I(t) in every pixel of a FLIM image is transformed into phasor plot coordinates according to:

$$S = \frac{\int_0^T I(t)\sin(n\omega t)dt}{\int_0^T I(t)dt} \qquad \text{(Eq 1)}$$

$$G = \frac{\int_0^T I(t)\cos(n\omega t)\,dt}{\int_0^T I(t)\,dt} \qquad \text{(Eq 2)}$$

where ω is the laser repetition angular frequency (2πf), the harmonic number n represents the integer number of whole cycles the trigonometric function has in the repetition period. T is the repetition frequency of the laser.

If the decay curve is single exponential $I(t) = Ae^{\frac{-t}{\tau}}$, the Eqs. 1 and 2 can be solved to obtain the coordinates of the phasor by:

$$s = \frac{n\omega\tau}{1+(n\omega\tau)^2} \quad \text{(Eq 3)}$$

$$g = \frac{1}{1+(n\omega\tau)^2} \quad \text{(Eq 4)}$$

Combining Eqs. 3 and 4 gives the expression $s_i^2 = g_i - g_i^2$ where the pure decays (single exponential) lie, that is represented by a semi-circle in the phasor plot, which is called "universal circle". A phasor corresponding to a long lifetime will appear close to the (0,0) point, meanwhile one of short lifetime will appear closer to the point (1,0).

If the decay curve is a combination of exponential curves $I(t) = \sum_1^N A_i e^{\frac{-t}{\tau}}$, the coordinates of the phasor plot are the sum of the phasor transformations of the pure components:

$$\sum_1^N f_i s_i = S \quad \text{(Eq 6)}$$

$$\sum_1^N f_i g_i = G \quad \text{(Eq 7)}$$

Upper case $(S\ , G\ )$ are the coordinates of our data points, lower case $(s_i\ , g_i\ )$ are the unknown coordinates of the pure components and f_i their respective photon fractions. The fractions have to add up to unity $\sum_1^N f_i = 1$.

REFERENCES AND NOTES

(1) The chemicals and instruments required for the synthesis of macrocyclic β-sheet peptide 2AM-L and 2AT-L are similar to those used in our laboratory's previous publications. This information was either adapted from or taken verbatim from Kreutzer, A. G.; Yoo, S.; Spencer, R. K.; Nowick, J. S. Stabilization, Assembly, and Toxicity of Trimers Derived from Aβ. *J. Am. Chem. Soc.* **2017**, *139* (2), 966–975. https://doi.org/10.1021/jacs.6b11748.

(2) Haerianardakani, S.; Kreutzer, A. G.; Salveson, P. J.; Samdin, T. D.; Guaglianone, G. E.; Nowick, J. S. Phenylalanine Mutation to Cyclohexylalanine Facilitates Triangular Trimer Formation by β-Hairpins Derived from Aβ. *J. Am. Chem. Soc.* **2020**, *142* (49), 20708–20716. https://doi.org/10.1021/jacs.0c09281.

(3) Peptides were run on SDS-PAGE and silver stained following a protocol similar to those published previously in our laboratory. The procedures were either adapted from or taken verbatim from Kreutzer, A. G.; Yoo, S.; Spencer, R. K.; Nowick, J. S. Stabilization, Assembly, and Toxicity of Trimers Derived from Aβ. *J. Am. Chem. Soc.* **2017**, *139* (2), 966–975. https://doi.org/10.1021/jacs.6b11748.

(4) Schägger, H. Tricine-SDS-PAGE. *Nat. Protoc.* **2006**, *1*, 16–22.

(5) Simpson, R. J. Staining Proteins in Gels with Silver Nitrate. *Cold Spring Harb. Protoc.* **2007** doi: 10.1101/Pdb.Prot4727.

(6) Snyder, D. T.; Jones, B. J.; Lin, Y. F.; Cooper-Shepherd, D. A.; Hewitt, D.; Wildgoose, J.; Brown, J. M.; Langridge, J. I.; Wysocki, V. H. Surface-Induced Dissociation of Protein Complexes on a Cyclic Ion Mobility Spectrometer. *Analyst* **2021**, *146* (22), 6861–6873. https://doi.org/10.1039/d1an01407b.

(7) Fluorescently labeled 2AT-L analogues were imaged following a protocol similar to those published previously by our laboratory. This information was either adapted from or taken verbatim from Zhang, S.; Guaglianone, G.; Morris, M. A.; Yoo, S.; Howitz, W. J.; Xing, L.; Zheng, J. G.; Jusuf, H.; Huizar, G.; Lin, J.; Kreutzer, A. G.; Nowick, J. S. Expression of N-Terminal Cysteine Aβ42 and Conjugation to Generate Fluorescent and Biotinylated Aβ42. *Biochemistry* **2021**, *60* (15), 1191–1200. https://doi.org/10.1021/acs.biochem.1c00105.

(8) Zhang, S.; Guaglianone, G.; Morris, M. A.; Yoo, S.; Howitz, W. J.; Xing, L.; Zheng, J. G.; Jusuf, H.; Huizar, G.; Lin, J.; Kreutzer, A. G.; Nowick, J. S. Expression of N-Terminal Cysteine Aβ42and Conjugation to Generate Fluorescent and Biotinylated Aβ42. *Biochemistry* **2021**, *60* (15), 1191–1200. https://doi.org/10.1021/acs.biochem.1c00105.

(9) Digman, M. A.; Caiolfa, V. R.; Zamai, M.; Gratton, E. The Phasor Approach to Fluorescence Lifetime Imaging Analysis. *Biophys. J.* **2008**, *94* (2), 14–16. https://doi.org/10.1529/biophysj.107.120154.

(10) Malacrida, L.; Ranjit, S.; Jameson, D. M.; Gratton, E. The Phasor Plot: A Universal Circle to Advance Fluorescence Lifetime Analysis and Interpretation. *Annu. Rev. Biophys.* **2021**, *50*, 575–593. https://doi.org/10.1146/annurev-biophys-062920-063631.

(11) Jameson, D. M.; Gratton, E.; Hall, R. D. The Measurement and Analysis of Heterogeneous Emissions by Multifrequency Phase and Modulation Fluorometry. *Appl. Spectrosc. Rev.* **1984**, *20* (1), 55–106. https://doi.org/10.1080/05704928408081716.

(12) Clayton, A. H. A.; Hanley, Q. S.; Verveer, P. J. Graphical Representation and Multicomponent Analysis of Single-Frequency Fluorescence Lifetime Imaging Microscopy Data. *J. Microsc.* **2004**, *213* (1), 1–5. https://doi.org/10.1111/j.1365-

2818.2004.01265.x.

(13) Ranjit, S.; Malacrida, L.; Jameson, D. M.; Gratton, E. Fit-Free Analysis of Fluorescence Lifetime Imaging Data Using the Phasor Approach. *Nat. Protoc.* **2018**, *13* (9), 1979–2004. https://doi.org/10.1038/s41596-018-0026-5.

(14) Hinde, E.; Cardarelli, F.; Digman, M. A.; Gratton, E. Changes in Chromatin Compaction during the Cell Cycle Revealed by Micrometer-Scale Measurement of Molecular Flow in the Nucleus. *Biophys. J.* **2012**, *102* (3), 691–697. https://doi.org/10.1016/j.bpj.2011.11.4026.

(15) Giral, H.; Lanzano, L.; Caldas, Y.; Blaine, J.; Verlander, J. W.; Lei, T.; Gratton, E.; Levi, M. Role of PDZK1 Protein in Apical Membrane Expression of Renal Sodium-Coupled Phosphate Transporters. *J. Biol. Chem.* **2011**, *286* (17), 15032–15042. https://doi.org/10.1074/jbc.M110.199752.

(16) Torrado, B.; Malacrida, L.; Ranjit, S. Linear Combination Properties of the Phasor Space in Fluorescence Imaging. *Sensors* **2022**, *22* (3). https://doi.org/10.3390/s22030999.

Characterization Data

Characterization of peptide 2AM-L

Analytical HPLC trace

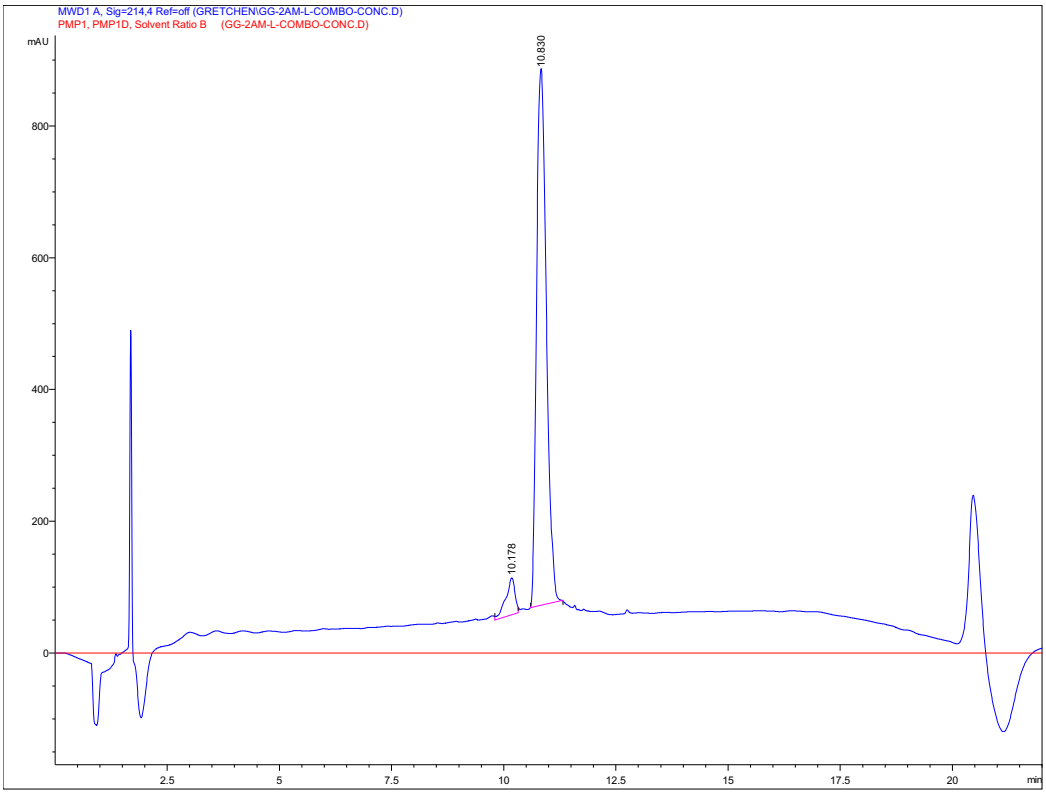

Signal 1: MWD1 A, Sig=214,4 Ref=off

Peak #	RetTime [min]	Type	Width [min]	Area [mAU*s]	Height [mAU]	Area %
1	10.178	MM	0.2374	795.36218	55.83872	6.0593
2	10.830	MM	0.2522	1.23309e4	814.92358	93.9407

Mass spectrum of peptide 2AM-L

Calculated $[M+H]^+$ of peptide 2AM-L: 2173.24

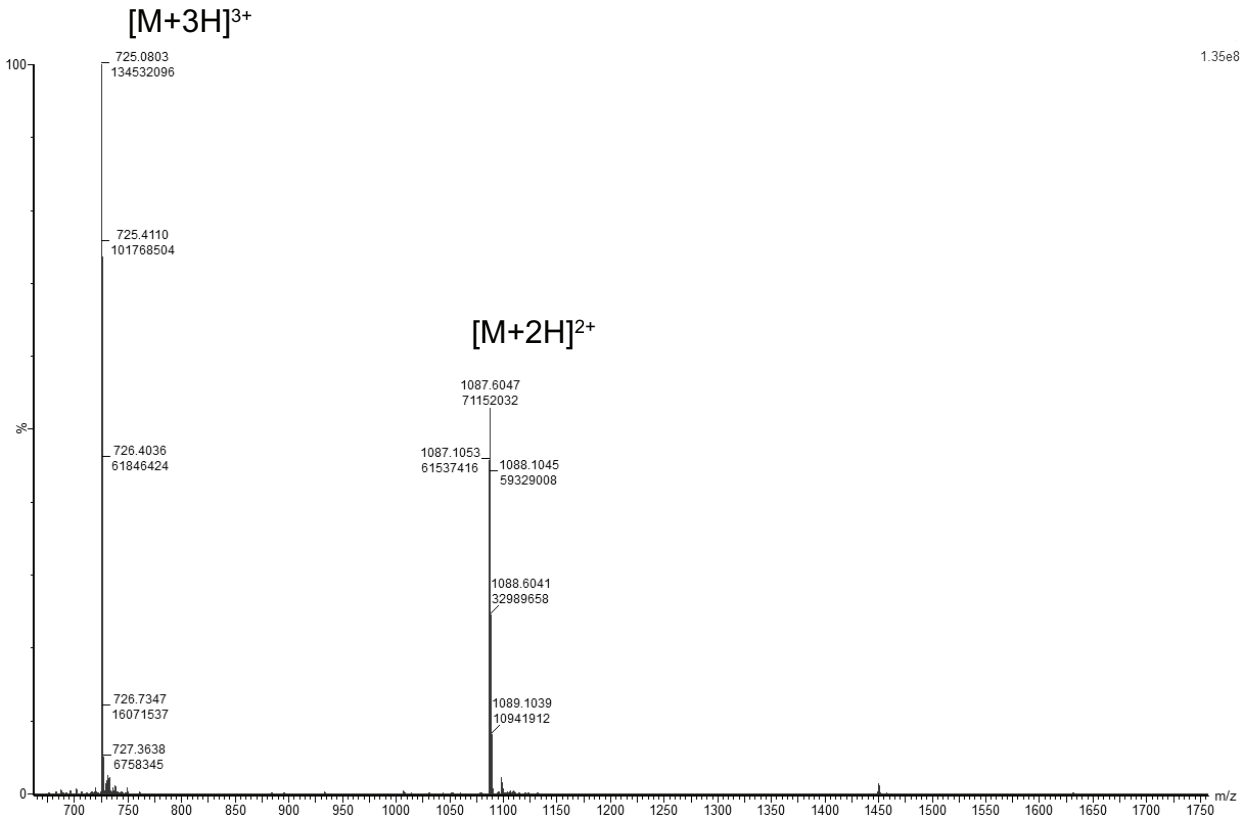

Expansion mass spectrum of peptide 2AM-L

Calculated $[M+H]^+$ of peptide 2AM-L: 2173.24

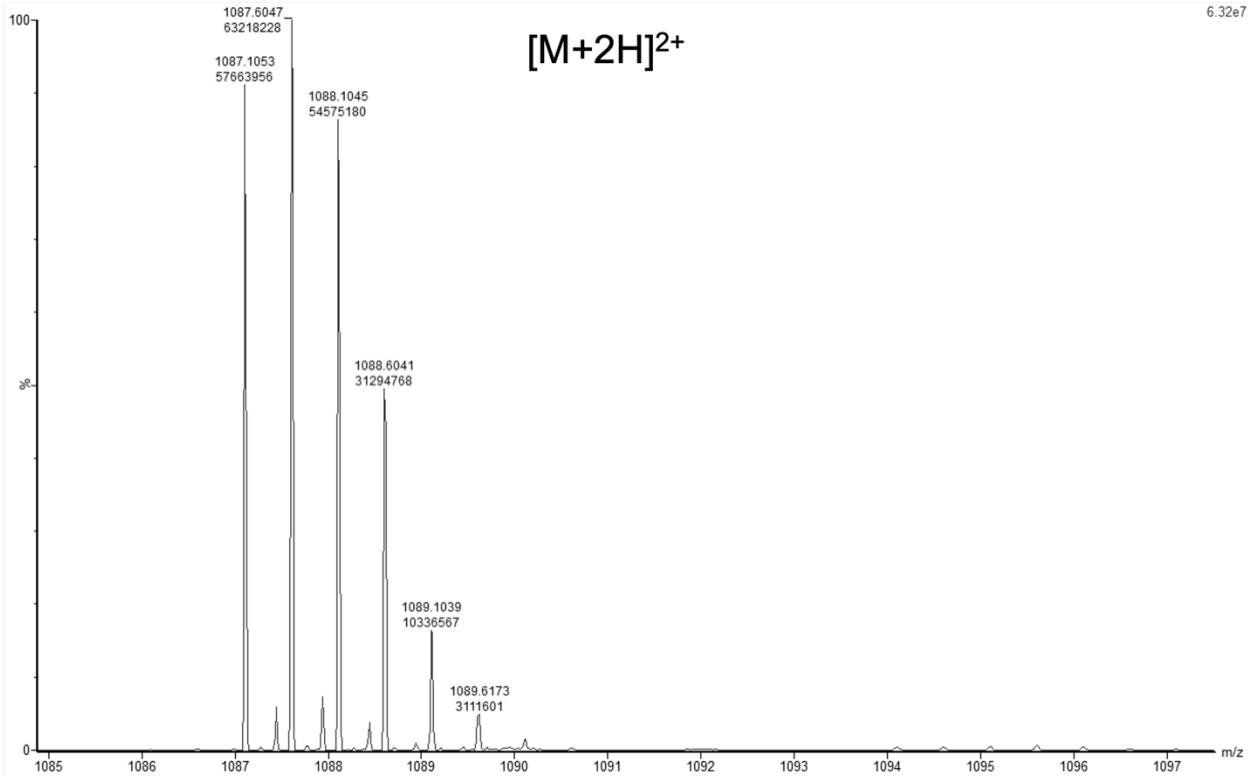

Expansion mass spectrum of peptide 2AM-L

Calculated $[M+H]^+$ of peptide 2AM-L: 2173.24

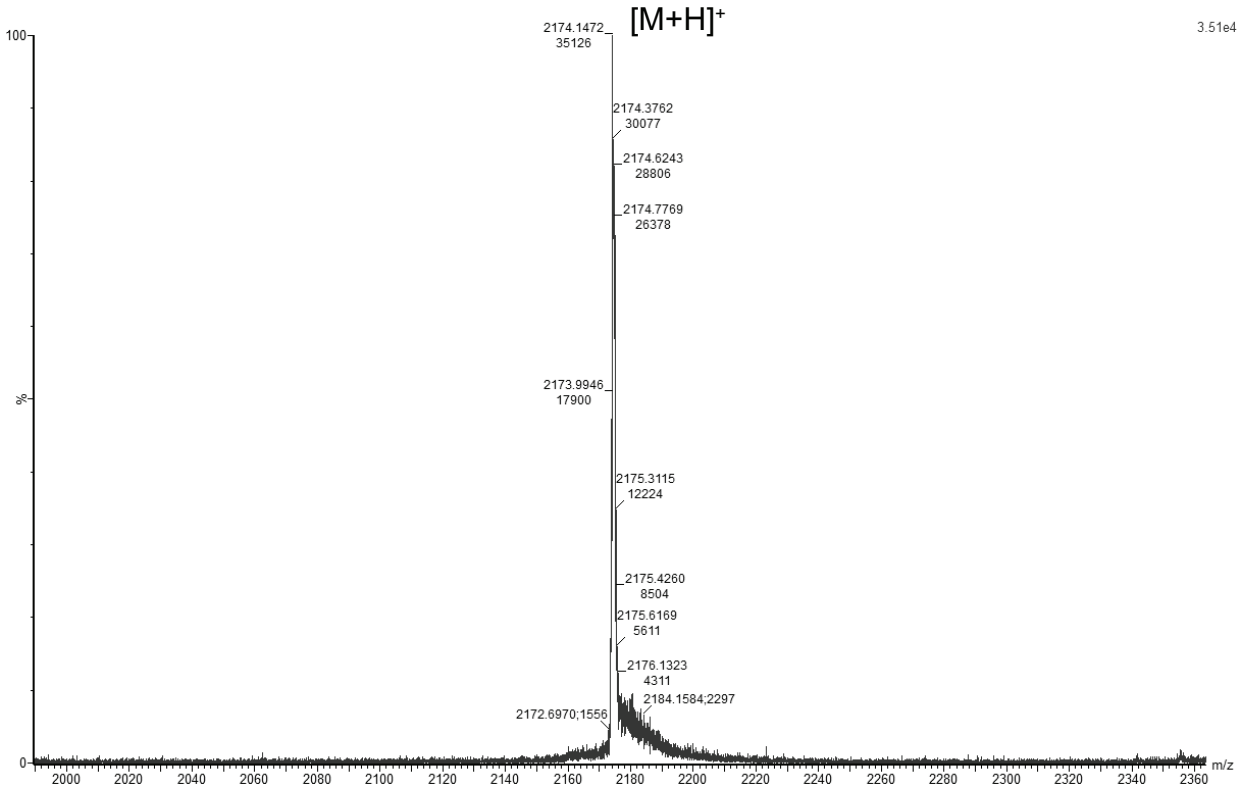

Characterization of peptide 2AM-L_{CC}

Analytical HPLC trace

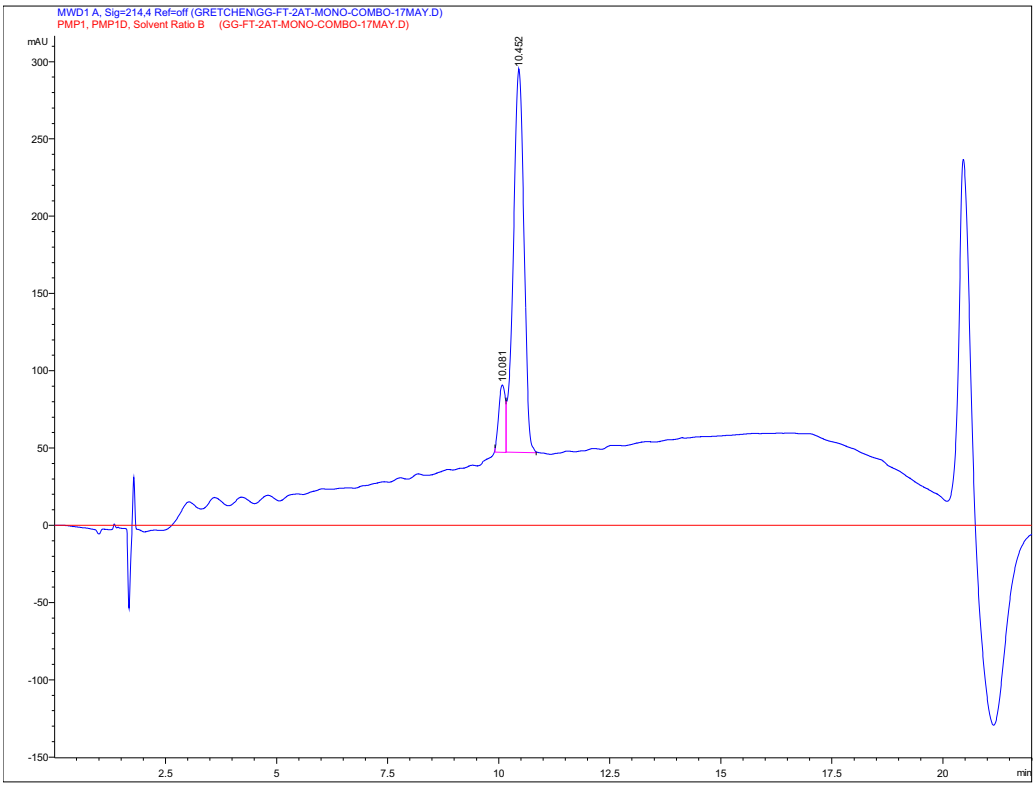

Signal 1: MWD1 A, Sig=214,4 Ref=off

Peak #	RetTime [min]	Type	Width [min]	Area [mAU*s]	Height [mAU]	Area %
1	10.081	MM	0.1710	445.97171	43.47296	9.7557
2	10.452	MM	0.2770	4125.44141	248.21205	90.2443

Mass spectrum of peptide 2AM-L_{CC}

Calculated $[M+H]^+$ of peptide 2AM-L_{CC}: 2195.14

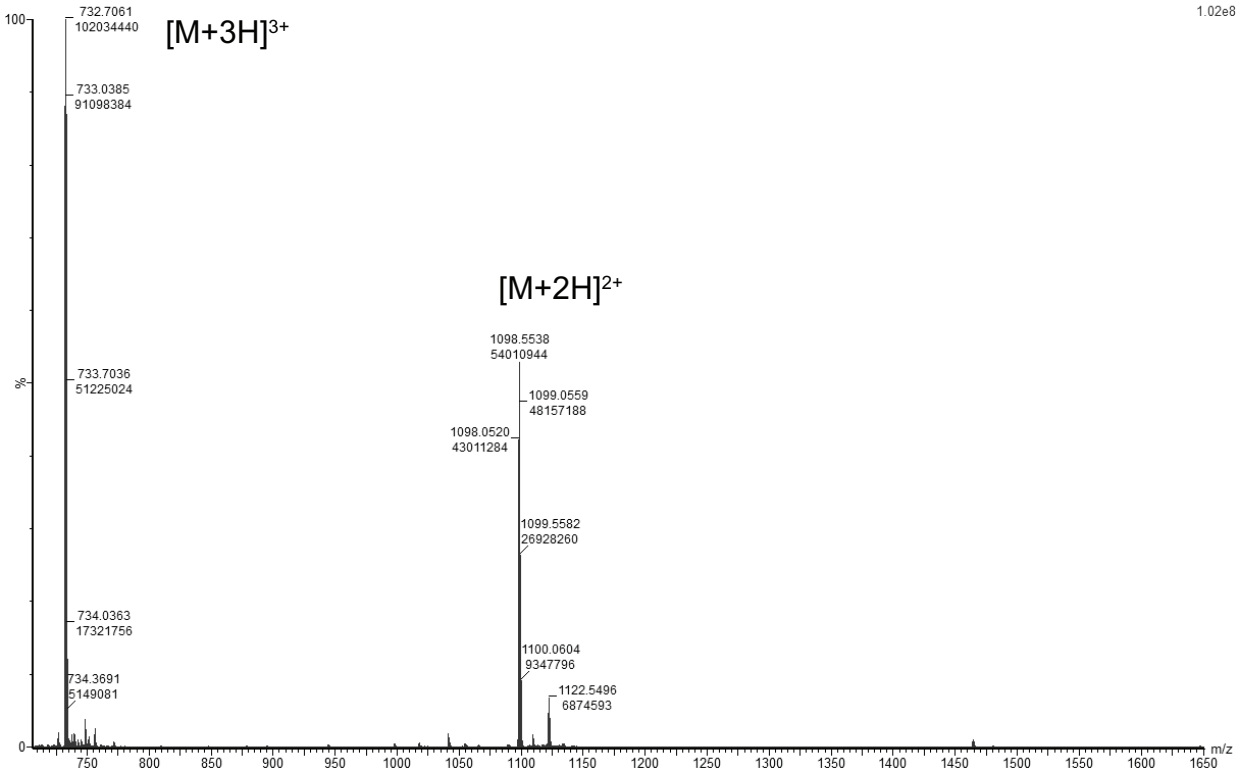

Expansion mass spectrum of peptide 2AM-L_{CC}

Calculated $[M+H]^+$ of peptide 2AM-L_{CC}: 2195.14

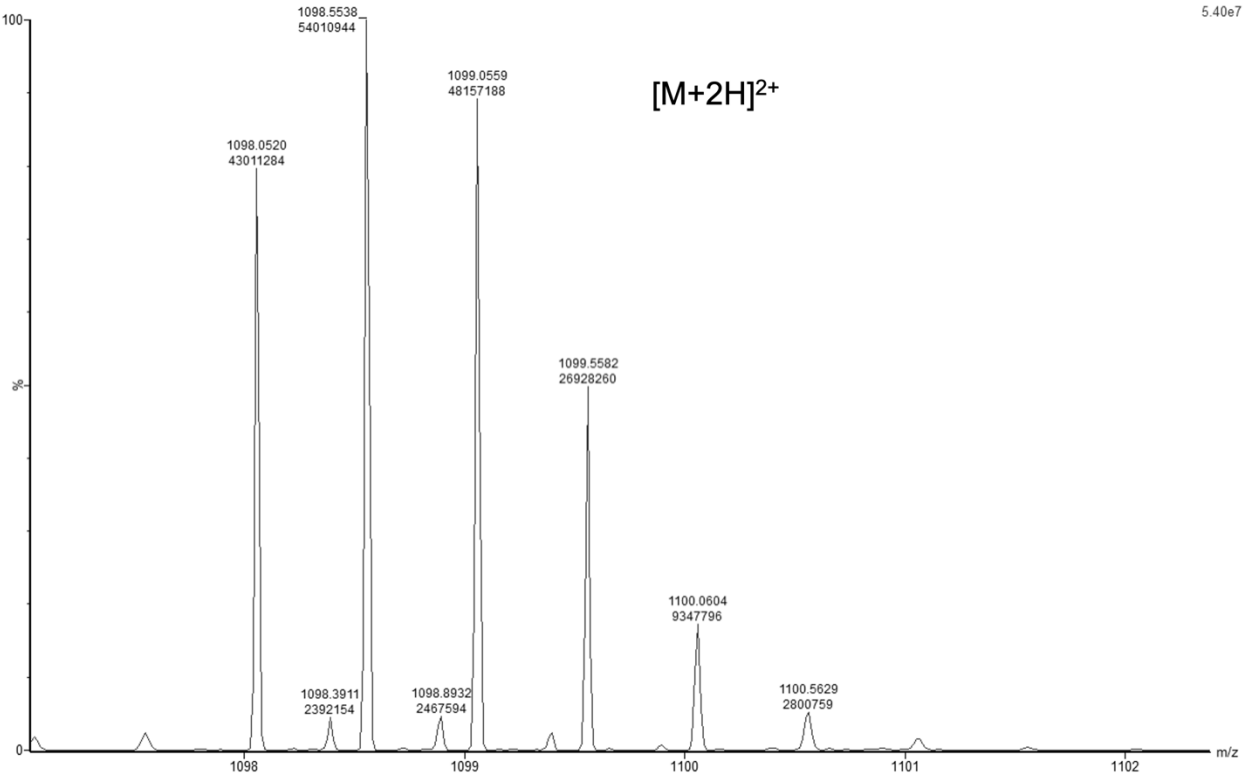

Expansion mass spectrum of peptide 2AM-L_{CC}

Calculated $[M+H]^+$ of peptide 2AM-L_{CC}: 2195.14

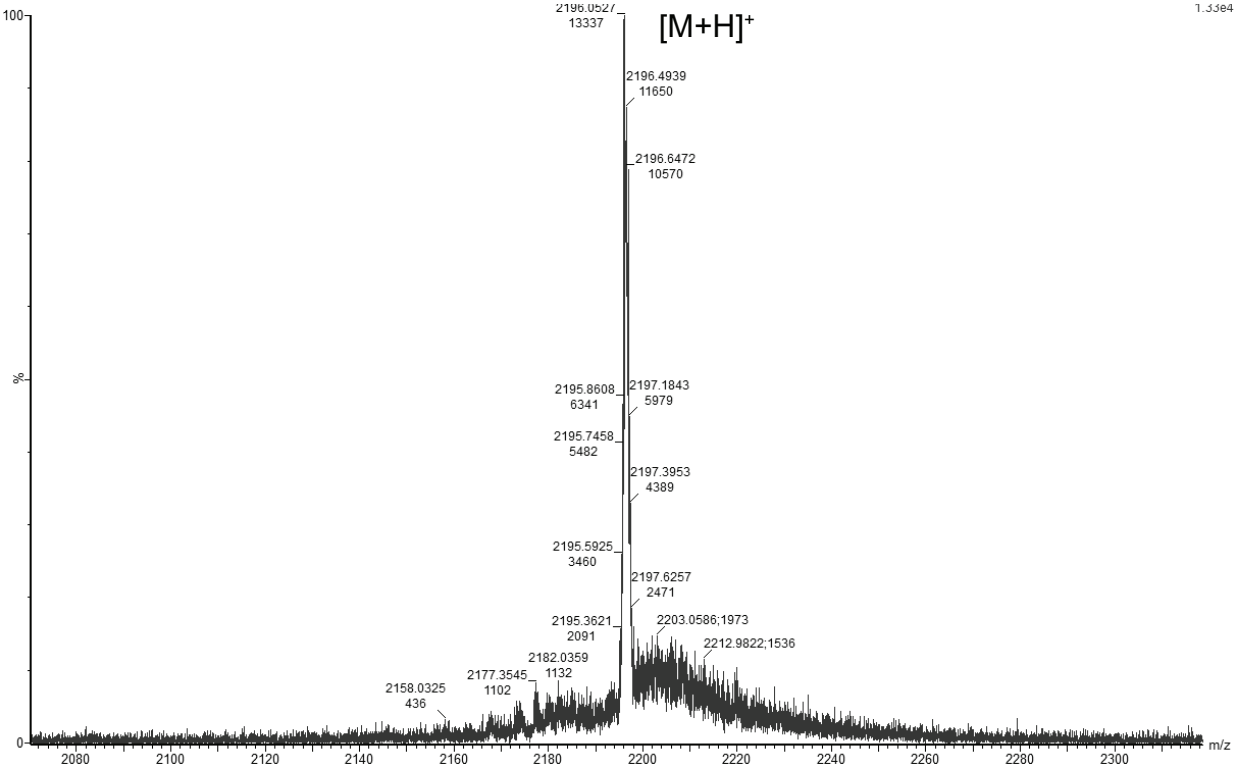

Characterization of trimer 2AT-L

Analytical HPLC trace

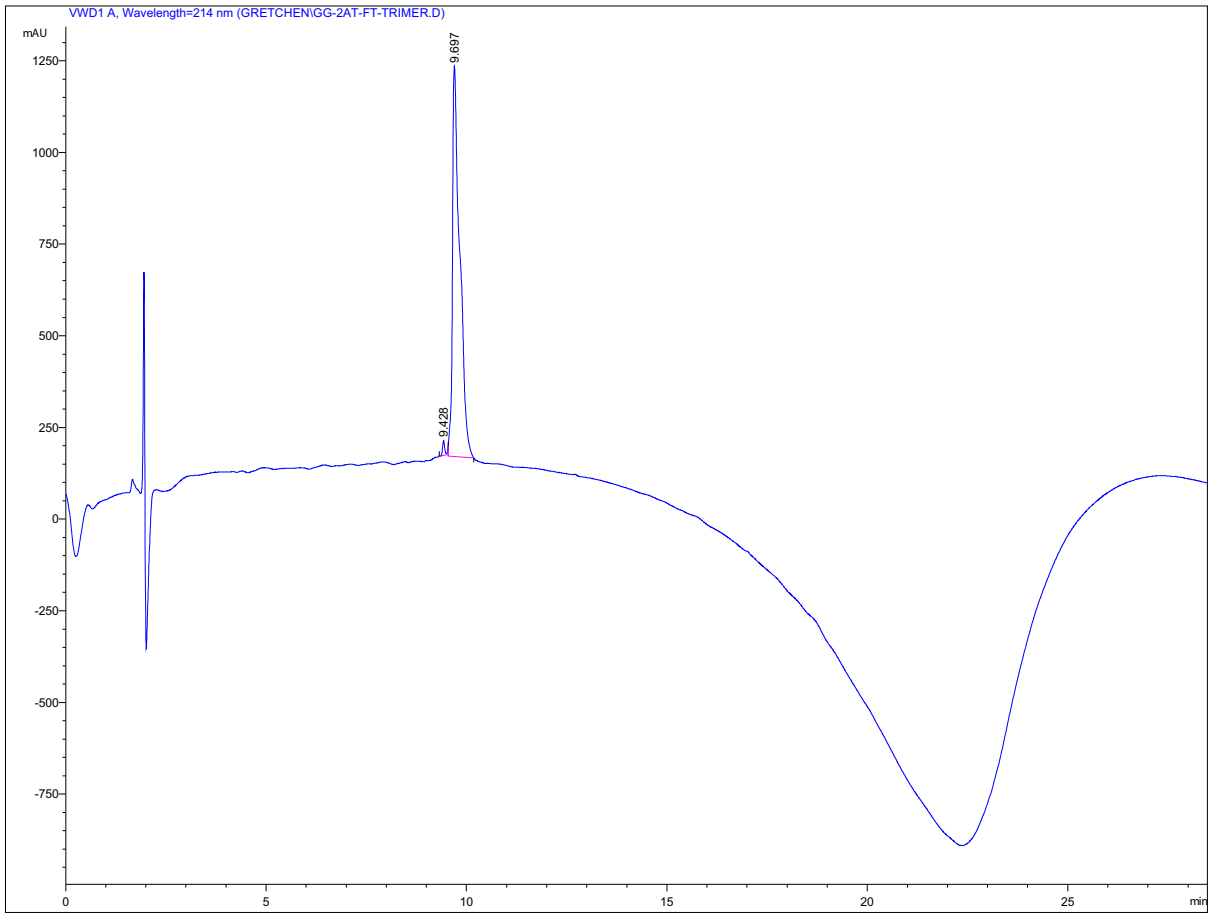

Signal 1: VWD1 A, Wavelength=214 nm

Peak #	RetTime [min]	Type	Width [min]	Area mAU *s	Height [mAU]	Area %
1	9.428	MM	0.0706	171.36655	40.45287	1.2561
2	9.697	MM	0.2106	1.34710e4	1066.05396	98.7439

Mass spectrum of trimer 2AT-L

Calculated $[M+H]^+$ of trimer 2AT-L: 6577.34

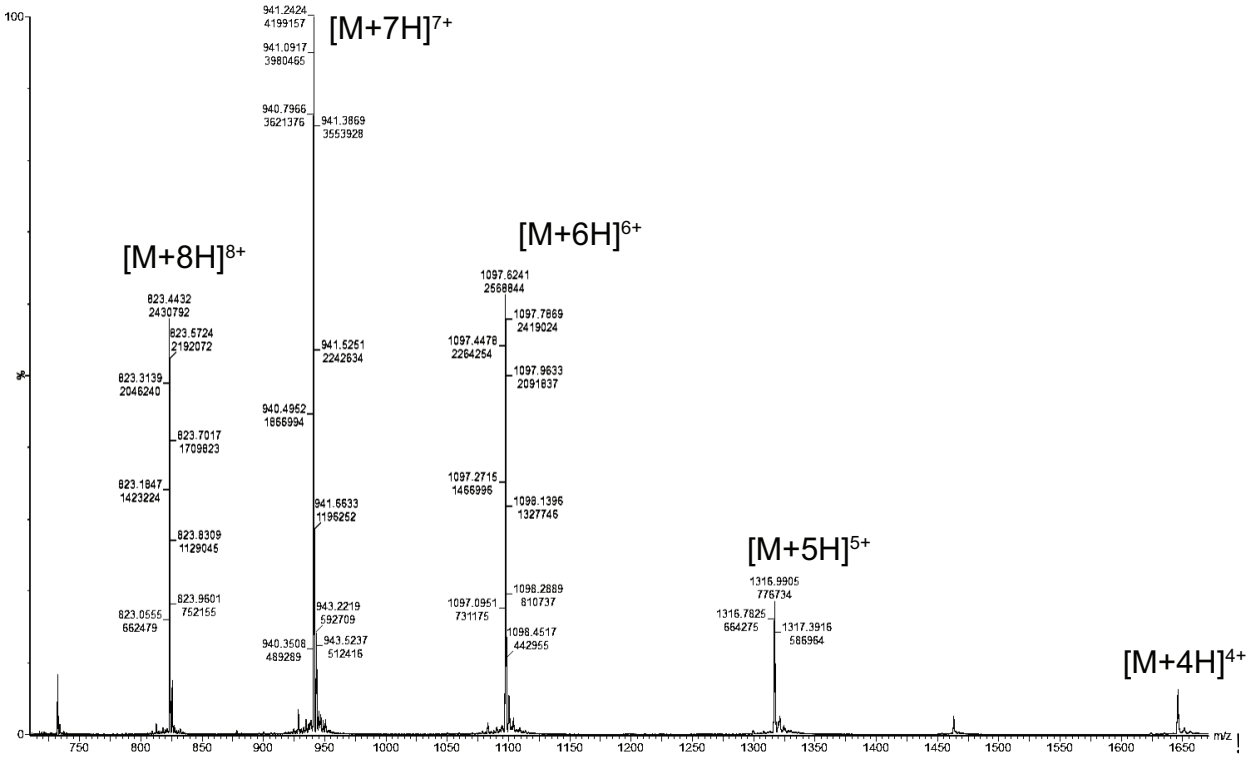

Expansion mass spectrum of trimer 2AT-L

Calculated $[M+H]^+$ of trimer 2AT-L: 6577.34

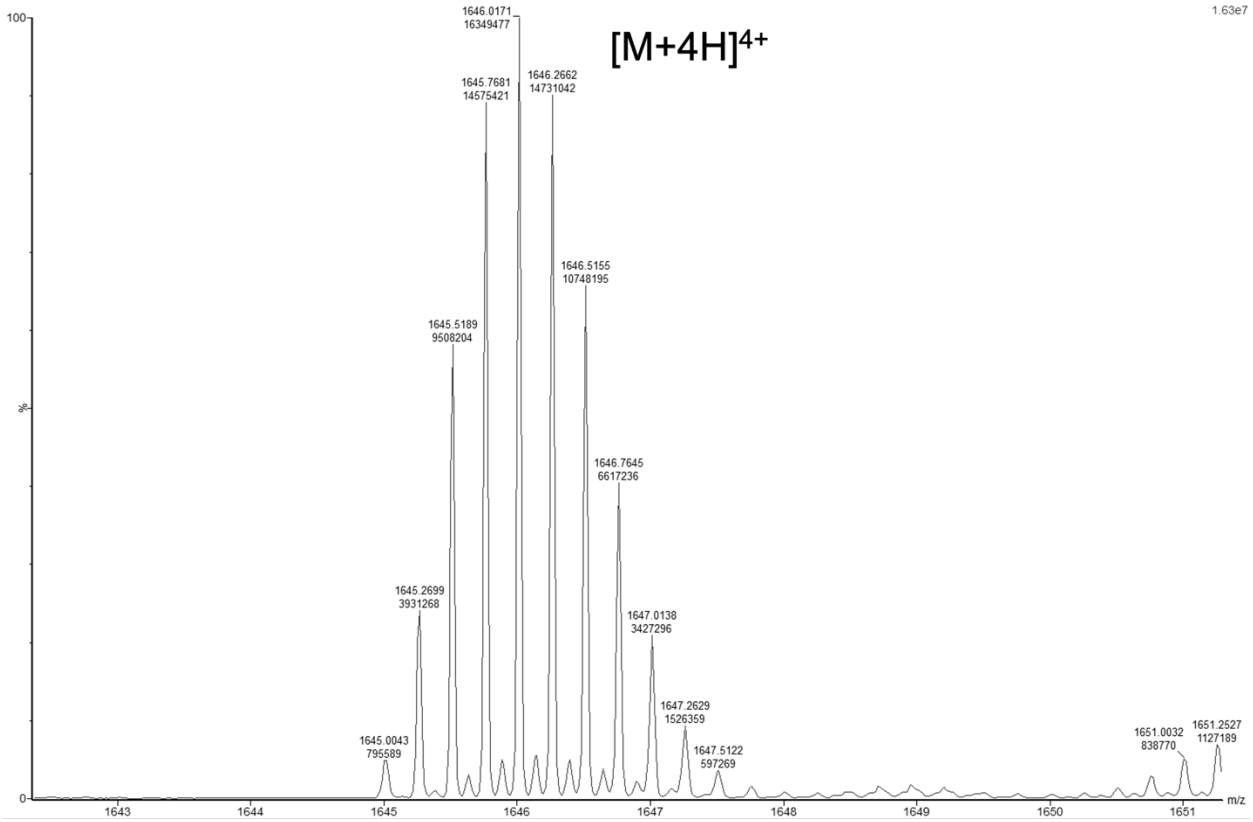

Deconvoluted mass spectrum of trimer 2AT-L

Exact mass of trimer 2AT-L: 6576.34

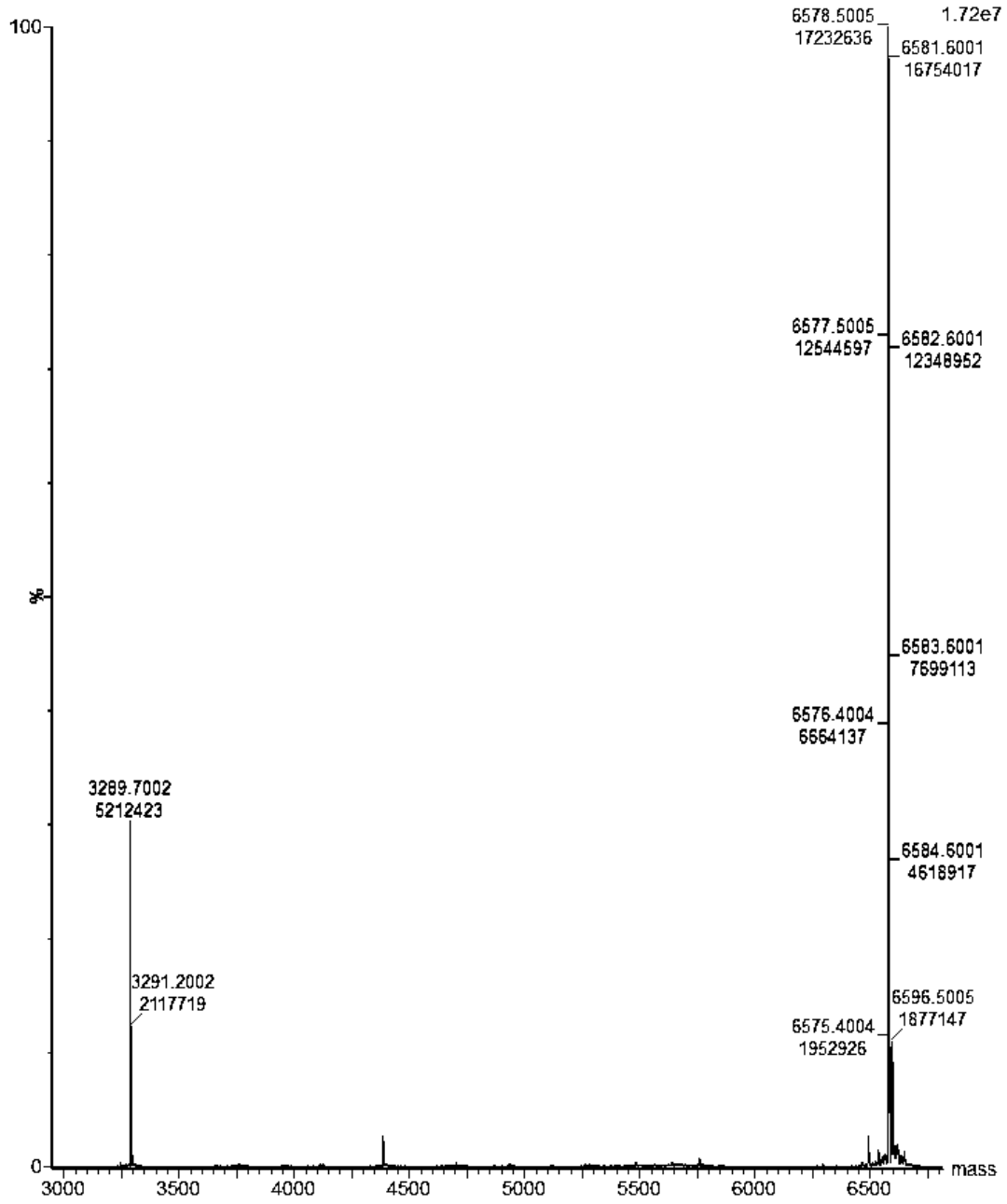

Deconvoluted mass spectrum of trimer 2AT-L

Exact mass of trimer 2AT-L: 6576.34

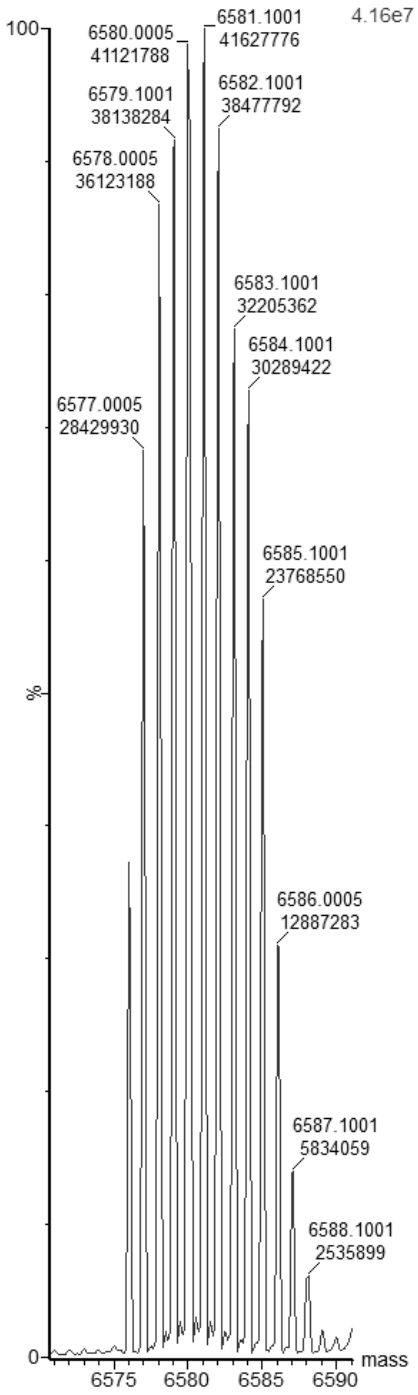

Characterization of trimer 2AT-L-sCy3

Analytical HPLC trace

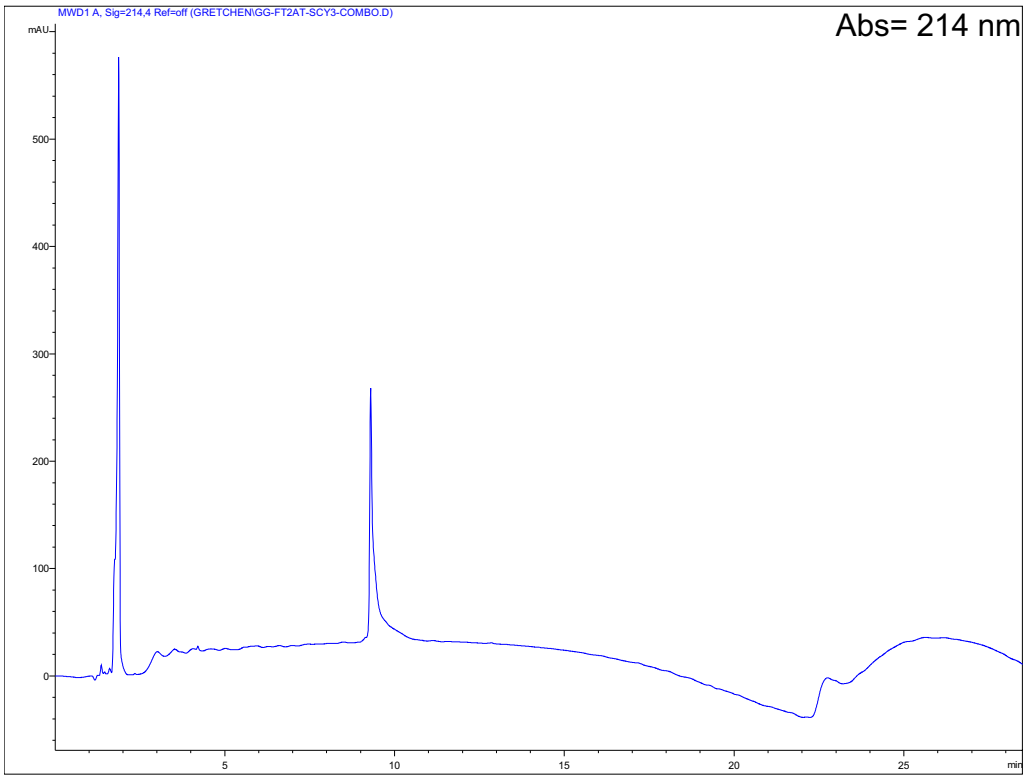

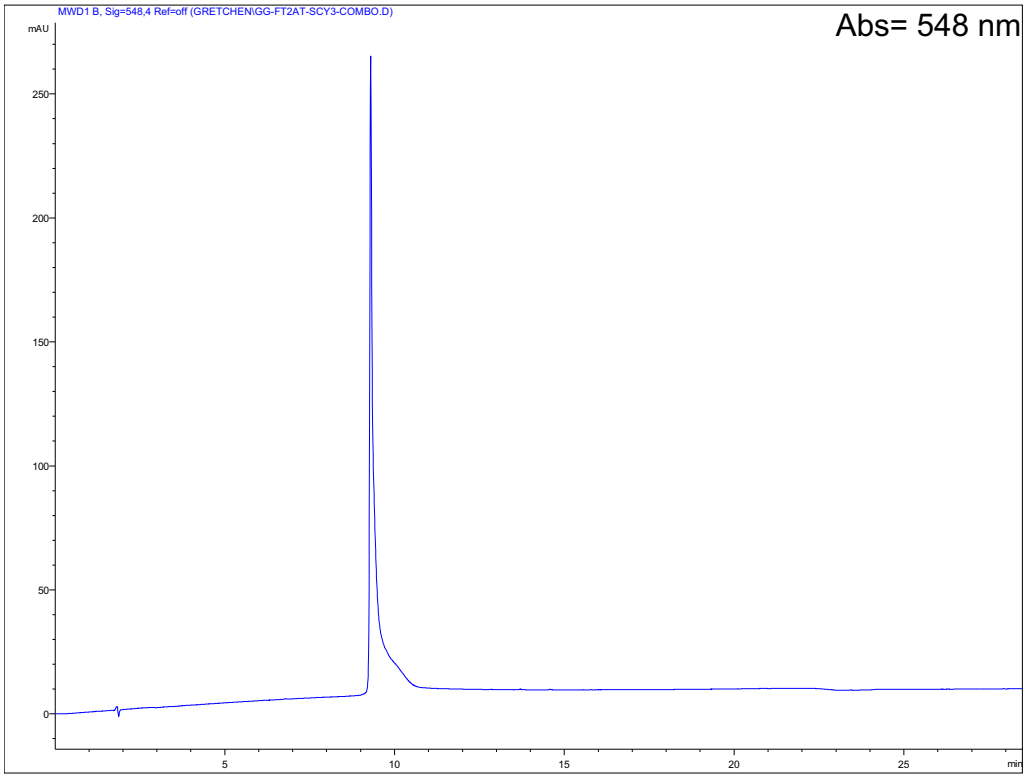

Mass spectrum of trimer 2AT-L-sCy3

Calculated $[M+H]^+$ of trimer 2AT-L-sCy3: 7175.52

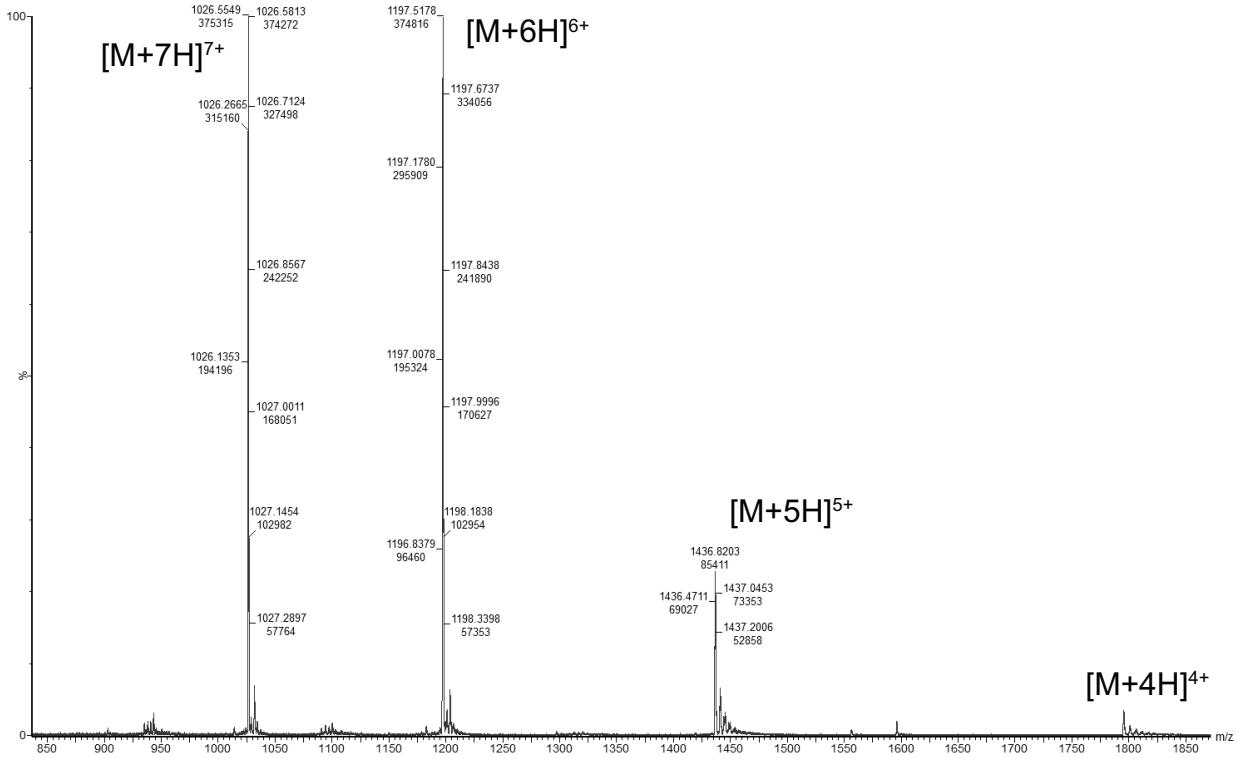

Expansion mass spectrum of trimer 2AT-L-sCy3

Calculated $[M+H]^+$ of trimer 2AT-L-sCy3: 7175.52

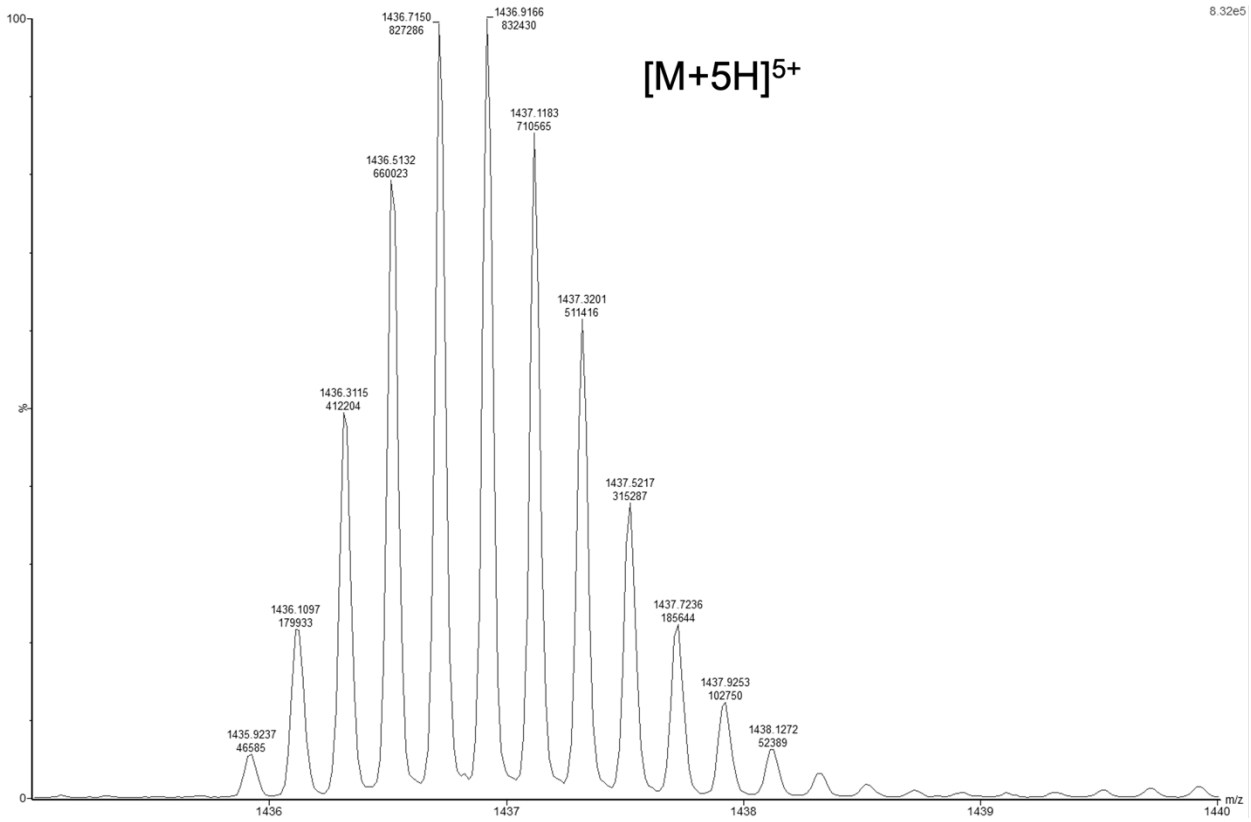

Deconvoluted mass spectrum of trimer 2AT-L-sCy3

Exact mass of trimer 2AT-L-sCy3: 7174.52

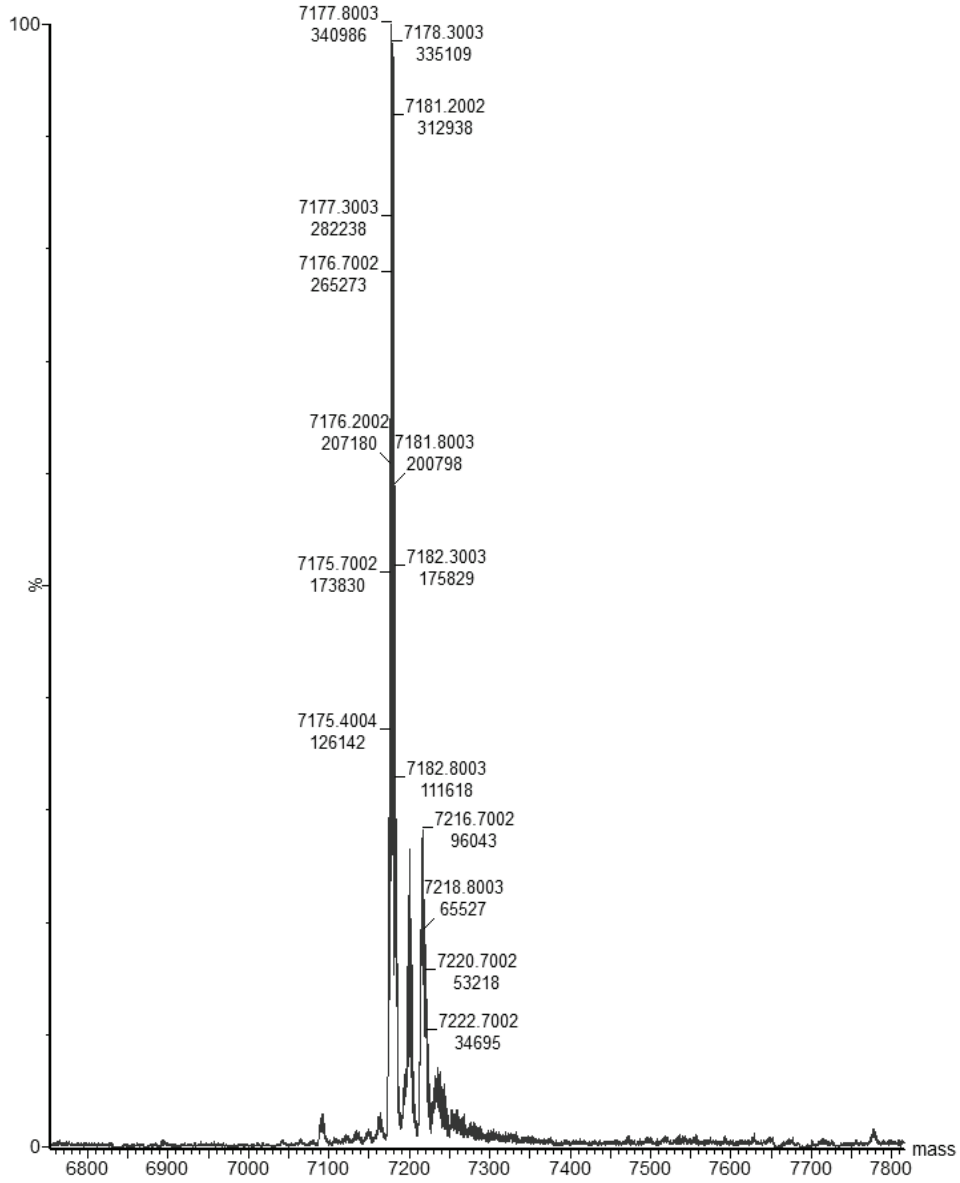

Deconvoluted mass spectrum of trimer 2AT-L-sCy3

Exact mass of trimer 2AT-L-sCy3: 7174.52

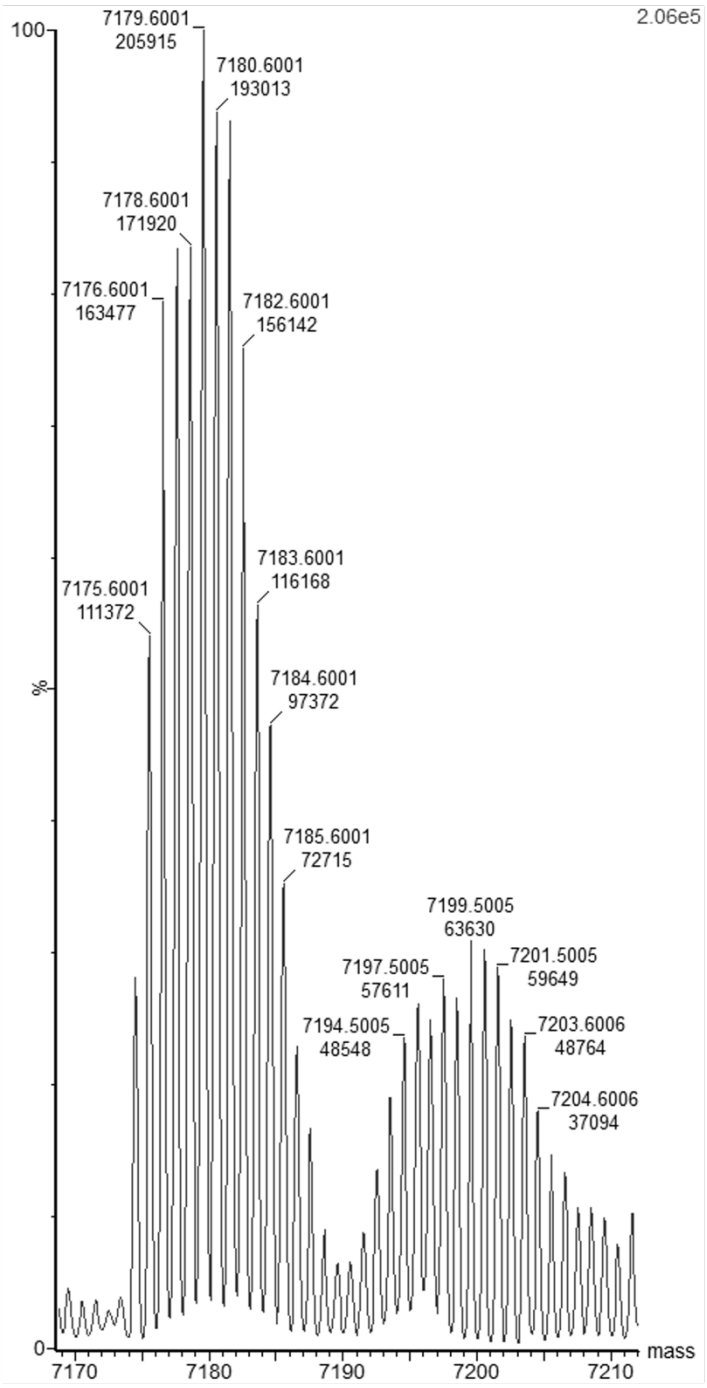

Characterization of trimer 2AT-L-sCy5

Analytical HPLC trace

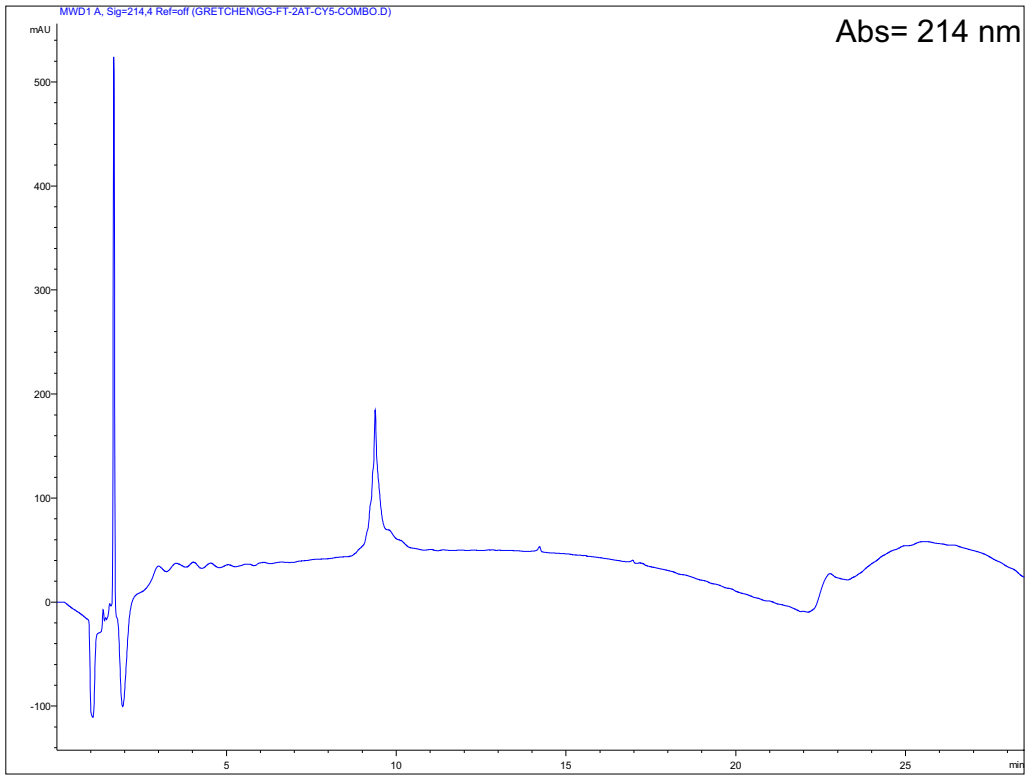

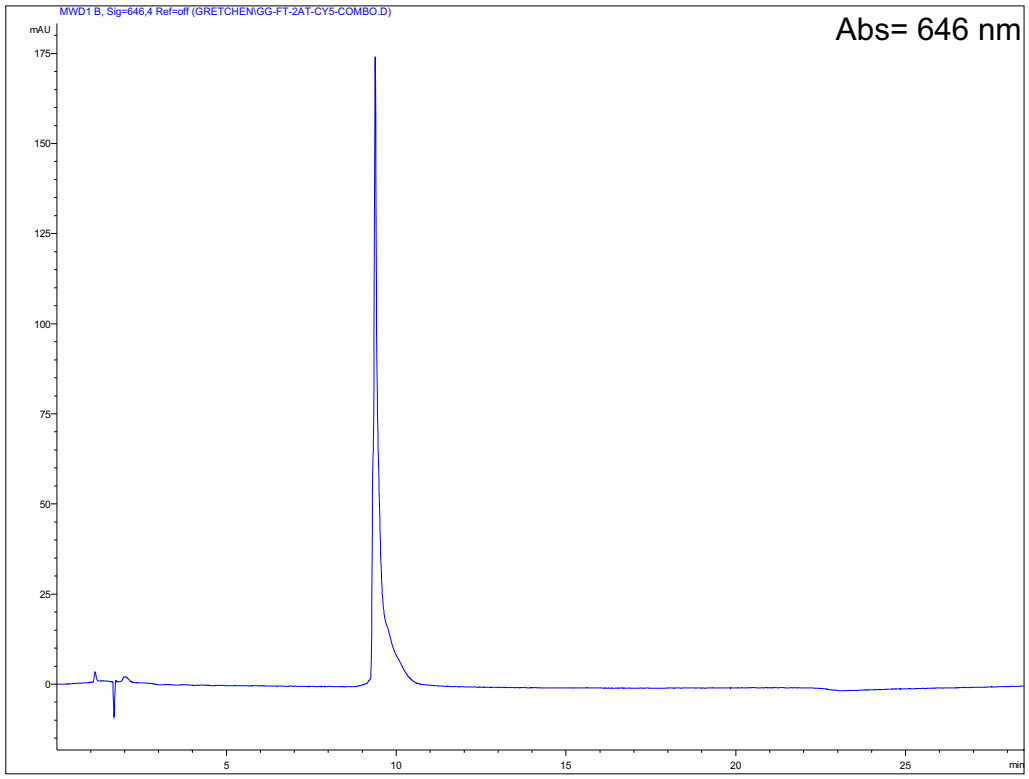

Mass spectrum of trimer 2AT-L-sCy5

Calculated $[M+H]^+$ of trimer 2AT-L-sCy5: 7201.54

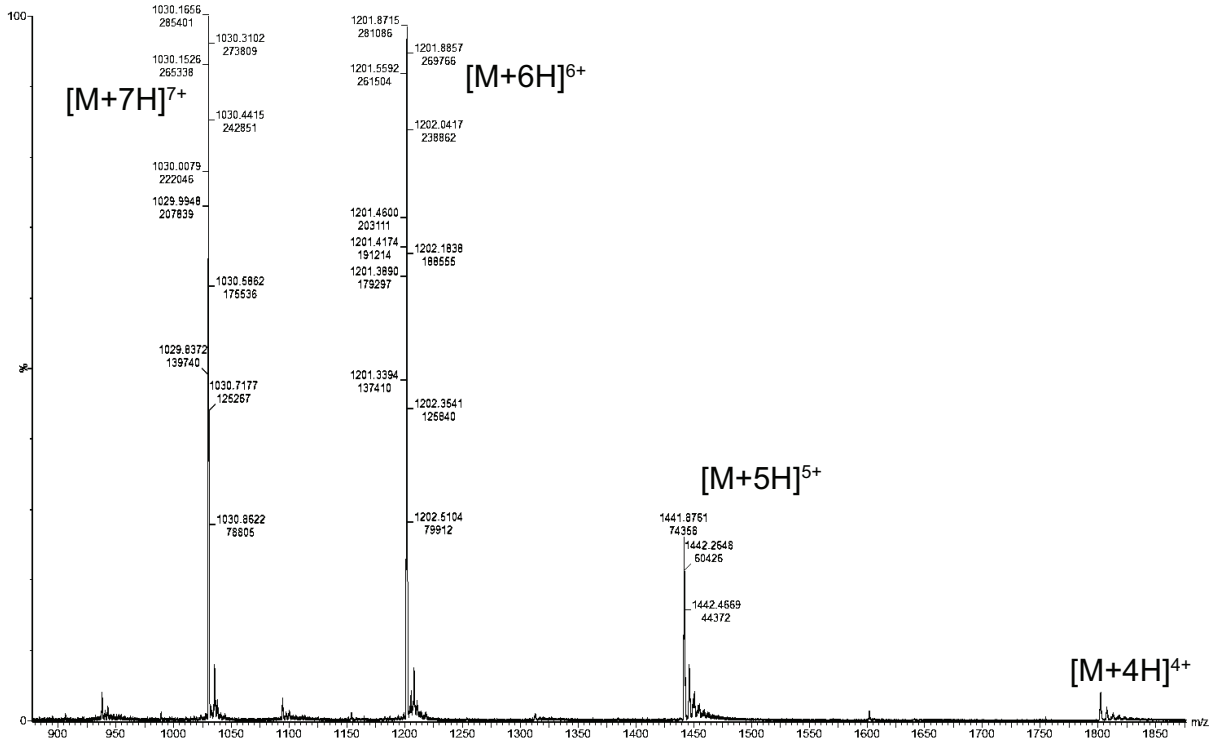

Mass spectrum of trimer 2AT-L-sCy5

Calculated $[M+H]^+$ of trimer 2AT-L-sCy5: 7201.54

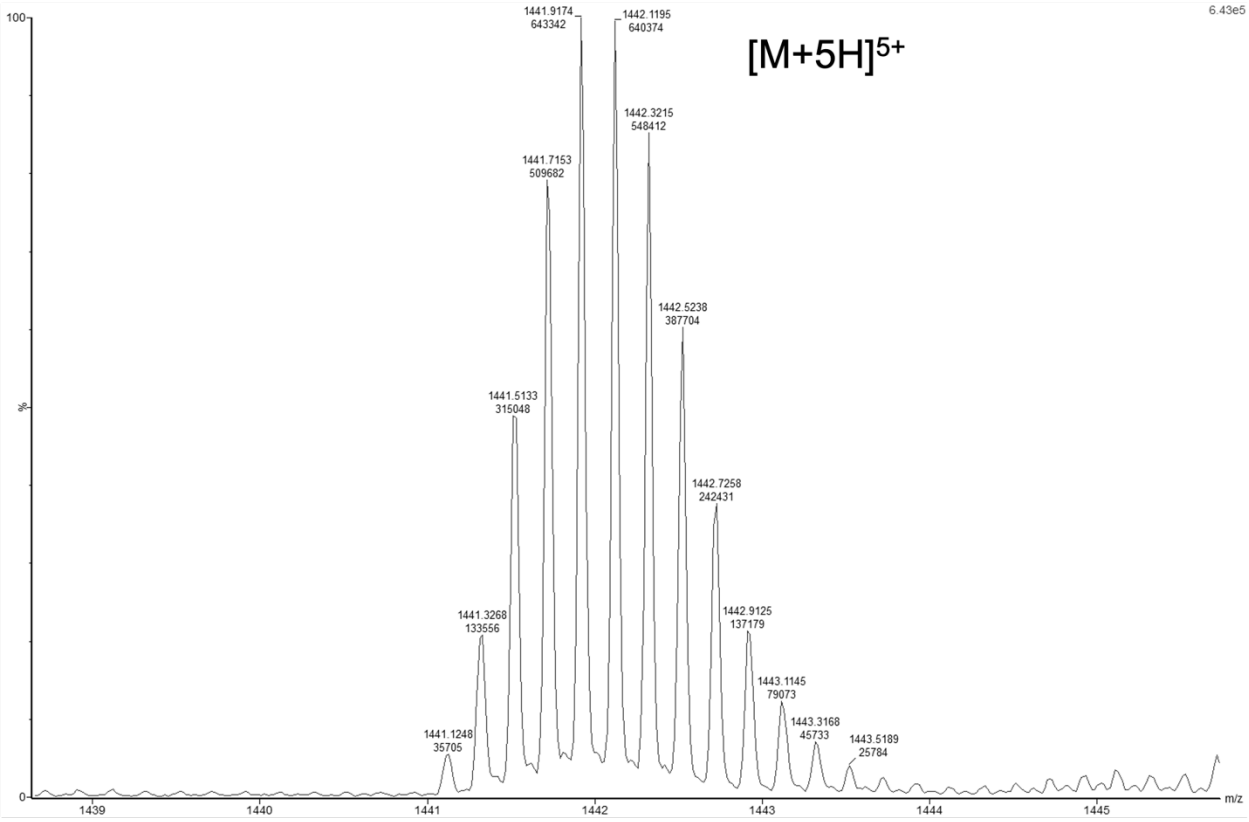

Deconvoluted mass spectrum of trimer 2AT-L-sCy5

Exact mass of trimer 2AT-L-sCy5: 7200.53

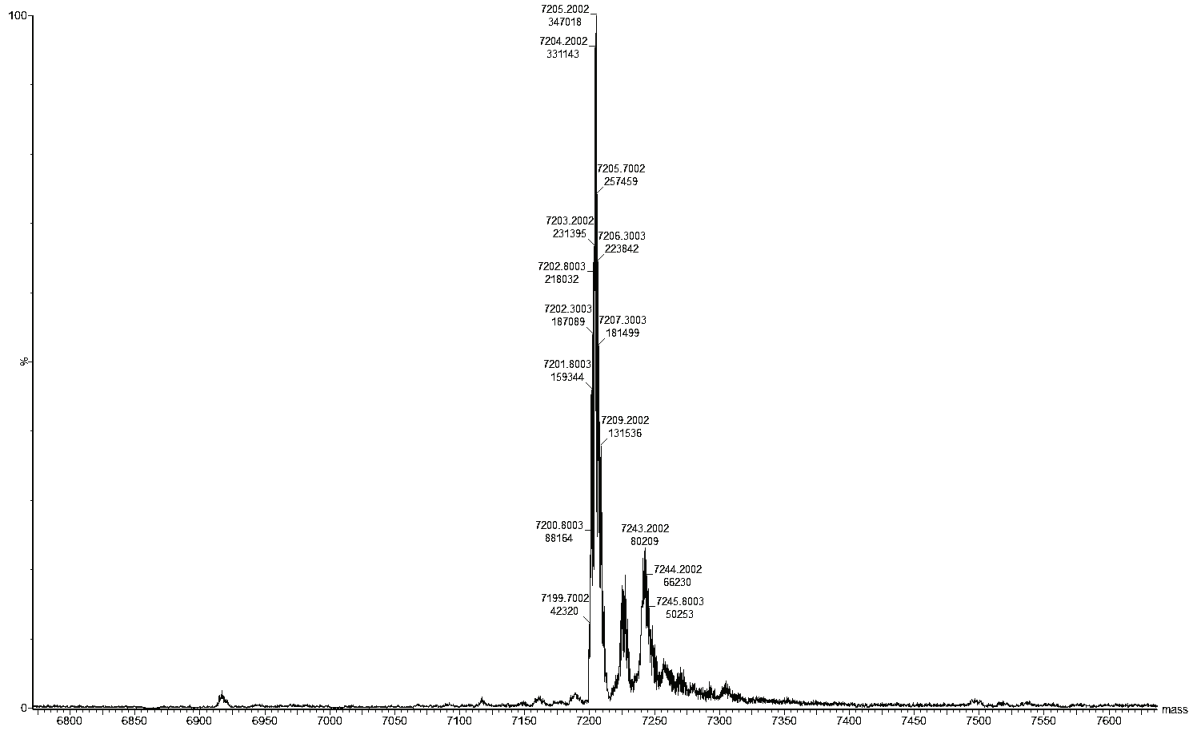

Deconvoluted mass spectrum of trimer 2AT-L-sCy5

Calculated mass of trimer 2AT-L-sCy5: 7200.53

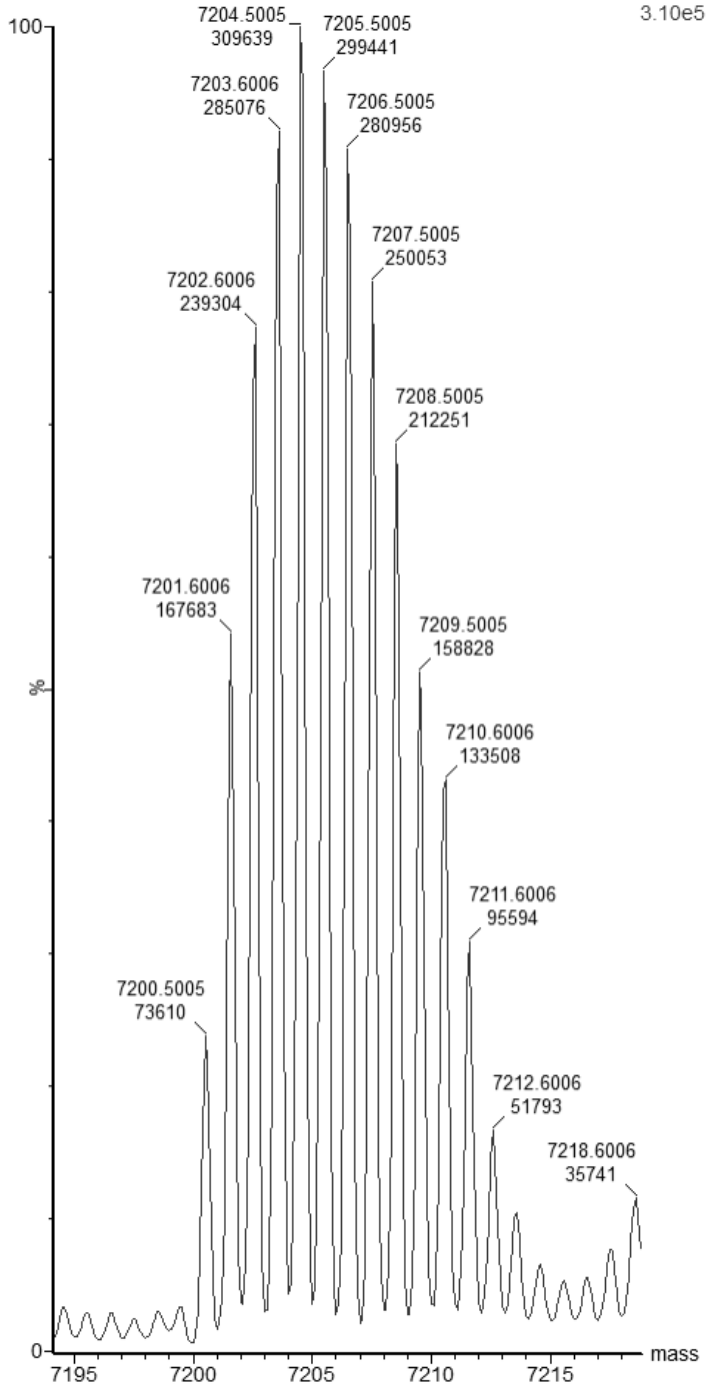

Chapter 3

Isomorphic trimers derived from Aβ exhibit different oligomerization and biological properties

Preface to Chapter 3

Chapter 3 is adapted from a collaborative project that I had the opportunity to work on with many colleagues under the leadership of Dr. Adam Kreutzer. This project introduces a new crosslinked trimer derived from Aβ, KLT, and details a variety of biophysical and biological studies as a comparison to our laboratory's well-characterized crosslinked trimer, 2AT. The design of this new macrocyclic β-hairpin peptide and the corresponding disulfide-stabilized trimer was led by Dr. Adam Kreutzer. I supported the optimization of the synthesis and purification with a team of undergraduate students. Dr. Kreutzer used X-ray crystallography to obtain a high-resolution structure of KLT, and I performed complementary SDS-PAGE experiments, which provided further insights into the supramolecular assembly of KLT. To continue to explore the differences in toxicity observed by Dr. Kreutzer, I pursued fluorescence labeling of the trimers for the purpose of studying the interactions of the trimers with cells by fluorescence microscopy. The work culminates with collaborative efforts from the Lai laboratory and Chelsea Parrocha to generate monoclonal antibodies against 2AT and KLT and use immunohistochemistry to determine if these antibodies recognize biogenic Aβ.

To delineate contributions, herein I have focused only on studies I have performed including SDS-PAGE, cellular cytotoxicity, fluorescence labeling, and fluorescence microscopy.

The work presented in Chapter 3 builds upon my previous experience in determining an efficient labeling procedure for trimer model systems and optimization of fluorescence microscopy with live cells and I am grateful to have had the opportunity to continue to hone these skills in contribution to this large collection of studies.

INTRODUCTION

The β-amyloid (Aβ) peptide accumulates in the brains of people with Alzheimer's disease (AD) and has been established as a leading contributor to neurodegeneration.[1–5] Aβ aggregates, forming smaller molecular weight oligomers and larger, insoluble fibrils. Significant evidence suggests oligomers are the primary toxic species and has identified trimers as key building blocks to these toxic oligomers.[5–12] Aβ oligomers have proven difficult to study as they are not a homogeneous species, but instead consist of heterogeneous mixtures of aggregates of different shapes and sizes in dynamic equilibrium.[13,14] The heterogeneity and metastability of oligomers have made them difficult to isolate in sufficient quantity that persist in solution, so the elucidation of high resolution structures of oligomers has proven challenging.[14,15]

The prevalence of β-sheet rich structures of Aβ, where the central and *C*-terminal regions fold to form a β-hairpin, has been established as important secondary structure of Aβ oligomers and fibrils, and the stability of some assemblies has been attributed to this β-turn.[13,16,17] However, structures of Aβ have demonstrated a great level of polymorphism.[13] One structure, published by Härd et al., revealed through nuclear magnetic resonance that $A\beta_{17–36}$ forms a hydrogen-bonded antiparallel β-sheet when bound to an affibody. In this structure, the top β-strand of residues 17–23 and the bottom β-strand of residues 30–36 are linked by residues 24–29 acting as a loop.[18] Alternatively, a structure reported by Tycko *et al.* revealed through cryo-electron microscopy that an endogenous Aβ fibril forms a parallel β-sheet composed of Aβ residues 16–36.[19] It is hypothesized that the polymorphism of Aβ structures, and specifically the alignment of the β-strands within the β-hairpin, may give rise to significant differences in the biophysical and biological properties of oligomers.[20]

Model systems of stabilized oligomers consisting of fragments of Aβ have emerged as tools to increase the understanding of the biophysical and biological properties of oligomers.[21–23] Our laboratory has previously reported a method to synthesize macrocyclic β-hairpin peptides derived from $A\beta_{16–36}$.[24–29] In each β-hairpin, δ-linked ornithine ($^{\delta}$Orn) turn units help enforce a folded β-hairpin conformation, and an *N*-methyl amino acid helps block uncontrolled aggregation. Macrocyclic β-hairpin 2AM contains residues 17–23 on the top strand and 30–36 on the bottom strand while macrocyclic β-hairpin KLM contains residues 16–22 on the top strand and 30–36 on the bottom strand.

In the crystal state, the monomers 2AM and KLM assemble to form respectively named 2AT and KLT triangular trimers, with adjacent molecules in proximity at each of the vertices.[30,31] In 2AT, residues 17 and 21 are replaced by cysteines, which allow for covalent crosslinks that hold the 2AT trimer together by connecting the monomer subunits at the vertices (Figure 3.1A,B). In KLT, residues 30 and 34 are replaced by cysteines, which allow for covalent crosslinks that hold the KLT trimer together (Figure 3.1C,D). The crosslinked trimers overcome some of the challenges of studying Aβ as they are more stable and homogeneous, and they mimic some of the biological properties of Aβ.

Herein, we describe the synthesis and study of isomorphic trimers 2AT and KLT. We compare the solution phase assembly of the trimers by SDS-PAGE and assess their biological role through caspase 3/7 activation. We then synthesize fluorescently labeled analogues of 2AT and KLT to study the trimers' interactions with cells by fluorescence microscopy. These studies allow the correlation of structure to function through a homogeneous model system and can provide further insight into the molecular basis of Alzheimer's disease.

RESULTS AND DISCUSSION

Synthesis of 2AT and KLT. 2AT was synthesized as previously reported.[27] We synthesized KLT by Fmoc-based solid phase peptide synthesis using similar procedures to those used to prepare 2AT.[27] We first prepared macrocyclic peptide KLM_{CC} by solid-phase peptide synthesis of the corresponding linear peptide on 2-chlorotrityl resin. Following synthesis, the peptide was cleaved from resin and cyclized in solution. The macrocyclic peptide underwent global deprotection, ether precipitation, and reversed-phase HPLC (RP-HPLC) yielding KLM_{CC}. KLM_{CC} was oxidized at 6 mM in 20% aqueous DMSO for 48 h to form intermolecular disulfide bonds. The trimer KLT was isolated from the oxidation reaction by RP-HPLC. Pure fractions were lyophilized, yielding KLT as the trifluoroacetate (TFA) salt.

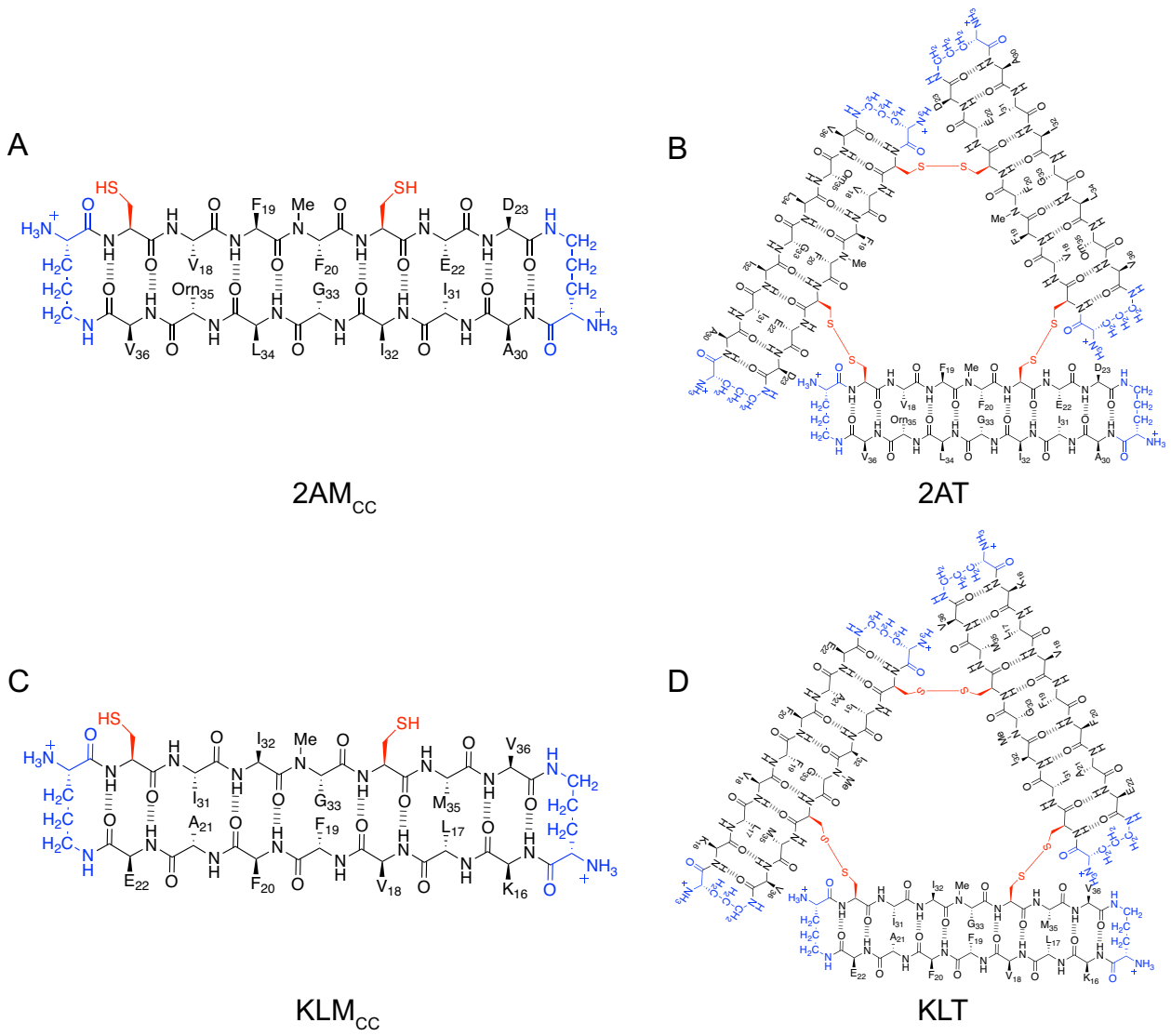

Figure 3.1 Chemical structures of β-hairpin peptides and the corresponding trimers. **(A)** Macrocyclic β-hairpin 2AM$_{CC}$ containing Aβ$_{17–23}$ and Aβ$_{30–36}$ with cysteine mutations at positions 17 and 21. **(B)** Three 2AM$_{CC}$ β-hairpins form covalently stabilized trimer 2AT through disulfide bonds. **(C)** Macrocyclic β-hairpin KLM$_{CC}$ containing Aβ$_{16–22}$ and Aβ$_{30–36}$ with cysteine mutations at positions 30 and 34. **(D)** Three KLM$_{CC}$ β-hairpins form covalently stabilized trimer KLT through disulfide bonds.

Assembly of 2AT and KLT by SDS-PAGE. We used SDS-PAGE to investigate the oligomerization of 2AT and KLT in solution. In the presence of SDS, silver staining of the gel reveals that 2AT and KLT migrate differently (Figure 3.2). Trimer 2AT forms a less intense band at a molecular weight consistent with a trimer (~5.3 kDa) and a much more intense band

spanning 22 kDa and 12 kDa. The diffuse shape of this band shows downward streaking, becoming less intense as it approaches the 12 kDa marker band. The streaking of this band suggests the equilibrium of multiple oligomers of ca. 2–4 trimers in size. In contrast, trimer KLT shows a much more diffuse band beginning above the 40 kDa marker band and streaking down to ca. 12 kDa, where a more compact band is observed. 1AT, a previously reported trimer from our group, forms an oligomer made up of 2 trimers.[27] Comparing 1AT to the compact band of KLT at 12 kDa, it is likely that this oligomer of KLT is made up of 3 trimers. These oligomers are consistent with observed Aβ oligomers that include trimers, hexamers, nonamers and dodecamers.[6,32–34]

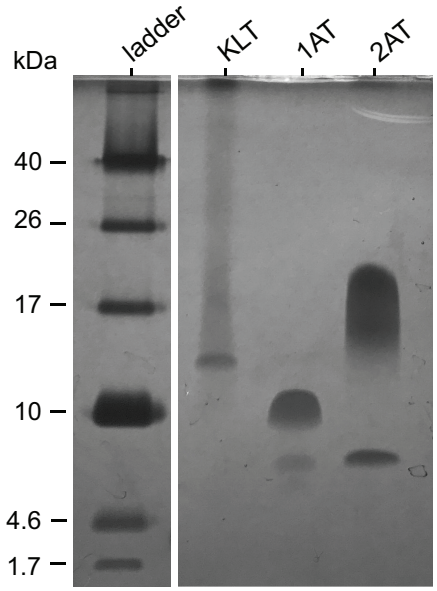

Figure 3.2 Silver-stained SDS-PAGE of trimers KLT, 1AT, and 2AT. SDS-PAGE was performed in Tris buffer at pH 6.8 with 2% (w/v) SDS on a 16% polyacrylamide gel with 5 μL of 30 μM solutions of trimer in each lane.

Investigating the cytotoxicity of 2AT and KLT. To explore whether or not the oligomerization differences observed by SDS-PAGE affected the trimers biological activity, we assessed cellular

cytotoxicity. Previous studies of Aβ have demonstrated that oligomers with similar sizes but different conformations can have significantly different toxicity profiles.[35] We hypothesized that 2AT and KLT may also show differences in toxicity. Aβ has been shown to be toxic to cells through many mechanisms, one of which being the activation of the caspase-3/7 pathway, indicating apoptosis and resulting in a decrease in cell viability. For this reason, we chose to investigate toxicity by measuring caspase 3/7 activation. SH-SY5Y cells were incubated with varying concentrations of 2AT and KLT for 72 hours before cell death was measured. Results showed a significant increase in caspase 3/7 activation from trimer 2AT in a dose-dependent fashion compared to trimer KLT, which showed minimal toxicity and no dose dependence (Figure 3.3). This difference may begin to reveal how the different Aβ oligomer models have different biological interactions.

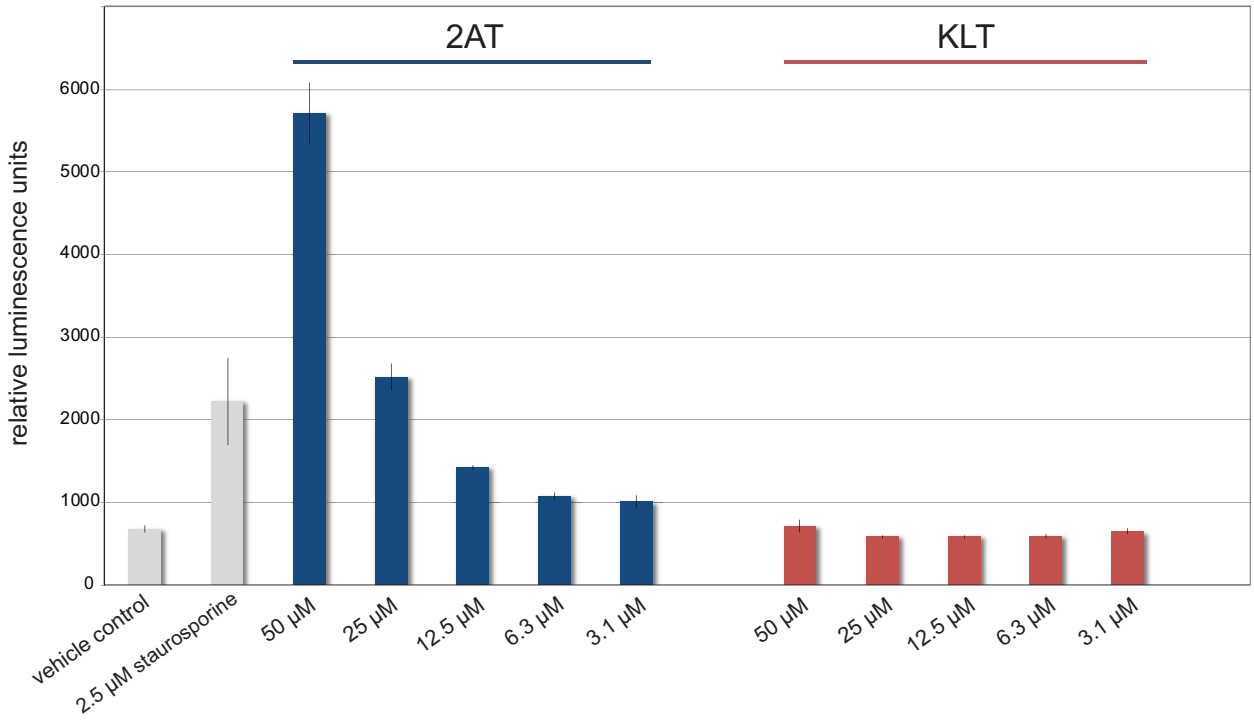

Figure 3.3 Caspase 3/7 activation assay (Promega) of 2AT and KLT. SH-SY5Y cells were treated with 2AT and KLT at concentrations of 50 μM, 25 μM, 12.5 μM, 6.3 μM, and 3.1 μM for 72 h. A solution of 2.5 μM staurosporine was used as a positive control and the vehicle (water) was used as a negative control.

Preparation of fluorescently labeled 2AT and KLT analogues. To further investigate the different interactions of 2AT and KLT with mammalian cells, we prepared fluorescently labeled 2AT and KLT analogues to use in fluorescence microscopy. We hypothesized that labeling the monomer subunits with a fluorophore prior to oxidation into the disulfide-linked trimer would prevent the formation of trimers in solution. Therefore, we approached the process of fluorescence labeling following the isolation of pure trimer. However, each trimer contains multiple reactive amines, allowing for the potential of multiple fluorophores to be conjugated via NHS-ester chemistry. We anticipated that the addition of multiple fluorophores to the trimer would begin to inhibit the self-assembling behavior unique to these trimers. Therefore, we refined a procedure to append one single fluorophore onto the trimer.

We developed a procedure in which excess molar equivalents of 2AT is treated with the commercially available sulfo-cyanine3 (sCy3) ester in a molar ratio of 20:1 trimer to fluorophore. The singly-labeled trimer (2AT-sCy3) is isolated by RP-HPLC, and the unlabeled trimer is collected and recycled. The reaction was then repeated to generate sCy3 labeled KLT (KLT-sCy3).

Fluorescence microscopy of 2AT-sCy3 and KLT-sCy3. We performed live-cell fluorescence microscopy to visualize the interactions of 2AT and KLT with cells to perhaps provide insight into the differences in cytotoxicity observed. SH-SY5Y cells were incubated either 2AT-sCy3 or KLT-sCy3 at a concentration of 1 μM for 8 h. Cells were then counterstained with Hoechst 33342 nuclear stain (blue), washed with phenol red-free DMEM:F12 media, and imaged. Fluorescence micrographs were collected with observed emission in the Cyanine3 channel to visualize the labeled trimers.

Fluorescence microscopy revealed key differences in the cellular interactions of 2AT and KLT. When SH-SY5Y cells are incubated with 2AT-sCy3, we observe the accumulation of 2AT-sCy3 as bright, intracellular puncta (Figure 3.4). The appearance of intracellular puncta was consistent with previous reports of Aβ which localized into late stage endosomes and lysosomes.

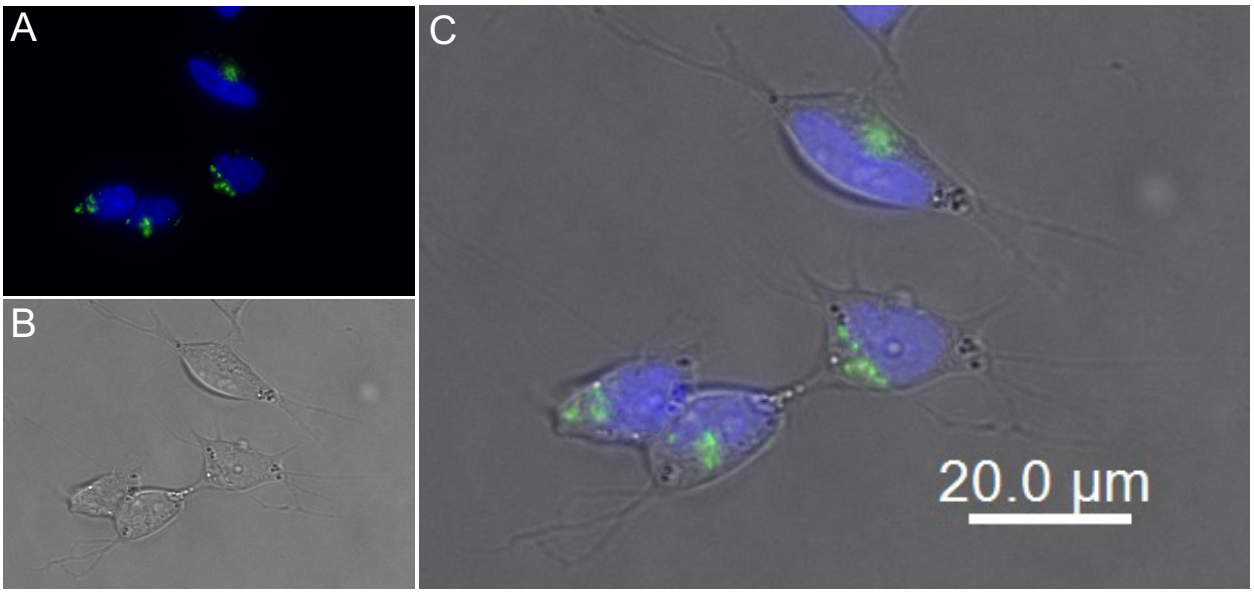

Figure 3.4 Micrographs illustrating intracellular localization of fluorescently labeled 2AT-sCy3 in SH-SY5Y cells. **(A)** 2AT-sCy3 (green). **(B)** Brightfield image. **(C)** Merged fluorescence and brightfield images. Cells were incubated with 1 µM 2AT-sCy3 for 8 h at 37°C, counterstained with Hoechst 33342 nuclear stain (blue), and imaged.

When SH-SY5Y cells are incubated with 2AT-sCy3 and the lysosomal marker Lysotracker Green, the 2AT-sCy3 puncta appear to co-localize with the marker, suggesting sequestration into the lysosomes (Figure 3.5). This observation of bright puncta localized to the lysosomes is consistent with previous reports of Aβ and is indicative of an endocytotic uptake mechanism.[36–38]

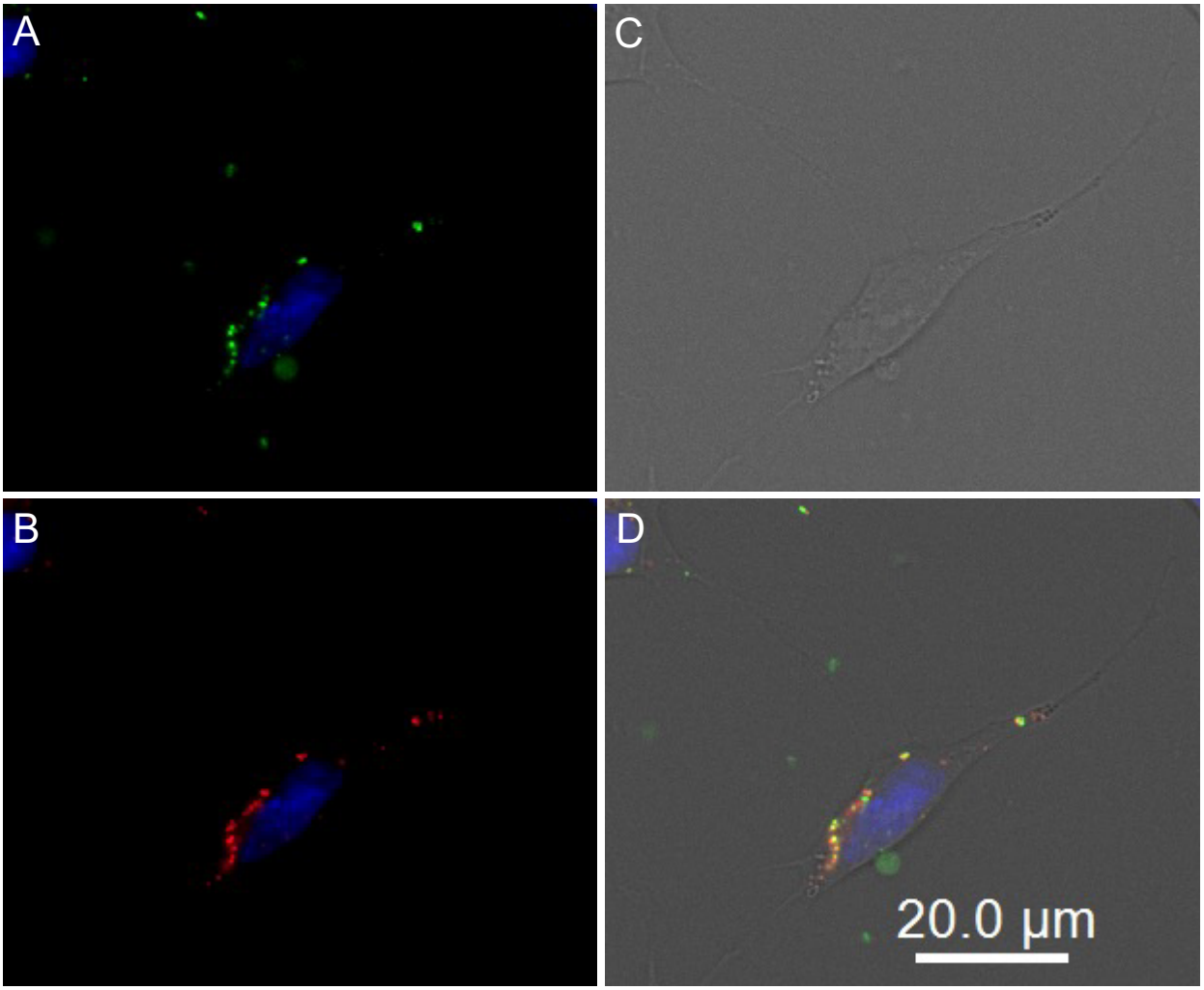

Figure 3.5 Micrographs illustrating intracellular co-localization of 2AT-sCy3 and Lysotracker Green in SH-SY5Y cells. **(A)** 2AT-sCy3 (green). **(B)** Lysotracker Green (red). **(C)** Brightfield image. **(D)** Merged fluorescence and brightfield images. Cells were incubated with 1 µM 2AT-sCy3 and 100 nM Lysotracker Green for 8 h at 37°C, counterstained with Hoechst 33342 nuclear stain (blue), and imaged.

Alternatively, when SH-SY5Y cells are incubated with KLT-sCy3, KLT-sCy3 appears to remain extracellular on the plasma membrane with minimal fluorescence observed within the cell (Figure 3.6).

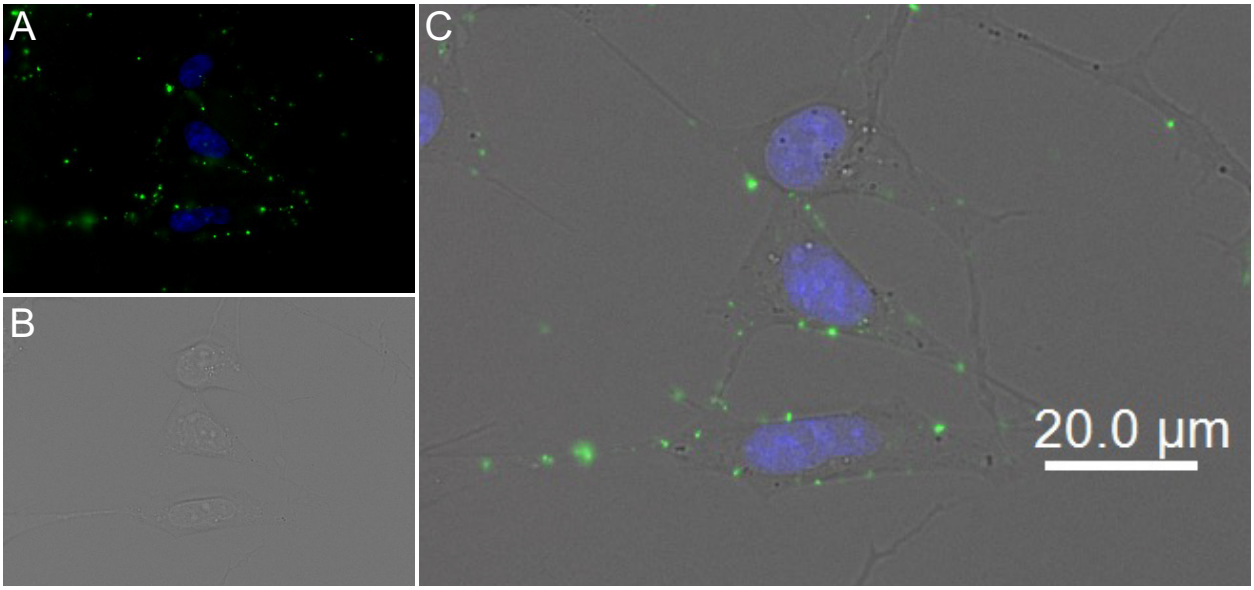

Figure 3.6 Micrographs illustrating intracellular localization of fluorescently labeled KLT-sCy3 in SH-SY5Y cells. **(A)** KLT-sCy3 (green). **(B)** Brightfield image. **(C)** Merged fluorescence and brightfield images. Cells were incubated with 1 µM KLT-sCy3 for 8 h at 37°C, counterstained with Hoechst 33342 nuclear stain (blue), and imaged.

Unsurprisingly, when SH-SY5Y cells are incubated with KLT-sCy3 and the lysosomal marker Lysotracker Green, there is little to no co-localization. The lysosomal marker forms intracellular puncta and KLT-sCy3 remains on the cellular membrane (Figure 3.7). While the interactions of KLT-sCy3 with cells differs considerably from the interactions of 2AT-sCy3 with cells, some reported preparations of Aβ have yielded oligomers that behave similarly to KLT-sCy3. In these reports, fluorescence microscopy revealed that the preparation of crosslinked oligomers of Aβ adhered to the cell membrane and did not show appreciable amounts of internalized oligomers.[2,39]

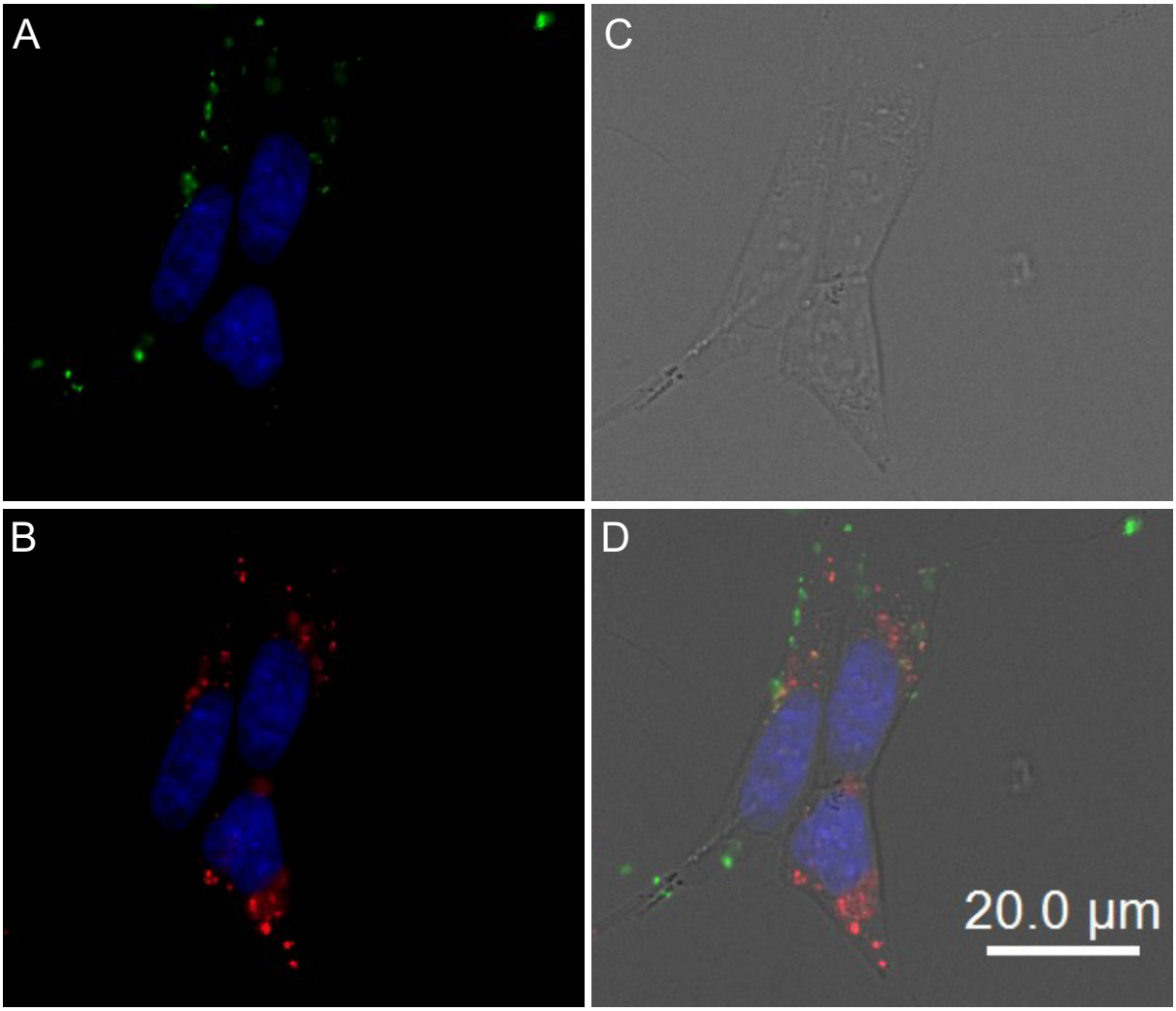

Figure 3.7 Micrographs illustrating the absence of co-localization of KLT-sCy3 and Lysotracker Green in SH-SY5Y cells. **(A)** 2AT-sCy3 (green). **(B)** Lysotracker Green (red). **(C)** Brightfield image. **(D)** Merged fluorescence and brightfield images. Cells were incubated with 1 µM 2AT-sCy3 and 100 nM Lysotracker Green for 8 h at 37°C, counterstained with Hoechst 33342 nuclear stain (blue), and imaged.

We then wanted to investigate the incubation of 2AT and KLT together with cells to determine if the two oligomer models would interact. To do this, we used the established labeling procedure to synthesize 2AT labeled with sulfo-cyanine5 (2AT-sCy5). We treated SH-SY5Y cells with 1 µM KLT-sCy3 and 1 µM 2AT-sCy5 for 8 h. Cells were then counterstained with Hoechst 33342 nuclear stain (blue), washed with phenol red-free DMEM:F12 media, and imaged. When 2AT-sCy5 and KLT-sCy3 are co-incubated, 2AT-sCy5 appears to form fewer

intracellular puncta; instead, it appears to co-localize on the membrane with KLT-sCy3 (Figure 3.8). This co-localization may indicate an interaction occurring between the two oligomer models in which the presence of KLT affects the uptake of 2AT. While some studies have suggested that the interactions of different oligomers can have an overall protective effect, further investigation of these oligomer interactions would be required to determine the significance of the observed co-localization.[33]

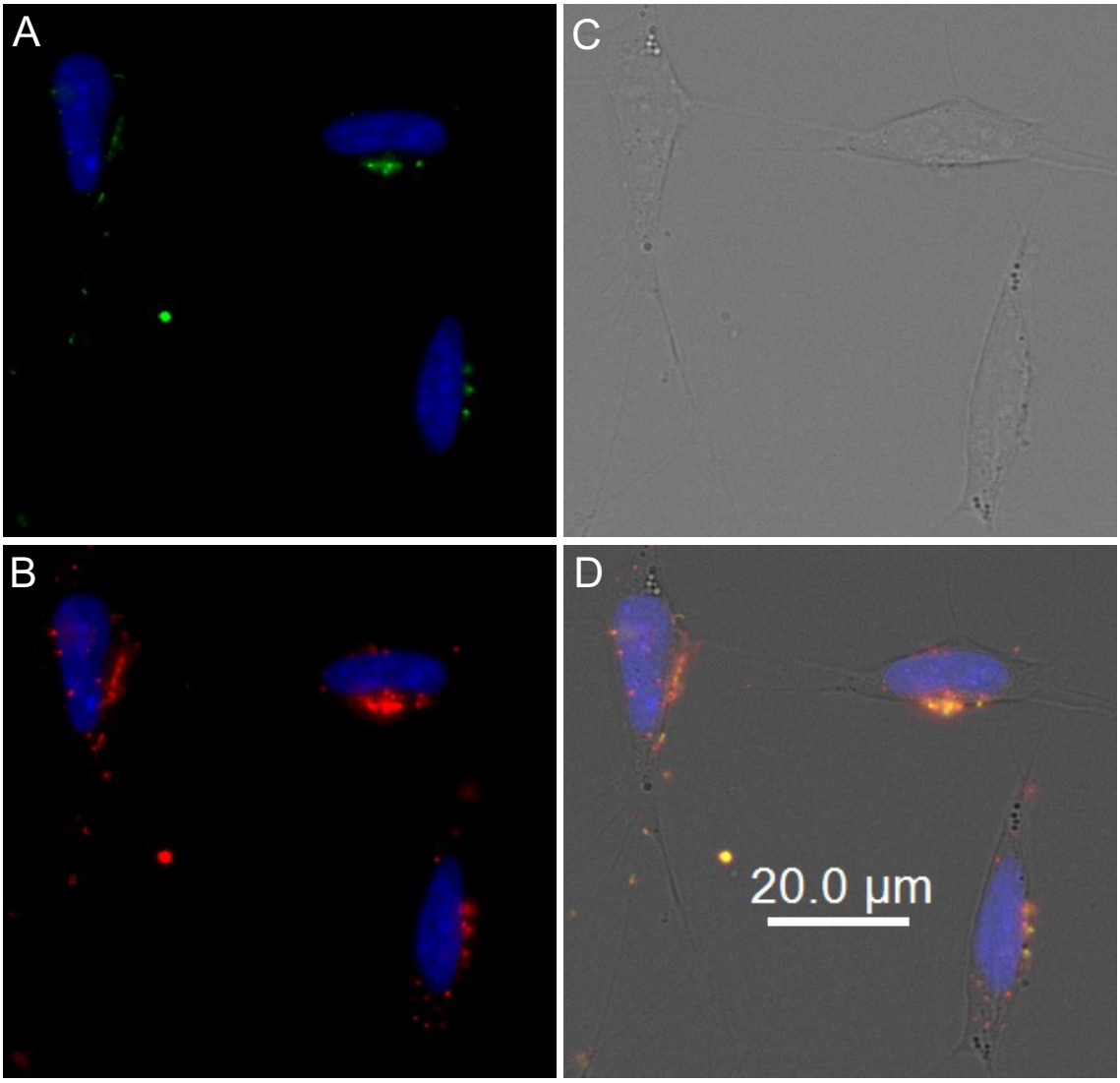

Figure 3.8 Micrographs illustrating localization of KLT-sCy3 and 2AT-sCy5 in SH-SY5Y cells. **(A)** KLT-sCy3 (green). **(B)** 2AT-sCy5 (red). **(C)** Brightfield image. **(D)** Merged fluorescence and brightfield images. Cells were incubated with 1 µM KLT-sCy3 and 1 µM 2AT-sCy5 for 8 h at 37°C, counterstained with Hoechst 33342 nuclear stain (blue), and imaged.

SUMMARY AND CONCLUSIONS

Understanding Aβ oligomers is necessary to better understand Alzheimer's disease. Specifically, understanding the relation of structure and function is important to begin to elucidate the differences in harmful and benign Aβ species.[40] High resolution structures of Aβ oligomers have remained elusive because Aβ forms heterogenous mixtures that are metastable. Using an Aβ oligomer model system, we can synthesize and study homogeneous mixtures of oligomers to improve the correlation of structure to function. Here, we study two oligomer models that differ in β-strand registration. By SDS-PAGE, 2AT and KLT both assemble to form higher order oligomers. 2AT shows a diffuse band of hexamers, nonamers, and dodecamers in equilibrium, while KLT forms a more compact band of nonamers. Species of hexamers, nonamers, and dodecamers have all been observed as oligomers formed by Aβ and suggest that these model systems recapitulate assemblies of Aβ oligomers.[6,32–34] 2AT appears to activate the caspase 3/7 pathway in SH-SY5Y cells and initiate apoptosis more significantly than KLT, which may be due to their different, preferred assemblies observed by SDS-PAGE. Though KLT did not show toxicity through the caspase 3/7 pathway, studies of Aβ have demonstrated toxicity through multiple mechanisms. Further investigate may reveal KLT elicits toxicity through one of these alternative pathways.

To continue investigate the observed differences in toxicity, we studied fluorescently labeled analogues of 2AT and KLT in the presence of SH-SY5Y cells. Fluorescence microscopy revealed significantly different interactions of the two oligomer models with cells. 2AT-sCy3 was readily uptaken and internalized by cells, indicative of endocytosis. In contrast, KLT-sCy3 remained membrane-bound and did not appear to be internalized. Again, we observed these isomorphic trimers recapitulate behavior of different preparations of Aβ oligomers. Aβ

oligomers have been reported as both intracellular puncta and membrane bound puncta when investigated with fluorescence microscopy.[2,36–39] Collectively, these studies of two stabilized Aβ-derived oligomers provide evidence that the trimers are appropriate models for Aβ oligomers and suggest that the alignment of the β-hairpin can have biophysical and biological effects. Future studies continue to investigate the biological relevance of these isomorphs through the generation of antibodies from these two trimer antigens.

REFERENCES AND NOTES

(1) Cline, E. N.; Bicca, M. A.; Viola, K. L.; Klein, W. L. The Amyloid-Oligomer Hypothesis: Beginning of the Third Decade. *J. Alzheimer's Dis.* **2018**, *64*, 567–610. https://doi.org/10.3233/JAD-179941.

(2) Lacor, P. N.; Buniel, M. C.; Chang, L.; Fernandez, S. J.; Gong, Y.; Viola, K. L.; Lambert, M. P.; Velasco, P. T.; Bigio, E. H.; Finch, C. E.; Krafft, G. A.; Klein, W. L. Synaptic Targeting by Alzheimer's-Related Amyloid β Oligomers. *J. Neurosci.* **2004**, *24* (45), 10191–10200. https://doi.org/10.1523/JNEUROSCI.3432-04.2004.

(3) Näslund, J.; Haroutunian, V.; Mohs, R.; Davis, K. L.; Davies, P.; Greengard, P.; Buxbaum, J. D. Correlation between Elevated Levels of Amyloid β-Peptide in the Brain and Cognitive Decline. *J. Am. Med. Assoc.* **2000**, *283* (12), 1571–1577. https://doi.org/10.1001/jama.283.12.1571.

(4) Dickson, D. W. The Pathogenesis of Senile Plaques. *J. Neuropathol. Exp. Neurol.* **1997**, *56* (4), 321–339.

(5) Larson, M. E.; Lesné, S. E. Soluble Aβ Oligomer Production and Toxicity. *J. Neurochem.* **2012**, *120* (SUPPL. 1), 125–139. https://doi.org/10.1111/j.1471-4159.2011.07478.x.

(6) Townsend, M.; Shankar, G. M.; Mehta, T.; Walsh, D. M.; Selkoe, D. J. Effects of Secreted Oligomers of Amyloid β-Protein on Hippocampal Synaptic Plasticity: A Potent Role for Trimers. *J. Physiol.* **2006**, *572* (2), 477–492. https://doi.org/10.1113/jphysiol.2005.103754.

(7) Podlisny, M. B.; Ostaszewski, B. L.; Squazzo, S. L.; Koo, E. H.; Rydell, R. E.; Teplow, D. B.; Selkoe, D. J. Aggregation of Secreted Amyloid β-Protein into Sodium Dodecyl Sulfate- Stable Oligomers in Cell Culture. *J. Biol. Chem.* **1995**, *270* (16), 9564–9570.

https://doi.org/10.1074/jbc.270.16.9564.

(8) Walsh, D. M.; Tseng, B. P.; Rydel, R. E.; Podlisny, M. B.; Selkoe, D. J. The Oligomerization of Amyloid β-Protein Begins Intracellularly in Cells Derived from Human Brain. *Biochemistry* **2000**, *39* (35), 10831–10839. https://doi.org/10.1021/bi001048s.

(9) Walsh, D. M.; Klyubin, I.; Fadeeva, J. V.; Cullen, W. K.; Anwyl, R.; Wolfe, M. S.; Rowan, M. J.; Selkoe, D. J. Naturally Secreted Oligomers of Amyloid β Protein Potently Inhibit Hippocampal Long-Term Potentiation in Vivo. *Nature* **2002**, *416* (6880), 535–539. https://doi.org/10.1038/416535a.

(10) Haass, C.; Selkoe, D. J. Soluble Protein Oligomers in Neurodegeneration: Lessons from the Alzheimer's Amyloid β-Peptide. *Nat. Rev. Mol. Cell Biol.* **2007**, *8* (2), 101–112. https://doi.org/10.1038/nrm2101.

(11) Cline, E. N.; Bicca, M. A.; Viola, K. L.; Klein, W. L. The Amyloid-β Oligomer Hypothesis: Beginning of the Third Decade. *J. Alzheimer's Dis.* **2018**, *64*, S567–S610. https://doi.org/10.3233/JAD-179941.

(12) Yang, T.; Li, S.; Xu, H.; Walsh, D. M.; Selkoe, D. J. Large Soluble Oligomers of Amyloid β-Protein from Alzheimer Brain Are Far Less Neuroactive than the Smaller Oligomers to Which They Dissociate. *J. Neurosci.* **2017**, *37* (1), 152–163. https://doi.org/10.1523/JNEUROSCI.1698-16.2016.

(13) Fändrich, M. Oligomeric Intermediates in Amyloid Formation: Structure Determination and Mechanisms of Toxicity. *J. Mol. Biol.* **2012**, *421* (4–5), 427–440. https://doi.org/10.1016/j.jmb.2012.01.006.

(14) Hong, W.; Wang, Z.; Liu, W.; O'Malley, T. T.; Jin, M.; Willem, M.; Haass, C.; Frosch,

M. P.; Walsh, D. M. Diffusible, Highly Bioactive Oligomers Represent a Critical Minority of Soluble Aβ in Alzheimer's Disease Brain. *Acta Neuropathol.* **2018**, *136* (1), 19–40. https://doi.org/10.1007/s00401-018-1846-7.

(15) De, S.; Wirthensohn, D. C.; Flagmeier, P.; Hughes, C.; Aprile, F. A.; Ruggeri, F. S.; Whiten, D. R.; Emin, D.; Xia, Z.; Varela, J. A.; Sormanni, P.; Kundel, F.; Knowles, T. P. J.; Dobson, C. M.; Bryant, C.; Vendruscolo, M.; Klenerman, D. Different Soluble Aggregates of Aβ42 Can Give Rise to Cellular Toxicity through Different Mechanisms. *Nat. Commun.* **2019**, *10* (1), 1541. https://doi.org/10.1038/s41467-019-09477-3.

(16) Millucci, L.; Ghezzi, L.; Bernardini, G.; Santucci, A. Conformations and Biological Activities of Amyloid Beta Peptide 25-35. *Curr. Protein Pept. Sci.* **2010**, *11* (1), 54–67. https://doi.org/10.2174/1389209197511882037.

(17) Greenwald, J.; Riek, R. Biology of Amyloid: Structure, Function, and Regulation. *Structure* **2010**, *18* (10), 1244–1260. https://doi.org/10.1016/j.str.2010.08.009.

(18) Hoyer, W.; Grönwall, C.; Jonsson, A.; Ståhl, S.; Härd, T. Stabilization of a β-Hairpin in Monomeric Alzheimer's Amyloid-β Peptide Inhibits Amyloid Formation. *Chemtracts* **2008**, *20* (12), 499–500.

(19) Ghosh, U.; Thurber, K. R.; Yau, W. M.; Tycko, R. Molecular Structure of a Prevalent Amyloid-β Fibril Polymorph from Alzheimer's Disease Brain Tissue. *Proc. Natl. Acad. Sci. U. S. A.* **2021**, *118* (4), 1–9. https://doi.org/10.1073/pnas.2023089118.

(20) Lu, J. X.; Qiang, W.; Yau, W. M.; Schwieters, C. D.; Meredith, S. C.; Tycko, R. XMolecular Structure of β-Amyloid Fibrils in Alzheimer's Disease Brain Tissue. *Cell* **2013**, *154* (6), 1257. https://doi.org/10.1016/j.cell.2013.08.035.

(21) Benilova, I.; Karran, E.; De Strooper, B. The Toxic Aβ Oligomer and Alzheimer's

Disease: An Emperor in Need of Clothes. *Nat. Neurosci.* **2012**, *15* (3), 349–357. https://doi.org/10.1038/nn.3028.

(22) Hawk, L. M. L.; Pittman, J. M.; Moore, P. C.; Srivastava, A. K.; Zerweck, J.; Williams, J. T. B.; Hawk, A. J.; Sachleben, J. R.; Meredith, S. C. β-Amyloid Model Core Peptides: Effects of Hydrophobes and Disulfides. *Protein Sci.* **2020**, *29* (2), 527–541. https://doi.org/10.1002/pro.3778.

(23) Straub, J. E.; Thirumalai, D. Principles Governing Oligomer Formation in Amyloidogenic Peptides. *Curr. Opin. Struct. Biol.* **2010**, *20* (2), 187–195. https://doi.org/10.1016/j.sbi.2009.12.017.

(24) Kreutzer, A. G.; Nowick, J. S. Elucidating the Structures of Amyloid Oligomers with Macrocyclic β-Hairpin Peptides: Insights into Alzheimer's Disease and Other Amyloid Diseases. *Acc. Chem. Res.* **2018**, *51* (3), 706–718. https://doi.org/10.1021/acs.accounts.7b00554.

(25) Kreutzer, A. G.; Spencer, R. K.; McKnelly, K. J.; Yoo, S.; Hamza, I. L.; Salveson, P. J.; Nowick, J. S. A Hexamer of a Peptide Derived from Aβ16-36. *Biochemistry* **2017**, *56* (45), 6061–6071. https://doi.org/10.1021/acs.biochem.7b00831.

(26) Wang, Y.; Kreutzer, A. G.; Truex, N. L.; Nowick, J. S. A Tetramer Derived from Islet Amyloid Polypeptide. *J. Org. Chem.* **2017**, *82* (15), 7905–7912. https://doi.org/10.1021/acs.joc.7b01116.

(27) Kreutzer, A. G.; Yoo, S.; Spencer, R. K.; Nowick, J. S. Stabilization, Assembly, and Toxicity of Trimers Derived from Aβ. *J. Am. Chem. Soc.* **2017**, *139* (2), 966–975. https://doi.org/10.1021/jacs.6b11748.

(28) Kreutzer, A. G.; Samdin, T. D.; Guaglianone, G.; Spencer, R. K.; Nowick, J. S. X-Ray

Crystallography Reveals Parallel and Antiparallel β-Sheet Dimers of a β-Hairpin Derived from Aβ16-36that Assemble to Form Different Tetramers. *ACS Chem. Neurosci.* **2020**, *11* (15), 2340–2347. https://doi.org/10.1021/acschemneuro.0c00290.

(29) Haerianardakani, S.; Kreutzer, A. G.; Salveson, P. J.; Samdin, T. D.; Guaglianone, G. E.; Nowick, J. S. Phenylalanine Mutation to Cyclohexylalanine Facilitates Triangular Trimer Formation by β-Hairpins Derived from Aβ. *J. Am. Chem. Soc.* **2020**, *142* (49), 20708–20716. https://doi.org/10.1021/jacs.0c09281.

(30) Salveson, P. J.; Spencer, R. K.; Kreutzer, A. G.; Nowick, J. S. X-Ray Crystallographic Structure of a Compact Dodecamer from a Peptide Derived from Aβ16-36. *Org. Lett.* **2017**, *19* (13), 3462–3465. https://doi.org/10.1021/acs.orglett.7b01445.

(31) Spencer, R. K.; Li, H.; Nowick, J. S. X-Ray Crystallographic Structures of Trimers and Higher-Order Oligomeric Assemblies of a Peptide Derived from Aβ17-36. *J. Am. Chem. Soc.* **2014**, *136* (15), 5595–5598. https://doi.org/10.1021/ja5017409.

(32) Bleiholder, C.; Dupuis, N. F.; Wyttenbach, T.; Bowers, M. T. Ion Mobility-Mass Spectrometry Reveals a Conformational Conversion from Random Assembly to β-Sheet in Amyloid Fibril Formation. *Nat. Chem.* **2011**, *3* (2), 172–177. https://doi.org/10.1038/nchem.945.

(33) Bleiholder, C.; Bowers, M. T. The Solution Assembly of Biological Molecules Using Ion Mobility Methods: From Amino Acids to Amyloid β-Protein. *Annu. Rev. Anal. Chem.* **2017**, *10*, 365–386. https://doi.org/10.1146/annurev-anchem-071114-040304.

(34) Durell, S. R.; Kayed, R.; Guy, H. R. The Amyloid Concentric B-barrel Hypothesis: Models of Amyloid Beta 42 Oligomers and Annular Protofibrils. *Proteins Struct. Funct. Bioinforma.* **2022**, 1–20. https://doi.org/10.1002/prot.26301.

(35) Ladiwala, A. R. A.; Litt, J.; Kane, R. S.; Aucoin, D. S.; Smith, S. O.; Ranjan, S.; Davis, J.; Van Nostrand, W. E.; Tessier, P. M. Conformational Differences between Two Amyloid Boligomers of Similar Size and Dissimilar Toxicity. *J. Biol. Chem.* **2012**, *287* (29), 24765–24773. https://doi.org/10.1074/jbc.M111.329763.

(36) Wesén, E.; Jeffries, G. D. M.; Dzebo, M. M.; Esbjörner, E. K. Endocytic Uptake of Monomeric Amyloid-β Peptides Is Clathrin- A Nd Dynamin-Independent and Results in Selective Accumulation of Aβ(1-42) Compared to Aβ(1-40). *Sci. Rep.* **2017**, *7* (1), 1–14. https://doi.org/10.1038/s41598-017-02227-9.

(37) Dutta, S.; Finn, T. S.; Kuhn, A. J.; Abrams, B.; Raskatov, J. A. Chirality Dependence of Amyloid β Cellular Uptake and a New Mechanistic Perspective. *ChemBioChem* **2019**, *20* (8), 1023–1026. https://doi.org/https://doi.org/10.1002/cbic.201800708.

(38) Esbjörner, E. K.; Chan, F.; Rees, E.; Erdelyi, M.; Luheshi, L. M.; Bertoncini, C. W.; Kaminski, C. F.; Dobson, C. M.; Kaminski Schierle, G. S. Direct Observations of Amyloid β Self-Assembly in Live Cells Provide Insights into Differences in the Kinetics of Aβ(1-40) and Aβ(1-42) Aggregation. *Chem. Biol.* **2014**, *21* (6), 732–742. https://doi.org/10.1016/j.chembiol.2014.03.014.

(39) Cline, E. N.; Das, A.; Bicca, M. A.; Mohammad, S. N.; Schachner, L. F.; Kamel, J. M.; DiNunno, N.; Weng, A.; Paschall, J. D.; Bu, R. Lo; Khan, F. M.; Rollins, M. G.; Ives, A. N.; Shekhawat, G.; Nunes-Tavares, N.; de Mello, F. G.; Compton, P. D.; Kelleher, N. L.; Klein, W. L. A Novel Crosslinking Protocol Stabilizes Amyloid β Oligomers Capable of Inducing Alzheimer's-Associated Pathologies. *J. Neurochem.* **2019**, *148* (6), 822–836. https://doi.org/10.1111/jnc.14647.

(40) Darling, A. L.; Shorter, J. Atomic Structures of Amyloid-β Oligomers Illuminate a

Neurotoxic Mechanism. *Trends Neurosci.* **2020**, *43* (10), 740–743.

https://doi.org/10.1016/j.tins.2020.07.006.

Supporting information for:

Isomorphic Trimers Derived from Aβ Exhibit Different Oligomerization and Interactions with Cells

Table of Contents

General Information 118

Synthesis of the Macrocyclic Peptides $2AM_{CC}$ and KLM_{CC} 119

Oxidation of Peptide KLM_{CC} to Trimer KLT 119

SDS-PAGE 120

Cell Culture 121

Caspase 3/7 Assay 121

Synthesis of Fluorescently labeled 2AT and KLT 122

Fluorescence Microscopy 123

References and Notes 125

Characterization Data

- Characterization of $2AT_{CC}$ 127
- Characterization of 2AT 130
- Characterization of KLT_{CC} 134
- Characterization of KLT 137
- Characterization of 2AT-sCy3 141
- Characterization of KLT -sCy3 145
- Characterization of 2AT-sCy3 149

General Information[1]

All Fmoc-protected amino acids including the unnatural amino acid, Boc-ornithine(Fmoc)-OH, were purchased from Chem-Impex or Anaspec. 2-Chlorotrityl chloride resin was purchased from Chem-Impex. Trifluoroacetic acid (TFA), and HPLC grade acetonitrile (MeCN) were purchased from Fischer Scientific. Water was purified to 18 MΩ with a ThermoFisher Barnstead Nanopure water purification system. All other solvents and chemicals were purchased from Alfa Aesar and Sigma Aldrich. All amino acids, resins, solvents, and chemicals were used as received, with the exception that dichloromethane (DCM) and *N,N*-dimethylformamide (DMF) were dried by passage through dry alumina under argon. Analytical HPLC chromatograms were obtained using an Agilent 1260 Infinity II HPLC equipped with Phenomenex bioZen C18 column (150 mm × 4.6 mm, 2.6 μm particle size). HPLC grade acetonitrile (ACN) and 18 MΩ deionized water, each containing 0.1% trifluoroacetic acid, were used as the mobile phase running at 1 mL/min flow rate. Peaks for peptides without fluorophores were detected at 214 nm. Sulfo-cyanine3 labeled peptides were detected at 548 nm and sulfo-cyanine5 labeled peptides were detected at 646 nm in addition to 214 nm. All peptides were monitored using the provided HPLC OpenLAB software.

Preparative-scale purification of $2AM_{CC}$, 2AT, KLM_{CC}, and KLT were done using an Agilent Zorbax SB-C18 PrepHT column (21.2 mm x 250 mm, 7 μm particle size) on a Rainin Dynamax HPLC with a flow rate of 12.0 mL/min, monitored at 214 nm with the accompanying DA Rainin HPLC software. HPLC grade acetonitrile (ACN) and 18 MΩ deionized water, each containing 0.1% trifluoroacetic acid, were used as the mobile phase. Semi-preparative scale purification of fluorescently labeled peptides was done using an Agilent Zorbax 300SB-C18 semi-preparative column (9.4 mm x 250 mm, 5 μm particle size) with a ZORBAX 300SB-C3

preparative guard column (9.4 x 15 mm) on a Rainin Dynamax HPLC with a flow rate of 5.0 mL/min. The C18 column and the guard column were heated to 60 °C in a water bath. Elution was monitored at 214 nm with the accompanying DA Rainin HPLC software. Liquid chromatography-mass spectrometry was performed using a Waters Xevo XS UPLC-QTOF. Spectra were analyzed using the accompanying Waters MassLynx software.

Synthesis of the Macrocyclic Peptides $2AM_{CC}$ and KLM_{CC}

The synthesis, purification, and characterization of $2AM_{CC}$ has been reported previously.[2] The synthesis of KLM_{CC} followed procedures similar to those previously reported and involved the following sequence of operations: (1) resin loading and capping, (2) solid-phase amino acid couplings, (3) cleavage of the linear peptides from the resin, (4) solution-phase cyclization of the linear peptides, (5) global deprotection of acid-labile protecting groups, and (6) purification with preparative reverse-phase HPLC. Clean fractions were combined and lyophilized. The purified peptide was characterized by analytical HPLC and liquid chromatography-mass spectrometry.

Oxidation of Peptide KLM_{CC} to Trimer KLT

A 6 mM solution of lyophilized peptide was prepared gravimetrically by dissolving the peptide in an appropriate amount of 20% (v/v) aqueous DMSO prepared with deionized water. The reaction was carried out in a capped 25-mL glass scintillation vial with rocking at room temperature for 48 h. After 48 h, the reaction mixture was immediately subjected to RP-HPLC purification. Pure fractions were concentrated by rotary evaporation and lyophilized. The purified trimer was characterized by analytical HPLC and liquid chromatography-mass spectrometry.

SDS-PAGE[3]

Solutions of the peptides were prepared gravimetrically by dissolving the lyophilized peptide in the appropriate amount of 18 MΩ deionized water to achieve a 10 mg/mL stock. Aliquots of the 10 mg/mL stock solutions were diluted with 18 MΩ deionized water to create 50 μM solutions. 1 μL of 6X SDS-PAGE sample loading buffer (G Biosciences) was added per 5 μL sample solution to create working solutions. A 5 μL aliquot of each working solution was run on a 16% polyacrylamide gel with a 4% stacking polyacrylamide gel. The gel was run at a constant 60 volts for approximately 4 h. Reagents and gels for Tricine SDS-PAGE were prepared according to recipes and procedures detailed in Schägger, H. *Nat. Protoc*. **2006**, *1*, 16–22.[4]

Staining with silver nitrate was used to visualize the peptides in the SDS-PAGE gel. Reagents for silver staining were prepared according to procedures detailed in Simpson, R. J. *Cold Spring Harb. Protoc.* **2007**.[5] Briefly, the gel was removed from the casting glass and rocked in fixing solution (50% (v/v) methanol and 5% (v/v) acetic acid in 18 MΩ deionized water) for 20 min. Next, the fixing solution was discarded and the gel was rocked in 50% (v/v) aqueous methanol for 10 min. The 50% methanol was subsequently discarded and the gel was rocked in 18 MΩ deionized water for 10 min. After the water was discarded, the gel was rocked in 0.02% (w/v) sodium thiosulfate in 18 MΩ deionized water for 1 min. The sodium thiosulfate was discarded and the gel was rinsed with 18 MΩ deionized water for 1 min (2x). After the last rinse, the gel was submerged in chilled 0.1% (w/v) silver nitrate in 18 MΩ deionized water and rocked at 4 °C for 20 min. The silver nitrate solution was then discarded and the gel was rinsed with 18 MΩ deionized water for 30 s (2x). To develop the gel, the gel was incubated in developing solution (2% (w/v) sodium carbonate, 0.04% (w/v) formaldehyde) until the desired intensity of staining was reached (~2–5 min). When the desired intensity of staining was reached,

the development was stopped by discarding the developing solution and submerging the gel in 5% aqueous acetic acid.

Cell Culture

SH-SY5Y neuroblastoma cell cultures (ATCC® CRL-2266™) were maintained in 1:1 mixture of Dubelcco's modified Eagle medium and Ham's F12 (DMEM:F12) medium supplemented with 10% heat-inactivated fetal bovine serum (FBS), 100 U/mL penicillin and 100 µg/mL streptomycin at pH 7.4 in a humidified 5% CO2 atmosphere at 37 °C using a Fischer Scientific Forma Series 3 Water Jacketed CO_2 Incubator. All experiments were performed using ca. 60–80% confluent cells on passages ranging from 2–10.

Caspase 3/7 Assay

SH-SY5Y cells were seeded at 30,000 cells per well in the inner 60 wells of half area 96-well plates to a total volume of 50 µL using 1:1 DMEM/F12 media supplemented with 10% FBS, 100 U/mL penicillin and 100 µg/mL streptomycin at pH 7.4. The outer wells of the plate were filled with 100 µL of media without any cells. The cells were incubated for 24 h after plating. Prior to treatment, the media of the inner 60 wells was removed by pipet. Solutions of the peptides were prepared gravimetrically by dissolving the lyophilized peptide in the appropriate amount of 18 MΩ deionized water to achieve a 10 mg/mL stock. From the 10 mg/mL stock solutions, 50 µM solutions were made by dilution with serum-free, phenol-red free 1:1 DMEM/F12 media with no added penicillin or streptomycin. 2-fold serial dilutions of the 50 µM solutions were prepared by diluting with serum-free, phenol-red free 1:1 DMEM/F12 media with no added penicillin or streptomycin resulting in solutions with concentrations of 50 µM, 25

μM, 12.5 μM, 6.3 μM, and 3.2 μM. 50 μL of a solution was added to the wells containing cells and each treatment was run in triplicate. An additional six wells were used as controls. Three wells received a solution of serum-free, phenol-red free 1:1 DMEM/F12 media with 7% 18 MΩ deionized water (vehicle, negative control) and the other three wells were left untreated, to be subsequently treated with 2.5 μM staurosporine (positive control) 6 h prior to development. Cells were incubated for 72 hours.

After 72 hours, the Caspase 3/7 Assay (Caspase-Glo® 3/7 Assay System, Promega) was performed according to the manufacturer's instructions. Data were collected on a Promega GloMax Discover and analyzed.

Synthesis of Fluorescently Labeled 2AT and KLT

5 mg of NHS-ester sulfo-cyanine3 and NHS-ester sulfo-cyanine5 were purchased from Lumiprobe. The powder was dissolved in water and transferred into Eppendorf tubes in 17 μg aliquots. Eppendorf tubes containing aliquoted fluorophore were immediately moved to a -80 °C freezer and remained overnight. The Eppendorf tubes were then lyophilized.

A 75 mM sodium carbonate buffer solution was prepared gravimetrically and the pH was adjusted to 9.6. A 10 mg/mL solution of 2AT or KLT was prepared gravimetrically by dissolving the lyophilized peptide in the appropriate amount of 18 MΩ deionized water. To a clean Eppendorf tube, 300 μL of 10 mg/mL solution of trimer was added to 700 μL of 75 mM sodium carbonate buffer. 40 μL of the reaction mixture was transferred into an Eppendorf tube containing 17 μg of NHS-ester fluorophore. The dissolved fluorophore and reaction mixture was transferred back to the larger reaction mixture. The reaction was protected from light with black felt and rocked gently for 1 h. After 1 h, the reaction was directly injected onto an HPLC.

The fluorescently labeled trimers were purified by semi-preparative reverse-phase HPLC using an Agilent Zorbax 300SB-C18 semi-preparative column (9.4 mm x 250 mm, 5 μm particle size) with a ZORBAX 300SB-C3 preparative guard column (9.4 x 15 mm) on a Rainin Dynamax HPLC with a flow rate of 5.0 mL/min. The C18 column and the guard column were heated to 60 °C in a water bath. The trimers were eluted from 20–45% over 90 minutes. Elution was monitored at 214 nm with the accompanying DA Rainin HPLC software. Pure fractions were combined and lyophilized. The purified peptide was characterized by analytical HPLC and liquid chromatography-mass spectrometry.

Stock solutions of fluorescently labeled analogues were prepared spectrophotometrically. Lyophilized peptide was dissolved in 18 MΩ deionized water and the absorbance was measured using the λ_{max} of the respective fluorophore (2AT-L-sCy3 λ_{max}= 548 nm, 2AT-L-sCy5 λ_{max}= 646 nm). The published molar extinction coefficients were used to calculate sample concentration.

Fluorescence Microscopy[6]

Cell Preparation, Treatment, and Imaging. SH-SY5Y cells were plated in an Ibidi μ-Slide 8 Well Chamber Slide (Ibidi catalog number 80826) at 80,000 cells per well. Cells were incubated in 500 μL of a 1:1 mixture of DMEM:F12 media supplemented with 10% fetal bovine serum, 100 U/mL penicillin, and 100 μg/mL streptomycin at 37 °C in a 5% CO_2 atmosphere and allowed to adhere to the bottom of the slide for 48 hours. A solution of 100 nM of lysotracker-containing media was prepared by adding Lysotracker Green DND-26 (ThermoFischer) into serum-free, phenol red-free 1:1 DMEM/F12 media. Solutions of 2AT-sCy3, KLT-sCy3, or 2AT-sCy5 were prepared to a final volume of 200 μL and a final concentration of 1 μM in either

serum-free, phenol red-free 1:1 DMEM/F12 media or serum-free, phenol red-free 1:1 DMEM/F12 media with Lysotracker Green DND-26.

After cells were incubated for 48 hours, the media was removed and replaced with solutions of fluorescently labeled analogues with and without Lysotracker Green DND-26. Control wells were treated with media containing no peptide. The slide was incubated in the microscope chamber for 8 hours. The media was removed from the well slide containing the cells and replaced with 200 μL of 1 μg/mL Hoechst 33342 in serum-free, phenol red-free 1:1 DMEM:F12 media. After 30 minutes, the Hoechst-containing media was removed and replaced with 200 μL of serum-free, phenol red-free 1:1 DMEM:F12 media. The cells were imaged using a Keyence BZ-X810 fluorescence microscope. Images were collected with a 60x oil immersion objective lens. Micrographs of treated cells were recorded using the DAPI filter cube [excitation wavelength = 350/50 nm (325–375 nm) and emission wavelength = 460/50 nm (435–485nm)] for Hoechst nuclear marker, the Cy3 filter cube [excitation wavelength = 545/25 nm (532.5–557.5 nm) and emission wavelength = 605/70 nm (570–640 nm)] for 2AT-L-sCy3, the Cy5 filter cube [excitation wavelength = 620/60 nm (590–650 nm) and emission wavelength = 700/75 nm (662.5–737.5 nm)] for 2AT-L-sCy5, and the GFP filter cube [excitation wavelength = 470/40 nm (450–490 nm) and emission wavelength = 525/50 nm (500–550 nm)] for Lysotracker Green DND-26 (ThermoFischer).The image brightness of the channels was adjusted using BZ-X810 Analyzer software.

REFERENCES AND NOTES

(1) The chemicals and instruments required for the synthesis of macrocyclic β-sheet peptide KLT and 2AT are similar to those used in our laboratory's previous publications. This information was either adapted from or taken verbatim from Kreutzer, A. G.; Yoo, S.; Spencer, R. K.; Nowick, J. S. Stabilization, Assembly, and Toxicity of Trimers Derived from Aβ. *J. Am. Chem. Soc.* **2017**, *139* (2), 966–975. https://doi.org/10.1021/jacs.6b11748.

(2) Kreutzer, A. G.; Yoo, S.; Spencer, R. K.; Nowick, J. S. Stabilization, Assembly, and Toxicity of Trimers Derived from Aβ. *J. Am. Chem. Soc.* **2017**, *139* (2), 966–975. https://doi.org/10.1021/jacs.6b11748.

(3) Peptides were run on SDS-PAGE and silver stained following a protocol similar to those published previously in our laboratory. The Procedures Were Either Adapted from or Taken Verbatim from: Kreutzer, A. G.; Yoo, S.; Spencer, R. K.; Nowick, J. S. Stabilization, Assembly, and Toxicity of Trimers Derived from Aβ. *J. Am. Chem. Soc.* **2017**, *139* (2), 966–975. https://doi.org/10.1021/jacs.6b11748.

(4) Schägger, H. Tricine-SDS-PAGE. *Nat. Protoc.* **2006**, *1,* 16–22.

(5) Simpson, R. J. Staining Proteins in Gels with Silver Nitrate. *Cold Spring Harb. Protoc.* **2007**, Doi: 10.1101/Pdb.Prot4727.

(6) Fluorescently labeled 2AT and KLT analogues were imaged following a protocol similar to those published previously by our laboratory. This information was either adapted from or taken verbatim from Zhang, S.; Guaglianone, G.; Morris, M. A.; Yoo, S.; Howitz, W. J.; Xing, L.; Zheng, J. G.; Jusuf, H.; Huizar, G.; Lin, J.; Kreutzer, A. G.; Nowick, J. S. Expression of N-Terminal Cysteine Aβ42 and Conjugation to Generate Fluorescent and

Biotinylated Aβ42. *Biochemistry* **2021**, *60* (15), 1191–1200.

https://doi.org/10.1021/acs.biochem.1c00105.

Characterization Data

Characterization of peptide 2AT$_{CC}$

Analytical HPLC trace

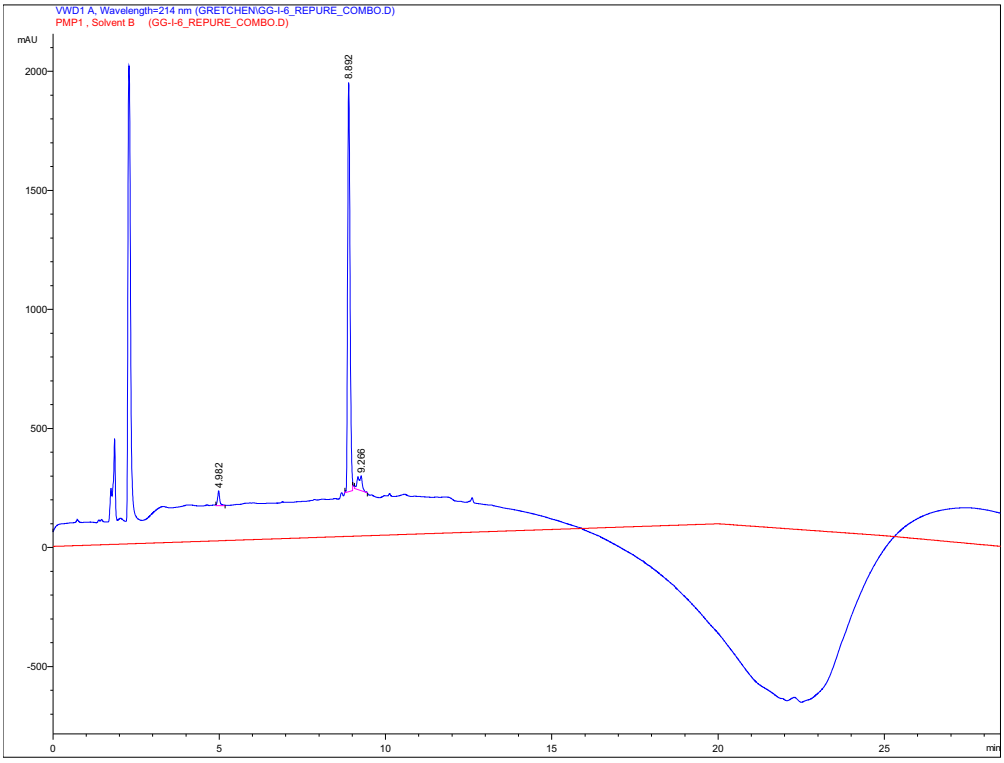

Signal 1: VWD1 A, Wavelength=214 nm

Peak #	RetTime [min]	Type	Width [min]	Area mAU *s	Height [mAU]	Area %
1	4.982	MM	0.0764	288.73434	62.96883	2.7267
2	8.892	MM	0.0828	8546.16309	1721.23706	80.7065
3	9.266	MM	0.1569	589.23090	62.61000	5.5645

Mass spectrum of $2AT_{CC}$

Calculated $[M+H]^+$ of $2AT_{CC}$: 1766.93

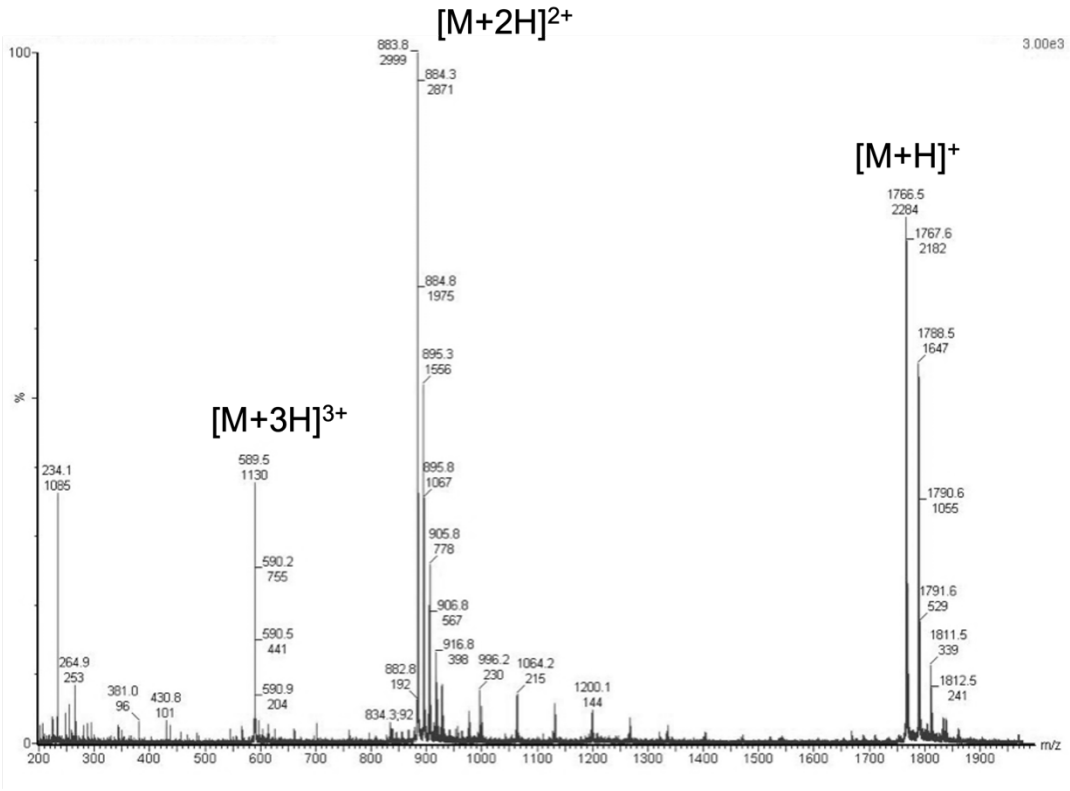

Mass spectrum of $2AT_{CC}$

Calculated $[M+H]^+$ of $2AT_{CC}$: 1766.93

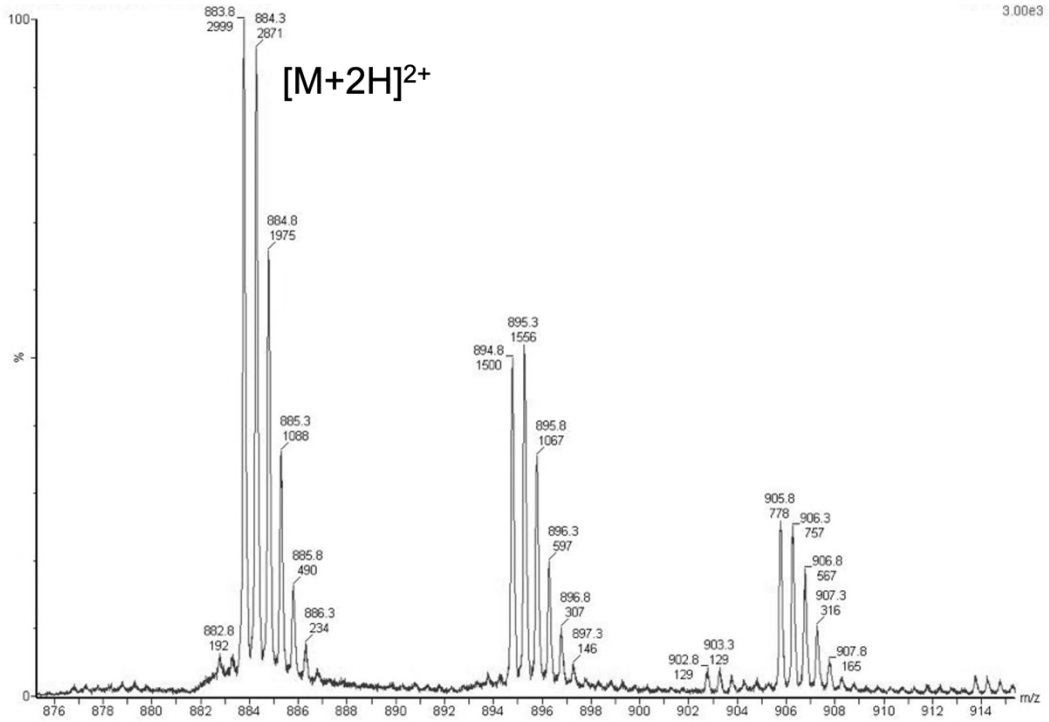

Characterization of trimer 2AT

Analytical HPLC trace

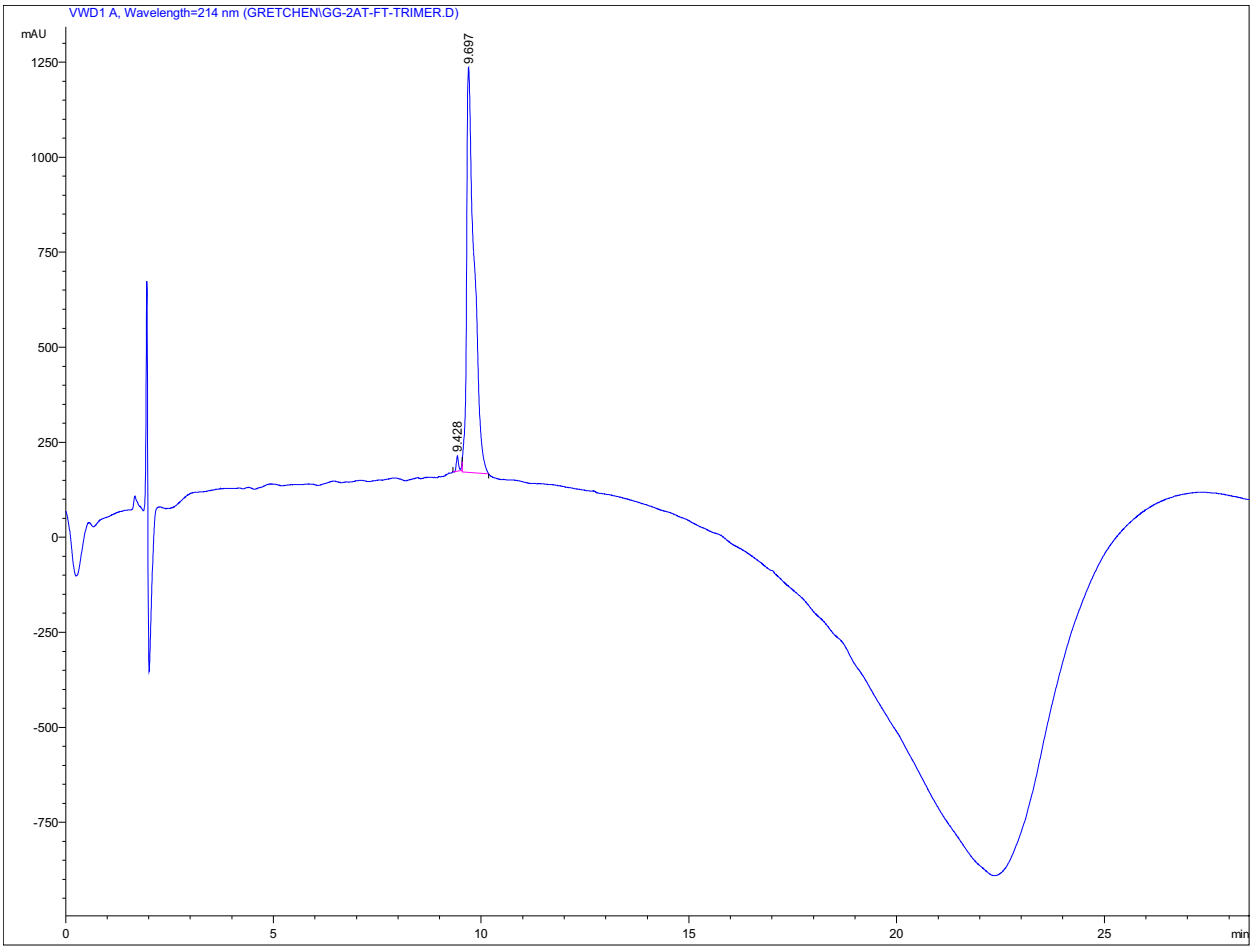

Signal 1: VWD1 A, Wavelength=214 nm

Peak #	RetTime [min]	Type	Width [min]	Area mAU *s	Height [mAU]	Area %
1	9.428	MM	0.0706	171.36655	40.45287	1.2561
2	9.697	MM	0.2106	1.34710e4	1066.05396	98.7439

Mass spectrum of 2AT

Calculated $[M+H]^+$ of 2AT: 5292.74

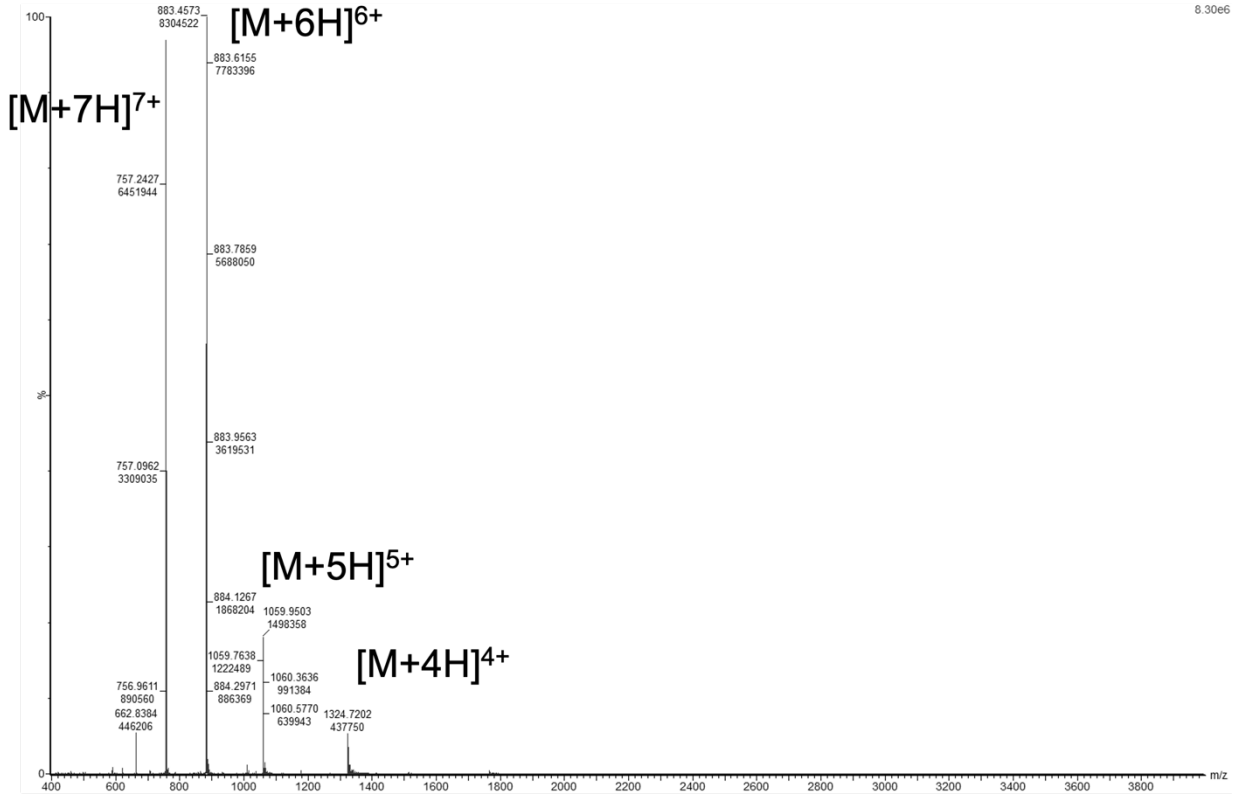

Expansion mass spectrum of 2AT

Calculated $[M+H]^+$ of 2AT: 5292.74

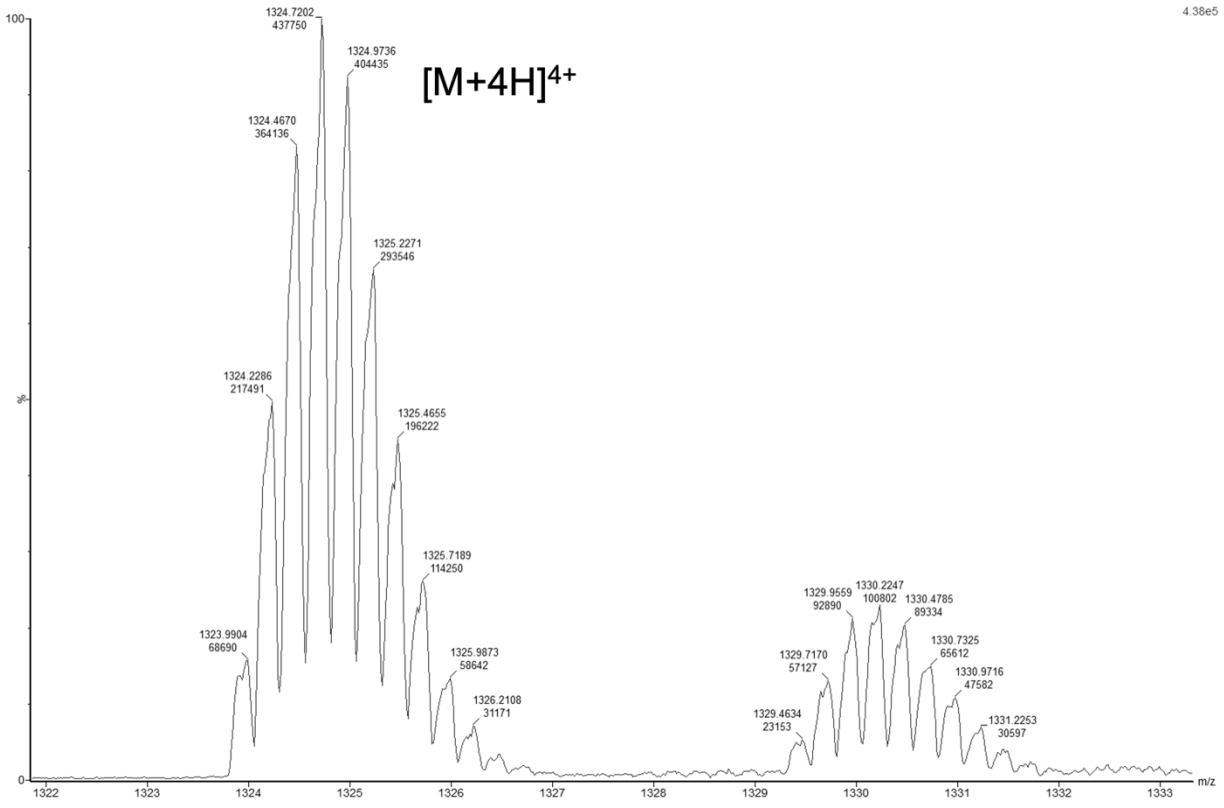

Deconvolution mass spectrum of 2AT

Exact mass of 2AT: 5291.73

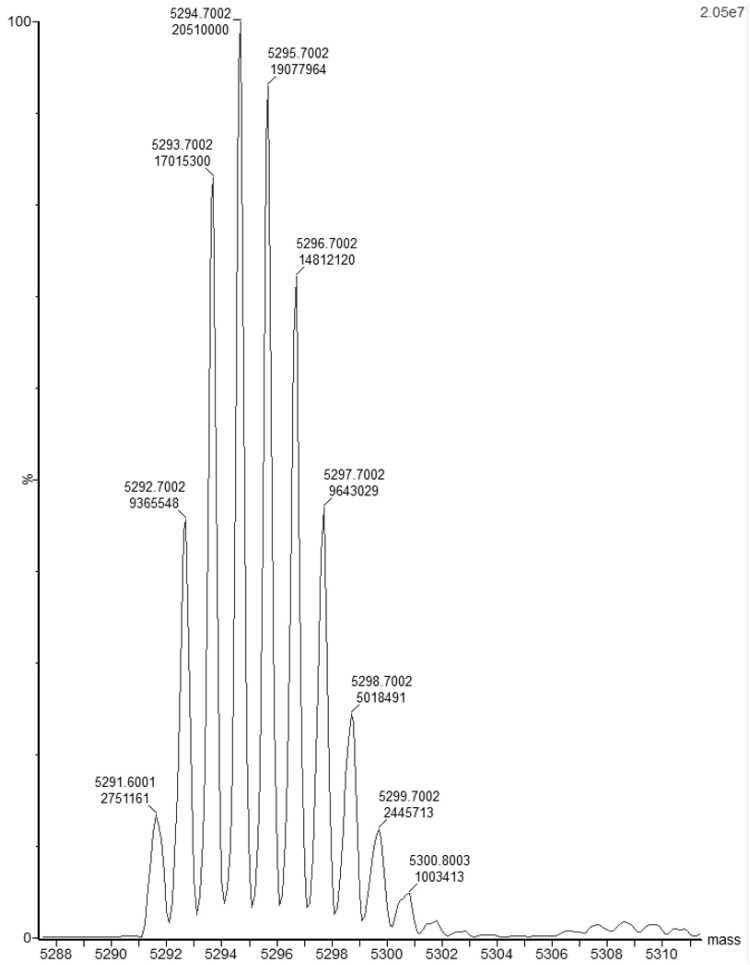

Characterization of peptide KLT_{CC}

Analytical HPLC trace

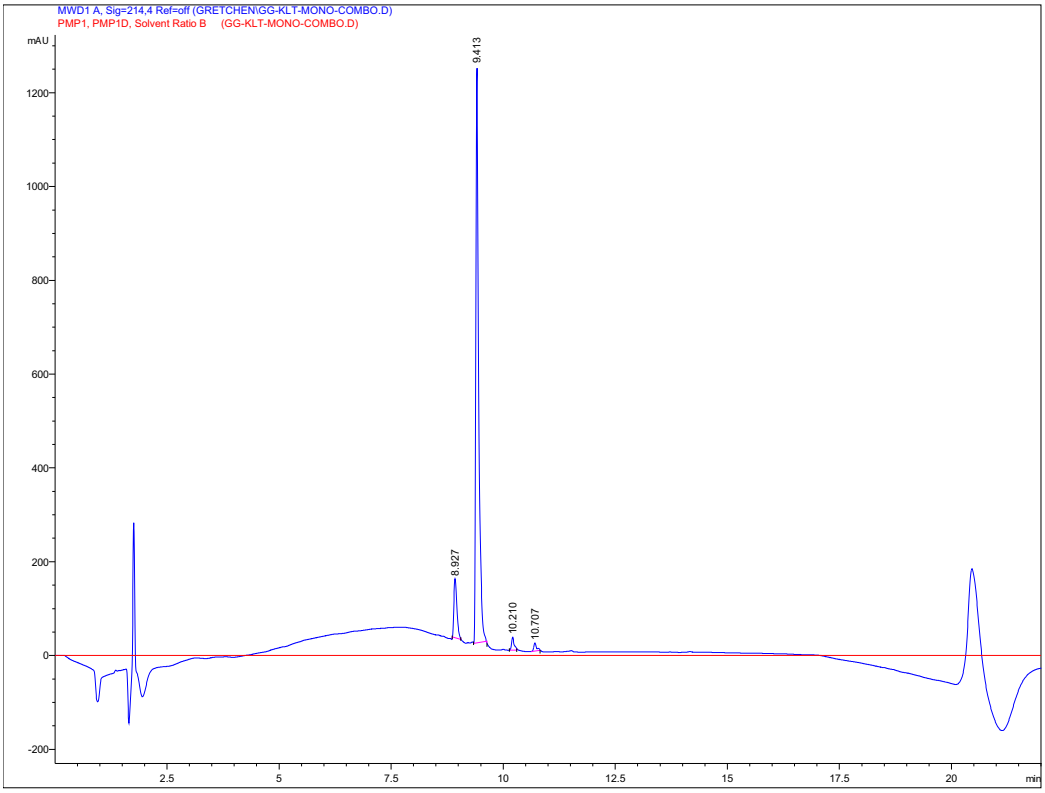

Signal 1: MWD1 A, Sig=214,4 Ref=off

Peak #	RetTime [min]	Type	Width [min]	Area [mAU*s]	Height [mAU]	Area %
1	8.927	MM	0.0783	595.82605	126.90630	9.6829
2	9.413	MM	0.0739	5436.47900	1225.67163	88.3493
3	10.210	MM	0.0537	76.02363	23.57573	1.2355
4	10.707	MM	0.0583	45.06036	12.88971	0.7323

The observed peak that elutes at 8.927 min is observed when methionine oxidation occurs.

Mass spectrum of KLT_{CC}

Calculated $[M+H]^+$ of KLT_{CC}: 1796.96

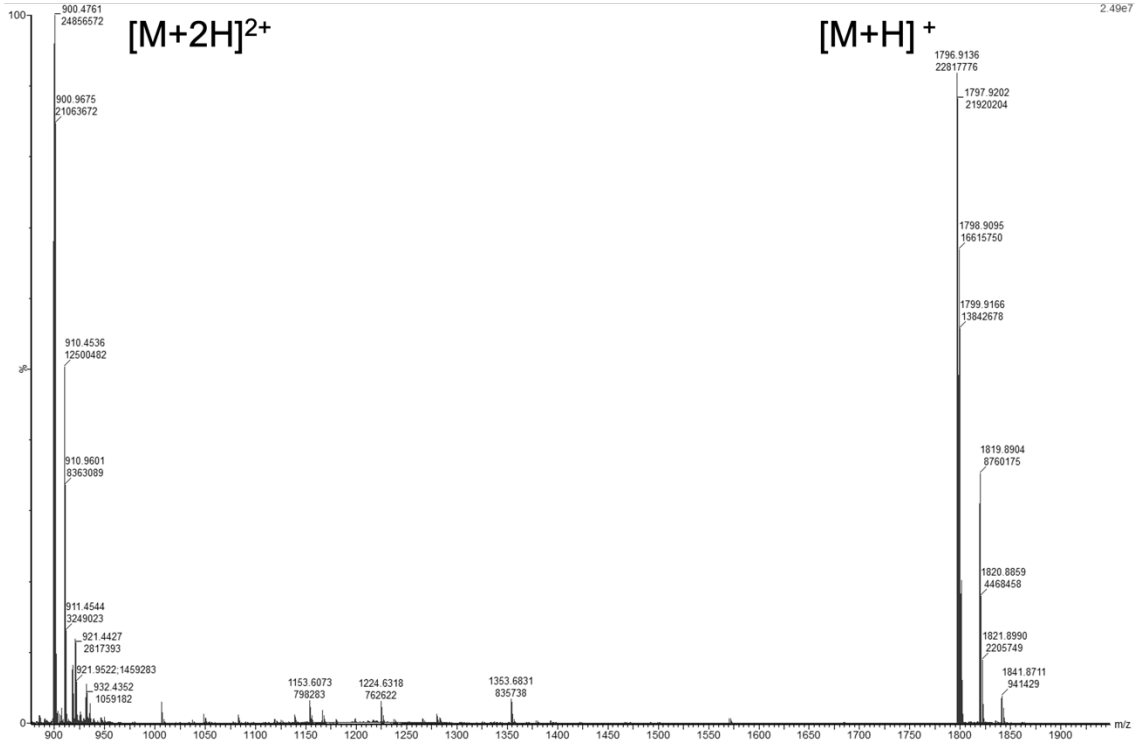

Mass spectrum of KLT_{CC}

Calculated $[M+H]^+$ of KLT_{CC}: 1796.96

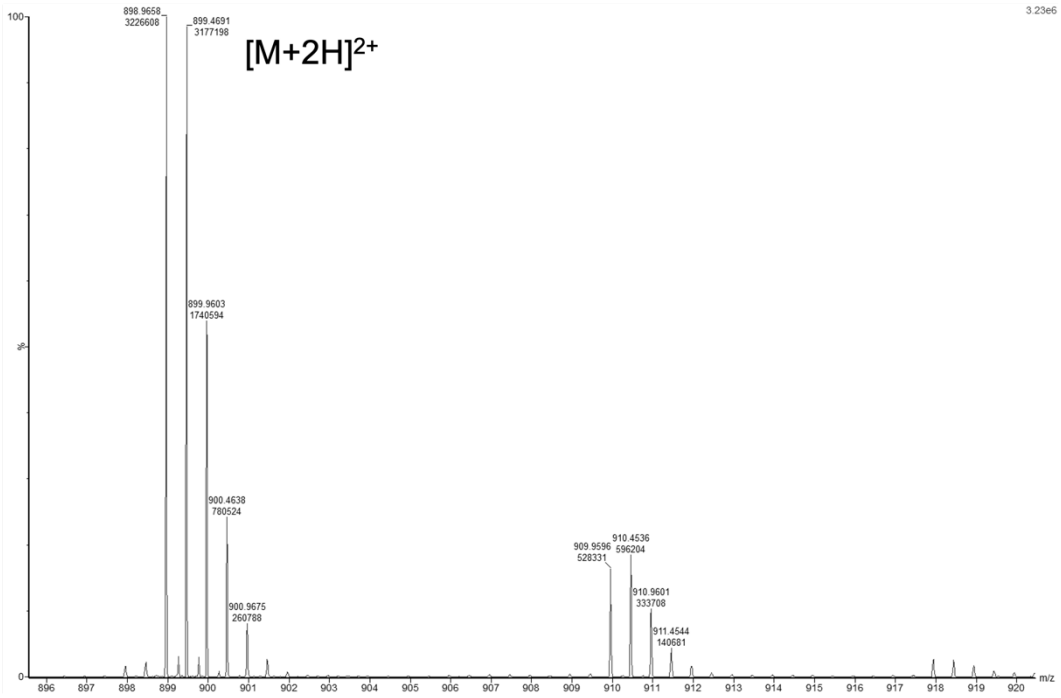

Characterization of trimer KLT

Analytical HPLC trace

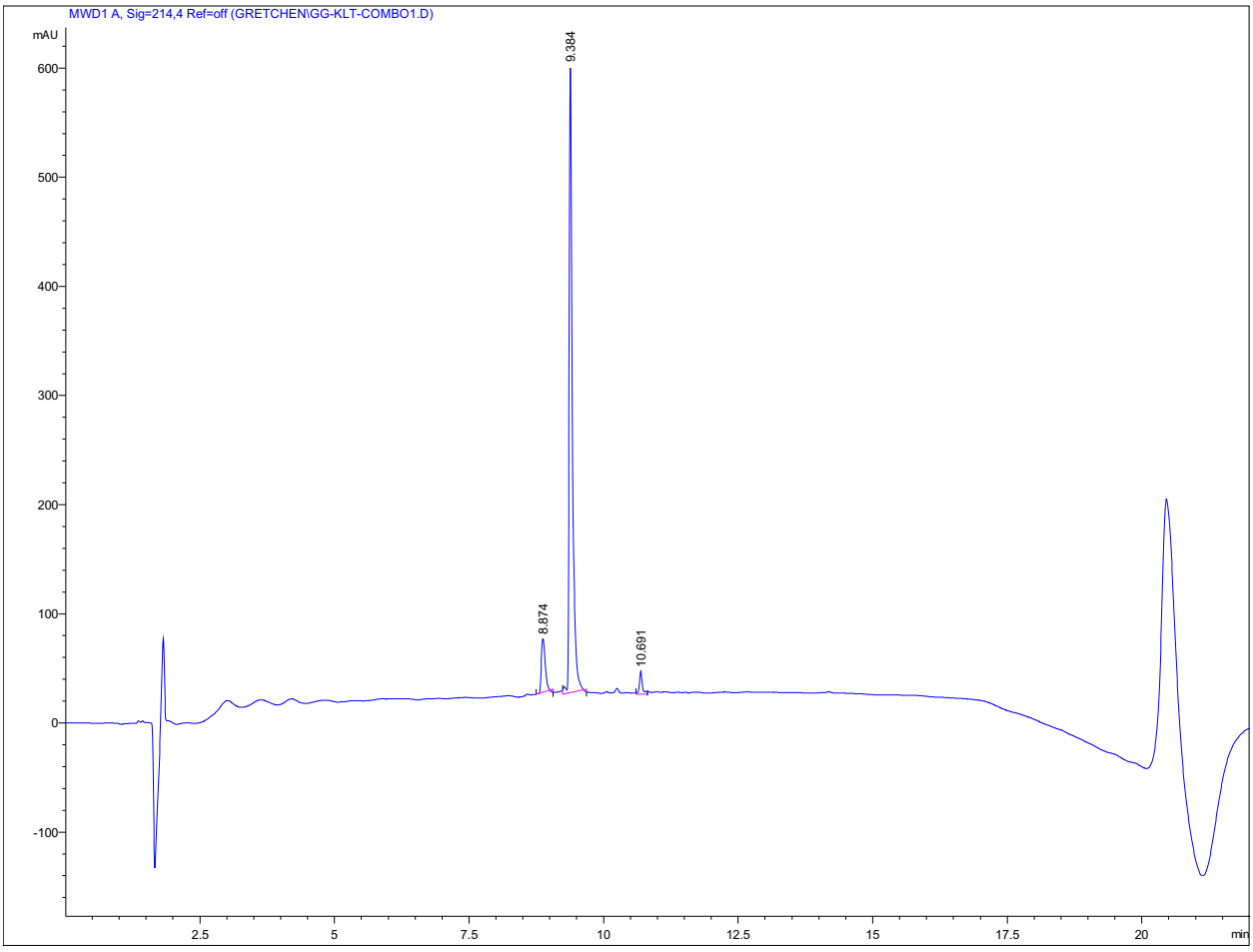

Signal 1: MWD1 A, Sig=214 nm Ref=off

Peak #	RetTime [min]	Type	Width [min]	Area [mAU*s]	Height [mAU]	Area %
1	8.874	MM	0.0815	241.49431	49.37487	9.0355
2	9.384	MM	0.0681	2345.10425	574.30060	87.7422
3	10.691	MM	0.0671	86.12202	21.39272	3.2223

The observed peak that elutes at 8.874 min is observed when methionine oxidation occurs.

Mass spectrum of KLT

Calculated $[M+H]^+$ of KLT: 5382.83

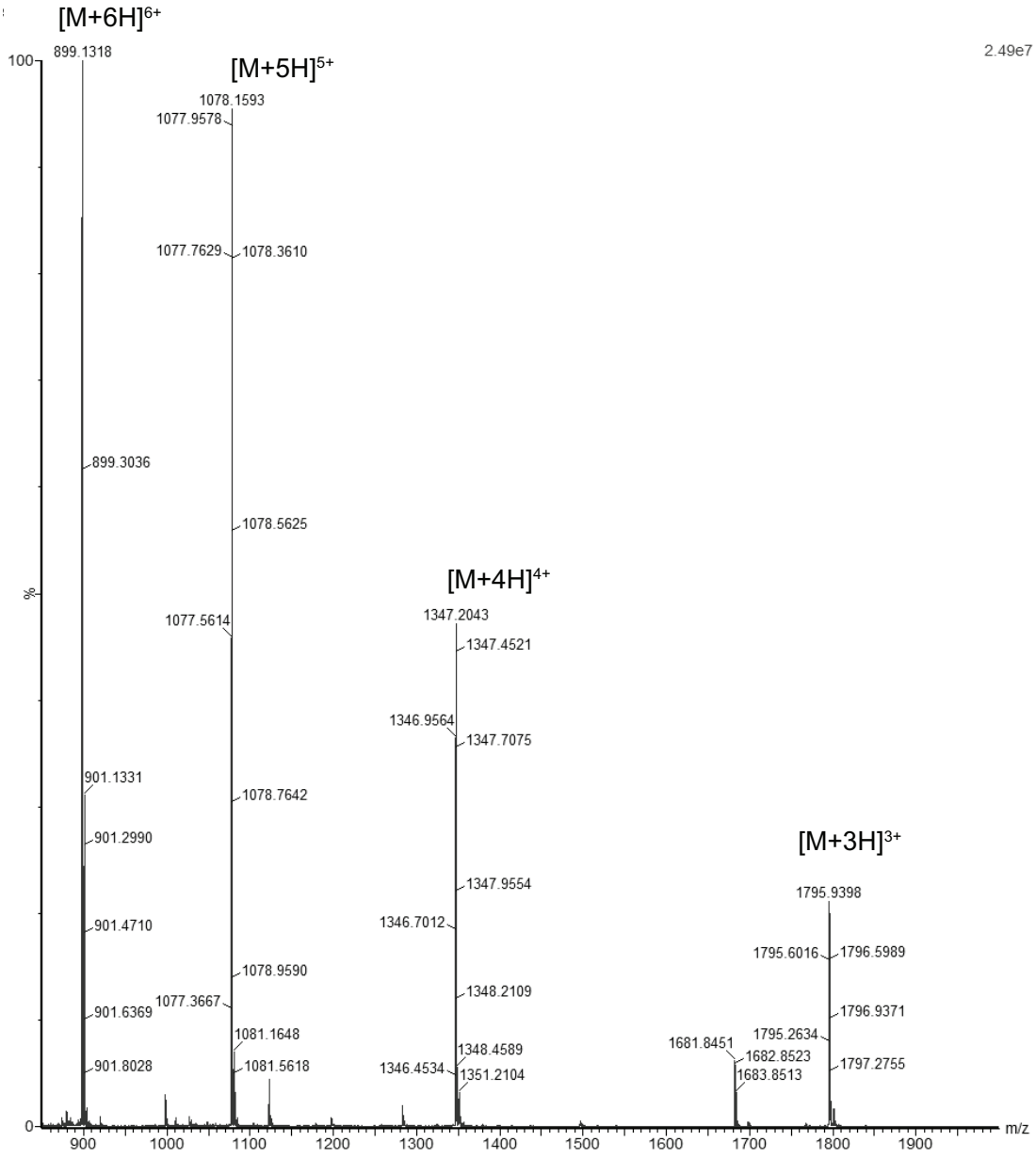

Expansion mass spectrum of KLT

Calculated $[M+H]^+$ of KLT: 5382.83

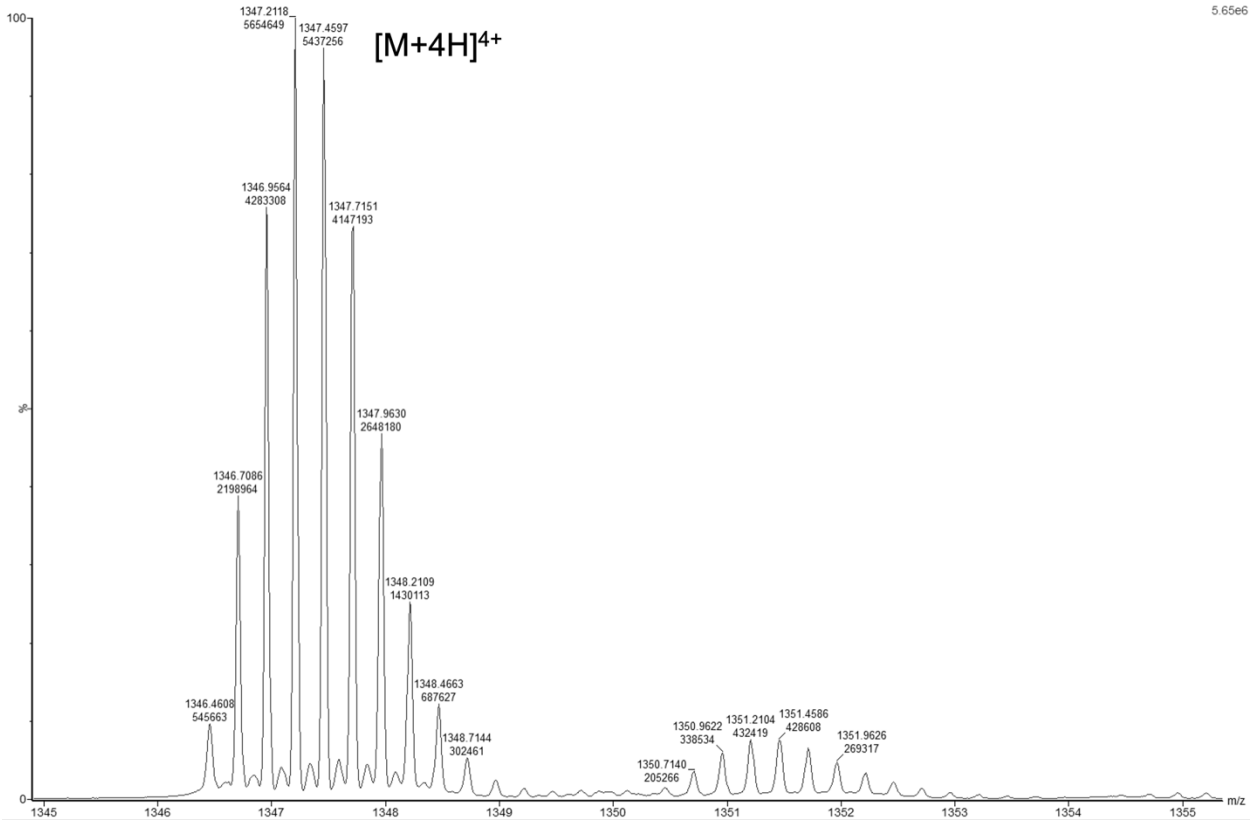

Deconvolution mass spectrum of KL

Exact mass of KLT: 5381.82

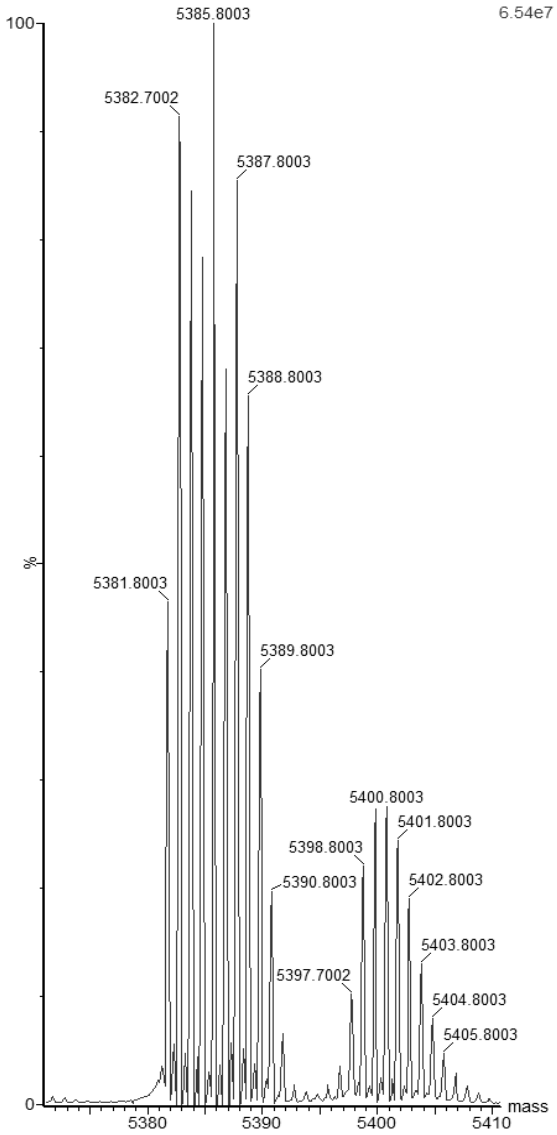

Characterization of 2AT-sCy3

Analytical HPLC trace

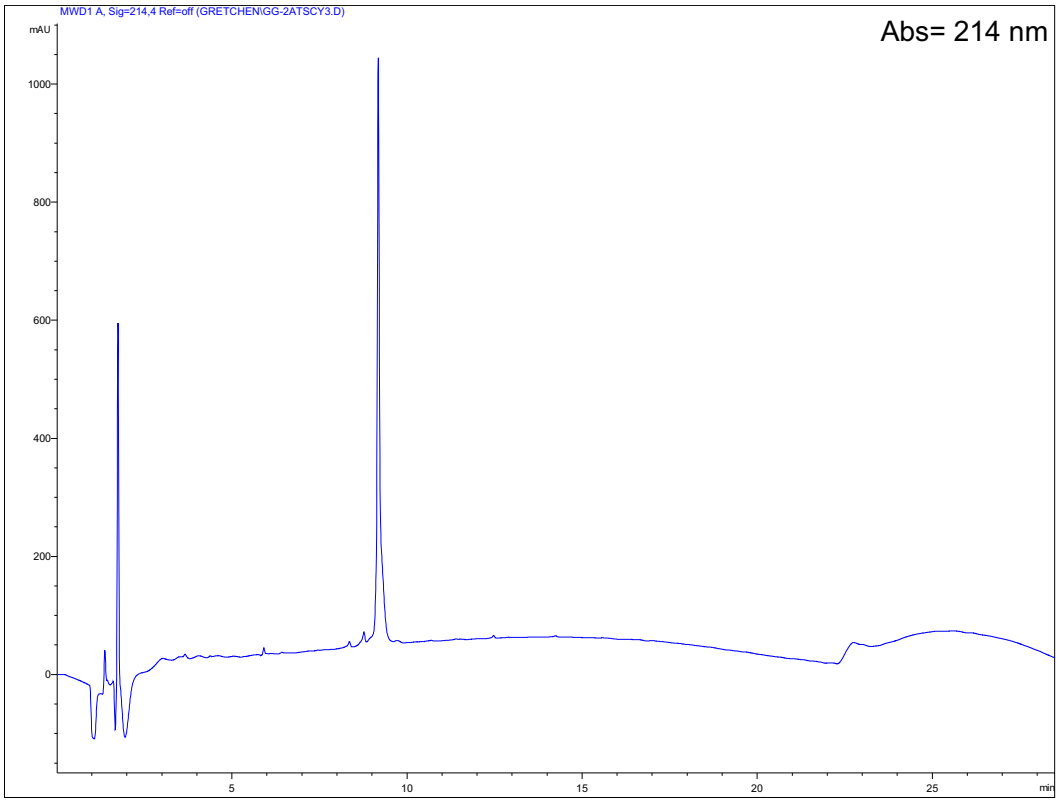

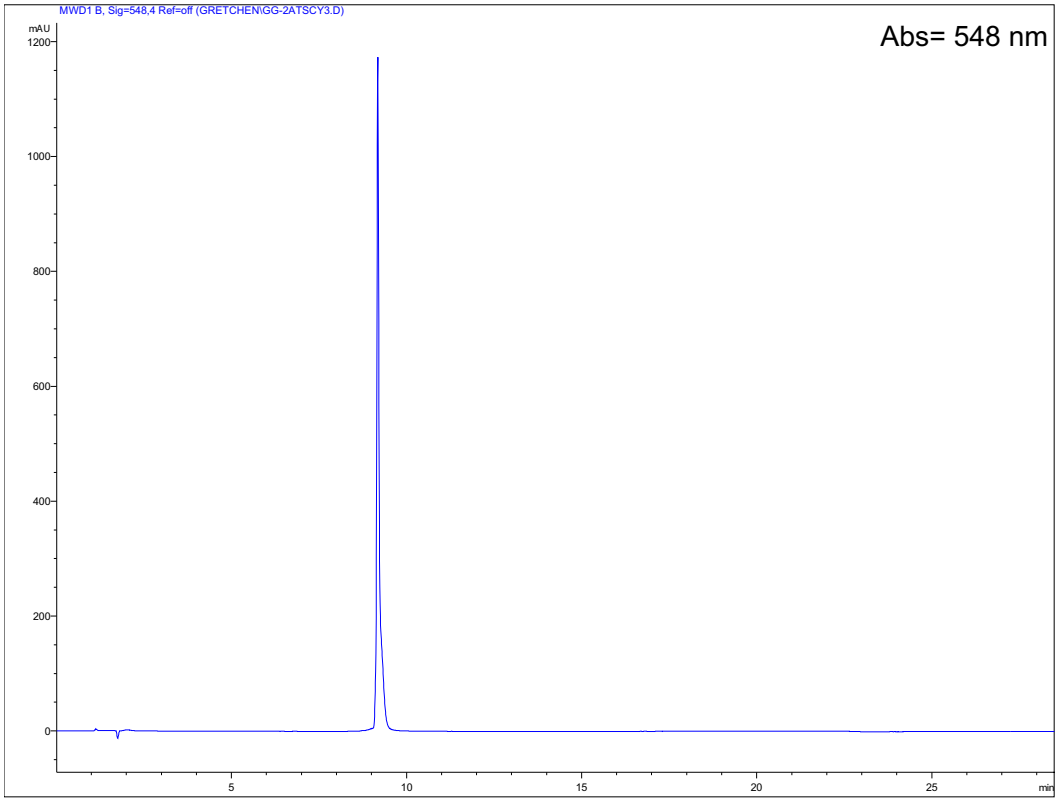

Mass spectrum of 2AT-sCy3

Calculated $[M+H]^+$ of 2AT-sCy3: 5890.92

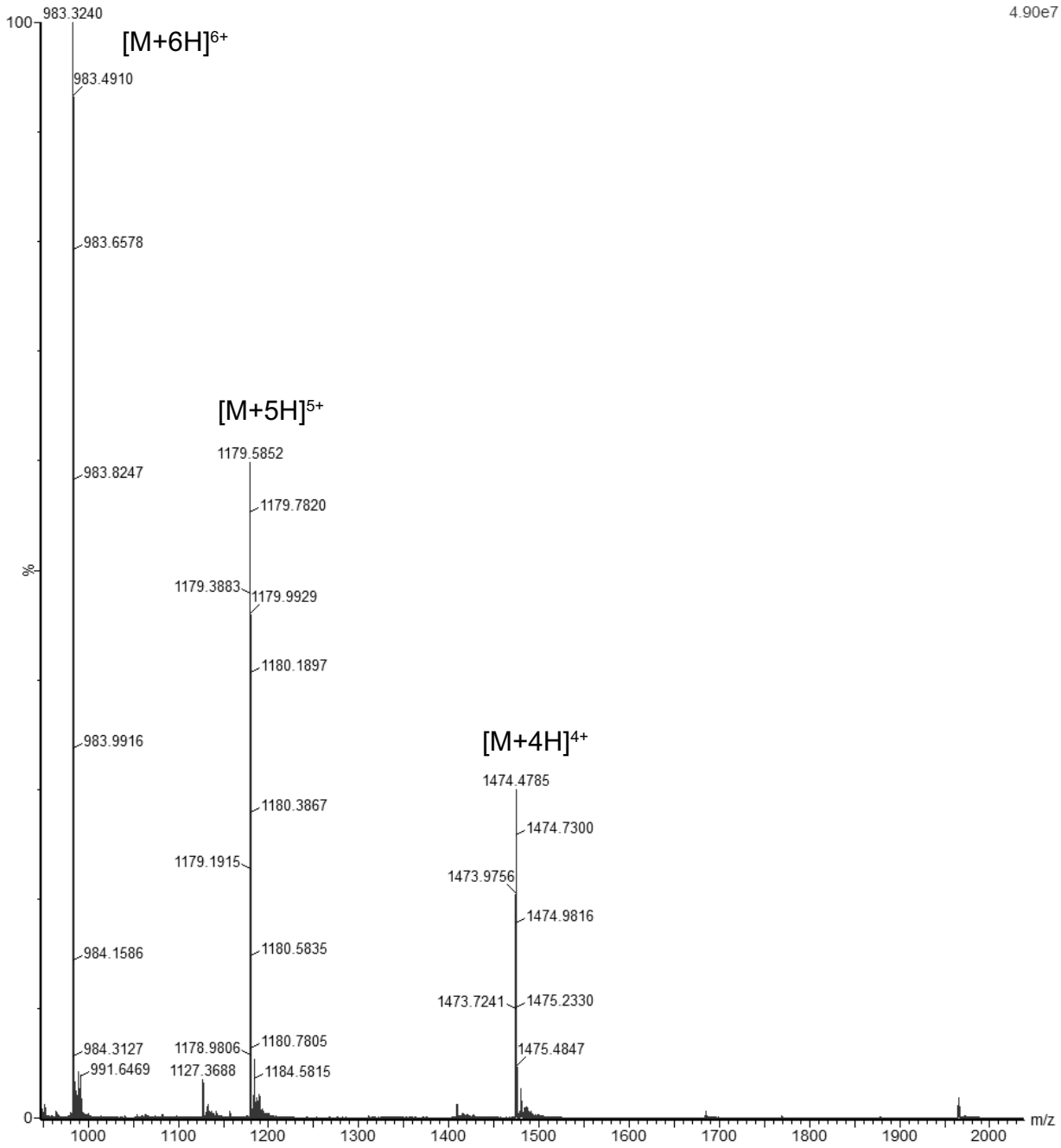

Mass spectrum of 2AT-sCy3

Calculated $[M+H]^+$ of 2AT-sCy3: 5890.92

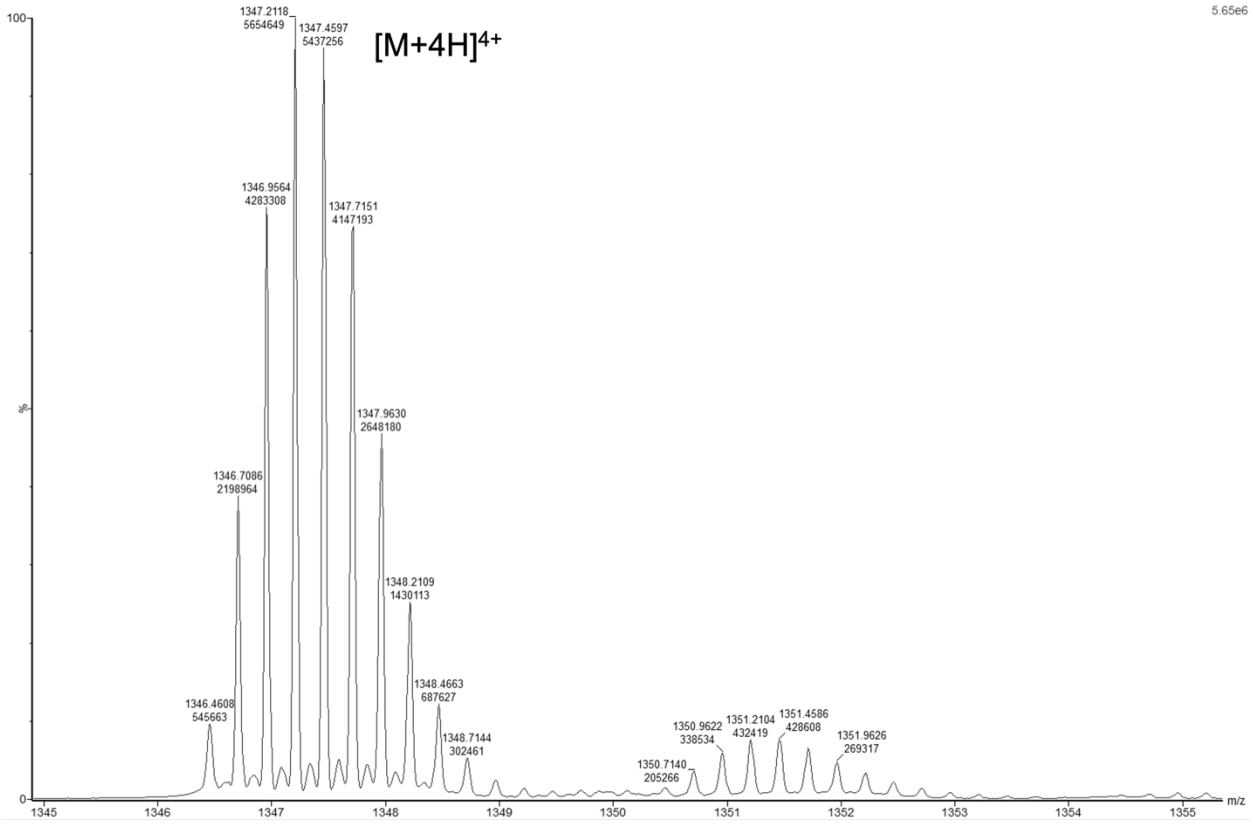

Deconvolution mass spectrum of 2AT-sCy3

Exact mass of 2AT-sCy3: 5889.91

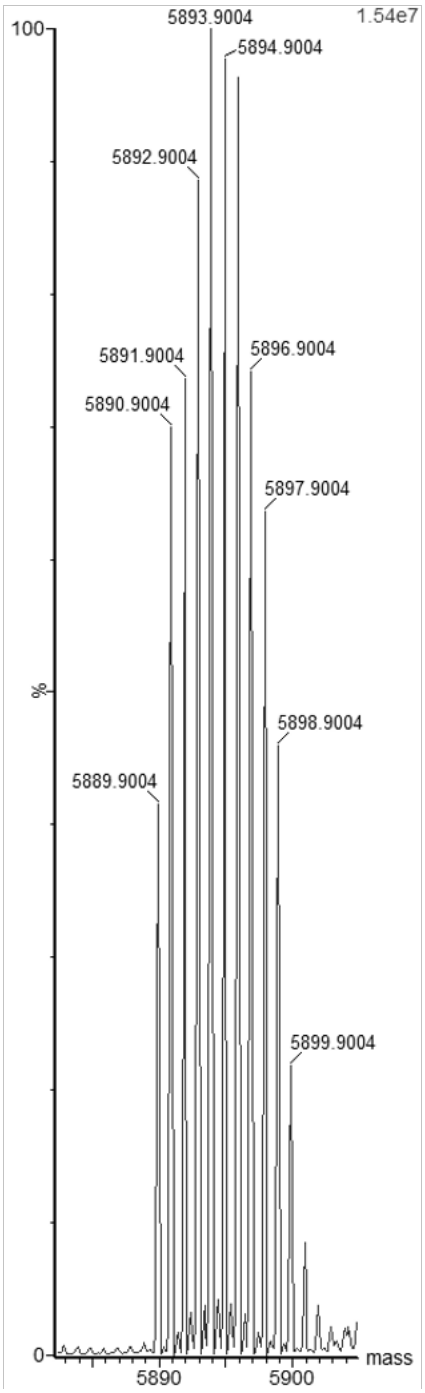

Characterization of KLT-sCy3

Analytical HPLC trace

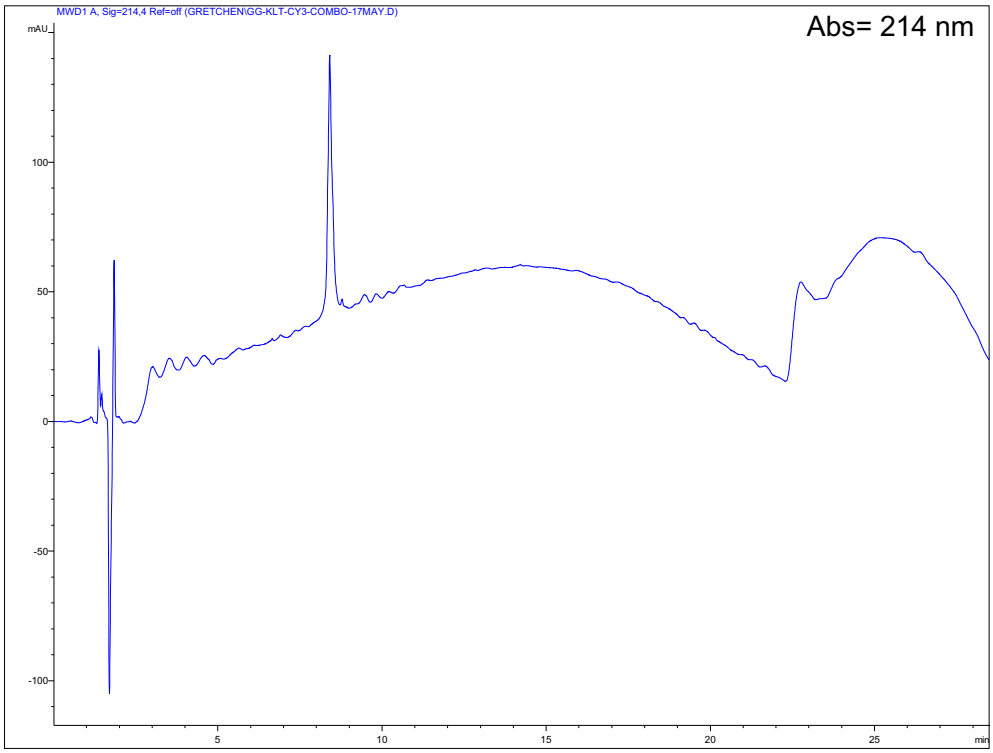

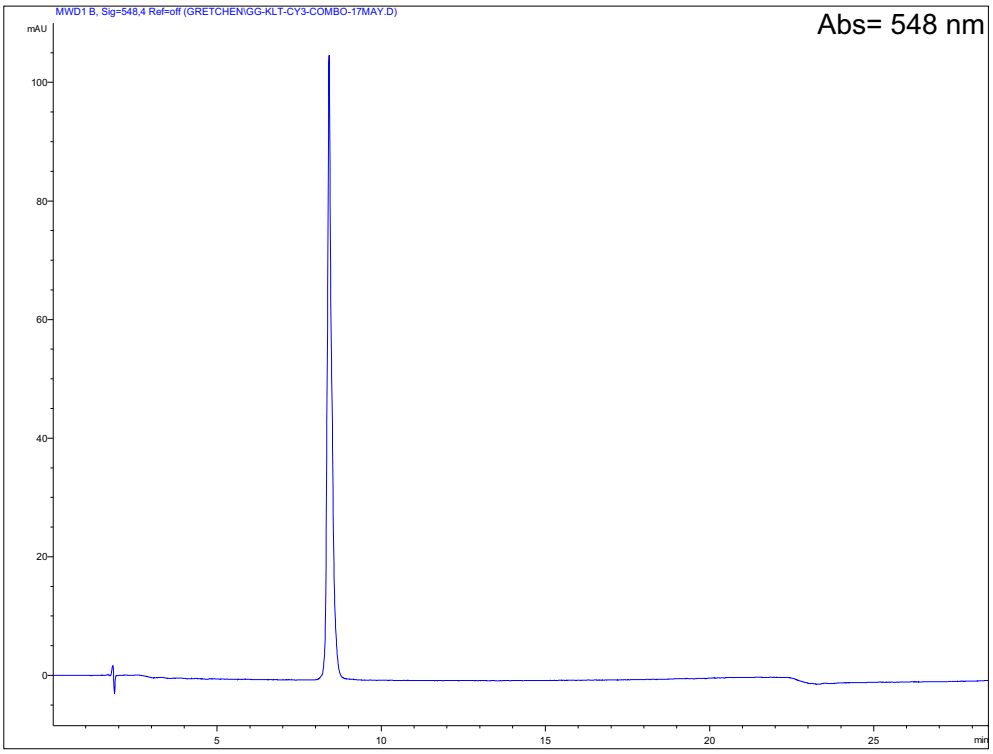

Mass spectrum of KLT-sCy3

Calculated $[M+H]^+$ of KLT-sCy3: 5980.01

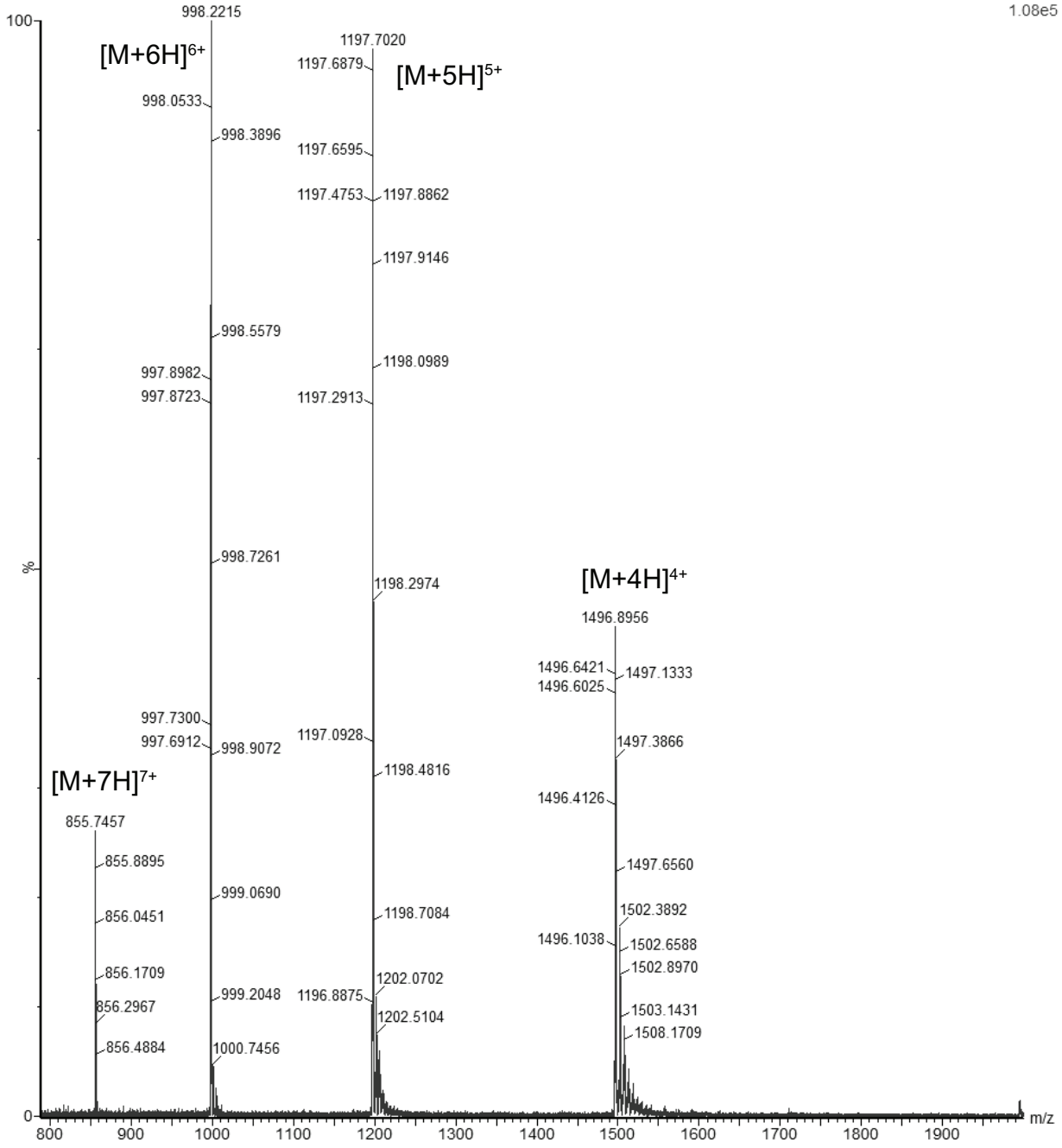

Mass spectrum of KLT-sCy3

Calculated $[M+H]^+$ of KLT-sCy3: 5980.01

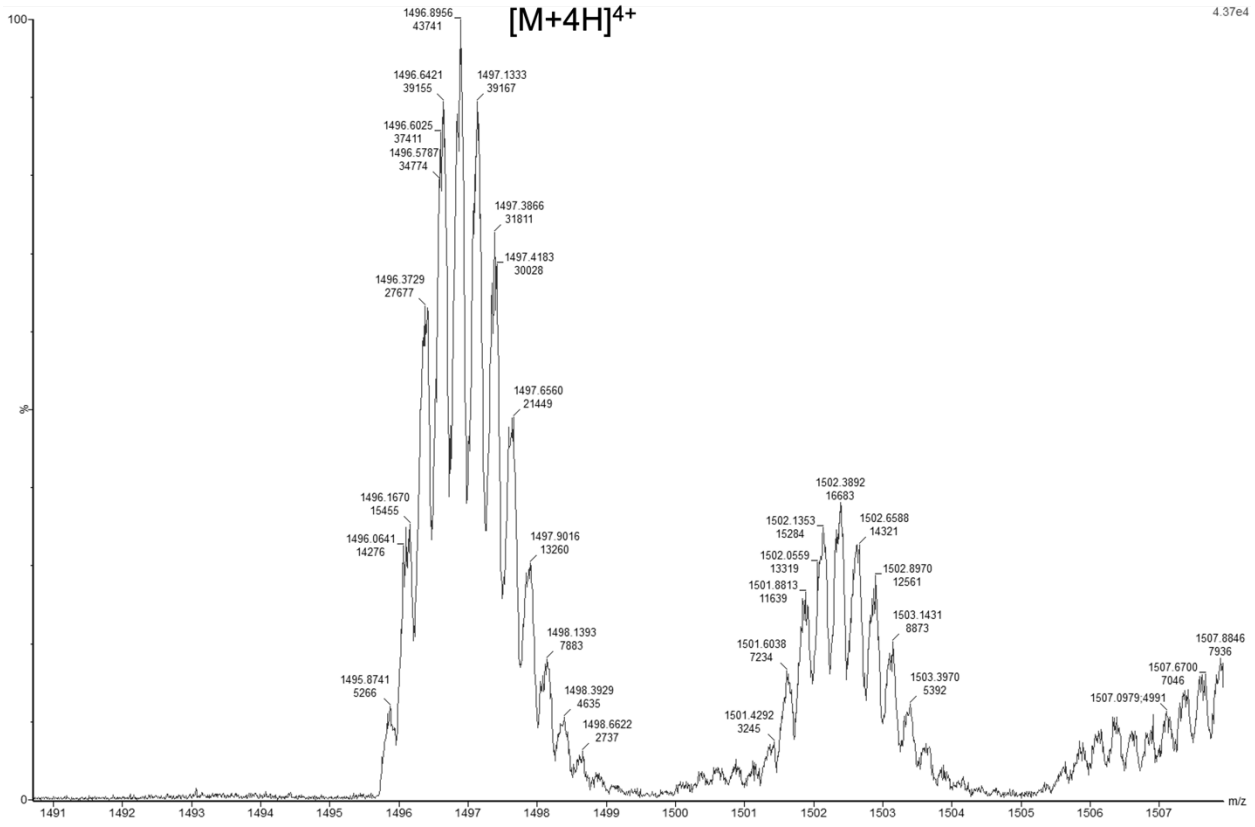

Deconvolution mass spectrum of KLT-sCy3

Exact mass of KLT-sCy3: 5979.99

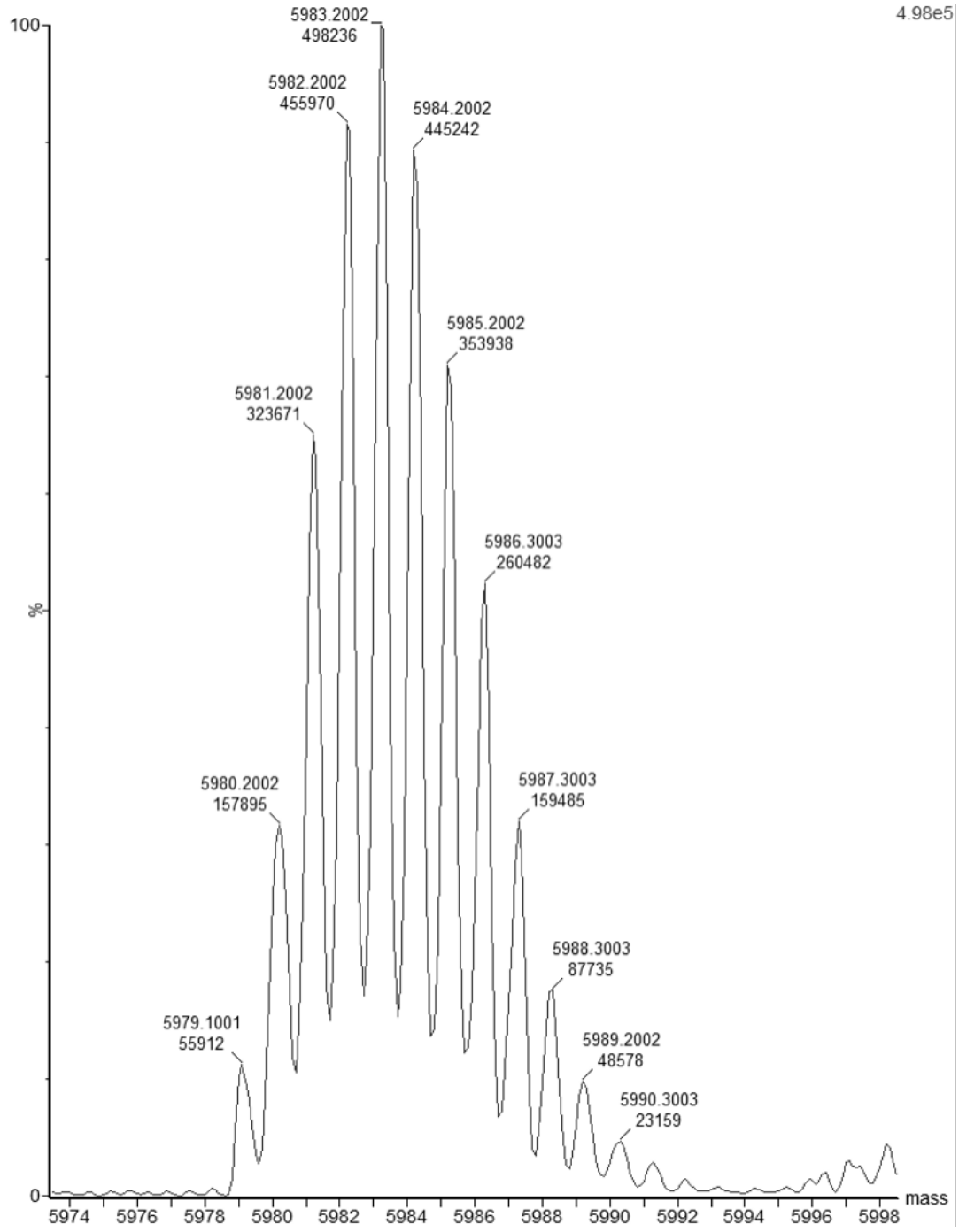

Characterization of 2AT-sCy5

Analytical HPLC trace

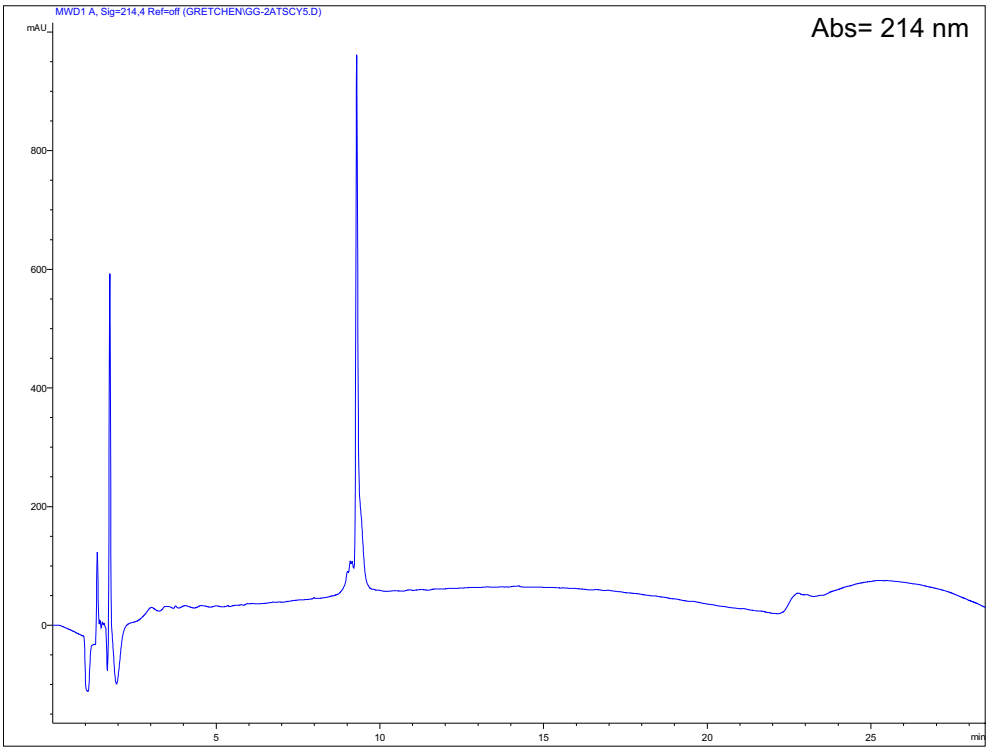

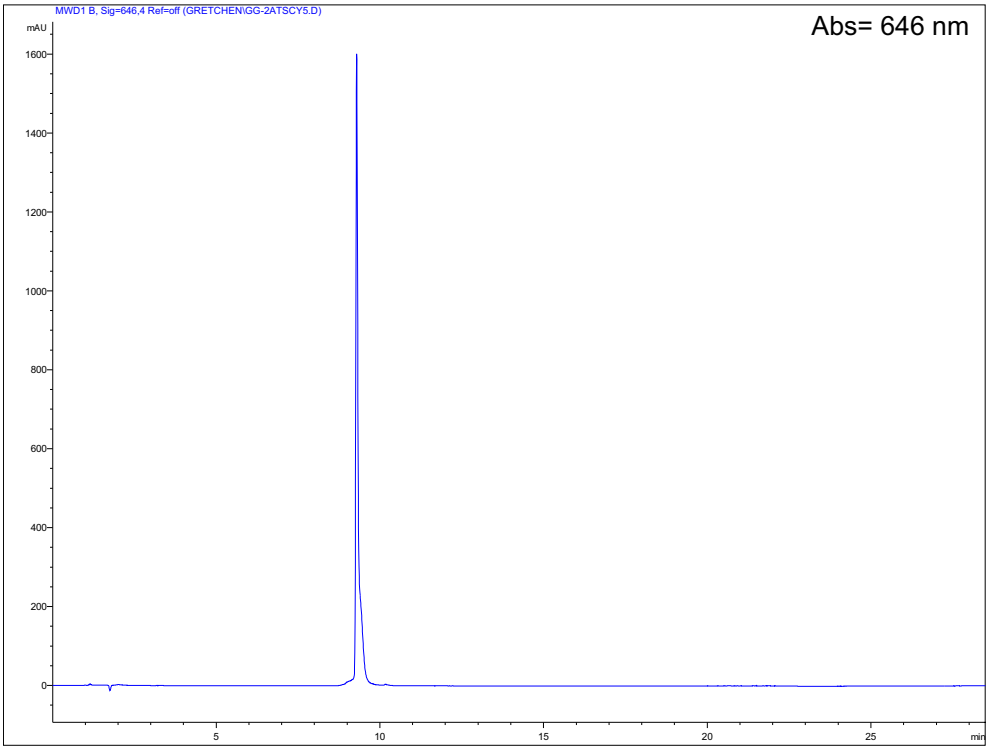

Mass spectrum of 2AT-sCy5

Calculated $[M+H]^+$ of 2AT-sCy5: 5916.93

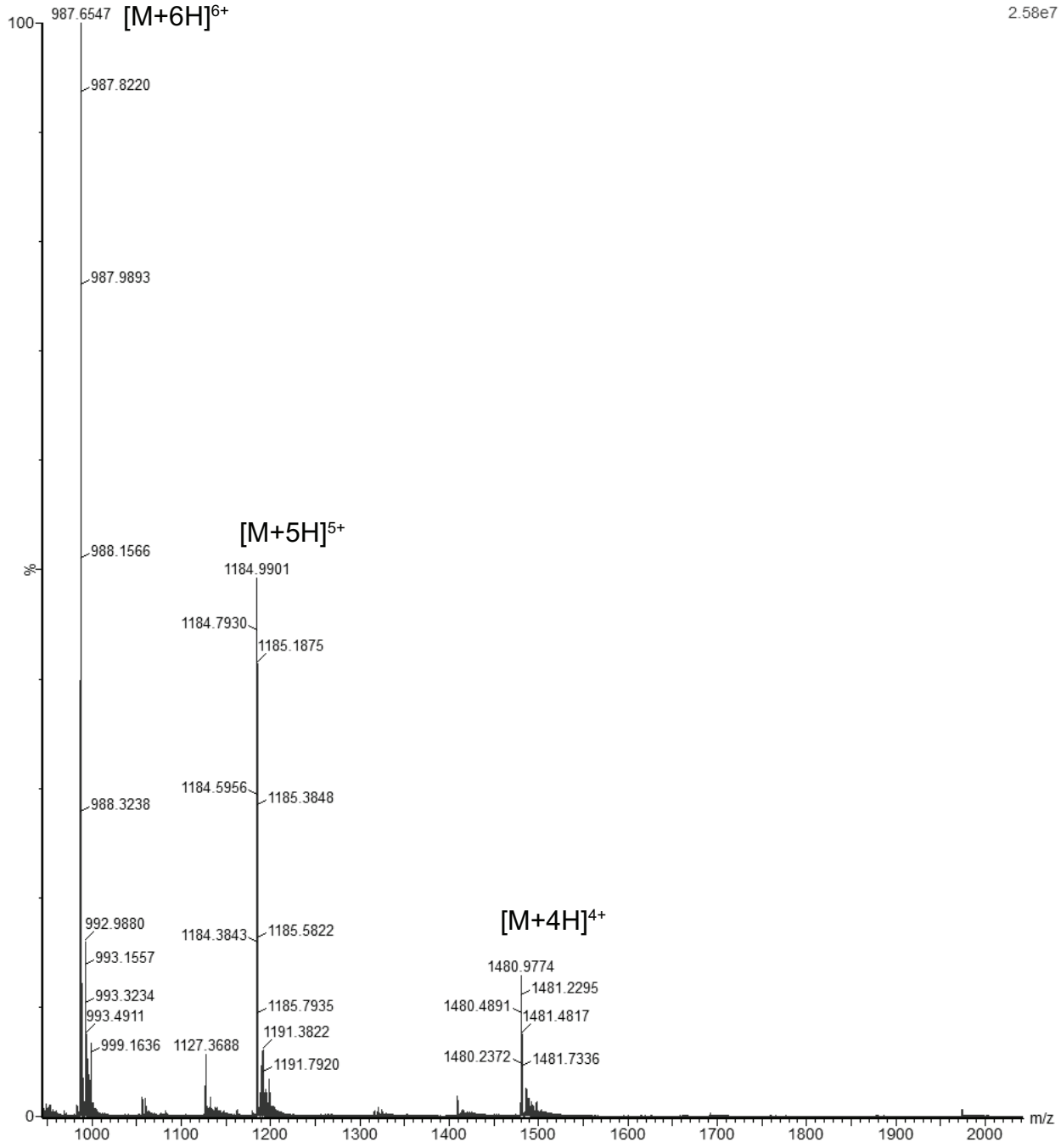

Mass spectrum of 2AT-sCy5

Calculated $[M+H]^+$ of 2AT-sCy5: 5916.93

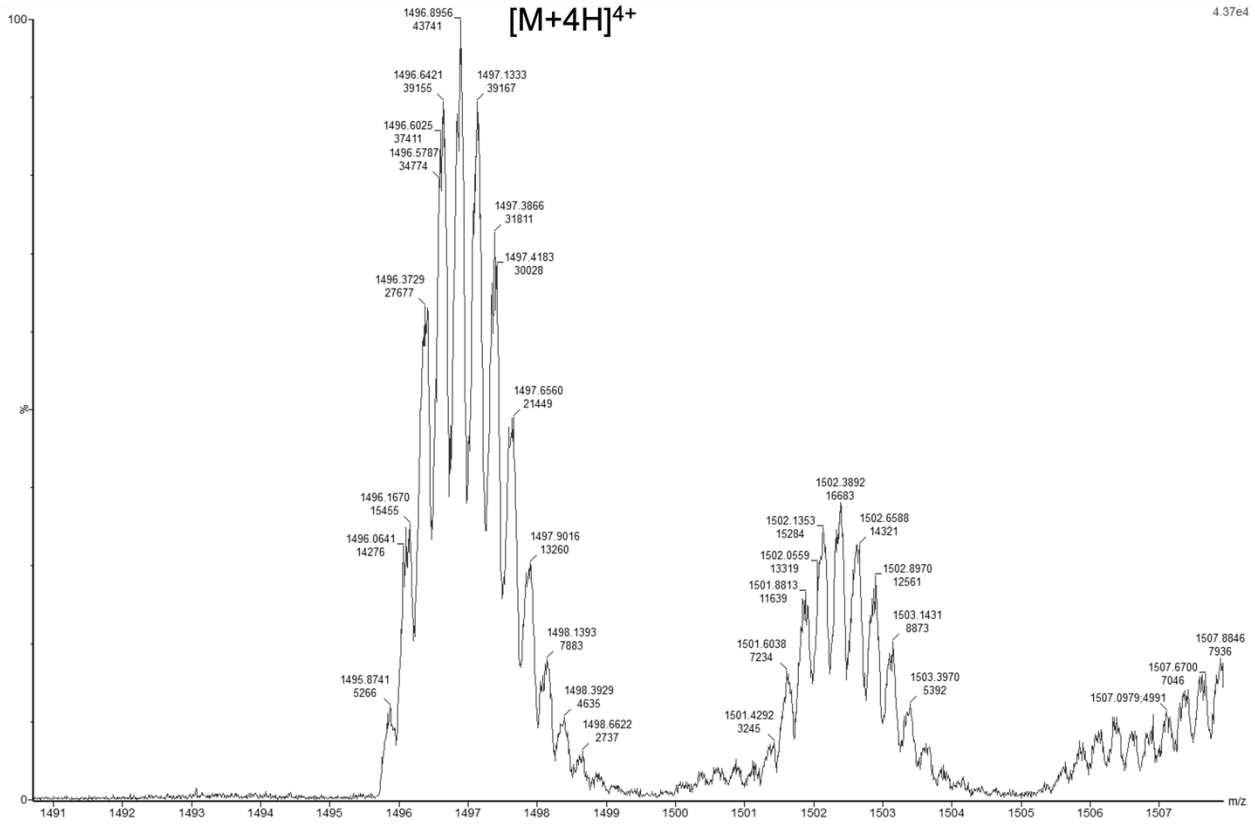

Deconvolution mass spectrum of 2AT-sCy5

Exact mass of 2AT-sCy5: 5915.93

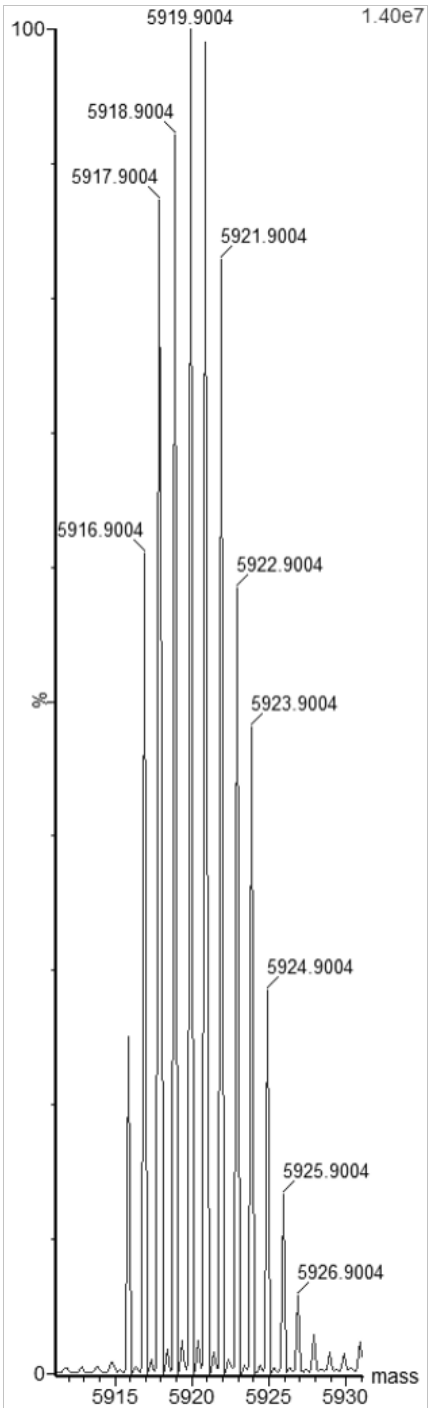

Chapter 4

Investigating the gas- and solution-phase assembly of three trimers derived from Aβ

Preface to Chapter 4

The assays described in Chapter 4 were accomplished with the support of the Wysocki laboratory and Prof. Vicki Wysocki. The Wysocki laboratory is a leader in the field of mass spectrometry and graciously hosted my visit to their laboratory to learn from the members of their group and use their instruments. Graduate student Leon Lin taught me how to use a variety of the instruments required for this study and offered his expertise in the evaluation and interpretation of the results. I am appreciative of the time he dedicated to training me while visiting the group and his ongoing support and troubleshooting as questions arise.

INTRODUCTION

Mass spectrometry is a leading analytical tool for the study of complex mixtures, offering advantages in its sensitivity and accuracy in mass detection and the ability to analyze heterogeneous species that range in size, oligomeric state, and stoichiometry.[1–3] Specifically, native mass spectrometry (native MS) has emerged as a powerful technique for the study of non-covalent assemblies as this approach retains native protein structure, including complex assemblies, when transferred into the gas phase.[3–7] This advancement led to native and other mass spectrometry techniques being utilized as powerful complementary tools in structural biology for the study of amyloidogenic diseases, including Alzheimer's disease.[8–10]

Aggregation of the β-amyloid peptide (Aβ) is a hallmark of Alzheimer's disease, where monomers of Aβ assemble into β-sheet-rich oligomers and fibrils.[11–13] While fibrils can be observed as plaques in the brains of people with Alzheimer's disease, extensive research has established soluble Aβ oligomers as the main synaptotoxic species.[5,14–20] Of many oligomeric species, dimers, trimers, and tetramers have been observed as prevalent endogenous oligomers.[21–25] Variations in Aβ oligomers are suspected to be of great importance, as structural differences have been shown to impact biological activity, but the study of oligomers is challenging because oligomers are inherently transient, polymorphic, and heterogeneous.[26] Therefore, the need for techniques that can characterize oligomers without disrupting structure are required for a better understanding of the biophysical and biological relevance of Aβ oligomers.[11]

Many techniques have been utilized to investigate and characterize oligomers of Aβ, each with their own advantages and disadvantages. Sodium dodecyl sulfate–polyacrylamide gel electrophoresis (SDS-PAGE) is a popular tool frequently used to analyze the oligomeric state of

Aβ, but reports of SDS-induced oligomer formation have reduced the reliability of SDS-PAGE.[27–30] Nuclear magnetic resonance (NMR) can provide high-resolution structural information but the transient nature of oligomer mixtures and the need for higher concentrations of each species make this technique challenging to use to characterize complex oligomer mixtures.[2,31] Similarly, X-ray crystallography can be used to study static complexes, where atomic structures are generated at angstrom resolution, but this technique does not capture the dynamic nature of oligomers.[3,32] Mass spectrometry can provide a snapshot of the equilibrium of oligomeric species present in solution, even those of low abundance, but is frequently paired with other high resolution structural techniques and biological investigation to elucidate further information.[3,13] Overall, a combination of complementary, orthogonal techniques is necessary to study Aβ oligomers.[2,3,11,20]

Important to the structure of oligomers is the propensity for Aβ to adopt a folded conformation in which the central and *C*-terminal regions fold to form a β-hairpin. The β-hairpin alignment and the hydrogen bonding contacts created can introduce polymorphism within Aβ structures. It is hypothesized these differences may give rise to significant changes in the biophysical and biological properties of oligomers.[33] Multiple high resolution structures of Aβ have been reported that describe β-hairpins with varying alignment, including those detailed by Härd et al., Tycko et al., and Carulla et al.[34–36] In the structure reported by Härd et al., Val_{36} is across from Leu_{17}; in the structure reported by Tycko et al., Val_{36} is across from Lys_{16}; and in the structure reported by Carulla et al., Val_{36} is across from Gln_{15}. The differences in these β-hairpin alignments may have biological implications but need further investigation.

The application of model systems have emerged as a tool to study more stable and homogeneous mixtures of oligomers to further understand the molecular basis of Alzheimer's

disease. In this study, we use our laboratory's established synthesis of covalently stabilized chemical models derived from Aβ to synthesize three isomorphic β-hairpin peptides based on the alignments reported by Härd et al., Tycko et al., and Carulla et al.[37–45] We investigate the three oligomer models using mass spectrometry, as well as mass photometry, SDS-PAGE, and cytotoxicity.

RESULTS AND DISCUSSION

Design and Synthesis of 2AT, KLT, and QKT. Trimer oligomer models are made up of three macrocyclic β-hairpins, in which each β-hairpin is derived from the central and *C*-terminal region of Aβ. Two δ-linked ornithine ($^{\delta}$Orn) turn units stabilize two heptapeptide β-strands to help enforce a folded β-hairpin conformation, and an *N*-methyl group is introduced onto the peptide backbone to help block uncontrolled aggregation. Crystallographic studies of macrocyclic β-hairpins revealed the assembly of triangular trimers, where three monomer peptides make up the sides of each triangular trimer, coming into close proximity at the vertices. The mutations of residues within each monomer—one at each vertex—to cysteine allows for the formation of disulfide-stabilized trimers in solution. Using our lab's established template, we synthesized three isomorphic macrocyclic β-hairpin peptides, $2AM_{CC}$, KLM_{CC}, and QKM_{CC}, with varying β-sheet alignments (Figure 4.1A,B,C). One β-strand in each peptide is derived from Aβ30–36 while the second β-strand introduces variation in alignment. The second β-strand of $2AM_{CC}$ is derived from Aβ residues 17–23; the second β-strand of KLM_{CC} is derived from Aβ residues 16–22; and the second β-strand of QKM_{CC} is derived from Aβ residues 15–21.

From these three distinct monomers we synthesized the corresponding stabilized, isomorphic trimers, 2AT, KLT, and QKT. Trimers 2AT and KLT were synthesized as previously

described.[43,46] Trimer QKT was synthesized by similar procedures. First, macrocyclic peptide QKM_{CC} was synthesized by solid-phase peptide synthesis of the corresponding linear peptide on 2-chlorotrityl resin The resulting protected peptide is cleaved from the resin and subjected to solution-phase macrocyclization. The macrocycle proceeds through side chain deprotection and ether precipitation. The macrocycle QKM_{CC} is purified by reversed-phase HPLC (RP-HPLC) and pure fractions are collected and lyophilized. The lyophilized macrocycle is subjected to oxidation at 6 mM in 20% aqueous DMSO for 48 h to form disulfide-stabilized trimers. The trimers were isolated from the oxidation reaction by RP-HPLC. Pure fractions were lyophilized and trimers were isolated as the trifluoroacetate (TFA) salt.

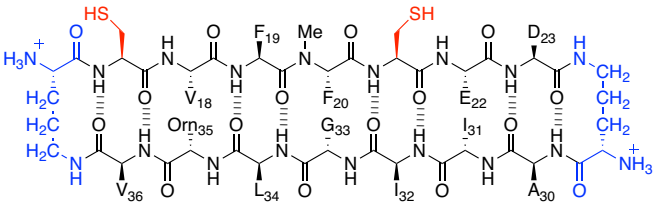

2AM$_{CC}$

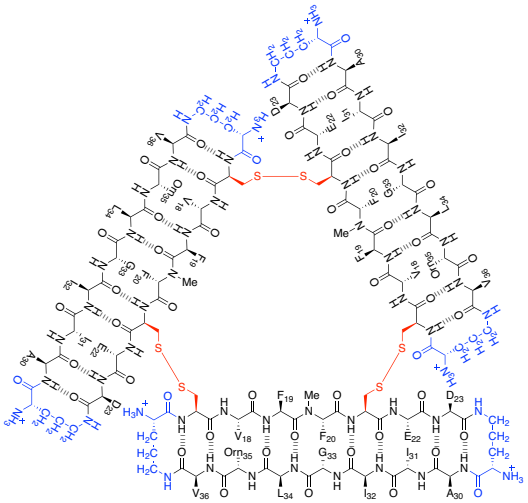

2AT

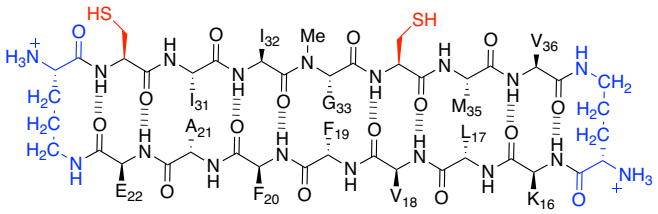

KLM$_{CC}$

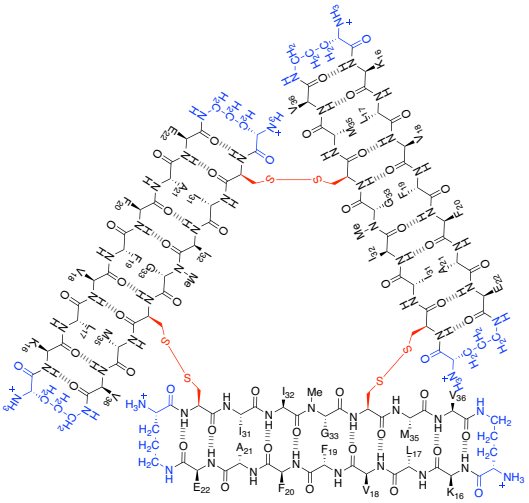

KLT

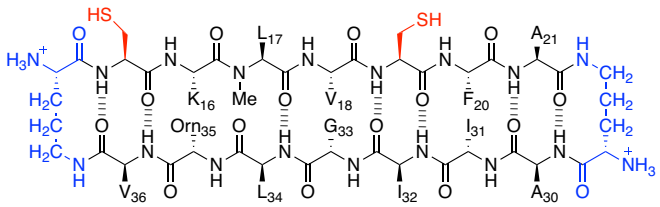

QKM$_{CC}$

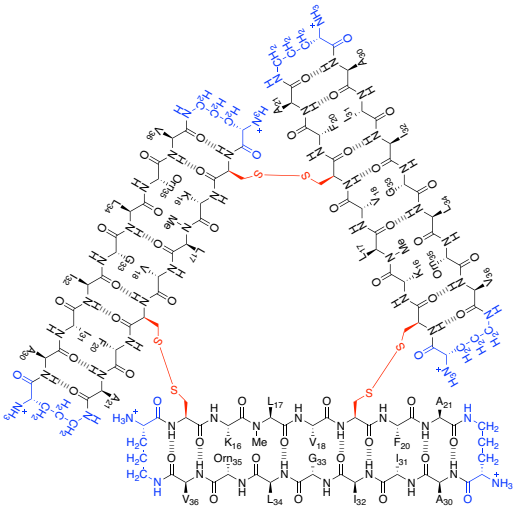

QKT

Figure 4.1 Chemical structures of β-hairpin peptides derived from the central and *C*-terminus of Aβ. Macrocyclic β-hairpins incorporate an *N*-methyl residue to prevent uncontrolled aggregation and two $^{\delta}$Orn turn (blue) mimics to enforce a β-hairpin conformation. Three β-hairpins form covalently stabilized trimers through disulfide bonds. **(A)** 2AM$_{CC}$. **(B)** 2AT. **(C)** KLM$_{CC}$. **(D)** KLT. **(E)** QKM$_{CC}$. **(F)** QKT.

Oligomers of 2AT, KLT, and QKT observed by native MS. After synthesizing trimers 2AT, KLT, and QKT, we studied their oligomeric assembly in solution by native MS. Critical to native MS is non-disrupting ionization to transfer solution-phase oligomers to the gas phase.[4] This is typically accomplished by nano-electrospray ionization (nano-ESI) where gentle desolvation and instrument conditions are applied for ionization.[3,4,47] Additionally, samples are prepared in non-denaturing electrolyte solutions compatible with mass spectrometry. In this study, samples of 2AT, KLT, and QKT were prepared at a concentration of 40 μM in 200 mM ammonium acetate (AmAc) and run immediately after preparation on a Thermo QExactive Ultra High Mass Range (UHMR) Orbitrap MS. Data were analyzed and deconvolved using UniDec.[48]

Analysis of 2AT on the UHMR instrument revealed higher order oligomers form in solution. Oligomers of 2AT up to 10-mers (10 trimers) were observed by native MS (Figure 4.2A,B). Analysis of KLT on the UHMR revealed oligomers of 4-mers (4 trimers), in addition to 1-mers (1 trimer) (Figure 4.2C,D). In contrast, analysis of QKT revealed only 1-mers (1 trimer) in solution and show no evidence of higher order oligomer formation (Figure 4.2E,F). These differences in assembly between the three isomorphic trimers may begin to indicate how β-sheet alignment may affect structure and higher order oligomer formation. To further investigate the oligomers in solution and determine if oligomer formation is time-dependent, we studied the three trimers in a time course experiment using native ion mobility mass spectrometry (native IM-MS).

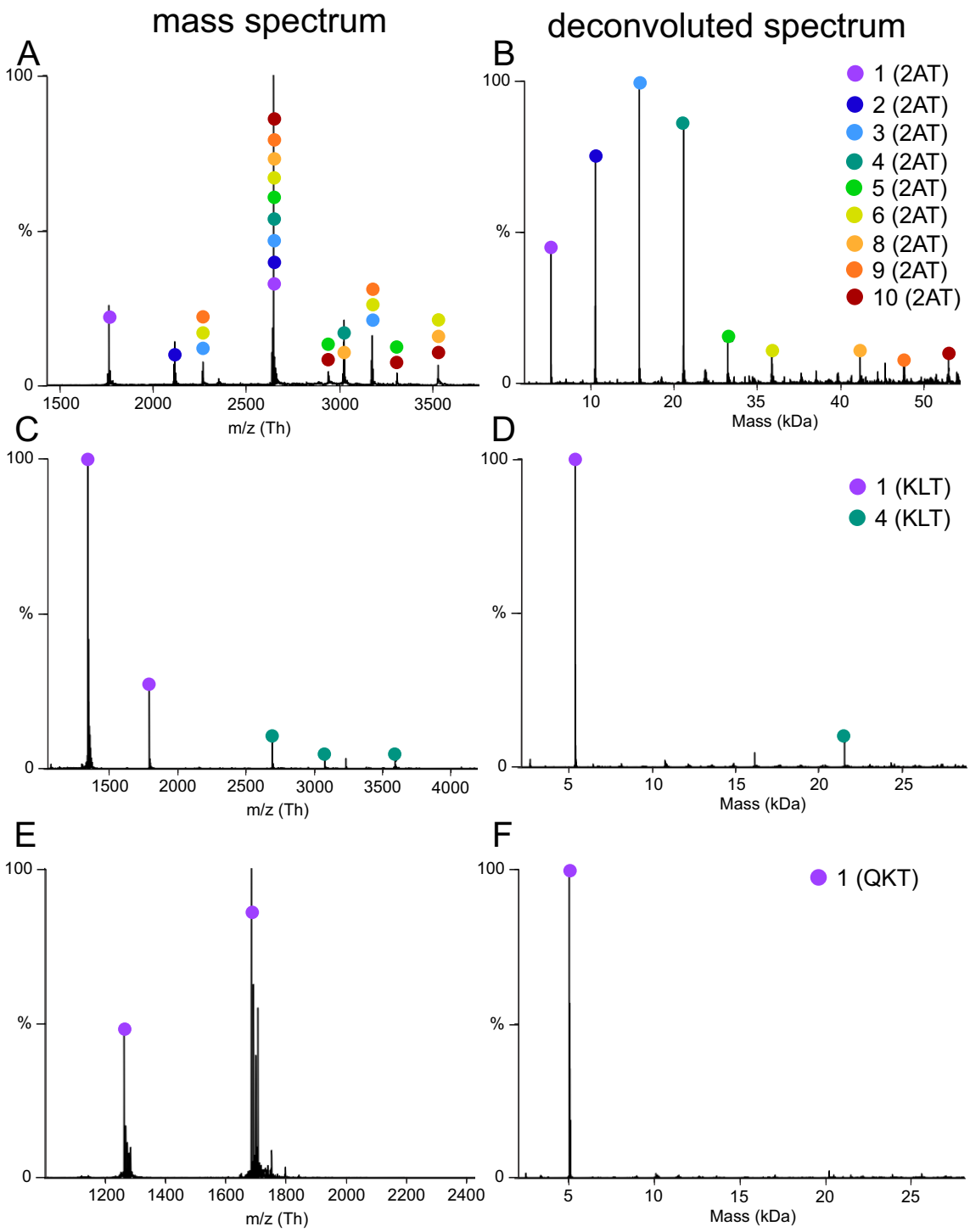

Figure 4.2 Mass spectra and deconvoluted spectra of three trimers acquired on the UHMR. Samples were prepared at 40 µM in 200 mM AmAc and run immediately following preparation. **(A)** Mass spectrum of 2AT. **(B)** Deconvoluted spectrum of 2AT. **(C)** Mass spectrum of KLT. **(D)** Deconvoluted mass spectrum of KLT. **(E)** Mass spectrum of QKT. **(F)** Deconvoluted mass spectrum of QKT.

Oligomers of 2AT, KLT, and QKT observed by native IM-MS. We investigated the oligomer formation of 2AT, KLT, and QKT over time by native IM-MS. Coupling native mass spectrometry to ion mobility spectrometry allows the separation of ions in the gas phase before mass analysis. In the ion mobility cell, a traveling wave electric field is applied to carry ions through a drift gas, where ions are separated by size, shape, and charge.[2,49–51] Ions then exit the ion mobility cell and proceed to be analyzed by time-of-flight mass spectrometry where both mass-to-charge (*m/z*) and arrival time are measured.[52] The commercialization of a cyclic ion mobility device has an increased drift length that provides increased resolution and separation to study oligomers.[53] Here, we use the Waters SELECT SERIES Cyclic Ion Mobility Spectrometer (cIMS) to study the oligomers formed by the three isomorphic trimers.

The charging of oligomers by nano-ESI can result in oligomers of different sizes having overlapping *m/z* peaks.[3] Using the two dimensional separation of ions provided by IM-MS—arrival time and *m/z*—data can be represented in a 2D mobiligram. In a mobiligram, the arrival time is plotted against mass-to-charge ratio (*m/z*), with the relative intensity displayed as a heat map. This representation can more easily differentiate oligomers of different sizes even with overlapping charge states.

Samples of 2AT, KLT, and QKT were prepared at 40 μM in 200 mM AmAc and run at 0 h and 6 h timepoints. Samples were run on the cIMS instrument with instrument conditions kept consistent between timepoints. The data were analyzed using Waters Driftscope software. The resulting mobiligrams reveal differences in trimer assemblies that vary with time. Mobiligrams of 2AT show small differences in the assembly of 2AT between the 0 h and 6 h timepoints. The mobiligram at 0 h shows that 2AT forms 2-mers, in addition to the trimer (Figure S4.2A). The mobiligram at 6 h shows the emergence of 3-mers as well as 2-mers and the trimer (Figure

4.3A). Mobiligrams of KLT show no differences between the 0 h and 6 h timepoints. The mobiligram at 0 h shows that KLT forms 2-mers in solution, in addition to the trimer (Figure S4.2B). The mobiligram at 6 h again shows that KLT forms 2-mers in solution, in addition to the trimer (Figure 4.3B). In contrast, the mobiligram for QKT shows more significant differences between the 0 h and 6 h timepoints. The mobiligram at 0 h shows that QKT forms 2- and 3-mers in solution, in addition to the trimer (Figure S4.2C|). Interestingly, the mobiligram at 6 h shows that QKT forms 2-, 3-, 4-, and 5-mers in solution, in addition to the trimer (Figure 4.3C).

These results show some time-dependent oligomer formation. QKT shows two new oligomers emerge after 6 h whereas 2AT shows one new oligomer emerge after 6 h and KLT does not show any new oligomers. In comparison to the native MS results on the UHMR instrument, native IM-MS on the cIMS instrument shows some disparity. 2AT forms many oligomer species on the UHMR instrument that are not observed on the cIMS instrument. This may indicate one set of instrument conditions ionizes 2AT oligomers better than the other. KLT shows 4-mers on the UHMR instrument but only up to 2-mers on the cIMS. Alternatively, QKT shows no oligomer formation on the UHMR instrument but shows up to 5-mers on the cIMS instrument that increased with time. This may indicate QKT preferentially forms oligomers when incubated in AmAc solution or is slower to form oligomers than 2AT. Again, we cannot discount that one set of instrument conditions ionizes some species better than others.

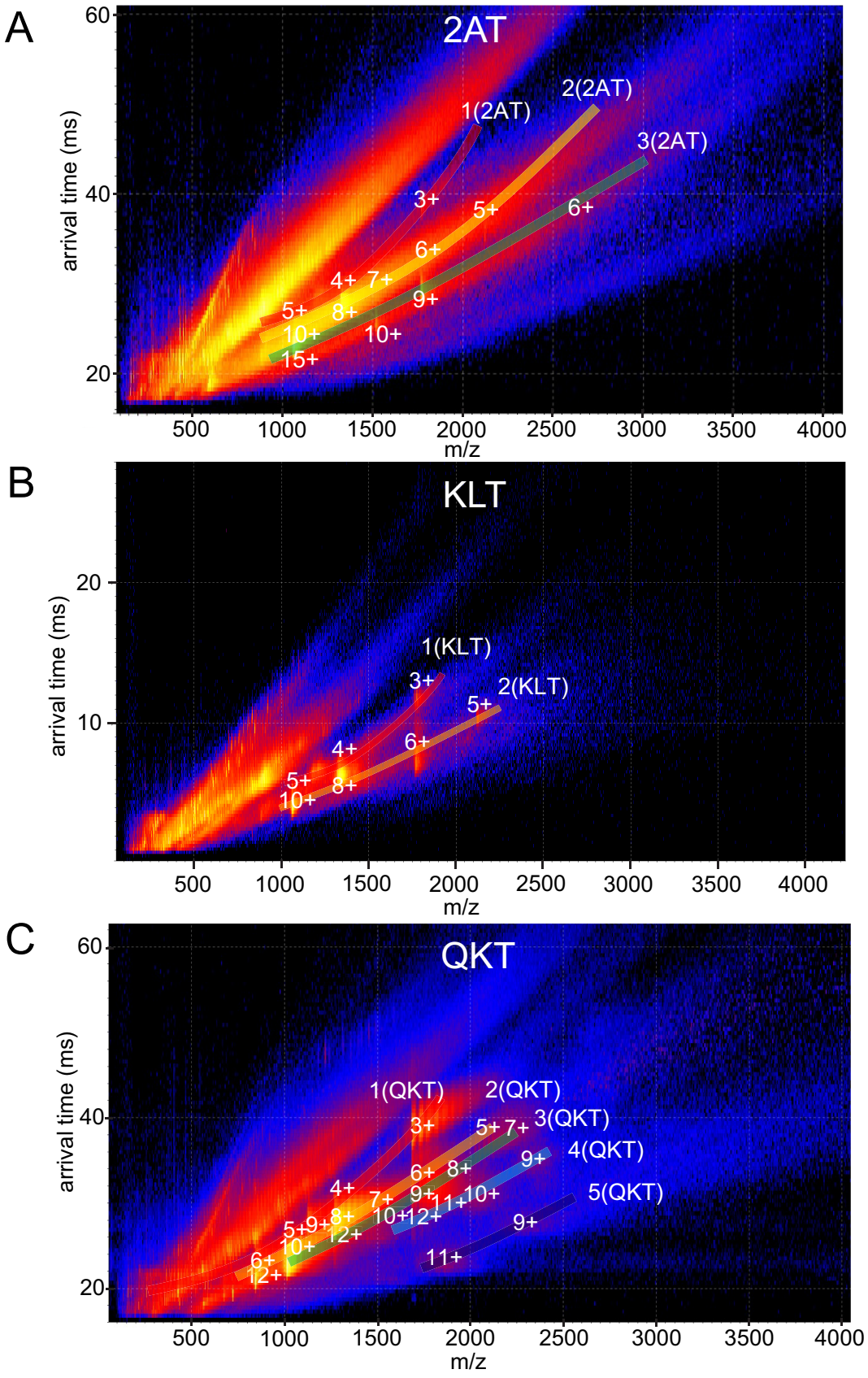
A
2AT
1(2AT)
2(2AT)
3(2AT)
3+
5+
6+
6+
4+
7+
9+
5+
8+
10+
10+
15+
arrival time (ms)
60
40
20
500
1000
1500
2000
2500
3000
3500
4000
m/z
B
KLT
1(KLT)
2(KLT)
3+
5+
4+
6+
5+
8+
10+
arrival time (ms)
20
10
500
1000
1500
2000
2500
3000
3500
4000
m/z
C
QKT
1(QKT)
2(QKT)
3(QKT)
4(QKT)
5(QKT)
3+
5+
7+
6+
8+
9+
4+
7+
9+
11+
10+
5+
9+
8+
10+
12+
9+
12+
10+
6+
12+
11+
arrival time (ms)
60
40
20
500
1000
1500
2000
2500
3000
3500
4000
m/z

Figure 4.3 Native IM-MS of 2AT, KLT, and QKT after 6 h incubation. **(A,B,C)** Mobiligrams of 2AT, KLT, and QKT. Samples of trimers were prepared at a concentration of 40 μM in 200 mM AmAc and native IM-MS was performed on a SELECT SERIES Cyclic IMS Q-cIMS-TOF (cIMS) instrument (Waters Corporation). Numeric labels indicate the charge state of the corresponding oligomeric species.

Oligomers of 2AT, KLT, and QKT observed by mass photometry. With the suspicion that ionization may be affecting the oligomeric species we observe from the three isomorphic trimers, we sought to use a technique that did not require ionization. Thus, we studied 2AT, KLT, and QKT by mass photometry. Mass photometry is a label-free, ionization-free technique that uses small quantities of sample to assess the size of assemblies in solution. Mass photometry measures assemblies based on light scattering from individual complexes. These complexes undergo binding events, where complexes in solution interact with the glass surface on which the solution is placed, and results in a change to the refractive index.[54] These binding events are recorded and the contrast from binding events can be correlated with molecular weight to obtain a size distribution of complexes in solution. While complexes below 30 kDa can be difficult to resolve, mass photometry can reveal large oligomers in solution that ionization-based mass spectrometry may not.

Samples of 2AT, KLT, and QKT were prepared at a concentration of 650 nM in 200 mM AmAc. Prior to running trimer samples, a protein ladder in 200 mM AmAc was run to establish a calibration curve for analysis. Mass photometry analysis of 2AT (5.3 kDa) reveals a distribution with a maximum at 31 kDa (Figure 4.4A). This maximum likely indicates oligomers of 6–7 trimers with a distribution of other oligomers in solution. Mass photometry analysis of KLT (5.4 kDa) reveals a distribution with a maximum at 43 kDa (Figure 4.4B). This likely indicates oligomers of 8 KLT trimers with a distribution of other oligomers in solution. Mass photometry

analysis of QKT (5.1 kDa) reveals a distribution with a maximum at 79 kDa (Figure 4.4C). This maximum likely indicates oligomers of 15–16 trimers with a wide distribution of other oligomers in solution.

For 2AT, mass photometry analysis reveals species similar to those observed by native MS on the UHMR instrument. In contrast, mass photometry shows evidence of much larger oligomers of KLT and QKT that were not observed on the UHMR or cIMS instruments. Likely there are higher concentrations of smaller oligomers in solution that preferentially ionize and prevent the observation of these larger, less prevalent, and less ionizable species by native MS. As mass photometry does not well-characterize species under 30 kDa, we are likely not observing the higher concentrations of smaller oligomers that dominate in ionization-based techniques. To address this, we then used SDS-PAGE as it is a technique that does not require ionization but can better characterize smaller oligomers that mass photometry cannot.

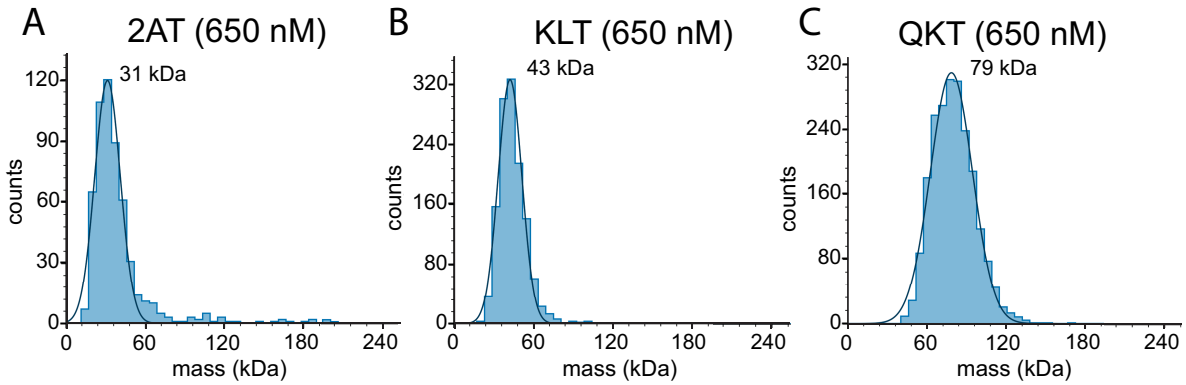

Figure 4.4 Distribution of oligomers formed when observed by mass photometry. (A) Oligomer distribution from a sample of 650 nM 2AT in 200 mM AmAc with a peak at 31 kDa. **(B)** Oligomer distribution from a sample of 650 nM KLT in 200 mM AmAc with a peak at 48 kDa. **(C)** Oligomer distribution from a sample of 650 nM QKT in 200 mM AmAc with a peak at 79 kDa. All samples were prepared from 10 mg/mL stock solutions and were run on a Refeyn TwoMP instrument.

Oligomers of 2AT, KLT, and QKT observed by SDS-PAGE. We explored the assembly of 2AT, KLT, and QKT by an additional technique that does not require ionization. The assembly of trimers was studied in the membrane-like environment of SDS-PAGE. Samples of 2AT, KLT, and QKT were prepared to a concentration of 75 μM in water with 2% (w/v) SDS. The trimers were then visualized in the gel by silver staining (Figure 4.5). In SDS-PAGE, all trimers assemble to form higher-order oligomers. As previously reported, when 2AT (5.3 kDa) is run in SDS-PAGE, it forms a downward-streaking band from ca. 26 kDa to ca. 10 kDa and a compact band below 10 kDa.[43] This migration suggests assembly into oligomers ca. 2–5 trimers in size in addition to unassembled trimer (Figure 4.5). As we have previously observed, when KLT (5.4 kDa) is run in SDS-PAGE, it forms a streaking band from the top of the gel that migrates to just under ca. 10 kDa.[46] This migration suggests assembly into oligomers ca. 2 trimers in size, likely with other larger oligomers in equilibrium. When QKT (5.1 kDa) is run in SDS-PAGE and visualized by silver staining, it also forms a streaking band from the top of the gel to ca. 16 kDa. In addition to the streaking band, there is a compact band at ca. 26 kDa. This migration likely indicates the propensity of QKT to form oligomers ca. 3–4 trimers in size, in addition to other larger but less abundant oligomers in equilibrium.

Overall, SDS-PAGE reveals the isomorphic trimers all form different higher order oligomers in SDS. These differences in assemblies have also been revealed through mass spectrometry and mass photometry techniques, though not all techniques converge on the most favored oligomers from each isomorph. We continued to investigate the effects of these oligomerization differences between the isomorphic trimers on biological interactions through cell cytotoxicity.

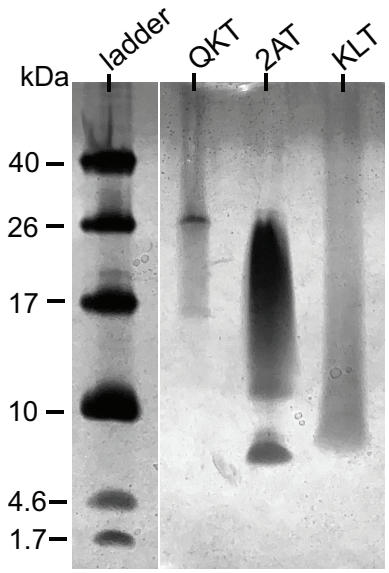

Figure 4.5 Silver stained SDS-PAGE of trimers 2AT, KLT, QKT. SDS-PAGE was performed in Tris buffer at pH 6.8 with 2% (w/v) SDS on a 16% polyacrylamide gel with 75 μM solutions of trimer in each lane.

Cell viability of SH-SY5Y cells treated with 2AT, KLT, and QKT. To explore the biological activity of the three isomorphic trimers, we treated SH-SY5Y cells with each trimer and assessed the cell viability after 72 h. In this assay, cell-permeable substrate enters intact cells and is cleaved by live-cell proteases to generate fluorescence; therefore, a larger fluorescence output in this assay indicates more intact and viable cells. Cells were treated with a 2-fold dilution series of 2AT, KLT, and QKT from 50 μM to 1.6 μM. After 72 h, the health of the cells was assessed (Figure 4.6). All treated cells show a dose-dependent response to the trimers. Cells treated with 2AT show the highest level of cell viability and cells treated with KLT show slightly decreased levels of cell viability compared to 2AT. QKT shows the lowest levels of cell viability at all concentrations.

In contrast, when a specific pathway of cytotoxicity is measured, QKT shows the lowest level of cytotoxicity (Figure S4.3). In this assay, the activation of a known marker of apoptosis (caspase 3/7) is measure. The caspase 3/7 pathway has been shown as one of the pathways by which Aβ is toxic.[55] The results of this assay suggest more cells undergo apoptosis in the presence of 2AT than the other isomorphs. The results of these two assays together suggest QKT and KLT may decrease cell viability through other pathways that we have not yet assayed.

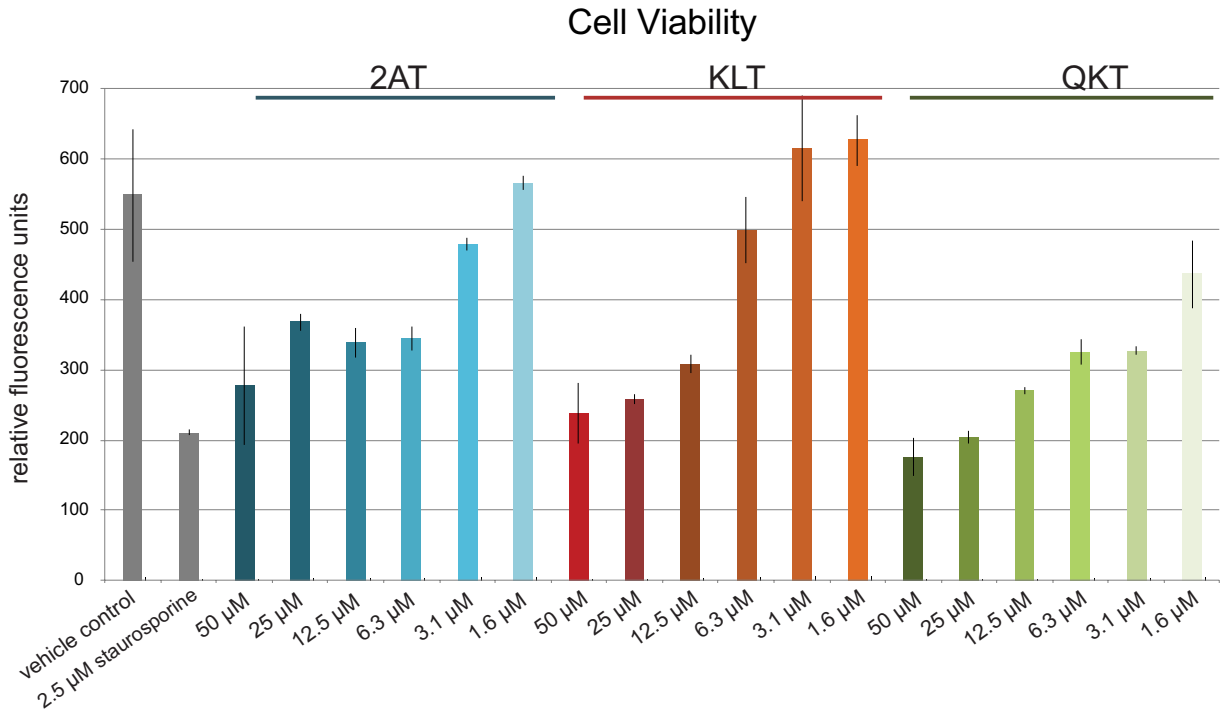

Figure 4.6 Promega ApoLive-Glo™ Multiplex Assay of SH-SY5Y cells treated with 2AT, KLT, or QKT. Data represent the mean of three replicate wells, with the error bars corresponding to the standard deviation.

SUMMARY AND CONCLUSIONS

Understanding the complex assembly of Aβ oligomers is key to treating Alzheimer's disease. This area of research has placed even more emphasis on the need for tools to study these dynamic, polymorphic, and heterogeneous mixtures of oligomers. To mitigate the complexity of

these mixtures, the use of a chemical model system of oligomers derived from Aβ and the application of multiple orthogonal techniques have been applied.

The trimers in this study–2AT, KLT, and QKT–are inspired from high-resolution structures of Aβ reported by Härd et al., Tycko et al., and Carulla et al. that show shifts in β-sheet alignment. By native MS on a UHMR instrument, 2AT shows significantly more oligomerization than KLT or QKT, but by native IM-MS on a cIMS instrument, QKT shows more oligomerization than 2AT or KLT with some time dependence for oligomerization. Mass photometry revealed QKT had the largest oligomers in solution, followed by KLT with intermediate-sized oligomers, and finally 2AT with the smallest oligomers. Mass photometry revealed much larger oligomers for KLT and QKT that were not observed by nano-ESI-based mass spectrometry techniques, but correlated with the oligomers of 2AT observed on the UHMR instrument. SDS-PAGE showed similar oligomerization trends as mass photometry, where QKT and KLT showed streaking bands from the top of the gel indicating larger oligomeric assemblies than 2AT. Finally, cell viability studies indicate that cells treated with QKT were less viable than cells treated with 2AT or KLT. The results from these studies of Aβ-derived model systems reflect studies of Aβ which demonstrated that structure can influence biological function.[12]

Excluding native MS data collected on the UHMR instrument, QKT shows the largest oligomers in solution and the least viable cells after treatment. Admittedly, not all techniques used converge on the most prevalent oligomers formed by each isomorphic trimer and many factors could contribute to the observed differences in assembly and toxicity including net charge of the trimers. Overall, these studies suggest that structural differences in β-sheet alignment can affect the solution-phase assembly and biological interactions of oligomers derived from Aβ but also reinforce the need for multiple techniques to accurately characterize oligomers to ultimately

better understand the role of Aβ oligomers in the progression of Alzheimer's disease. Continued characterization is ongoing, including efforts to obtain a high-resolution structure by X-ray crystallography.

MATERIALS AND METHODS

Peptides 2AT, KLT, and QKT were synthesized by procedures analogous to those described previously.[43] SDS-PAGE and silver staining were performed as described previously.[43] Procedures for native MS, native IM-MS studies, mass photometry, and cell viability can be found in the Supporting Information.

ACKNOWLEDGMENTS

We thank the Wysocki lab for helpful guidance and the use of their cIMS, UHMR, and mass photometry instruments. We thank the UCI Mass Spectrometry Core Facility for funding to travel to the Wysocki lab at The Ohio State University. We thank the National Institutes of Health (NIH) for funding (AG072587).

REFERENCES AND NOTES

(1) Zakharova, N. V.; Kononikhin, A. S.; Indeykina, M. I.; Bugrova, A. E.; Strelnikova, P.; Pekov, S.; Kozin, S. A.; Popov, I. A.; Mitkevich, V.; Makarov, A. A.; Nikolaev, E. N. Mass Spectrometric Studies of the Variety of Beta-amyloid Proteoforms in Alzheimer's Disease. *Mass Spec. Rev.* **2022**, 1–19. https://doi.org/10.1002/mas.21775.

(2) Hoffmann, W.; von Helden, G.; Pagel, K. Ion Mobility-Mass Spectrometry and Orthogonal Gas-Phase Techniques to Study Amyloid Formation and Inhibition. *Curr. Opin. Struct. Biol.* **2017**, *46*, 7–15. https://doi.org/10.1016/j.sbi.2017.03.002.

(3) Benesch, J. L. P.; Ruotolo, B. T. Mass Spectrometry: Come of Age for Structural and Dynamical Biology. *Curr. Opin. Struct. Biol.* **2011**, *21* (5), 641–649. https://doi.org/10.1016/j.sbi.2011.08.002.

(4) Karch, K. R.; Snyder, D. T.; Harvey, S. R.; Wysocki, V. H. Native Mass Spectrometry: Recent Progress and Remaining Challenges. *Annu. Rev. Biophys.* **2022**, *51* (1), 157-179. https://doi.org/10.1146/annurev-biophys-092721-085421.

(5) Kulenkampff, K.; Wolf Perez, A. M.; Sormanni, P.; Habchi, J.; Vendruscolo, M. Quantifying Misfolded Protein Oligomers as Drug Targets and Biomarkers in Alzheimer and Parkinson Diseases. *Nat. Rev. Chem.* **2021**, *5* (4), 277–294. https://doi.org/10.1038/s41570-021-00254-9.

(6) Heck, A. J. R. Native Mass Spectrometry: A Bridge between Interactomics and Structural Biology. *Nat. Methods* **2008**, *5* (11), 927–933. https://doi.org/10.1038/nmeth.1265.

(7) Leney, A. C.; Heck, A. J. R. Native Mass Spectrometry: What Is in the Name? *J. Am. Soc. Mass Spectrom.* **2017**, *28* (1), 5–13. https://doi.org/10.1007/s13361-016-1545-3.

(8) Zakharova, N. V.; Bugrova, A. E.; Kononikhin, A. S.; Indeykina, M. I.; Popov, I. A.;

Nikolaev, E. N. Mass Spectrometry Analysis of the Diversity of Aβ Peptides: Difficulties and Future Perspectives for AD Biomarker Discovery. *Expert Rev. Proteomics* **2018**, *15* (10), 773–775. https://doi.org/10.1080/14789450.2018.1525296.

(9) Ştefănescu, R.; Stanciu, G. D.; Luca, A.; Caba, I. C.; Tamba, B. I.; Mihai, C. T. Contributions of Mass Spectrometry to the Identification of Low Molecular Weight Molecules Able to Reduce the Toxicity of Amyloid-β Peptide to Cell Cultures and Transgenic Mouse Models of Alzheimer's Disease. *Molecules* **2019**, *24* (6), 1–17. https://doi.org/10.3390/molecules24061167.

(10) Grasso, G. Mass Spectrometry Is a Multifaceted Weapon to Be Used in the Battle against Alzheimer's Disease: Amyloid Beta Peptides and Beyond. *Mass Spectrom. Rev.* **2019**, *38* (1), 34–48. https://doi.org/10.1002/mas.21566.

(11) Elizabeth Pryor, N.; Moss, M. A.; Hestekin, C. N. Unraveling the Early Events of Amyloid-ß Protein (Aß) Aggregation: Techniques for the Determination of Aβ Aggregate Size. *Int. J. Mol. Sci.* **2012**, *13* (3), 3038–3072. https://doi.org/10.3390/ijms13033038.

(12) Darling, A. L.; Shorter, J. Atomic Structures of Amyloid-β Oligomers Illuminate a Neurotoxic Mechanism. *Trends Neurosci.* **2020**, *43* (10), 740–743. https://doi.org/10.1016/j.tins.2020.07.006.

(13) Grasso, G. The Use of Mass Spectrometry to Study Amyloid-β Peptides. *Mass Spectrom. Rev.* **2011**, *30* (3), 347–365. https://doi.org/10.1002/mas.20281.

(14) Oren, O.; Taube, R.; Papo, N. Amyloid β Structural Polymorphism, Associated Toxicity and Therapeutic Strategies. *Cell. Mol. Life Sci.* **2021**, *78* (23), 7185–7198. https://doi.org/10.1007/s00018-021-03954-z.

(15) Shea, D.; Daggett, V. Amyloid-β Oligomers: Multiple Moving Targets. *Biophysica* **2022**,

2, 91–110.

(16) Urban, A. S.; Pavlov, K. V.; Kamynina, A. V.; Okhrimenko, I. S.; Arseniev, A. S.; Bocharov, E. V. Structural Studies Providing Insights into Production and Conformational Behavior of Amyloid-β Peptide Associated with Alzheimer's Disease Development. *Molecules* **2021**, *26* (10), 2897. https://doi.org/10.3390/molecules26102897.

(17) Xie, Y.; Wang, Y.; Jiang, S.; Xiang, X.; Wang, J.; Ning, L. Novel Strategies for the Fight of Alzheimer's Disease Targeting Amyloid-β Protein. *J. Drug Target.* **2022**, *30* (3), 259–268. https://doi.org/10.1080/1061186X.2021.1973482.

(18) Wells, C.; Brennan, S.; Keon, M.; Ooi, L. The Role of Amyloid Oligomers in Neurodegenerative Pathologies. *Int. J. Biol. Macromol.* **2021**, *181*, 582–604. https://doi.org/10.1016/j.ijbiomac.2021.03.113.

(19) Mrdenovic, D.; Pieta, I. S.; Nowakowski, R.; Kutner, W.; Lipkowski, J.; Pieta, P. Amyloid β Interaction with Model Cell Membranes – What Are the Toxicity-Defining Properties of Amyloid β? *Int. J. Biol. Macromol.* **2022**, *200*, 520–531. https://doi.org/10.1016/j.ijbiomac.2022.01.117.

(20) Madhu, P.; Mukhopadhyay, S. Distinct Types of Amyloid-β Oligomers Displaying Diverse Neurotoxicity Mechanisms in Alzheimer's Disease. *J. Cell. Biochem.* **2021**, *122* (11), 1594–1608. https://doi.org/10.1002/jcb.30141.

(21) Larson, M. E.; Lesné, S. E. Soluble Aβ Oligomer Production and Toxicity. *J. Neurochem.* **2012**, *120* (SUPPL. 1), 125–139. https://doi.org/10.1111/j.1471-4159.2011.07478.x.

(22) Walsh, D. M.; Selkoe, D. J. Aβ Oligomers - A Decade of Discovery. *J. Neurochem.* **2007**, *101* (5), 1172–1184. https://doi.org/10.1111/j.1471-4159.2006.04426.x.

(23) Gorman, P. M.; Yip, C. M.; Fraser, P. E.; Chakrabartty, A. Alternate Aggregation

Pathways of the Alzheimer β-Amyloid Peptide: Aβ Association Kinetics at Endosomal PH. *J. Mol. Biol.* **2003**, *325* (4), 743–757. https://doi.org/10.1016/S0022-2836(02)01279-2.

(24) Cleary, J. P.; Walsh, D. M.; Hofmeister, J. J.; Shankar, G. M.; Kuskowski, M. A.; Selkoe, D. J.; Ashe, K. H. Natural Oligomers of the Amyloid-β Protein Specifically Disrupt Cognitive Function. *Nat. Neurosci.* **2005**, *8* (1), 79–84. https://doi.org/10.1038/nn1372.

(25) Townsend, M.; Shankar, G. M.; Mehta, T.; Walsh, D. M.; Selkoe, D. J. Effects of Secreted Oligomers of Amyloid β-Protein on Hippocampal Synaptic Plasticity: A Potent Role for Trimers. *J. Physiol.* **2006**, *572* (2), 477–492. https://doi.org/10.1113/jphysiol.2005.103754.

(26) Ladiwala, A. R. A.; Litt, J.; Kane, R. S.; Aucoin, D. S.; Smith, S. O.; Ranjan, S.; Davis, J.; Van Nostrand, W. E.; Tessier, P. M. Conformational Differences between Two Amyloid Boligomers of Similar Size and Dissimilar Toxicity. *J. Biol. Chem.* **2012**, *287* (29), 24765–24773. https://doi.org/10.1074/jbc.M111.329763.

(27) Pujol-Pina, R.; Vilaprinyó-Pascual, S.; Mazzucato, R.; Arcella, A.; Vilaseca, M.; Orozco, M.; Carulla, N. SDS-PAGE Analysis of Aβ Oligomers Is Disserving Research into Alzheimer's Disease: Appealing for ESI-IM-MS. *Sci. Rep.* **2015**, *5* (May), 1–13. https://doi.org/10.1038/srep14809.

(28) Yu, L.; Edalji, R.; Harlan, J. E.; Holzman, T. F.; Lopez, A. P.; Labkovsky, B.; Hillen, H.; Barghorn, S.; Ebert, U.; Richardson, P. L.; Miesbauer, L.; Solomon, L.; Bartley, D.; Walter, K.; Johnson, R. W.; Hajduk, P. J.; Olejniczak, E. T. Structural Characterization of a Soluble Amyloid β-Peptide Oligomer. *Biochemistry* **2009**, *48* (9), 1870–1877. https://doi.org/10.1021/bi802046n.

(29) Bitan, G.; Fradinger, E. A.; Spring, S. M.; Teplow, D. B. Neurotoxic Protein Oligomers - What You See Is Not Always What You Get. *Amyloid* **2005**, *12* (2), 88–95. https://doi.org/10.1080/13506120500106958.

(30) Watt, A. D.; Perez, K. A.; Rembach, A.; Sherrat, N. A.; Hung, L. W.; Johanssen, T.; McLean, C. A.; Kok, W. M.; Hutton, C. A.; Fodero-Tavoletti, M.; Masters, C. L.; Villemagne, V. L.; Barnham, K. J. Oligomers, Fact or Artefact? SDS-PAGE Induces Dimerization of β-Amyloid in Human Brain Samples. *Acta Neuropathol.* **2013**, *125* (4), 549–564. https://doi.org/10.1007/s00401-013-1083-z.

(31) Harvey, S. R.; Vanaernum, Z. L.; Wysocki, V. H. Surface-Induced Dissociation of Anionic vs Cationic Native-Like Protein Complexes. *J. Am. Chem. Soc.* **2021**, *143* (20), 7698–7706. https://doi.org/10.1021/jacs.1c00855.

(32) Russel, D.; Lasker, K.; Phillips, J.; Schneidman-Duhovny, D.; Velázquez-Muriel, J. A.; Sali, A. The Structural Dynamics of Macromolecular Processes. *Curr. Opin. Cell Biol.* **2009**, *21* (1), 97–108. https://doi.org/10.1016/j.ceb.2009.01.022.

(33) Lu, J. X.; Qiang, W.; Yau, W. M.; Schwieters, C. D.; Meredith, S. C.; Tycko, R. XMolecular Structure of β-Amyloid Fibrils in Alzheimer's Disease Brain Tissue. *Cell* **2013**, *154* (6), 1257. https://doi.org/10.1016/j.cell.2013.08.035.

(34) Hoyer, W.; Grönwall, C.; Jonsson, A.; Ståhl, S.; Härd, T. Stabilization of a β-Hairpin in Monomeric Alzheimer's Amyloid-β Peptide Inhibits Amyloid Formation. *Chemtracts* **2008**, *20* (12), 499–500.

(35) Ghosh, U.; Thurber, K. R.; Yau, W. M.; Tycko, R. Molecular Structure of a Prevalent Amyloid-β Fibril Polymorph from Alzheimer's Disease Brain Tissue. *Proc. Natl. Acad. Sci. U. S. A.* **2021**, *118* (4). https://doi.org/10.1073/pnas.2023089118.

(36) Serra-Batiste, M.; Ninot-Pedrosa, M.; Bayoumi, M.; Gairí, M.; Maglia, G.; Carulla, N. Aβ42 Assembles into Specific β-Barrel Pore-Forming Oligomers in Membrane-Mimicking Environments. *Proc. Natl. Acad. Sci. U. S. A.* **2016**, *113* (39), 10866–10871. https://doi.org/10.1073/pnas.1605104113.

(37) Benilova, I.; Karran, E.; De Strooper, B. The Toxic Aβ Oligomer and Alzheimer's Disease: An Emperor in Need of Clothes. *Nat. Neurosci.* **2012**, *15* (3), 349–357. https://doi.org/10.1038/nn.3028.

(38) Hawk, L. M. L.; Pittman, J. M.; Moore, P. C.; Srivastava, A. K.; Zerweck, J.; Williams, J. T. B.; Hawk, A. J.; Sachleben, J. R.; Meredith, S. C. β-Amyloid Model Core Peptides: Effects of Hydrophobes and Disulfides. *Protein Sci.* **2020**, *29* (2), 527–541. https://doi.org/10.1002/pro.3778.

(39) Straub, J. E.; Thirumalai, D. Principles Governing Oligomer Formation in Amyloidogenic Peptides. *Curr. Opin. Struct. Biol.* **2010**, *20* (2), 187–195. https://doi.org/10.1016/j.sbi.2009.12.017.

(40) Kreutzer, A. G.; Nowick, J. S. Elucidating the Structures of Amyloid Oligomers with Macrocyclic β-Hairpin Peptides: Insights into Alzheimer's Disease and Other Amyloid Diseases. *Acc. Chem. Res.* **2018**, *51* (3), 706–718. https://doi.org/10.1021/acs.accounts.7b00554.

(41) Kreutzer, A. G.; Spencer, R. K.; McKnelly, K. J.; Yoo, S.; Hamza, I. L.; Salveson, P. J.; Nowick, J. S. A Hexamer of a Peptide Derived from Aβ16-36. *Biochemistry* **2017**, *56* (45), 6061–6071. https://doi.org/10.1021/acs.biochem.7b00831.

(42) Wang, Y.; Kreutzer, A. G.; Truex, N. L.; Nowick, J. S. A Tetramer Derived from Islet Amyloid Polypeptide. *J. Org. Chem.* **2017**, *82* (15), 7905–7912.

https://doi.org/10.1021/acs.joc.7b01116.

(43) Kreutzer, A. G.; Yoo, S.; Spencer, R. K.; Nowick, J. S. Stabilization, Assembly, and Toxicity of Trimers Derived from Aβ. *J. Am. Chem. Soc.* **2017**, *139* (2), 966–975. https://doi.org/10.1021/jacs.6b11748.

(44) Kreutzer, A. G.; Samdin, T. D.; Guaglianone, G.; Spencer, R. K.; Nowick, J. S. X-Ray Crystallography Reveals Parallel and Antiparallel β-Sheet Dimers of a β-Hairpin Derived from Aβ16-36that Assemble to Form Different Tetramers. *ACS Chem. Neurosci.* **2020**, *11* (15), 2340–2347. https://doi.org/10.1021/acschemneuro.0c00290.

(45) Haerianardakani, S.; Kreutzer, A. G.; Salveson, P. J.; Samdin, T. D.; Guaglianone, G. E.; Nowick, J. S. Phenylalanine Mutation to Cyclohexylalanine Facilitates Triangular Trimer Formation by β-Hairpins Derived from Aβ. *J. Am. Chem. Soc.* **2020**, *142* (49), 20708–20716. https://doi.org/10.1021/jacs.0c09281.

(46) Kreutzer, A. G.; Malonis, R. J.; Parrocha, M. T.; Guaglianone, G.; Tong, K.; Yoo, S.; Nguyen, J. T.; Howitz, W. J.; Diab, M. N.; Hamza, I. L.; Lai, J. R.; Nowick, J. S. Two Isomorphic Triangular Trimers Derived from Aβ Exhibit Different Biological, Biophysical, and Immunological Properties. Manuscript in preparation.

(47) Snyder, D. T.; Harvey, S. R.; Wysocki, V. H. Surface-Induced Dissociation Mass Spectrometry as a Structural Biology Tool. *Chem. Rev.* **2022**, *122* (8), 7442–7487. https://doi.org/10.1021/acs.chemrev.1c00309.

(48) Marty, M. T.; Baldwin, A. J.; Marklund, E. G.; Hochberg, G. K. A.; Benesch, J. L. P.; Robinson, C. V. Bayesian Deconvolution of Mass and Ion Mobility Spectra: From Binary Interactions to Polydisperse Ensembles. *Anal. Chem.* **2015**, *87* (8), 4370–4376. https://doi.org/10.1021/acs.analchem.5b00140.

(49) Kanu, A. B.; Dwivedi, P.; Tam, M.; Matz, L.; Hill, H. H. Ion Mobility-Mass Spectrometry. *J. Mass Spectrom.* **2008**, *43* (1), 1–22. https://doi.org/10.1002/jms.1383.

(50) Shvartsburg, A. A.; Smith, R. D. Fundamentals of Traveling Wave Ion Mobility Spectrometry. *Anal. Chem.* **2008**, *80* (24), 9689–9699. https://doi.org/10.1021/ac8016295.

(51) Dodds, J. N.; Baker, E. S. Ion Mobility Spectrometry: Fundamental Concepts, Instrumentation, Applications, and the Road Ahead. *J. Am. Soc. Mass Spectrom.* **2019**, *30* (11), 2185–2195. https://doi.org/10.1007/s13361-019-02288-2.

(52) Ben-Nissan, G.; Sharon, M. The Application of Ion-Mobility Mass Spectrometry for Structure/Function Investigation of Protein Complexes. *Curr. Opin. Chem. Biol.* **2018**, *42*, 25–33. https://doi.org/10.1016/j.cbpa.2017.10.026.

(53) Snyder, D. T.; Jones, B. J.; Lin, Y. F.; Cooper-Shepherd, D. A.; Hewitt, D.; Wildgoose, J.; Brown, J. M.; Langridge, J. I.; Wysocki, V. H. Surface-Induced Dissociation of Protein Complexes on a Cyclic Ion Mobility Spectrometer. *Analyst* **2021**, *146* (22), 6861–6873. https://doi.org/10.1039/d1an01407b.

(54) Sonn-Segev, A.; Belacic, K.; Bodrug, T.; Young, G.; VanderLinden, R. T.; Schulman, B. A.; Schimpf, J.; Friedrich, T.; Dip, P. V.; Schwartz, T. U.; Bauer, B.; Peters, J. M.; Struwe, W. B.; Benesch, J. L. P.; Brown, N. G.; Haselbach, D.; Kukura, P. Quantifying the Heterogeneity of Macromolecular Machines by Mass Photometry. *Nat. Commun.* **2020**, *11* (1), 1–10. https://doi.org/10.1038/s41467-020-15642-w.

(55) Jana, M. K.; Cappai, R.; Pham, C. L. L.; Ciccotosto, G. D. Membrane-Bound Tetramer and Trimer Aβ Oligomeric Species Correlate with Toxicity towards Cultured Neurons. *J. Neurochem.* **2016**, *136* (3), 594–608. https://doi.org/10.1111/jnc.13443.

Supporting information for:

Investigating the Gas- and Solution-Phase Assembly of Three Trimers Derived from Aβ

Table of Contents

Figure S4.1 LC-MS of QKM_{CC} Oxidation Reaction 181

Figure S4.2 Native IM-MS of Trimers with 0 h Incubation 182

Figure S4.3 Caspase 3/7 Activation Assay 183

General Information 184

Synthesis of Macrocyclic Peptides 186

Oxidation of QKM_{CC} to QKT 188

Native Mass Spectrometry 188

Native IM-MS 189

Mass Photometry 190

SDS-PAGE 190

Cell Culture 191

Cell Viability and Caspase 3/7 Assay 191

References and Notes 193

Characterization Data

- Characterization of 2AT 195
- Characterization of KLT 199
- Characterization of QKM_{CC} 203
- Characterization of QKT 206

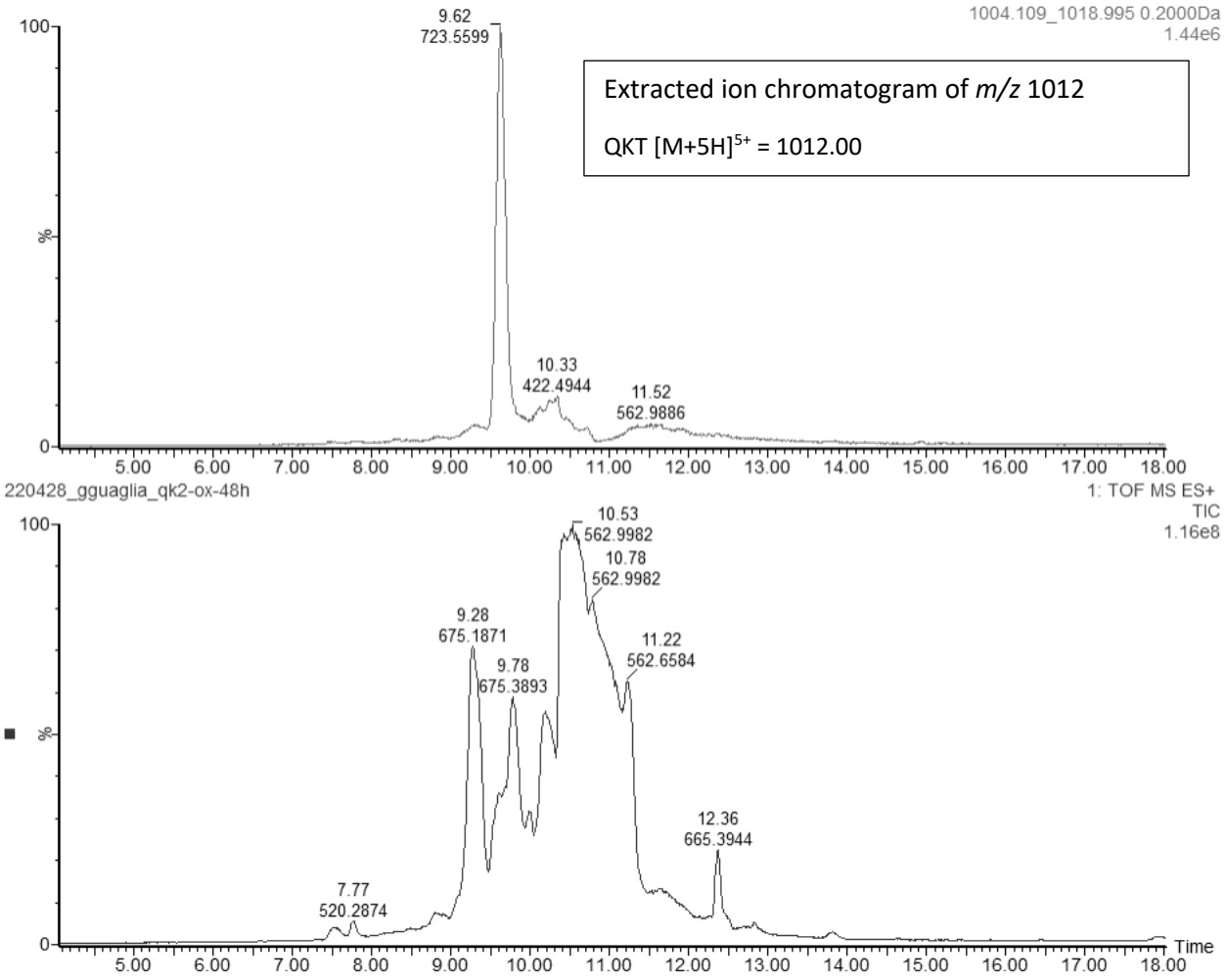

Figure S4.1 Liquid chromatograph-mass spectrometry ion chromatogram of the oxidation reaction of QKM_{CC} to form QKT in solution. The oxidation reaction of QKM_{CC} in 20% aqueous DMSO after 48 h was run on LC-MS and the reaction chromatogram (below) was integrated across all peaks to observe the masses of species present. The mass corresponding to $[M+5]^{5+}$ peak of QKT, a peak only present from the trimer species, was extracted from the mass spectrum back into the ion chromatogram. This extracted ion chromatogram indicates the retention of the trimer peak in context of the reaction mixture.

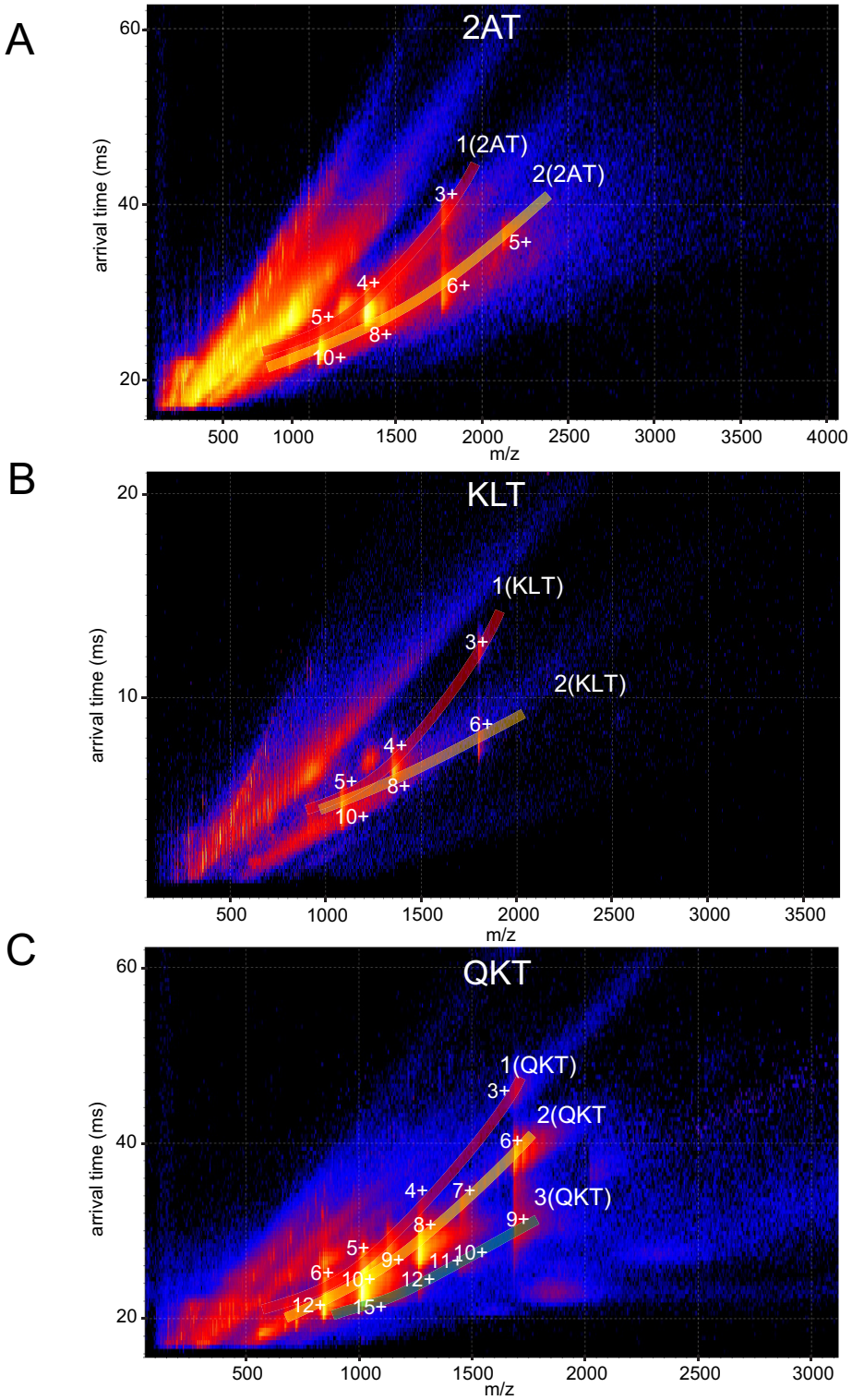

Figure S4.2 Native IM-MS of 2AT, KLT, and QKT after 0 h incubation. **(A,B,C)** Mobiligrams of 2AT, KLT, and QKT. Native IM-MS was performed on a SELECT SERIES Cyclic IMS Q-cIMS-TOF (cIMS) instrument (Waters Corporation). Numeric labels indicate the charge state of the corresponding oligomeric species. Samples of trimers were prepared at a concentration of 40 μM in 200 mM ammonium acetate.

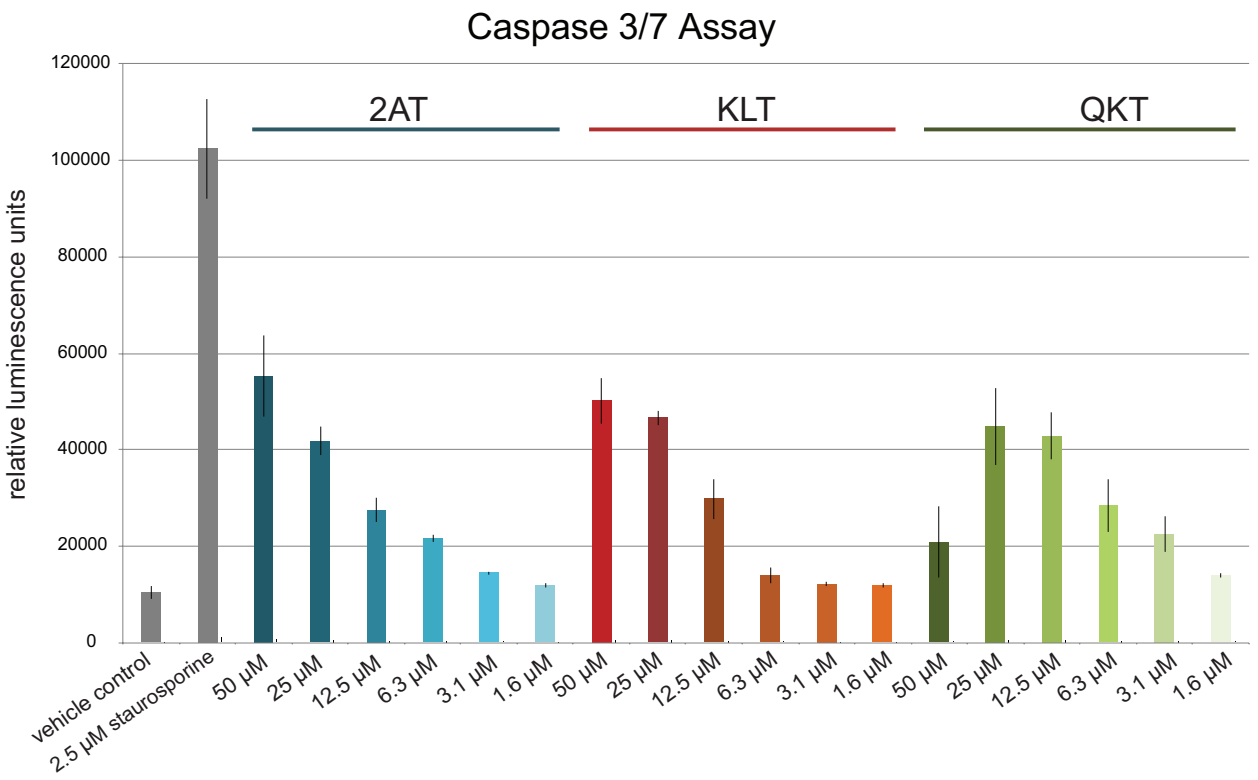

Figure S4.3 Caspase 3/7 assay of SH-SY5Y cells treated with 2AT, KLT, or QKT. Data represent the mean of three replicate wells, with the error bars corresponding to the standard deviation.

General Information[1]

All Fmoc-protected amino acids including the unnatural amino acid, Boc-ornithine(Fmoc)-OH, were purchased from Chem-Impex or Anaspec. 2-Chlorotrityl chloride resin was purchased from Chem-Impex. Trifluoroacetic acid (TFA), and HPLC grade acetonitrile (MeCN) were purchased from Fischer Scientific. Water was purified to 18 MΩ with a ThermoFisher Barnstead Nanopure water purification system. All other solvents and chemicals were purchased from Alfa Aesar and Sigma Aldrich. All amino acids, resins, solvents, and chemicals were used as received, with the exception that dichloromethane (DCM) and *N,N*-dimethylformamide (DMF) were dried by passage through dry alumina under argon. Analytical HPLC chromatograms were obtained using an Agilent 1260 Infinity II HPLC equipped with Phenomenex bioZen C18 column (150 mm × 4.6 mm, 2.6 μm particle size). HPLC grade acetonitrile (MeCN) and 18 MΩ deionized water, each containing 0.1% trifluoroacetic acid, were used as the mobile phase running at 1 mL/min flow rate. Peaks for peptides without fluorophores were detected at 214 nm. Sulfo-cyanine3 labeled peptides were detected at 548 nm and sulfo-cyanine5 labeled peptides were detected at 600 nm. All peptides were monitored using the provided HPLC OpenLAB software.

Preparative-scale purification of 2AM$_{CC}$, 2AT, KLM$_{CC}$, KLT, QKM$_{CC}$, and QKT was done using an Agilent Zorbax SB-C18 PrepHT column (21.2 mm x 250 mm, 7 μm particle size) on a Rainin Dynamax HPLC with a flow rate of 12.0 mL/min, monitored at 214 nm with the accompanying DA Rainin HPLC software. HPLC grade acetonitrile (MeCN) and 18 MΩ deionized water, each containing 0.1% trifluoroacetic acid, were used as the mobile phase. Liquid chromatography-mass spectrometry was performed using a Waters Xevo XS UPLC-QTOF. Spectra were analyzed using the accompanying Waters MassLynx software.

Abbreviations:

DCM	dichloromethane
DIPEA	diisopropylethylamine
DMF	*N*,*N*-dimethylformamide
HATU	*N*,*N*,*N*′,*N*′-tetramethyl-O-(7-azabenzotriazol-1-yl)uronium hexafluorophosphate
HBTU	*N*,*N*,*N*′,*N*′-tetramethyl-O-(1H-benzotriazol-1-yl)uronium hexafluorophosphate
HCTU	*N*,*N*,*N*′,*N*′-tetramethyl-O-(6-chlorobenzotriazol-1-yl)uraniumhexafluorophosphate
HFIP	1,1,1,3,3,3-hexafluoro-2-propanol
HPLC	high-performance liquid chromatography
HOBt	hydroxybenzotriazole
HOAt	1-Hydroxy-7-azabenzotriazole
NMM	*N*-Methylmorpholine
MeOH	methanol
MeCN	acetonitrile
TFA	trifluoroacetic acid
TIPS	triisopropylsilane

Synthesis of the Macrocyclic Peptides $2AM_{CC}$ and KLM_{CC} and Trimers 2AT and KLT

Peptides $2AM_{CC}$ and KLM_{CC} were synthesized as previously described.[2,3] Oxidation of $2AM_{CC}$ and KLM_{CC} to trimers 2AT and KLT was performed as previously described.[4,5]

Synthesis of the Macrocyclic Peptide QKM_{CC}

Peptide QKM_{CC} was synthesized in a fashion similar to $2AM_{CC}$ and KLM_{CC}. Synthesis proceeded through the following steps:

Resin Loading. 2-Chlorotrityl chloride resin (300 mg, 1.2 mmol/g) was added to a Bio-Rad Poly-Prep chromatography column (10 mL). The resin was suspended in dry DCM (10 mL) and allowed to swell for 30 min. The solution was drained from the resin and a solution of Boc-Orn(Fmoc)-OH (0.50 equiv, 82 mg, 0.18 mmol) in 6% (v/v) 2,4,6-collidine in dry DCM (8 mL) was added immediately and was rocked gently for 12 h. The solution was then drained and a mixture DCM/MeOH/ DIPEA (17:2:1, 10 mL) was added immediately. The mixture was gently rocked for 1 h to cap the unreacted 2-chlorotrityl chloride resin sites. The resin was then washed with dry DCM (3x 8 mL) and followed by a wash with dry DMF (3x 8 mL). The washed resin was transferred to a coupling vessel in DMF.

Peptide coupling. The Boc-Orn(Fmoc)-2-chlorotrityl resin generated from the previous step was submitted to cycles of peptide coupling with Fmoc-protected amino acid building blocks. Linear peptides were constructed from *C*- to *N*-terminus using Fmoc-protected amino acids (AAs), with each coupling step comprised of the following; 1) addition of 20% (v/v) piperidine in DMF to remove Fmoc from protected *N*-terminal amines (1 x 5 min.), 2) DMF washes (5 x 9 mL), 3) addition of Fmoc-AA-OH (0.75 mmol, 5.0 equiv.) and HCTU (0.68

mmol, 4.5 equiv.) in 20% (v/v) 2,4,6-collidine in DMF (6 mL) for peptide coupling (20 min. each), 4) repeat cycles from steps 2–4. Once the final AAs were coupled, one last round of Fmoc deprotection was conducted as described above. The resin was then removed from the coupling vessel and transferred into a Bio-Rad Poly-Prep chromatography column.

Cleavage of the peptide from the resin. The linear peptide was cleaved from the resin by gently rocking the resin for 1 h with a solution of HFIP in DCM. (11.5:3.5, 7 mL). The suspension was filtered and the filtrate was collected in a 250 mL round-bottomed flask. The resin was washed with additional HFIP in DCM (11.5:3.5, 7 mL). The combined filtrates were concentrated by rotary evaporation to give a white solid. The white solid was further dried by vacuum pump to afford the crude protected linear peptide, which was cyclized without further purification.

Cyclization of linear peptide. The crude protected linear peptide was dissolved in dry DMF (150 mL). HOAt (114 mg, 0.75 mmol, 5 equiv) and HATU (317 mg, 0.75 mmol, 5 equiv) were added to the solution. NMM (0.33 mL, 1.8 mmol, 12 equiv) was added to the solution and the mixture was stirred under nitrogen for 48 h. The mixture was concentrated by rotary evaporation to afford the crude protected cyclic peptide.

Global deprotection and ether precipitation of the cyclic peptide. The protected cyclic peptide was dissolved in TFA/TIPS/H_2O (18:1:1, 20 mL) in a 250 mL round-bottomed flask. The solution was stirred for 1 h. The reaction mixture was then ether precipitated. 40 mL of cold ether was added to 10 mL of the TFA/peptide solution in a 50 mL conical tube. The mixture was incubated in an ice bath for 10 min and then centrifuged. The supernatant was decanted and the pellet was transferred to a round bottom flask in acetonitrile. The mixture was dried by rotary

evaporation. The crude cyclic peptide was immediately subjected to purification by reversed-phase HPLC (RP-HPLC), as described below.

Reversed-phase HPLC purification. The peptide was dissolved in H_2O and MeCN (8:2, 10 mL), and the solution was filtered through a 0.2 μm syringe filter and purified by RP-HPLC (gradient elution with 20–50% MeCN over 60 min). Pure fractions were concentrated by rotary evaporation and lyophilized. Typical synthesis yielded ~50 mg of the peptide as the TFA salt.

Oxidation of Peptide QKM$_{CC}$ to Trimer QKT

Following purification, peptides with two free thiols from deprotected cysteine residues were oxidized in 20% aqueous dimethyl sulfoxide (DMSO). A 6 mM solution of lyophilized peptide was prepared gravimetrically by dissolving the peptide in an appropriate amount of 20% (v/v) aqueous DMSO prepared with HPLC-grade water. The reaction was carried out in a capped 25 mL glass scintillation vial with gentle shaking at room temperature for 48. The reaction mixture was subjected to RP-HPLC purification (gradient elution with 20-50% MeCN over 60 min). Pure fractions were concentrated by rotary evaporation and lyophilized. Typical synthesis yielded ~3 mg of trimer QKT. 10 mg/mL stock solutions were prepared gravimetrically by dissolving 1.0 mg of each compound in 100 μL of 18 MΩ deionized water.

Native Mass Spectrometry

A freshly prepared 10 mg/mL stock solution of each peptide was prepared by adding the appropriate amount of 18 MΩ deionized water to lyophilized peptide. The 10 mg/mL solution of each peptide was diluted to 40 μM in 200 mM ammonium acetate immediately before each mass spectrometric experiment. Experiments were conducted on a Thermo Q Exactive Ultra High

Mass Range (UHMR) Orbitrap MS (Bremen, Germany). All samples were ionized via static nanospray ionization using in-house pulled borosilicate capillaries with the electrospray voltage applied to a platinum wire in contact with the solution. A capillary temperature of 250 °C was applied and a trap gas flow rate of 3–4 was used. The resolution was set to 6k for all complexes studied. In-source trapping was set to 60 V or less. The injection flatapole rf was set to 400 V. The HCD cell rf amplitude was set to 500 V. The C-trap rf amplitude was set to 2950 V. The bent flatapole rf was set to 500 V.

Spectra were analyzed and deconvoluted using Unidec software with settings as follows: m/z range 1000–8000 Th, charge range 1–30, mass range 1500–70000 Da, and smooth charge state distributions on. Peak detection range was set to 500 Da and peak detection threshold was set to 0.05. Oligomers were identified with the *Oligomer and Mass Tools*.

Native IM-MS

A freshly prepared 10 mg/mL stock solution of each peptide was prepared by adding the appropriate amount of 18 MΩ deionized water to lyophilized peptide. The 10 mg/mL solution of each peptide was diluted to 40 μM in 200 mM ammonium acetate immediately before each mass spectrometric experiment. A Waters SELECT SERIES Cyclic Ion Mobility Spectrometry System[6] (cIMS) was used to conduct mass spectrometry analysis. Samples were ionized using nanoelectrospray ionization (nano-ESI). Nano-ESI glass capillary tips were pulled in-house using a Sutter Instruments P-97 micropipette tip puller (Novato, CA). When performing experiments on the cIMS, the cIMS was tuned as follows: capillary voltage, 0.4 to 0.6 kV; cone voltage, 20 V; source temperature, 25 °C; trap CE, 4 V; transfer CE, 4 V; trap and transfer gas,

N_2 at 7.0 mL/min; IMS pressure, 1.8 mbar; TW static height, 22 V; TW velocity, 375 m/s; pushes per bin, 2. Spectra were analyzed in Waters Driftscope software.

Mass Photometry

Mass photometry samples were prepared fresh before analysis. 10 mg/mL solutions of each peptide was diluted to 650 nM in 200 mM ammonium acetate. Microscope cover slips were washed with Milli-Q H_2O, followed by isopropanol, then dried under nitrogen. Clean gaskets were added on top of the cover slip to create wells. Samples of 200 mM ammonium acetate containing no peptide were used as controls. NativeMark Unstained Protein Standard (Thermo Fisher) in 200 mM ammonium acetate was used as a protein ladder to create a calibration curve. NativeMark contains proteins of 1236, 1048, 720, 480, 242, 146, 66, 20 kDa. For each acquisition, 20 µL of sample solution was introduced into the well and, following autofocus stabilization, movies of 60 s duration were recorded. Data was acquired using a TwoMP mass photometer (Refeyn Ltd, Oxford, UK) and analyzed using the associated software.

SDS-PAGE[7]

Solutions of the trimers were prepared gravimetrically by dissolving the lyophilized peptide in the appropriate amount of 18 MΩ deionized water to achieve a 10 mg/mL stock solutions. Stock solutions of all peptides were diluted with 18 MΩ deionized water to create 75 µM sample solutions.1 µL of 6X SDS-PAGE sample loading buffer (G Biosciences) was added per 5 µL of sample solution to create working solutions. A 5 µL aliquot of each working solution was run on a 16% polyacrylamide gel with a 4% stacking polyacrylamide gel. The gel was run at a constant 60 volts for approximately 4 h. Reagents and gels for Tricine SDS-PAGE were

prepared according to recipes and procedures detailed in Schägger, H. *Nat. Protoc*. **2006**, *1*, 16–22.[8]

Staining with silver nitrate was then used to visualize the peptides in the gel. Reagents for silver staining were prepared according to procedures detailed in Simpson, R. J. *Cold Spring Harb. Protoc.* **2007**.[9] The gel was then silver stained following the procedures previously described.[7]

Cell Culture

SH-SY5Y neuroblastoma cell cultures (ATCC® CRL-2266™) were maintained in 1:1 mixture of Dubelcco's modified Eagle medium and Ham's F12 (DMEM:F12) medium supplemented with 10% heat-inactivated fetal bovine serum (FBS), 100 U/mL penicillin and 100 μg/mL streptomycin at pH 7.4 in a humidified 5% CO_2 atmosphere at 37 °C using a Fischer Scientific Forma Series 3 Water Jacketed CO_2 Incubator. All experiments were performed using ca. 60–80% confluent cells on passages ranging from 2–10.

Cell Viability and Caspase 3/7 Assay

SH-SY5Y cells were seeded at 30,000 cells per well in the inner 60 wells of half area 96-well plates to a total volume of 50 μL using 1:1 DMEM/F12 media supplemented with 10% FBS, 100 U/mL penicillin and 100 μg/mL streptomycin at pH 7.4. The outer wells of the plate were filled with 100 μL of media without any cells. The cells were incubated for 24 h after plating. Prior to treatment, the media of the inner 60 wells was removed by pipet. Solutions of the peptides were prepared gravimetrically by dissolving the lyophilized peptide in the appropriate amount of 18 MΩ deionized water to achieve a 10 mg/mL stock. From the 10

mg/mL stock solutions, 50 μM solutions were made by dilution with serum-free, phenol-red free 1:1 DMEM/F12 media with no added penicillin or streptomycin. 2-fold serial dilutions of the 50 μM solutions were prepared by diluting with serum-free, phenol-red free 1:1 DMEM/F12 media with no added penicillin or streptomycin resulting in solutions with concentrations of 50 μM, 25 μM, 12.5 μM, 6.3 μM, and 3.2 μM. 50 μL of a solution was added to the wells containing cells and each treatment was run in triplicate. An additional six wells were used as controls. Three wells received serum-free, phenol-red free 1:1 DMEM/F12 media with 3% of 18 MΩ deionized water (vehicle, negative control) and the other three wells were left untreated, to be subsequently treated with 2.5 μM staurosporine (positive control) 6 h prior to development. Cells were incubated for 72 hours.

After 72 hours, the caspase 3/7 and cell viability assay (ApoLive-Glo™ Multiplex Assay, Promega) was performed according to the manufacturer's instructions. Data were collected on a Promega GloMax Discover and analyzed.

REFERENCES AND NOTES

(1) The chemicals and instruments required for the synthesis of macrocyclic β-sheet peptide 2AM-L and 2AT-L are similar to those used in our laboratory's previous publications. This information was either adapted from or taken verbatim from Kreutzer, A. G.; Hamza, I. L.; Spencer, R. K.; Nowick, J. S. X-Ray Crystallographic Structures of a Trimer, Dodecamer, and Annular Pore Formed by an Aβ17-36 β-Hairpin. *J. Am. Chem. Soc.* **2016**, *138* (13), 4634–4642. https://doi.org/10.1021/jacs.6b01332.

(2) Kreutzer, A. G.; Hamza, I. L.; Spencer, R. K.; Nowick, J. S. X-Ray Crystallographic Structures of a Trimer, Dodecamer, and Annular Pore Formed by an Aβ17-36 β-Hairpin. *J. Am. Chem. Soc.* **2016**, *138* (13), 4634–4642. https://doi.org/10.1021/jacs.6b01332.

(3) Salveson, P. J.; Spencer, R. K.; Kreutzer, A. G.; Nowick, J. S. X-Ray Crystallographic Structure of a Compact Dodecamer from a Peptide Derived from Aβ16-36. *Org. Lett.* **2017**, *19* (13), 3462–3465. https://doi.org/10.1021/acs.orglett.7b01445.

(4) Kreutzer, A. G.; Yoo, S.; Spencer, R. K.; Nowick, J. S. Stabilization, Assembly, and Toxicity of Trimers Derived from Aβ. *J. Am. Chem. Soc.* **2017**, *139* (2), 966–975. https://doi.org/10.1021/jacs.6b11748.

(5) Kreutzer, A. G.; Malonis, R. J.; Parrocha, M. T.; Guaglianone, G.; Tong, K.; Yoo, S.; Nguyen, J. T.; Howitz, W. J.; Diab, M. N.; Hamza, I. L.; Lai, J. R.; Nowick, J. S. Two Isomorphic Triangular Trimers Derived from Aβ Exhibit Different Biological, Biophysical, and Immunological Properties. *Manuscript in preparation.*

(6) Snyder, D. T.; Jones, B. J.; Lin, Y. F.; Cooper-Shepherd, D. A.; Hewitt, D.; Wildgoose, J.; Brown, J. M.; Langridge, J. I.; Wysocki, V. H. Surface-Induced Dissociation of Protein Complexes on a Cyclic Ion Mobility Spectrometer. *Analyst* **2021**, *146* (22), 6861–6873.

https://doi.org/10.1039/d1an01407b.

(7) Peptides were run on SDS-PAGE and silver stained following a protocol similar to those published previously in our laboratory. The procedures were either adapted from or taken verbatim from: Kreutzer, A. G.; Hamza, I. L.; Spencer, R. K.; Nowick, J. S. X-Ray Crystallographic Structures of a Trimer, Dodecamer, and Annular Pore Formed by an Aβ17-36 β-Hairpin. *J. Am. Chem. Soc.* **2016**, *138* (13), 4634–4642. https://doi.org/10.1021/jacs.6b01332.

(8) Schägger, H. Tricine-SDS-PAGE. *Nat. Protoc.* **2006**, *1*, 16–22.

(9) Simpson, R. J. Staining Proteins in Gels with Silver Nitrate. *Cold Spring Harb. Protoc.* **2007**, Doi: 10.1101/Pdb.Prot4727.

Characterization Data

Characterization of trimer 2AT

Analytical HPLC trace

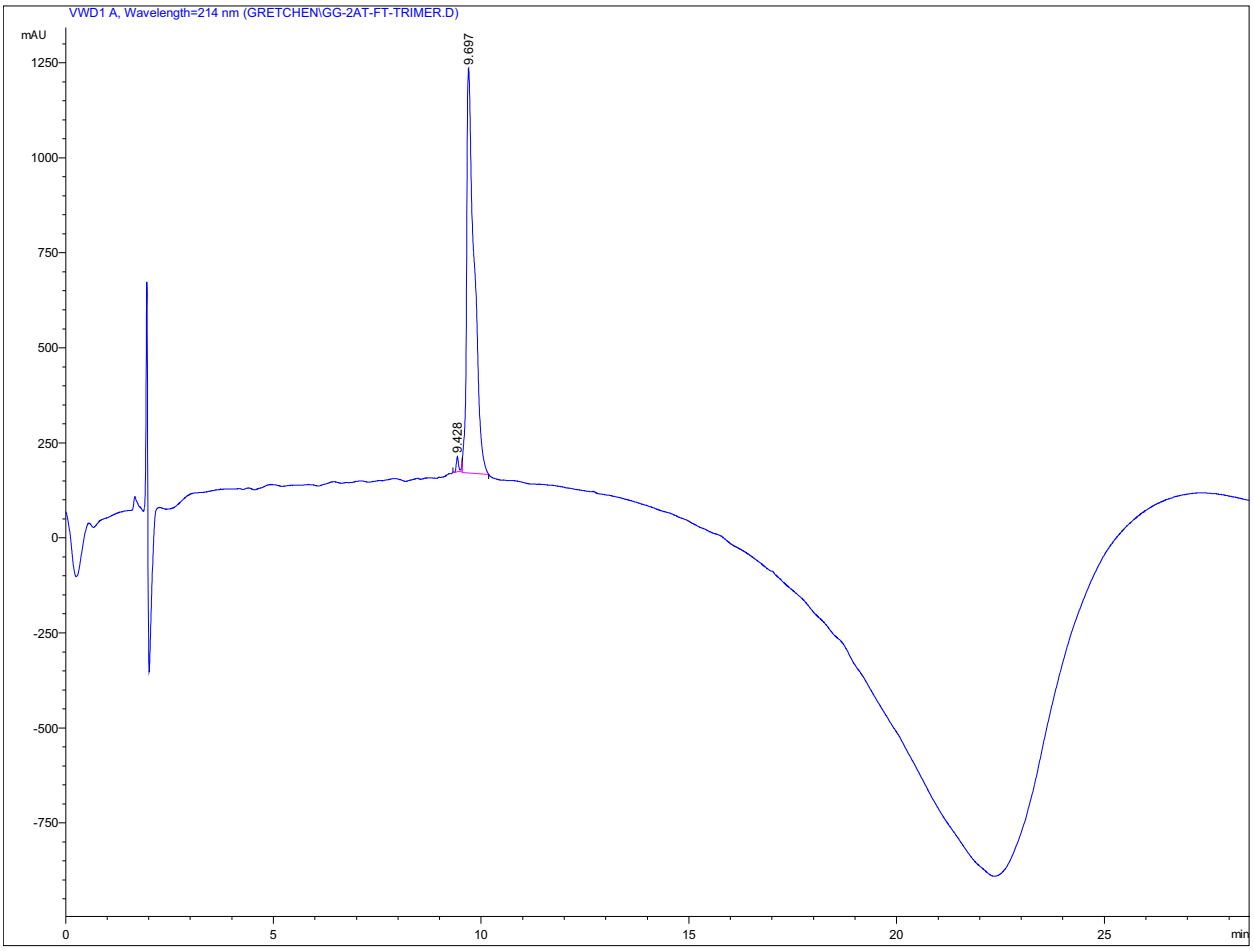

Signal 1: VWD1 A, Wavelength=214 nm

Peak #	RetTime [min]	Type	Width [min]	Area mAU *s	Height [mAU]	Area %
1	9.428	MM	0.0706	171.36655	40.45287	1.2561
2	9.697	MM	0.2106	1.34710e4	1066.05396	98.7439

Mass spectrum of trimer 2AT

Calculated $[M+H]^+$ of trimer 2AT: 5292.7

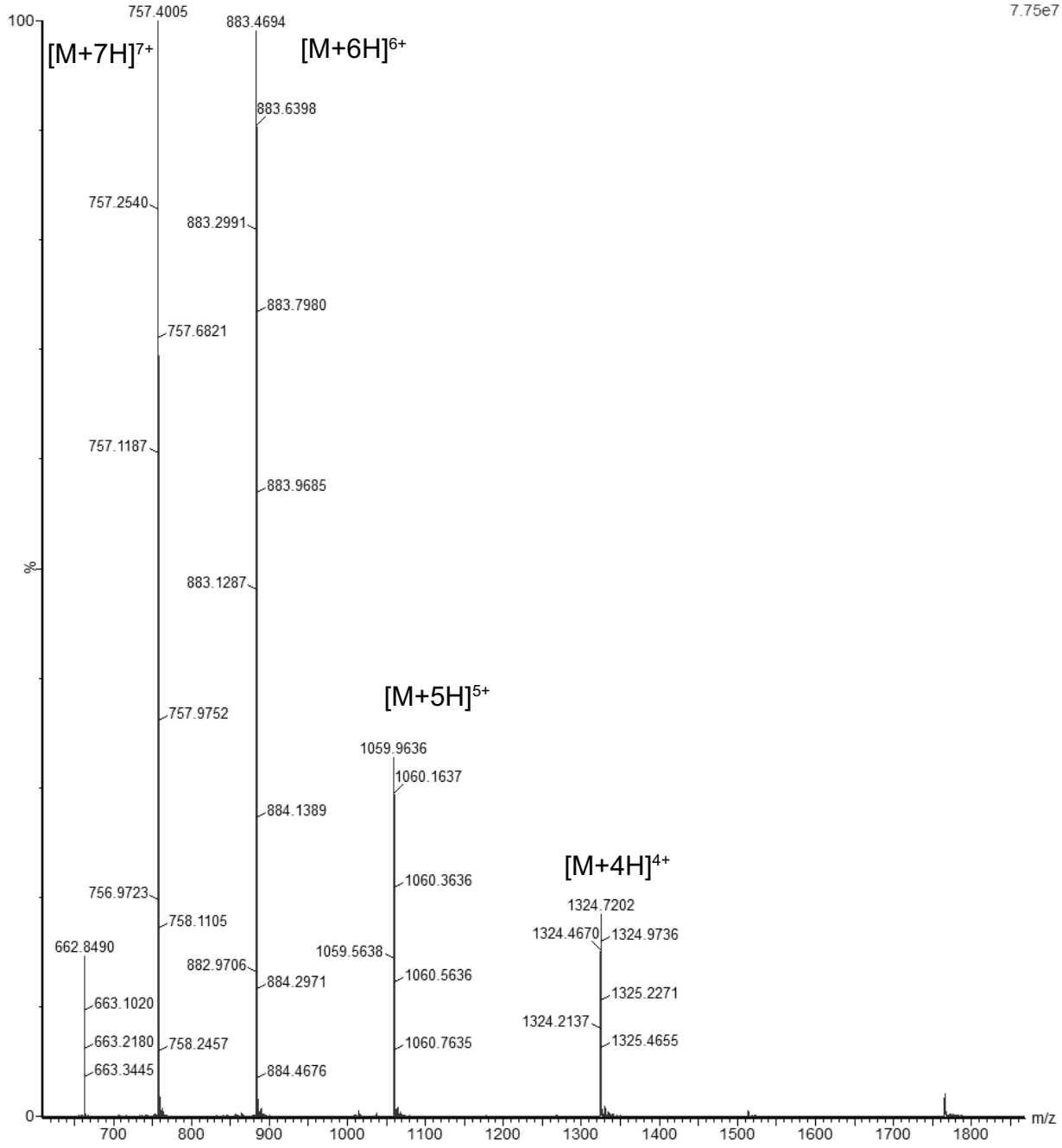

Expansion mass spectrum of trimer 2AT

Calculated $[M+H]^+$ of trimer 2AT: 5292.74

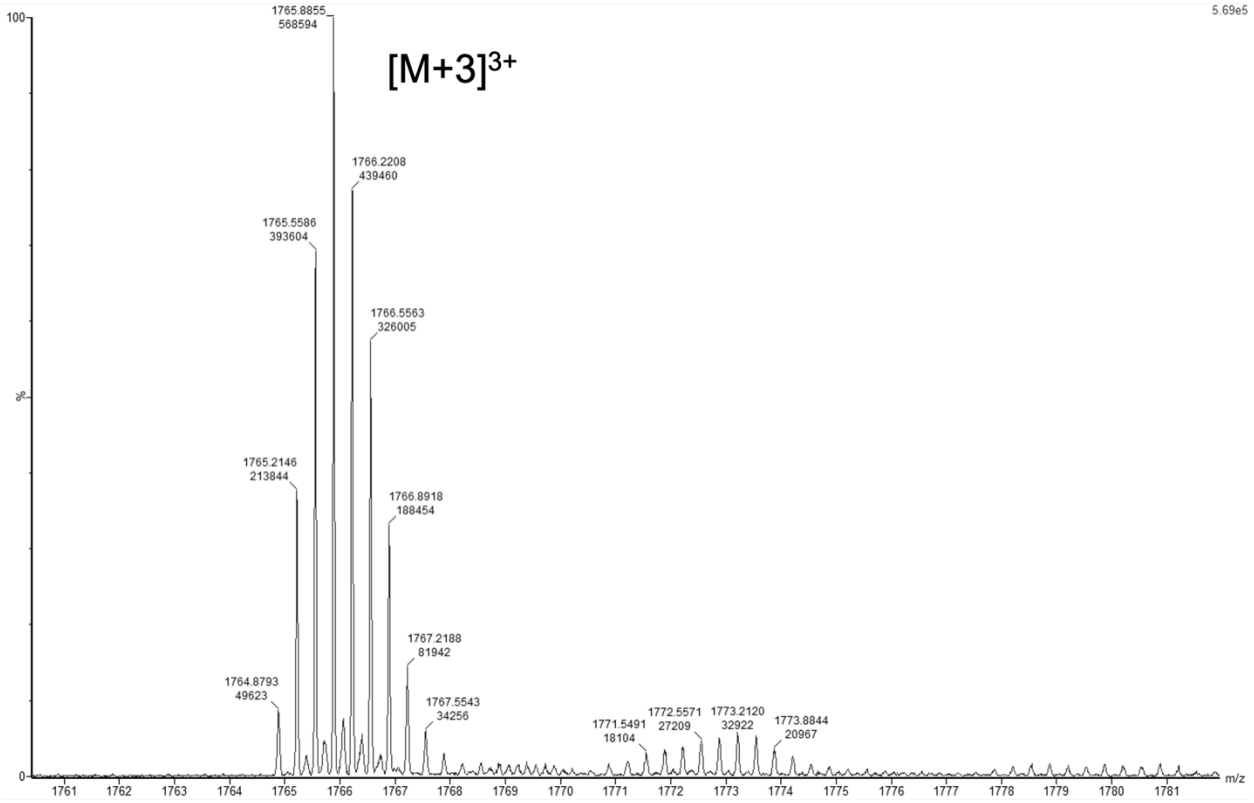

Deconvoluted mass spectrum of trimer 2AT

Exact mass of trimer 2AT: 5291.73

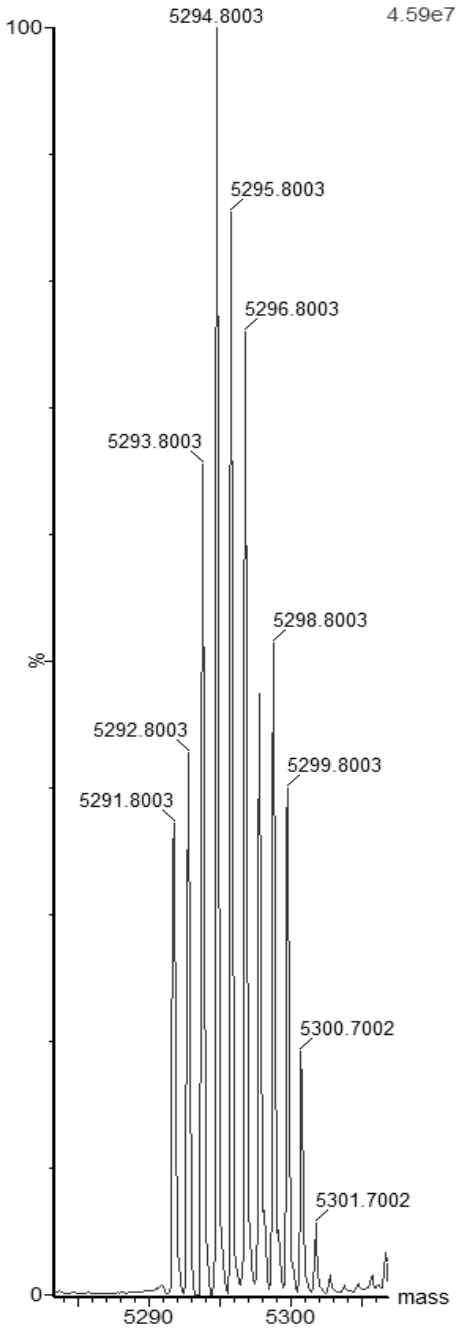

Characterization of trimer KLT

Analytical HPLC trace

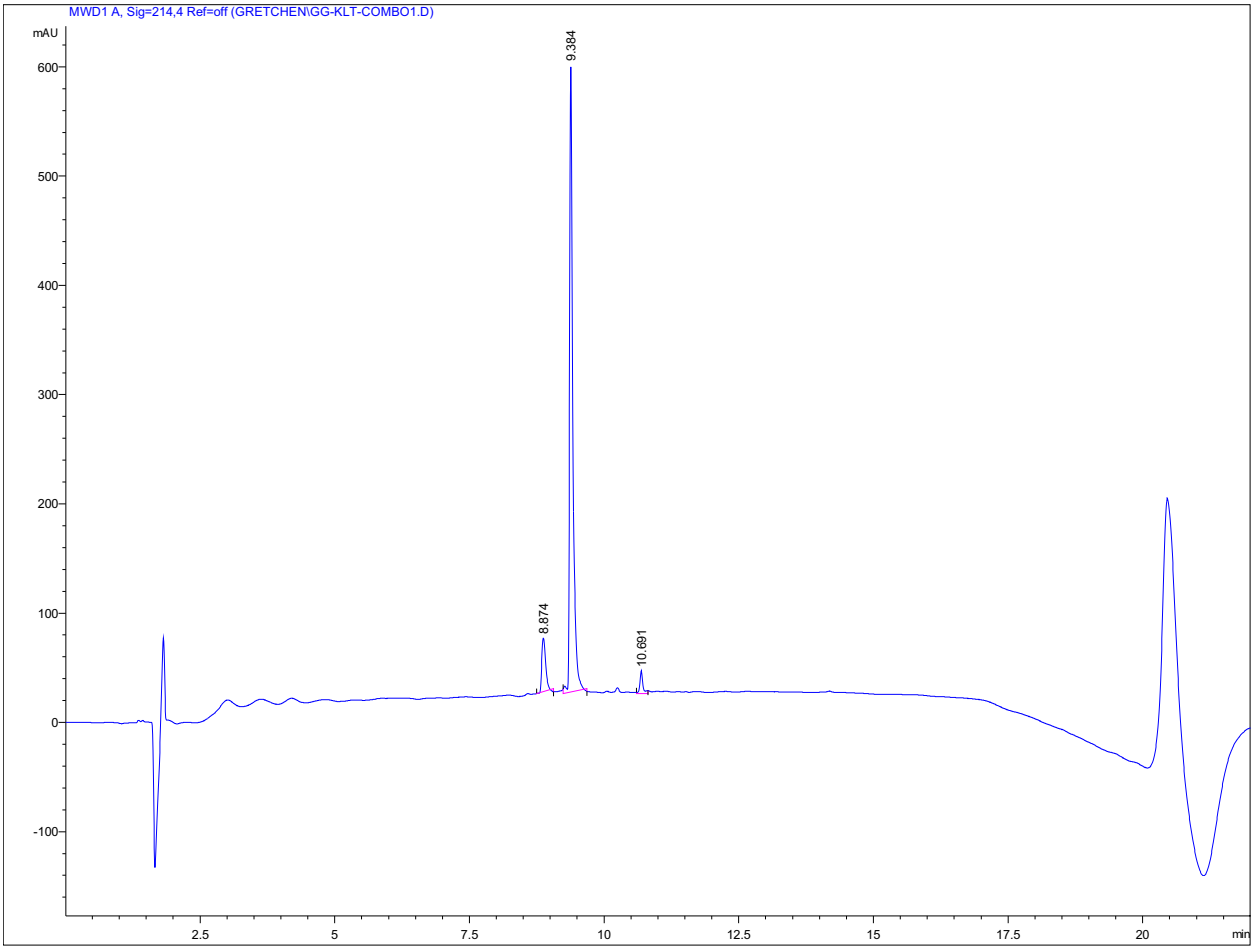

Signal 1: MWD1 A, Sig=214 nm Ref=off

Peak #	RetTime [min]	Type	Width [min]	Area [mAU*s]	Height [mAU]	Area %
1	8.874	MM	0.0815	241.49431	49.37487	9.0355
2	9.384	MM	0.0681	2345.10425	574.30060	87.7422
3	10.691	MM	0.0671	86.12202	21.39272	3.2223

The observed peak that elutes at 8.874 min is observed when methionine oxidation occurs.

Mass spectrum of trimer KLT

Calculated $[M+H]^+$ of trimer KLT: 5382.83

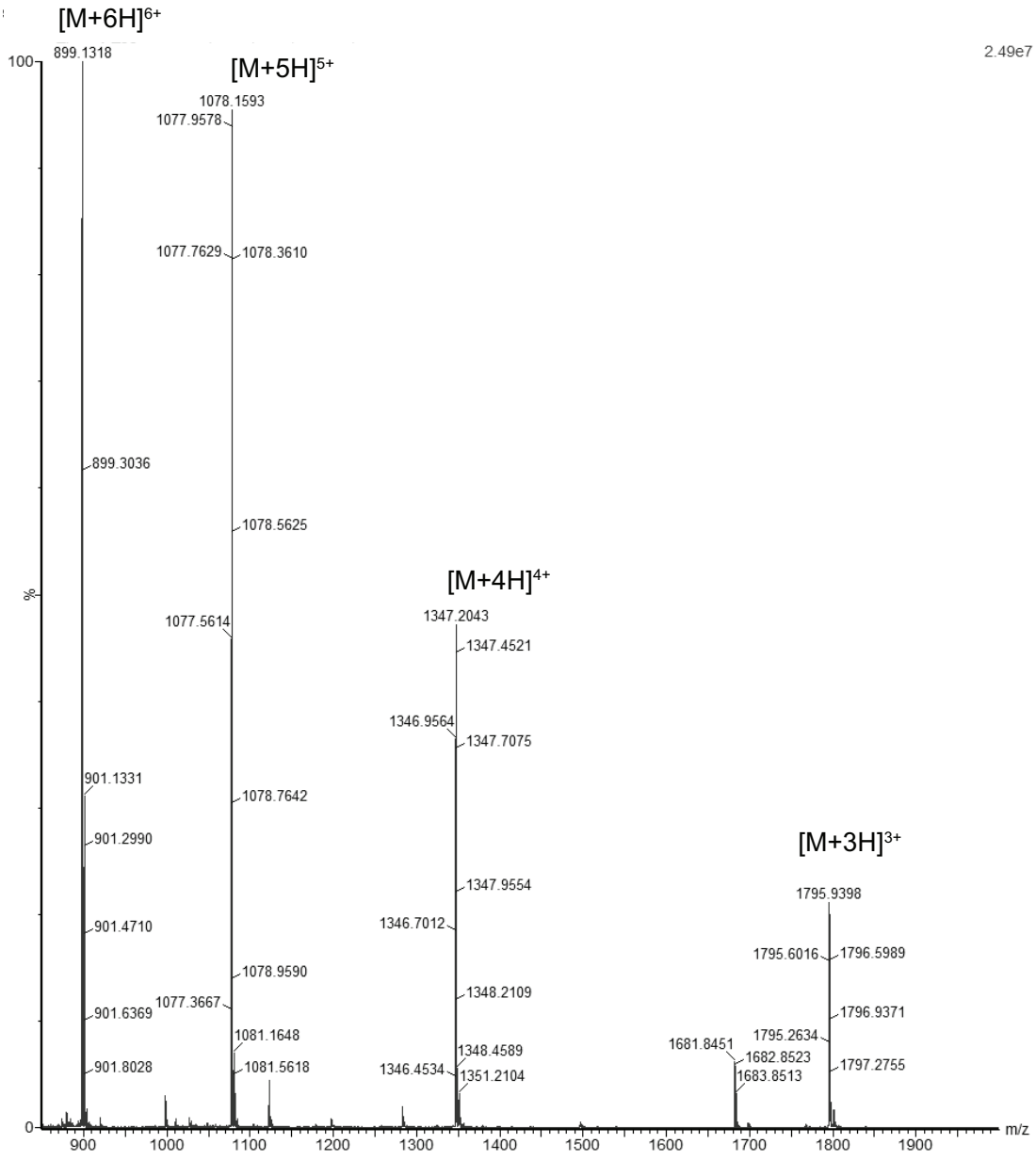

Expansion mass spectrum of trimer KLT

Calculated $[M+H]^+$ of trimer KLT: 5382.83

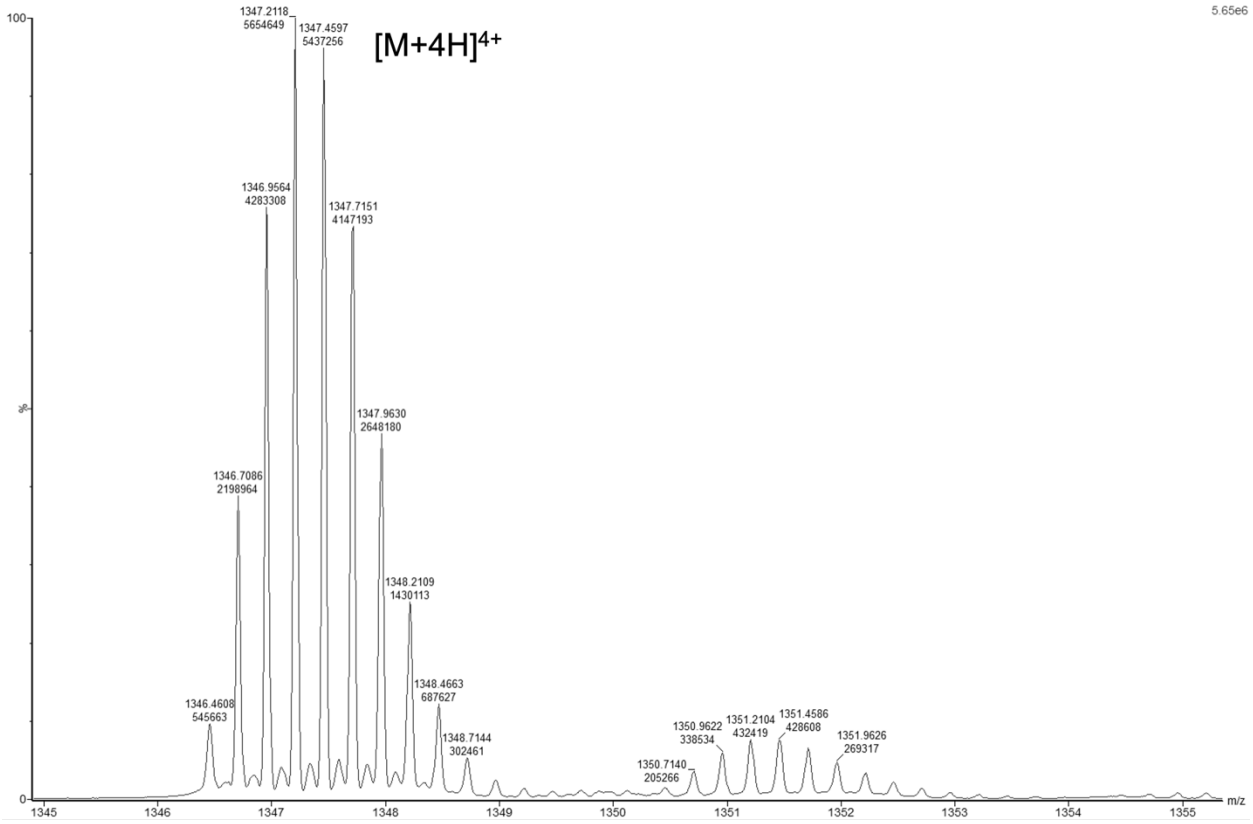

Deconvoluted mass spectrum of trimer KLT

Exact mass of trimer KLT: 5381.82

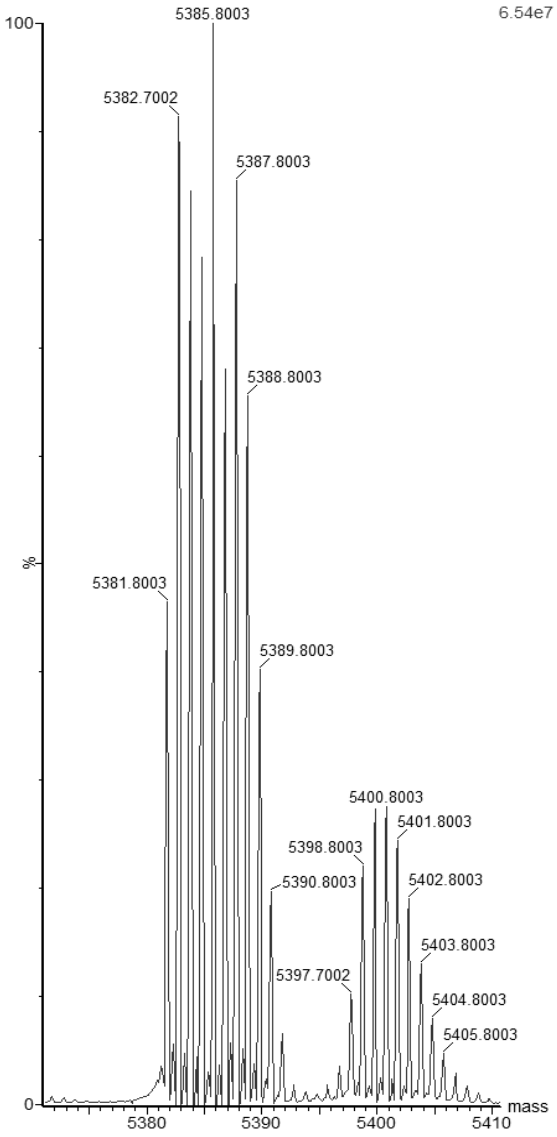

Characterization of peptide QKM_{CC}

Analytical HPLC trace

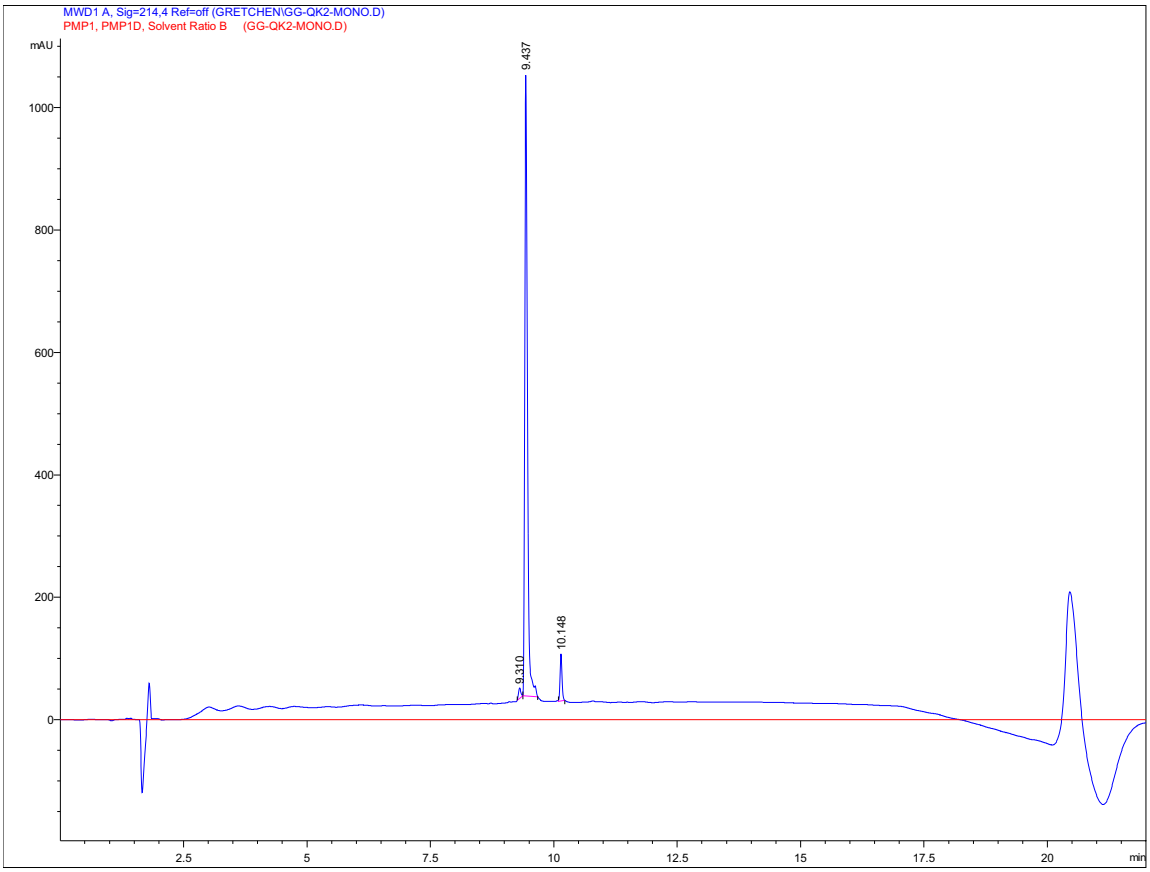

Signal 1: MWD1 A, Sig=214,4 Ref=off

Peak #	RetTime [min]	Type	Width [min]	Area [mAU*s]	Height [mAU]	Area %
1	9.310	MM	0.0541	55.99329	17.23619	1.3227
2	9.437	MM	0.0648	3954.08936	1017.77539	93.4078
3	10.148	MM	0.0478	223.06216	77.70994	5.2694

Mass spectrum of peptide QKM_{CC}

Calculated $[M+H]^+$ of peptide QKM_{CC}: 1688.01

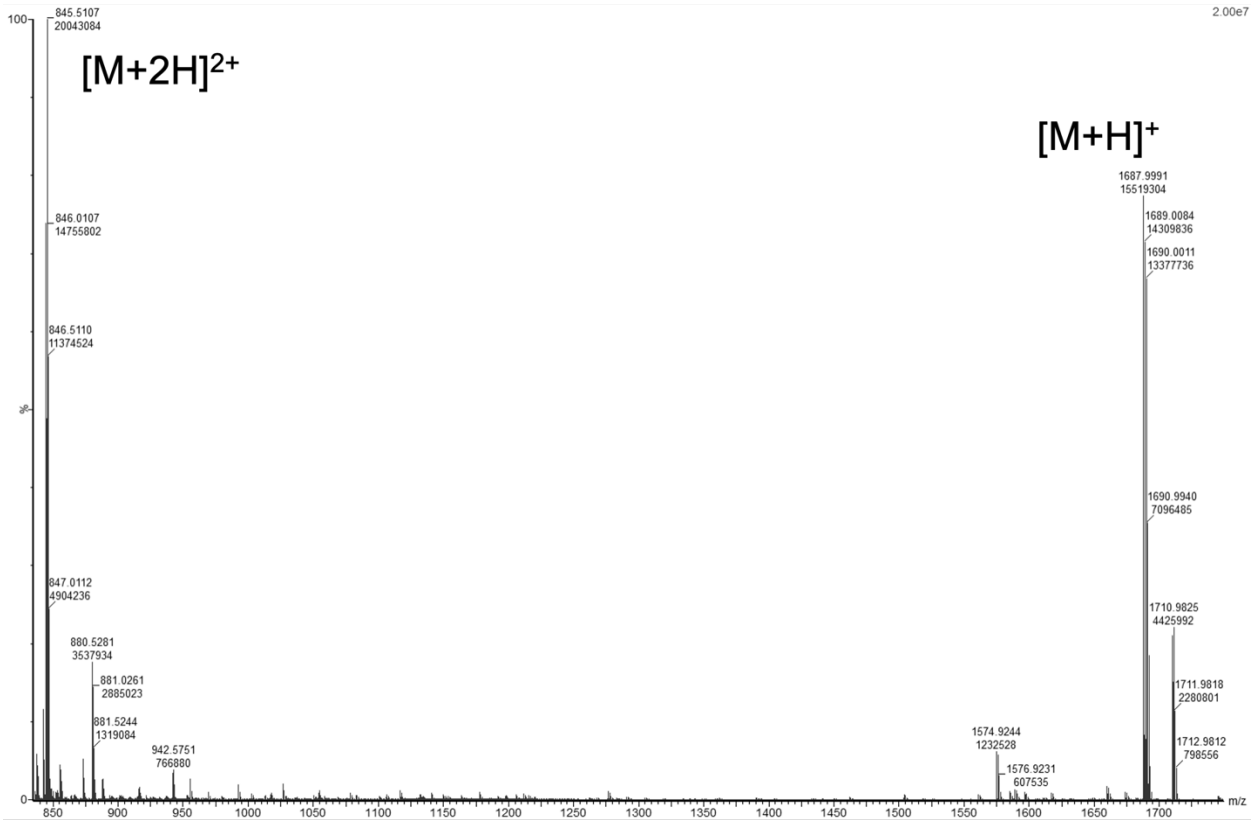

Mass spectrum of peptide QKM_{CC}

Calculated $[M+H]^+$ of peptide QKM_{CC}: 1688.01

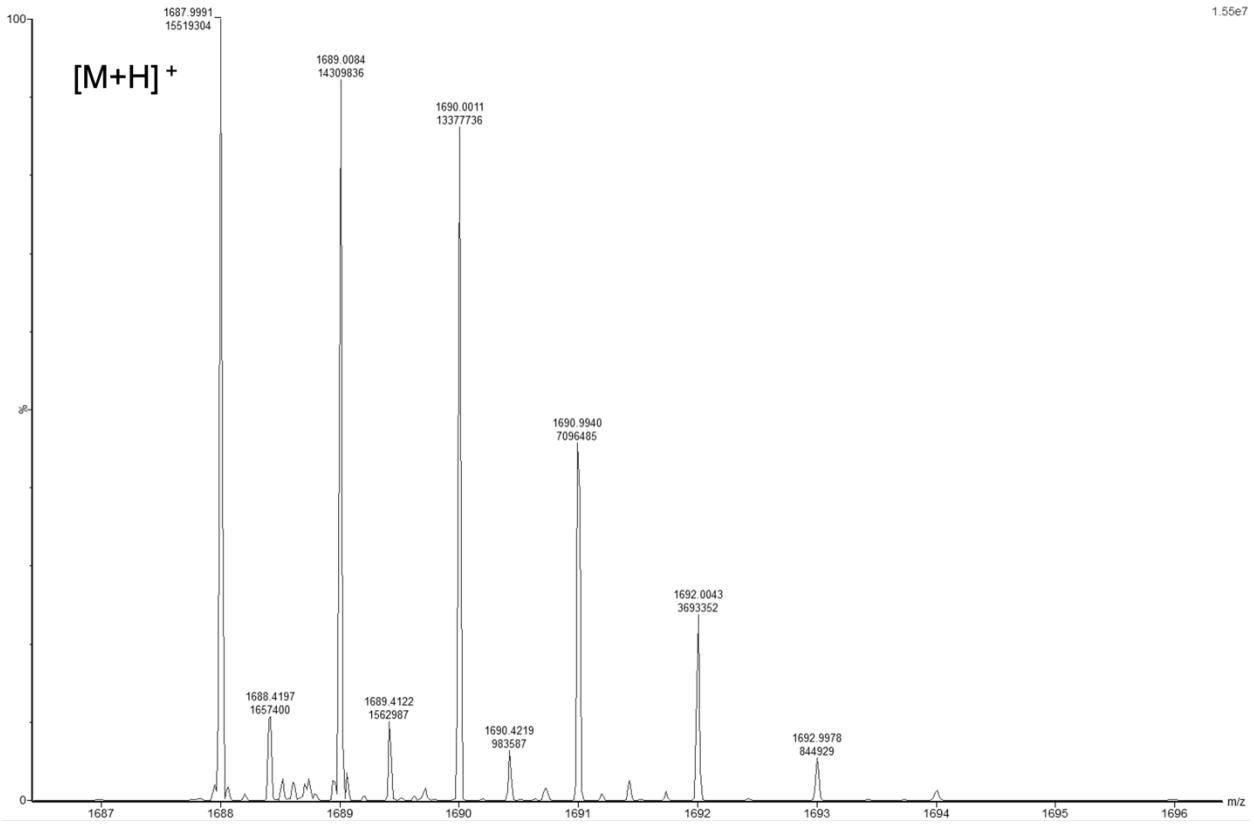

Characterization of trimer QKT

Analytical HPLC trace

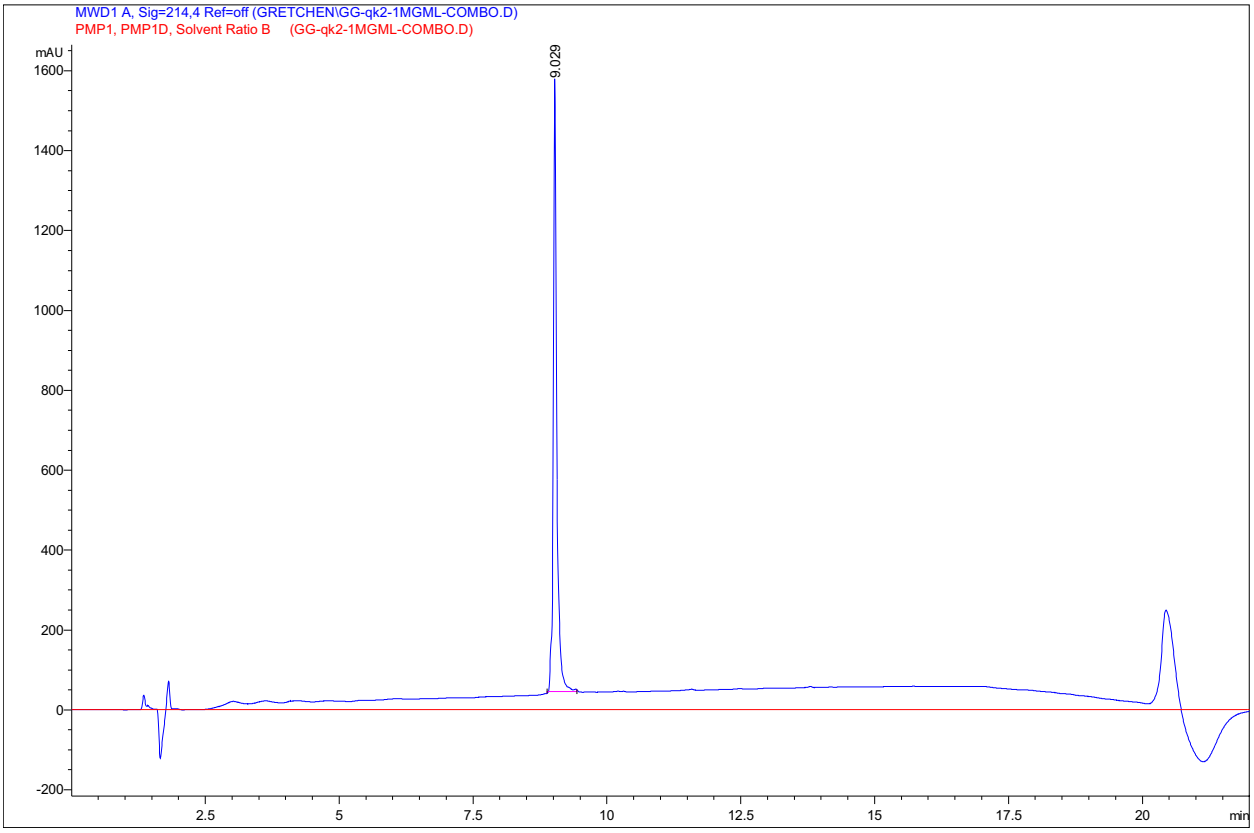

Mass spectrum of trimer QKT

Calculated $[M+H]^+$ of trimer QKT: 5055.97

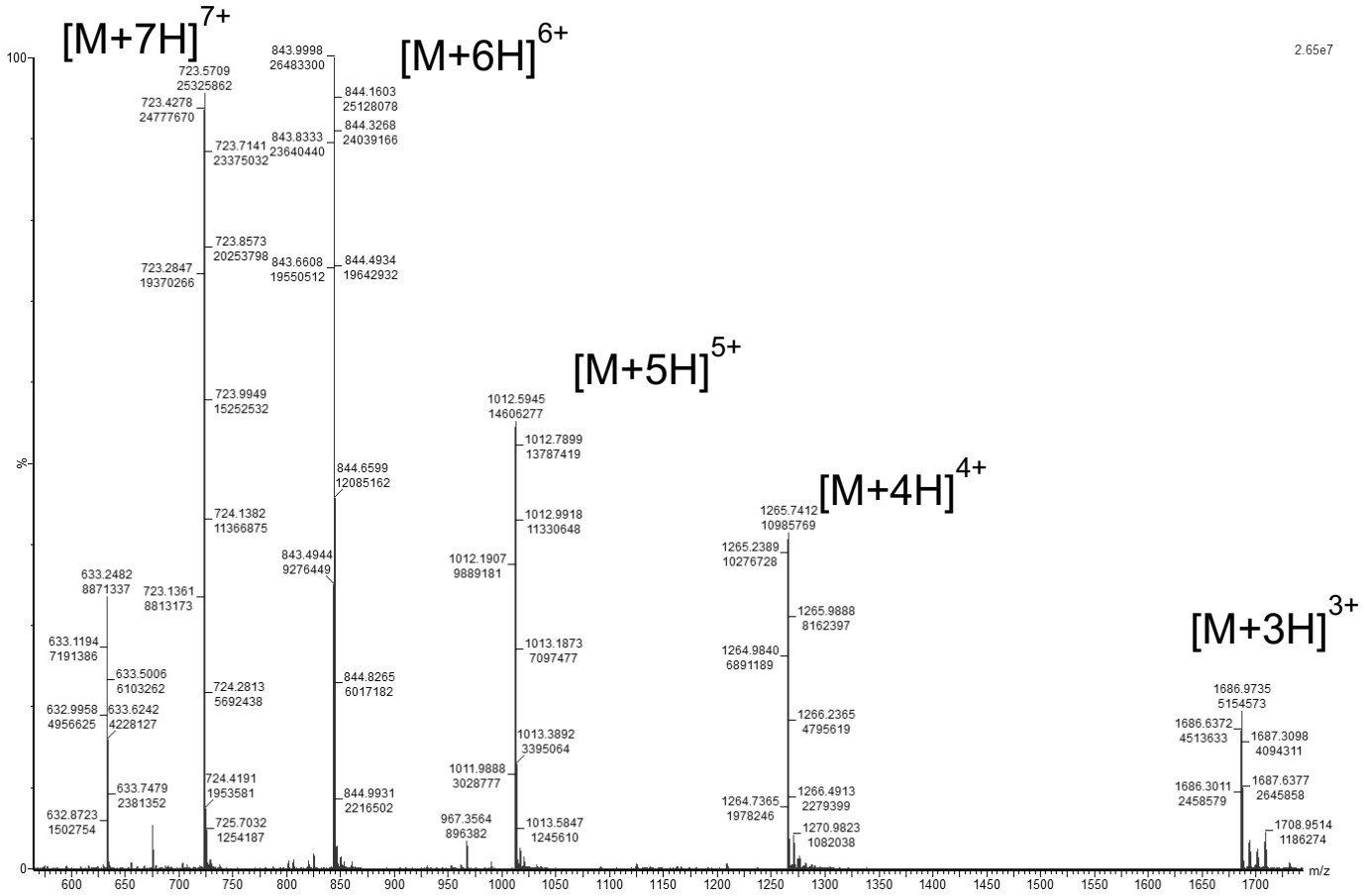

Expansion mass spectrum of trimer QKT

Calculated $[M+H]^+$ of trimer QKT: 5055.97

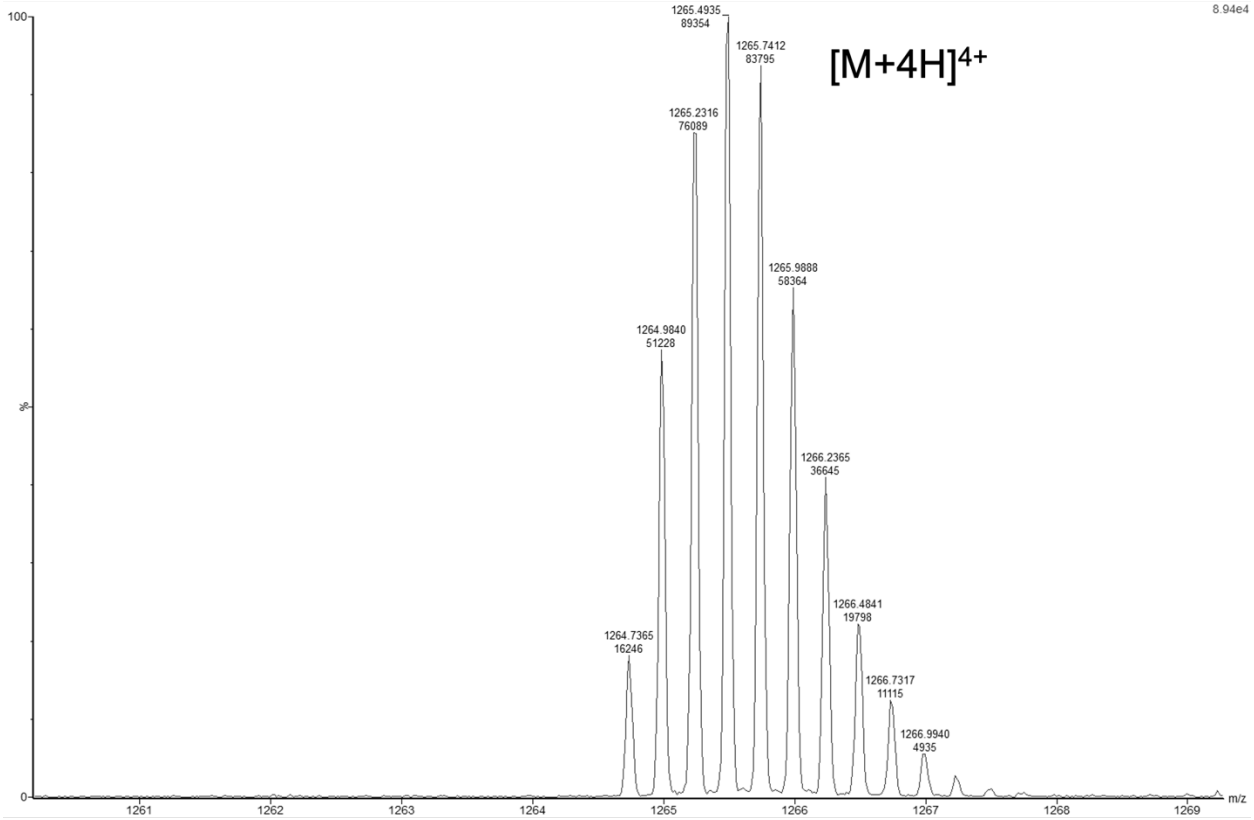

Deconvolution mass spectrum of trimer QKT

Exact mass of trimer QKT: 5054.97

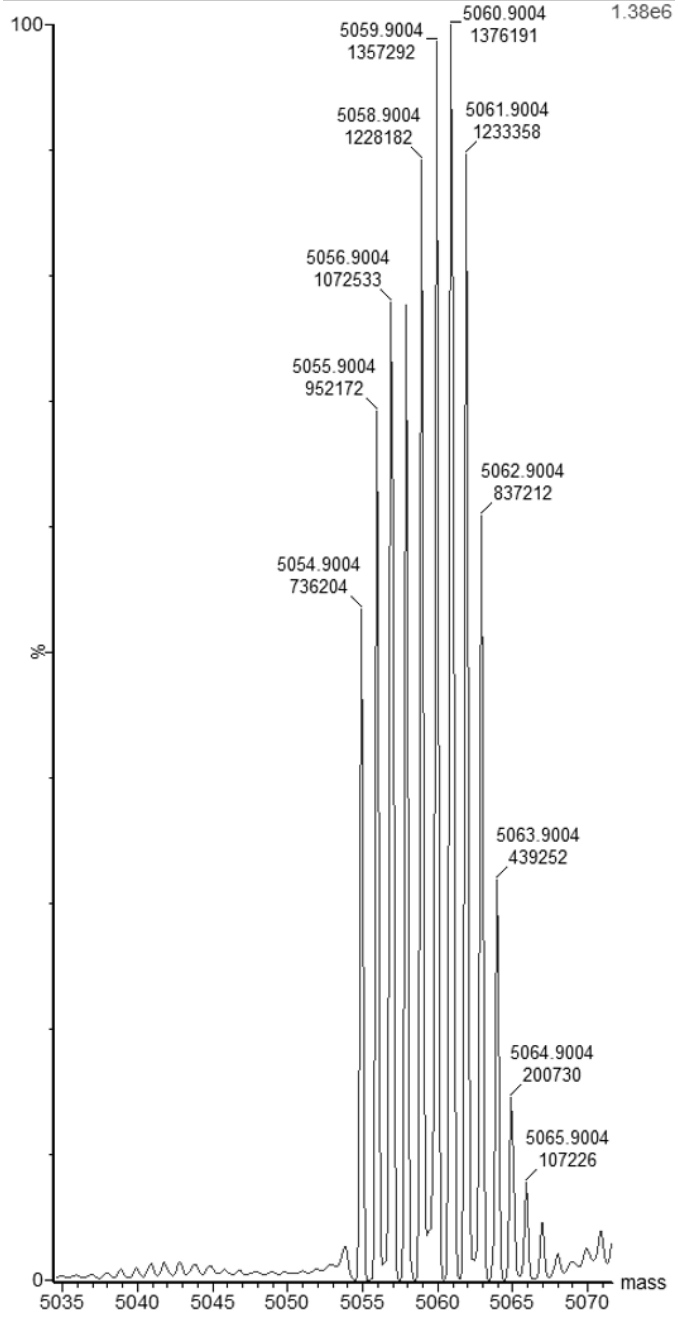

Chapter 5

Knowledge Acquired From My Experience As The Mass Spectrometry Fellow at UCI

INTRODUCTION

Early in graduate school I discovered my passion in mass spectrometry and gathered experience serving as the chemistry department Mass Spectrometry Fellow. Under the guidance of Director Dr. Felix Grün and protein specialist Benjamin Katz, I learned to troubleshoot and maintain all of the instruments in the UCI Mass Spectrometry Core Facility. I also had the opportunity to consult with other UCI scientists and advise them on the best sample preparation methods and instrument applications to progress their research. Through these experiences, I learned that mass spectrometry has applications far beyond simple mass determination and I began to apply these techniques in my own research projects. I have distilled the knowledge gathered through literature and experience into a simple guide which outlines the types of mass spectrometry instruments available in the UCI Mass Spectrometry Core Facility, sample preparation requirements and instrument compatibility, and data analysis resources.

5.1 General Principles and Instruments of Mass Spectrometry

All mass spectrometry follows the same general principle to transfer molecules to the gas phase with minimal disruption and acquire a charge to be analyzed using the mass-to-charge

ratio (*m/z*). While numerous separation, ionization, and mass analysis techniques exist, this section focuses only on those available in the UCI Mass Spectrometry Core Facility.

5.1.1 In-line separation techniques.

The instruments in UCI Mass Spectrometry Core Facility offer a variety of in-line separation techniques to analyze complex samples. A common form of in-line separation is reverse-phase liquid chromatography (LC).[1,2] This separation occurs prior to ionization and typically runs a combination of water and acetonitrile to elute sample off of a non-polar column in order of least hydrophobic to most hydrophobic. Another type of in-line liquid chromatography, known as size exclusion chromatography (SEC), allows large proteins and complexes to stay intact while separating components by size.[3] By SEC, larger molecules or complexes elute first followed by smaller molecules or smaller complexes. In-line SEC must be paired with a mass spectrometry-compatible solvent, which is most frequently ammonium acetate electrolyte solution.[4] When these chromatographic methods are paired with mass spectrometry, the instrument is known as an LC-MS.

Two types of gas-phase separation are available in the UCI Mass Spectrometry Core Facility. Gas chromatography (GC) separates vaporized molecules in a sample in the gas phase prior to ionization. This technique uses a carrier gas to separate molecules in the gas phase by polarity as they move through a separation column.[5] This technique is frequently applied to non-polar compounds that are not soluble in aqueous solutions. The second gas-separation technique is ion mobility spectrometry (IMS). IMS is a method of separation that occurs after molecules have been ionized. Ions travel through a mobility cell with buffer gas and an applied electric field separating ions by size and shape. The type of IMS in the UCI Mass Spectrometry Core

Facility is known as traveling wave ion mobility (TWIMS). TWIMS separates ions in an ion mobility cell by applying an oscillating electric field as ions move through a drift gas.[7] The oscillating electric field and collisions with the drift gas lead to smaller, more compact compounds traveling through the ion mobility cell quicker than larger, less compact compounds. Developments to IMS in recent years have paired this technique with mass spectrometry to analyze molecules by size, shape and charge.[6]

5.1.2 Methods of ionization.

Ionization is necessary to add charge to molecules for analysis of *m/z*. One of the most common methods of ionization is electrospray ionization (ESI).[8,9] ESI is a gentle form where liquid sample is sprayed through a charged capillary. ESI is used on seven instruments available in the UCI Mass Spectrometry Core Facility (Waters Xevo XS, Waters LCT #1 and #2, Waters ACQUITY QDa #1 and #2, Waters Quattro Premier XE, and Waters Synapt G2 HDMS #2). Recently, nano-electrospray ionization (nano-ESI) was developed as a variation of ESI to study non-covalent complexes. Nano-ESI uses a low flow emitter and applied voltage to ionize and transfer complexes into the gas phase with minimal disruption to the complexes.[10,11] Nano-ESI is available on one instrument in the UCI Mass Spectrometry Core Facility (Waters Synapt G2 HDMS #1).

Matrix-assisted laser desorption ionization (MALDI) is a technique where the sample is embedded in a matrix that desorbs UV light to ionize the molecules of interest.[12,13] Many sample types can be ionized by MALDI but specifically the development of MALDI has made analysis of tissue samples much more accessible.[14] This form of ionization is used on two instruments

available in the UCI Mass Spectrometry Core Facility (AB Sciex MALDI-TOF/TOF 8500 and Bruker ultrafleXtreme MALDI-TOF/TOF).

Electron impact (EI) and chemical ionization (CI) are some of the earliest developed ionization techniques that are still used in the core facility today. Both EI and CI require the sample to be in the gas phase before ionization can occur. EI is a form of hard ionization in which molecules are ionized through collisions with electrons.[15] In CI, a reagent gas is ionized through EI before interacting with the molecules of interest to form ions.[16] This ionization used on three instruments available in the UCI Mass Spectrometry Core Facility (Waters GCT, Thermo ISQ, and Thermo ISQ QD).

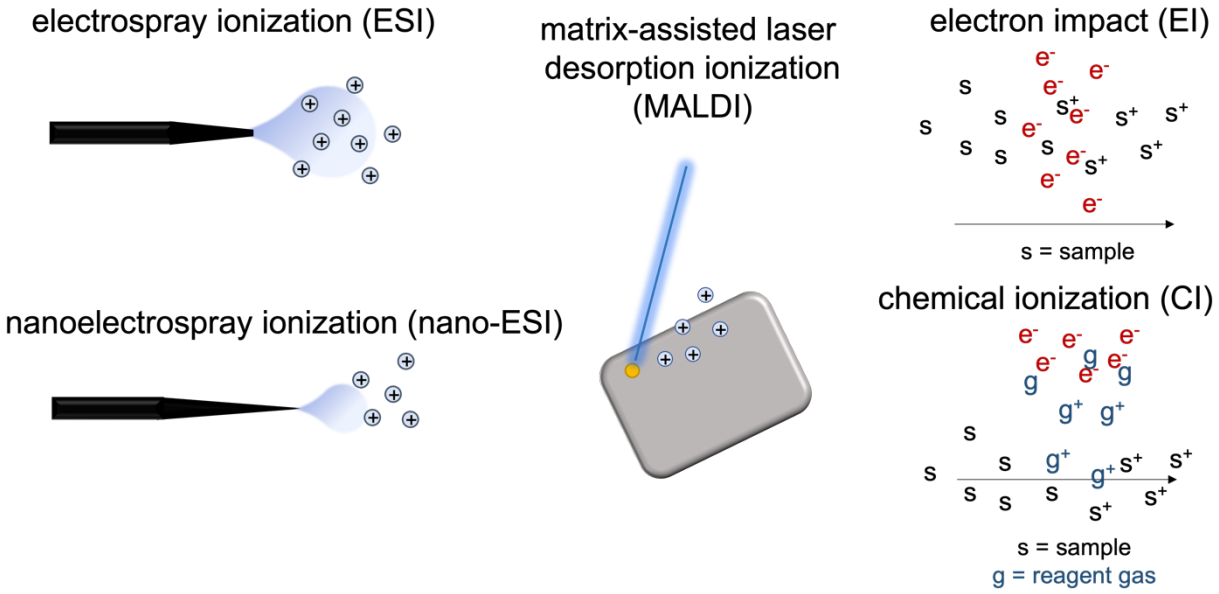

Figure 5.1. Schematic detailing ESI, nano-ESI, MALDI, EI, and CI types of ionization.

5.1.3 Types of mass analyzers.

There are four types of mass analyzers used frequently in the UCI Mass Spectrometry Core Facility. The appropriate mass analyzer is selected based on the size and resolution requirements of the sample.

Time-of-flight (TOF) mass analyzers push ions through a drift region using an applied electric field, separating them by mass-to-charge (*m/z*). In the earliest TOF instruments, this drift region was linear. The development of reflectron TOF, in which ions are reflected back down the drift region, has made significant progress in high mass resolution.[17] TOF analyzers are regularly paired with MALDI or ESI and are advantageous for their high sensitivity and wide mass range.[18]

A quadrupole (Q) mass analyzer is uses four parallel rods with oscillating electric fields to focus ions of interest while ejecting other ions. A single Q mass analyzer can be used on its own to analyze moderately sized molecules and is advantageous for its simple operation.[19] Q analyzers can also be used to apply high energy to traveling ions to cause collision-induced dissociation resulting in fragmentation of the molecule.[20,21] These fragments can provide valuable information about the parent ion. For this reason, the quadrupole is often paired with other mass analyzers to be used for fragmentation.

One of these instruments combines three in-line quadrupoles, known as a triple quadrupole (QqQ), where the second quadrupole is used as a collision cell to fragment ions.[22] QqQ instruments are best for the quantification and analysis of metabolites and biological samples where analyte concentration may be low. A Q mass analyzer can also be combined with a TOF analyzer (QTOF). This combination pairs fragmentation capability with the wide mass range and resolution of the TOF, making it a great tool for top-down proteomics.[23]

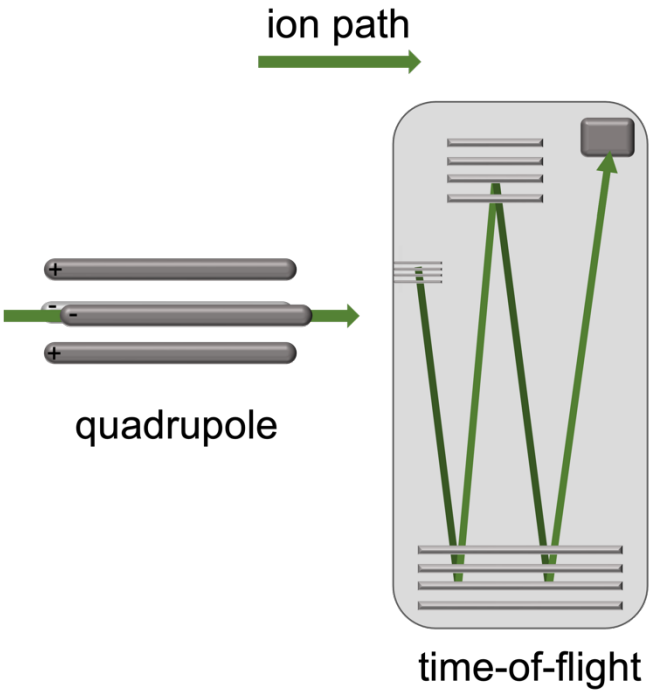

Figure 5.2. Schematic detailing ion path through Q and TOF mass analyzers.

5.2 Biomolecule Sample Preparations

There are a variety of instruments available for the analysis of biomolecules. Sample preparation and instrument selection are critical to optimizing investigation of the molecule or system.

5.2.1 Small molecules

The sample preparation and instrument selection for small molecules depends mainly on two factors: the sample solubility in selected solvents and heteroatoms present in the molecule. Typically, less hydrophobic molecules will be soluble in water, methanol, or acetonitrile and will contain more heteroatoms. Solutions of approximately 0.1 mg/mL in these solvents can be run on

the Waters LCT or Waters ACQUITY QDa LC-MS instruments. Molecules containing carboxylic acids or multiple alcohols may produce negatively charged ions by either the loss of a proton or the addition of a chloride and therefore would be best run in ESI^- mode. Otherwise, samples will likely ionize through the addition of a proton or sodium ion and would be run best in ESI^+ mode.

Molecules containing hydrocarbons with few heteroatoms are typically hydrophobic and will ionize best through EI or CI. These samples are prepared at 0.1 mg/mL in dichloromethane and run on the Waters GCT, the Thermo ISQ, or the Thermo ISQ QD GC-MS instruments.

5.2.2 RNA and DNA Oligos

Oligos can be difficult to ionize and are typically run on the Waters Xevo XS. If chromatographic separation is not desired, oligos can be prepared in water and ionized directly by ESI. If chromatography is desired, we have found that the preparation of oligos in water ionize well when separated by SEC in ammonium acetate and sprayed by ESI at a high desolvation temperature. Oligos can also be separated by reverse-phase liquid chromatography. This separation and ionization are most successful when hexafluoroisopropanol or triethylammonium acetate are added to the mobile phase solvents. While these additions help the oligos pick up charge, they can be damaging to the mass spectrometer, and a thorough cleaning of the instrument is recommended if following this protocol.

5.2.3 Peptides, Proteins, and Antibodies

Peptides, proteins, and antibodies can be run on many instruments within the facility. If chromatographic separation is not desired, MALDI-TOF instruments can be used. The correct

matrix must be selected for the sample. Typically, sinapic acid (SA) or α-cyano-4-hydroxycinnamic acid (CHCA) are used for the investigation of proteins and dihydrobenzoic acid (DHB) can be used for peptides. It is important to note that DHB can cleave disulfide bonds so it should only be used to investigate peptides that do not contain disulfide bonds. To prepare the sample, 0.5 μL of the selected matrix is spotted to the MALDI plate followed by 0.5 μL of sample. If the sample is not ionizing well, this procedure can be repeated, layering matrix and sample for better results.

If chromatographic separation is desired, 0.1 mg/mL solution of peptide or protein can be prepared in an aqueous or acetonitrile solution and run on an LC-MS instrument. Due to their size, proteins are typically run on the Waters Xevo XS (QTOF) as it has a wider mass range that can accommodate large proteins. Intact antibodies can be run similar to large proteins.

For further analysis of proteins and antibodies, the samples can be fragmented or chemically digested. Antibodies can often be highly glycosylated and treatment with PNGase enzymes can remove these modifications. Reduction of disulfide bonds with dithiothreitol (DTT) or tris(2-carboxyethyl)phosphine (TCEP) (performed at low pH) will yield sample with free thiol residues. In the case of an antibody, this will reduce the bonds holding together the light and heavy chains. The thiols can then be capped using an alkylating agent like iodoacetamide (IAA) to prevent the re-oxidation of disulfide bonds. Reduced and capped samples can be chemically digested or fragmented. Common enzymes used for digestion are trypsin and pepsin (performed at low pH). Formic acid or hydrochloric acid can also be used to chemically digest amide bonds. Samples are then diluted and subjected to LC-MS. On the Waters Xevo XS (QTOF) fragmentation within the mass spectrometer can be used in addition to or in replace of chemical digestion.

5.2.4 Tissue Samples

The investigation of molecules within tissue is quickly becoming a common mass spectrometry technique known as mass spectrometry imaging. Fresh frozen tissue is prepared by slicing 5 μm thick tissue sections on a cryostat. It is important when mounting or embedding tissue to use a mass spectrometry-compatible mounting medium. Many mounting mediums contain PEG, which will suppress ions and lead to extra signals in the mass spectrum. Mixtures of gelatin and sucrose are best for embedding. The sliced tissue sections are then mounted on indium tin oxide coated glass slides and placed in a desiccator before being stored at -80 °C. The duration of tissue storage has been shown to negatively affect signal, so minimal storage time is recommended. Different wash steps can be applied to the tissue to remove biomolecules that are not of interest and improve the observation of molecules that are of interest. For example, lipids can be removed by submerging tissue in hexanes or xylenes. Wash steps with a series of increasing aqueous ethanol concentrations (70%, 90%, 95%, 100%) can help remove salts and fix tissue. To maintain lipids in tissue, use water or aqueous buffers.

Matrix must be applied to the tissue for successful desorption and ionization. The matrix application can be done through sublimation or nebulization. Without an automated spraying system, we found that nebulization can lead to uneven distribution of matrix coating on the tissue and preferred to use sublimation for a more even coating. Sublimation protocols outline the best matrix selection and temperature required for sublimation as well as apparatus set up.[24] Sinapic acid (SA) or dihydroxyacetophenone (DHA) are good matrices for proteins and α-cyano-4-hydroxycinnamic acid (CHCA) works well for peptides. Once the matrix is applied, recrystallization of the matrix on the tissue has been shown to enhance signal. If recrystallization is done improperly, however, it can lead to poor spatial resolution in analysis.

After the tissue is prepared and matrix-coated, it is ready for imaging. A digital image of the tissue is obtained to overlay in data processing with the mass spectra. We have found that a digital scanner works well for this application. Once in the instrument, laser intensity must be optimized to avoid damaging the tissue. Once laser intensity is selected, most imaging can be automated to acquire sections of the tissue.

5.3 Analysis Tools

This section contains a list of mass spectrometry databases and tools, the majority of which are open access. This selection of tools can be used to search databases to assign observed species, predict fragments and b and y ions of proteins, predict isotope patterns of molecules, and assign observed oligomer species.

- MassBank of North America (MoNA) is a large database from which you can search LC-MS data to match species.
- METLIN is a MS/MS database for the identification of metabolites.
- Mascot is search engine used to identify proteins.
- Protein Prospector is a search tool designed to search multiple databanks to identify proteins.
- Human Metabolome Database (HMDB) allows a search by MS or MS/MS data of small molecules and metabolites.
- To search protein fragments, the National Center for Biotechnology Information (NCBI) hosts the program blastp.
- Global Natural Product Social Molecular Networking (GNPS) is a database to search natural products with GC-MS data.

Tools for analyzing protein fragmentation data include the following:

- PeptideCutter can be used to predict cleavage sites and fragments of a given protein sequence.
- PROTEOMICS TOOLKIT can predict b and y ions from input peptide fragments.
- BioharmaLynx (licensed through Waters) can evaluate fragmentation data and match b and y ions.
- Expasy Peptide Mass, mMass, envipat, and masslynx can model isotope patterns from given molecular formulas.
- UniDec, mMass, and Masslynx (licensed through Waters) can be used for analyzing data.
- UniDec has specific features helpful in the analysis of oligomers and nanodiscs.

CONCLUSIONS

In my time working in the UCI Mass Spectrometry Core Facility, I accumulated information about a variety of mass spectrometry instruments and techniques for the most successful analysis. I have assembled these learnings in this beginner's guide to mass spectrometry. As I progress in my career while working in an industry-sponsored mass spectrometry core facility, the knowledge gathered from my experience at UCI will provide a firm foundation and I am thankful to Dr. Felix Grün and Benjamin Katz for the mentorship and experience.

REFERENCES AND NOTES

(1) Bird, I. M. High Performance Liquid Chromatography: Principles and Clinical Applications. *Br. Med. J.* **1989**, *299* (6702), 783–787. https://doi.org/10.1136/bmj.299.6702.783.

(2) Bupp, C. R.; Wirth, M. J. Making Sharper Peaks for Reverse-Phase Liquid Chromatography of Proteins. *Annu. Rev. Anal. Chem.* **2020**, *13*, 363–380. https://doi.org/10.1146/annurev-anchem-061318-115009.

(3) Fekete, S.; Beck, A.; Veuthey, J. L.; Guillarme, D. Theory and Practice of Size Exclusion Chromatography for the Analysis of Protein Aggregates. *J. Pharm. Biomed. Anal.* **2014**, *101*, 161–173. https://doi.org/10.1016/j.jpba.2014.04.011.

(4) Štulík, K.; Pacáková, V.; Tichá, M. Some Potentialities and Drawbacks of Contemporary Size-Exclusion Chromatography. *J. Biochem. Biophys. Methods* **2003**, *56*, 1–13. https://doi.org/10.1016/S0165-022X(03)00053-8.

(5) Bartle, K. D.; Myers, P. History of Gas Chromatography. *Trends Anal. Chem.* **2002**, *21*, 547–557. https://doi.org/10.1038/1661000b0.

(6) Kanu, A. B.; Dwivedi, P.; Tam, M.; Matz, L.; Hill, H. H. Ion Mobility-Mass Spectrometry. *J. Mass Spectrom.* **2008**, *43* (1), 1–22. https://doi.org/10.1002/jms.1383.

(7) Dodds, J. N.; Baker, E. S. Ion Mobility Spectrometry: Fundamental Concepts, Instrumentation, Applications, and the Road Ahead. *J. Am. Soc. Mass Spectrom.* **2019**, *30* (11), 2185–2195. https://doi.org/10.1007/s13361-019-02288-2.

(8) Wilm, M. Principles of Electrospray Ionization. *Mol. Cell. Proteomics* **2011**, *10* (7), M111.009407. https://doi.org/10.1074/mcp.M111.009407.

(9) Fenn, J. B.; Mann, M.; Meng, C. K.; Wong, S. F. Electrospray Ionization-Principles and

Practice. **1990**, 37–70.

(10) Karas, M.; Bahr, U.; Dülcks, T. Nano-Electrospray Ionization Mass Spectrometry: Addressing Analytical Problems beyond Routine. *Fresenius. J. Anal. Chem.* **2000**, *366* (6–7), 669–676. https://doi.org/10.1007/s002160051561.

(11) Gibson, G. T. T.; Mugo, S. M.; Oleschuk, R. D. Nanoelectrospray Emitters: Trends and Perspective. *Mass Spectrom. Rev.* **2009**, *28* (6), 918–936. https://doi.org/10.1002/mas.20248.

(12) Jurinke, C.; Oeth, P.; Van Den Boom, D. MALDI-TOF Mass Spectrometry: A Versatile Tool for High-Performance DNA Analysis. *Appl. Biochem. Biotechnol. - Part B Mol. Biotechnol.* **2004**, *26* (2), 147–163. https://doi.org/10.1385/MB:26:2:147.

(13) Hosseini, S.; Martinez-Chapa, S. O. *Fundamentals of Tissue Engineering and Application of MALDI-ToF-MS in Analysis of the Scaffold Materials*; **2017**. https://doi.org/10.1007/978-981-10-2356-9_3.

(14) Francese, S.; Dani, F.; Traldi, P.; Mastrobuoni, G.; Pieraccini, G.; Moneti, G. MALDI Mass Spectrometry Imaging, from Its Origins up to Today: The State of the Art. *Comb. Chem. High Throughput Screen.* **2009**, *12* (2), 156–174. https://doi.org/10.2174/138620709787315454.

(15) Medhe, S. Ionization Techniques in Mass Spectrometry: A Review. *Mass Spectrom. Purif. Tech.* **2018**, *4* (1), 1–6. https://doi.org/10.4172/2469-9861.1000126.

(16) Richter, W. J.; Schwarz, H. Chemical Ionization-A Mass-Spectrometric Analytical Procedure of Rapidly Increasing Importance. *Angew. Chem. Ed. Engl.* **1978**, *17*, 424–439.

(17) Boesl, U. Time-of-Flight Mass Spectrometry: Introduction to the Basics. *Mass Spectrom. Rev.* **2017**, *36* (1), 86–109. https://doi.org/10.1002/mas.21520.

(18) Cotter, R. J. Time-of-flight Mass Spectrometry: An Increasing Role in the Life Sciences. *Biomed. Environ. Mass Spectrom.* **1989**, *18* (8), 513–532. https://doi.org/10.1002/bms.1200180803.

(19) Parasuraman, S.; Rao, A.; Balamurugan, S.; Muralidharan, S.; Jayaraj Kumar, K.; Vijayan, V. An Overview of Liquid Chromatography-Mass Spectroscopy Instrumentation. *Pharm. Methods* **2014**, *5* (2), 47–55. https://doi.org/10.5530/phm.2014.2.2.

(20) Douglas, D. J. Linear Quadrupoles in Mass Spectrometry. *Mass Spectrom. Rev.* **2009**, *28* (6), 937–960. https://doi.org/10.1002/mas.20249.

(21) Mitchell Wells, J.; McLuckey, S. A. Collision-Induced Dissociation (CID) of Peptides and Proteins. *Methods Enzymol.* **2005**, *402* (1993), 148–185. https://doi.org/10.1016/S0076-6879(05)02005-7.

(22) Hager, J. W. Recent Trends in Mass Spectrometer Development. *Anal. Bioanal. Chem.* **2004**, *378* (4), 845–850. https://doi.org/10.1007/s00216-003-2287-1.

(23) Allen, D. R.; McWhinney, B. C. Quadrupole Time-of-Flight Mass Spectrometry: A Paradigm Shift in Toxicology Screening Applications. *Clin. Biochem. Rev.* **2019**, *40* (3), 135–146. https://doi.org/10.33176/AACB-19-00023.

(24) Protocols available through National Research Resource Institute for Imaging Mass Spectrometry at Vanderbilt. https://medschool.vanderbilt.edu/ims/protocols/

Epilogue

Selected Collaborations from UCI

INTRODUCTION

In my time at UCI, I have had the opportunity to work closely with instructors and colleagues in contribution to many projects. Herein, I share the summaries of five collaborations that have shaped me both as a scientist and as a teammate. The time spent working with others taught me many valuable lessons. I learned effective communication which was critical to the completion of these projects. Verbal and written communication clearly outlining the goals of the experiment, the limitations of each technique, and the expected outcomes of the experiment were necessary to effectively execute the project. I also learned to listen to the ideas of teammates and facilitate productive discourse to design the best experiments for project success. These management skills I learned from collaborative projects will serve me in my future endeavors.

Expression of *N*-Terminal Cysteine Aβ42 and Conjugation to Generate Fluorescent and Biotinylated Aβ42[1]

In this project, Dr. Sheng Zhang designed and synthesized fluorescent derivatives of Aβ42 for the purpose of studying the interactions of Aβ42 with cells. He effectively expressed and purified Aβ42 with an *N*-terminal cysteine residue to use in conjugation chemistry. Dr. Zhang then appended FAM and TAMRA fluorophores to Aβ42 through thiol−maleimide labeling. Using the expertise I had developed in fluorescence microscopy and with Dr. Zhang's FAM-Aβ42 and TAMRA-Aβ42 in hand, I investigated the cellular interactions of the labeled peptides. Aβ42 is known to play a role in neurodegeneration and can cause toxicity to neurons as well as be cleared by macrophages in the brain. Knowing these interactions of Aβ42 in the brain, I studied both SH-SY5Y human neuroblastoma cells and RAW 264.7 macrophages in the presence of the fluorescent derivatives. We observed the uptake of Aβ42 in both cell types. The intracellular puncta in SH-SY5Y cells are smaller, possibly indicating uptake by endocytosis. The intracellular Aβ42 observed in macrophages are much larger, which is consistent with a phagocytosis mechanism. Through these studies, I was able to work with Aβ42, the peptide by which many of my projects were derived, as well as the experience of working with macrophages for the first time.

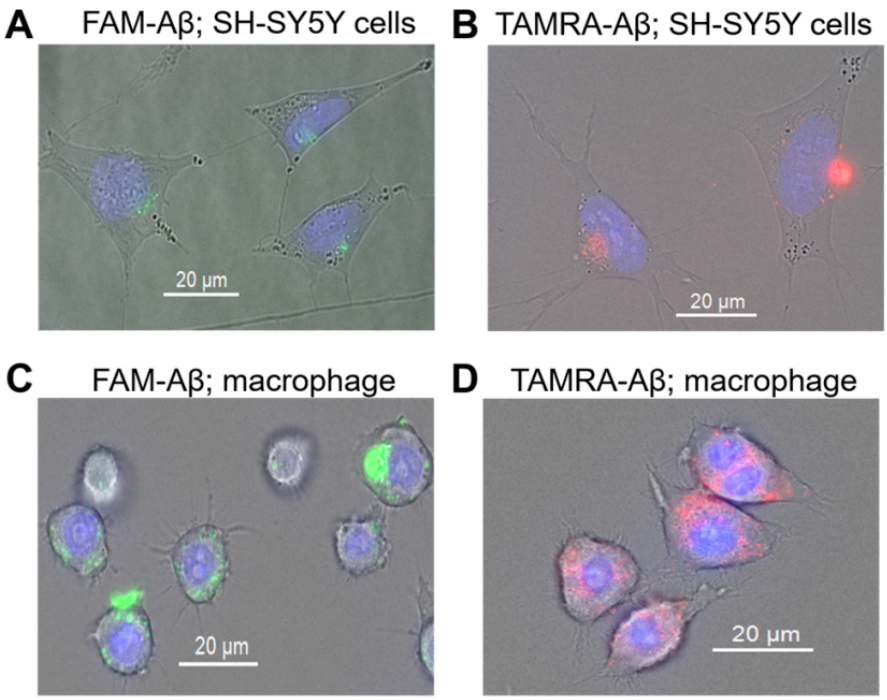

Figure 6.1 Fluorescence micrographs of labeled Aβ with mammalian cells and bacteria. **(A,B)** SH-SY5Y cells treated with 10 μM FAM- or 10 μM TAMRA-labeled Aβ for 3 h. **(C,D)** RAW 264.7 macrophage cells treated with 10 μM FAM- or 10 μM TAMRA-labeled Aβ for 4 h. Hoechst 33342 (blue) was used to stain the nuclei.

Macrocyclic Peptides Derived from Familial Alzheimer's Disease Mutants Show Charge-Dependent Oligomeric Assembly and Toxicity[2]

In this project, I worked closely with Dr. William Howitz to study the role of charge on peptide assembly. Dr. Howitz and coworkers designed and synthesized a wide range of peptides derived from known familial mutations of Aβ that affect the progression and severity of Alzheimer's disease. The oligomerization of the peptides was studied by SDS-PAGE and the membrane interactions were studied by cellular cytotoxicity and dye leakage of liposomes.

From Dr. Howitz I learned an important new technique to study membrane destabilization. The preparation of dye-filled large unilamellar vesicles (LUVs) was used to study the effect of charged peptides derived from Aβ to create pores within membrane mimetics. Dr. Howitz was also a great mentor who taught me the importance of delegation of tasks and team management to coordinate a large group towards a common goal.

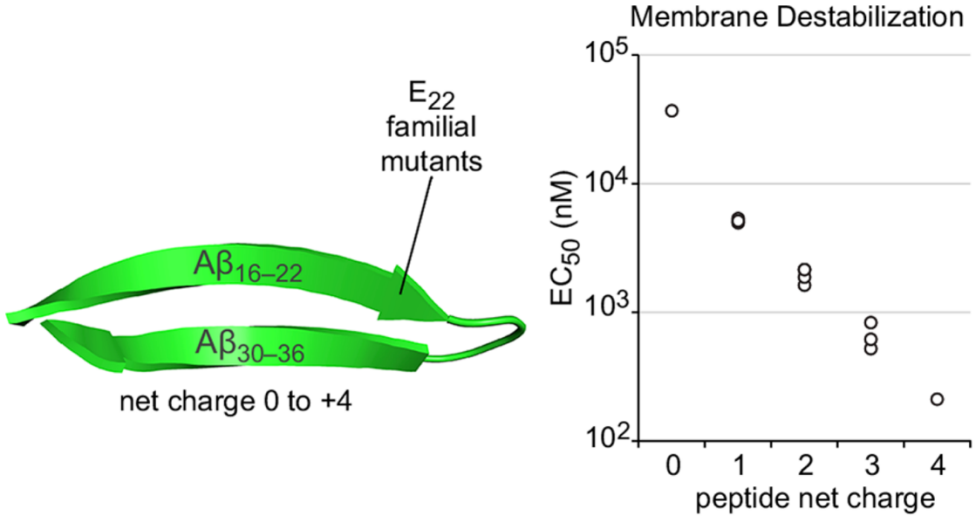

Figure 6.2 Peptides designed from known familial mutations of Aβ showed charge dependence in the ability to destabilize membranes.

Converting an Organic Chemistry Course to an Online Format in Two Weeks: Design, Implementation, and Reflection[3]

When the global pandemic and the spread of COVID-19 required the change of format of chemistry education, Dr. Susan King, Dr. Will Howitz, and I took on the challenge of adapting an organic chemistry course designed for in-person teaching to an online format. With this shift, we quickly found that there was a rapid learning curve for effectively teaching students reactions and mechanisms important to organic chemistry via computer. Based on our experience and online teaching methods, we put together a publication to guide others through the process.

As a teaching assistant, I was the team member most frequently interfacing with students through remote office hours and discussion sections. Keeping students engaged through a computer screen was challenging. Some adaptations we incorporated included using polls and surveys through Zoom to get student feedback and check conceptual understanding as well as using breakout rooms where students could engage with their peers. Overall, students responded positively to the course changes and demonstrated a grasp of concepts even with the hurdles presented by the global pandemic.

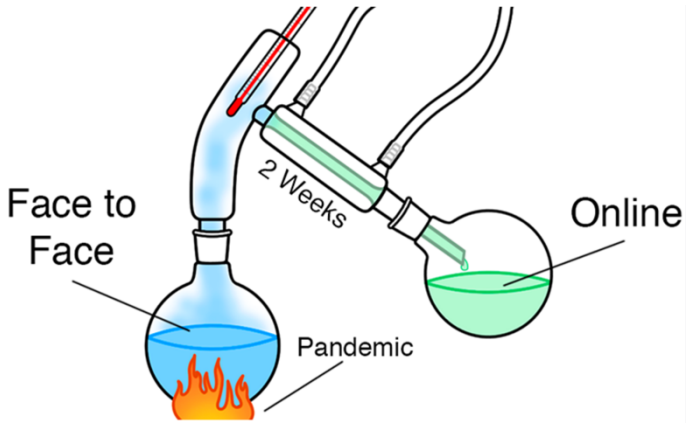

Figure 6.3 Graphic representation of the urgency created by the pandemic to distill information from a face-to-face organic chemistry course to an online course.

Teixobactin-Derived O-Acyl Isopeptide Prodrugs[4]

In this study, Chelsea Jones designed and synthesized teixobactin-derived prodrugs. Teixobactin is a highly effective antibiotic but has a high propensity to form gels in solution, making it a poor candidate for clinical development. Chelsea developed a solution to improve solubility by using an ester linkage within the peptide backbone that converts to an amide on the time scale of hours. In this work, I performed cytotoxicity studies on the nine peptides synthesized by Chelsea to determine if the prodrugs were toxic towards cells. Here, we used HeLa cells treated with the prodrugs for 48 h and measured live and dead cell enzymes present in solution.

In this collaboration, I was able to apply the skills I had obtained in the Nowick lab and train a new member of the lab in mammalian cell culture and cytotoxicity assays. This collaboration taught me the importance of mentorship and communication. I was challenged to not only convey the necessary technical information but also the learnings that came with years of cell culture.

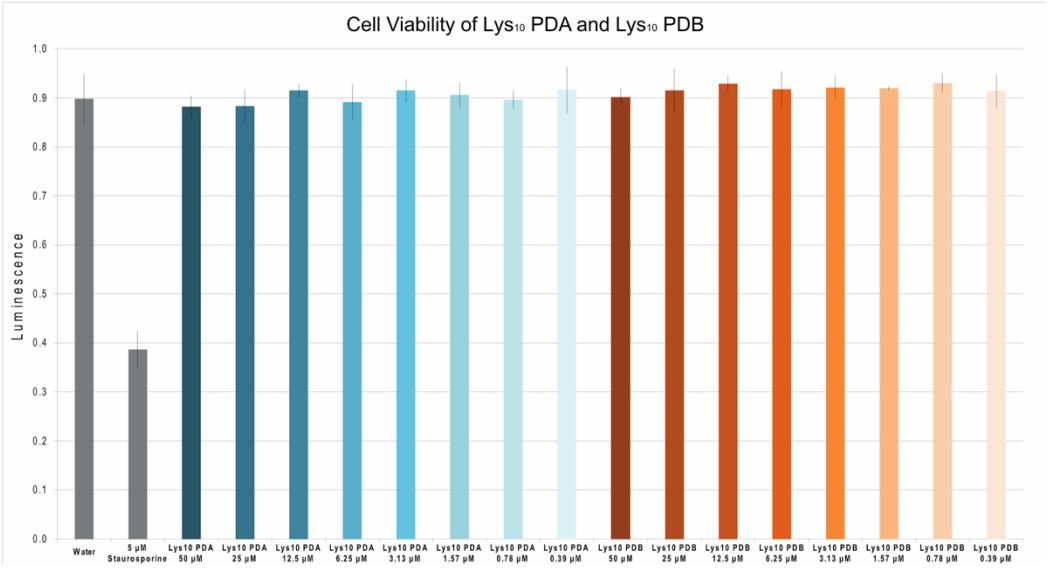

Figure 6.4 Representative image of cytotoxicity studies on two of nine prodrug compounds.

A β-Barrel-Like Tetramer Formed by a β-Hairpin Derived From Aβ[5]

In this project, Dr. Tuan Samdin designed, synthesized and studied β-hairpin peptides derived from Aβ12–40. By X-ray crystallography Dr. Samdin observed β-barrel-like tetramers that further assemble into octamers. Additionally, molecular dynamics simulations of the tetramer in a lipid bilayer membrane show disruption of the membrane. To further investigate the interactions of these peptides with cells, I performed cytotoxicity assays to analyze caspase 3/7 activation as an indicator of cells undergoing apoptosis.

Working with Dr. Samdin on this project taught me the importance of planning prior to execution and importance of knowing your field. He spent extensive time pouring over literature to design peptides, plan the goals of his project, and expertly assign the relevance of his work in the greater context of Aβ research. These skills were vital to making this project successful and are lessons I will take with me in my career.

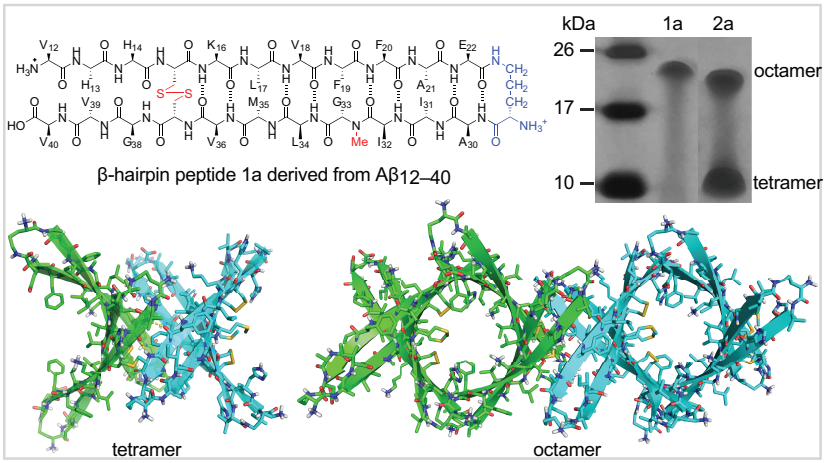

Figure 6.5 Representative structure of one of the β-hairpin peptides derived from Aβ12–40 with the oligomers observed by SDS-PAGE and X-ray crystallography.

REFERENCES

(1) Zhang, S.; Guaglianone, G.; Morris, M. A.; Yoo, S.; Howitz, W. J.; Xing, L.; Zheng, J. G.; Jusuf, H.; Huizar, G.; Lin, J.; Kreutzer, A. G.; Nowick, J. S. Expression of N-Terminal Cysteine Aβ42and Conjugation to Generate Fluorescent and Biotinylated Aβ42. *Biochemistry* **2021**, *60* (15), 1191–1200. https://doi.org/10.1021/acs.biochem.1c00105.

(2) Howitz, W. J.; Guaglianone, G.; McKnelly, K. J.; Haduong, K.; Ashby, S. N.; Laayouni, M.; Nowick, J. S. Macrocyclic Peptides Derived from Familial Alzheimer's Disease Mutants Show Charge-Dependent Oligomeric Assembly and Toxicity. *ACS Chem. Neurosci.* **2022**, *13* (6), 714–720. https://doi.org/10.1021/acschemneuro.1c00833.

(3) Howitz, W. J.; Guaglianone, G.; King, S. M. Converting an Organic Chemistry Course to an Online Format in Two Weeks: Design, Implementation, and Reflection. *J. Chem. Educ.* **2020**, *97* (9), 2581–2589. https://doi.org/10.1021/acs.jchemed.0c00809.

(4) Jones, C. R.; Guaglianone, G.; Lai, G. H.; Nowick, J. S. Teixobactin-Derived O-Acyl Isopeptide Prodrugs. *Submitted to ChemSci*.

(5) Samdin, T. D.; Guaglianone, G.; Kreutzer, A. G.; Freites, J. A.; Wierzbicki, M.; Nowick, J. S. A β-Barrel-Like Tetramer Formed by a β-Hairpin Derived From Aβ. *Submitted to Nat. Commun.*